AsCA'07 Taipei

Programme & Abstracts

November 4-7, 2007

www.asca2007.tw

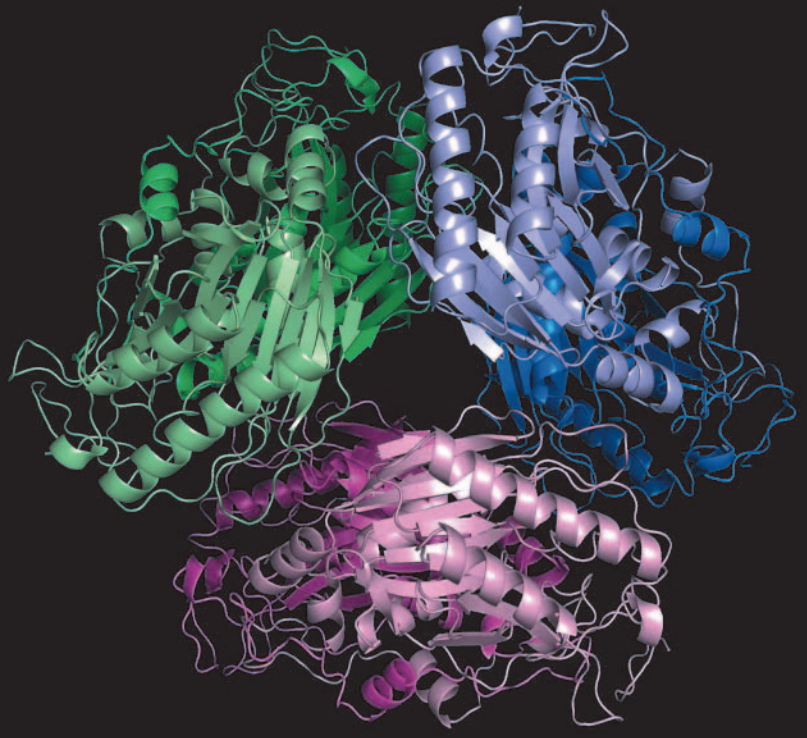

The 8th Conference of the Asian Crystallographic Association
Taipei, Taiwan

AsCA'07 Taipei

The 8th Conference of the Asian Crystallographic Association
Taipei, Taiwan

Committees

Asian Crystallographic Association

President: Prof. Mamannamana Vijayan
Indian Institute of Science, India

Vice President: Prof. Mitchell Guss
University of Sydney, Australia

Treasurer & Secretary: Prof. Ian Williams
Hong Kong University of Science & Technology, Hong Kong

International Program Committee

Chairman: Se Won Suh	Korea
Members:	
Amemiya, Yoshiyuki	Japan
Baker, Ted	New Zealand
Feng, Donglei	China
Kennedy, Brendan	Australia
Martin, Jennifer	Australia
Miki, Kunio	Japan
Murakami, Youichi	Japan
Ogawa, Keiichiro	Japan
Rao, Zihe	China
Row, T. N. Guru	India
Singh, T. P.	India
Wang, Andrew	Taiwan
Wang, Yu	Taiwan
Williams, Ian	Hong Kong

Organizing Committee

Chairman: Shih-Lin Chang	National Tsing Hua University
Members:	
Hsiao, Chwan-Deng	Academia Sinica
Jean, Yuch-Cheng	National Synchrotron Radiation Research Center
Lee, Chih-Hao	National Tsing Hua University
Liang, Keng S.	National Synchrotron Radiation Research Center
Lii, Kwang-Hwa	National Central University
Liu, Ling-Kang	Academia Sinica
Peng, Shie-Ming	National Taiwan University
Sheu, Hwo-Shuenn	National Synchrotron Radiation Research Center
Wang, Andrew	Academia Sinica
Wang,Yu	National Taiwan University
Yu, Shu-Cheng	National Cheng Kung University
Yuan, Hanna S.	Academia Sinica

IUCr Scientific Freedom Policy Statement

The Organizing Committee of the AsCA 2007 shall observe the basic policy of non-discrimination and affirms the right and freedom of scientists to associate in international scientific activity without regard to such factors as citizenship, religion, creed, political stance, ethnic origin, race, colour, language, age or gender, in accordance with the Statutes of the International Council for Science.

At AsCA 2007 no barriers will exist which would prevent the participation of bona fide scientists.

General Information

Registration and Reception

The Registration Desk is located on the 1F.

Opening Time: November 4, 13:30~18:00
November 5~7, 8:00~18:00

A name badge is required for all sessions.

Exhibition

The exhibitions are displayed on the 1F and 2F during the

Opening Time: November 5~6, 8:30~18:00
November 7, 8:30~12:00

Internet Access

Computers will be set up on 2F for attendees to access to the Internet. For every attendee's convenience, please limit Internet your access to 10 minutes, so that every attendee has the opportunity to use the Internet service. Free wireless Internet is available, but the speed is limited.

Luncheon & Coffee Break

Luncheon from November 5 to 7 will be served on the 2F (Yueshiang Restaurant) and on the B1 (Social Room) from 12:15 to 13:30.

280 seats are available at the 2F and 120 seats are available at the B1.

Vegetarian Service will be provided on the B1.

Coffee and tea are served during tea time on the 1F and 2F.

Shuttle Service

Free Shuttle Buses from and to the venues of two evening events, Dinner Buffet and Banquet, are provided.

Pre-event

Shuttles are available at the main entrance of the Howard International House on the 1F from 18:30 to 19:00.

Shuttles leave as soon as they are full.

The last shuttle leaves at 19:00.

Post-event

Please follow the staff in blue uniform handing "AsCA 2007" sign.

Shuttles leave as soon as they are full.

Shuttles do not serve any other stops except for Howard International House.

The last shuttle leaves 30 minutes after the end of the event.

Information for Authors and Presenters

Oral Presentations

A set of notebook PC and LCD projector will be ready in each hall/room. Each room has AsCA staffs in blue uniform. All presenters are kindly requested to come to the speaker ready room 30 minutes prior to your session and please hand your file or notebook to our site staffs.

What do Oral Codes stand for?

For example, “O1A05-M1”

O	is initial of Oral.
1	is Session number from 1 to 6.
A	indicate the room. “A”: Convention Hall, “B”: Conference Room, “C”: Room 103
05	means the presentation date.
M	indicate the time. “M”: Morning, “A”: Afternoon
1	is the presentation sequence.

Poster Presentations

Poster presentations are held in the corridors on the 2F to 4F in the Howard International House from 13:30 on Nov. 5 to 15:30 on Nov. 6.
All posters are scheduled to be displayed for 2 days.
Authors are kindly requested to set up posters between 10:30 and 13:30 on Nov. 5 and to remove them between 15:30 and 17:00 on Nov. 6.

What do Poster Codes stand for?

For example, “P05-116”

P	is initial of Poster.
05	indicates that the author of poster should have to present in person on November 5 from 13:30~15:30
116	the serial number of poster, which you can easily find your display board by following the number.

Poster Board Size

95cm(Width)X120cm(Height)

AsCA'07 Program Timetable

Nov.	4	5
	Sunday	**Monday**
08:00		**Registration** from 08:00
08:30		**Opening** 08:30 – 09:00 (A)
09:00		**Plenary 1** (20th Anniversary) 09:00 – 10:00 Dr. Zhong Lin Wang (A)
10:00		**Coffee Break** 10:00 – 10:15
10:15	-	**Oral Session 1** 10:15 – 12:15 MS-16/17: New methods for structural biology (A) MS-12: Crystallography of pharmaceuticals and natural products (B) MS-04: Advances in small angle X-ray and neutron scattering (C)
12:15		**Lunch** 12:15 – 13:30
13:30	**Registration** 13:30 – 18:00	**Poster – 1** 13:30 – 15:30 Corridor 2F, 3F, 4F
15:30		**Break** 15:30 – 16:00
16:00		**Oral Session 2** 16:00 – 18:30 MS-15: Macromolecular assemblies: proteins and nucleic acids (A) MS-09: Science of inorganic materials (B) MS-05: Electronic structure and bonding by X-ray diffraction and other techniques (C)
18:00		
18:30	**Welcome Mixer** **Rayonix& Marresearch** 18:30 – 21:00 2F, Howard International House	-
19:30		**Dinner Buffet** **Bruker – AXS** 19:30 – 21:30 Hall 201, NTU Internaitonal Convention Center
21:00	-	

(A): Convention Hall, (B): Conference Room, (C): Room 103

<table>
<tr><th rowspan="2">Nov.</th><th>6</th><th>7</th></tr>
<tr><th>Tuesday</th><th>Wednesday</th></tr>
<tr><td>08:00
08:30</td><td>-</td><td>-</td></tr>
<tr><td>09:00</td><td>Plenary 2 & 3 09:00 – 10:00
Dr. Jill Trewhella (A)
Dr. Krishan Lal (B)</td><td>Plenary 4 & 5 09:00 – 10:00
Dr. Osamu Nureki (A)
Dr. Kwang-Hwa Lii (B)</td></tr>
<tr><td>10:00</td><td colspan="2">Coffee Break 10:00 – 10:15</td></tr>
<tr><td>10:15</td><td>Oral session 3 10:15 – 12:15
MS-13: Membrane proteins - methods and structures (A)
MS-06: Scattering studies of novel electronic and magnetic systems (B)
MS-02: Synchrotron, instrumentation, time-resolved technique, and remote access (C)</td><td>Oral session 5 10:15 – 12:15
MS-18a: Cool structures in protein crystallography I (A)
MS-10: Science of organic materials (B)
MS-01: Neutron sources, instrumentation, and applications (C)</td></tr>
<tr><td>12:15</td><td colspan="2">Lunch 12:15 – 13:30</td></tr>
<tr><td>13:30</td><td>Poster – 2 13:30 – 15:30
Corridor 2F, 3F, 4F</td><td>Oral session 6 13:30 – 15:30
MS-18a: Cool structures in protein crystallography II (A)
MS-11: Dynamic aspects of molecular and solid state crystals (B)
MS-03: Advances in powder X-ray and neutron diffraction (C)</td></tr>
<tr><td>15:30</td><td colspan="2">Break 15:30 – 16:00</td></tr>
<tr><td>16:00</td><td rowspan="3">Oral session 4 16:00 – 18:30
MS-14: Proteins related to disease/drug discovery (A)
MS-07: Crystal engineering and supramolecular chemistry (B)
MS-08: Nano technology: structure, surface, and interface (C)</td><td>Plenary 6 (20th Anniversary) 16:00 – 17:00
Dr. Yigong Shi (A)</td></tr>
<tr><td>17:00</td><td>Closing ceremony (A) 17:00</td></tr>
<tr><td></td><td rowspan="2">Farewell Party 17:30 – 19:30
2F, Howard International House</td></tr>
<tr><td>18:30</td><td>-</td></tr>
<tr><td>19:30</td><td>Banquet
Rigaku
19:30 – 21:30
3F, Grand Formosa Regent Hotel</td><td>-</td></tr>
</table>

(A): Convention Hall, (B): Conference Room, (C): Room 103

November 05, Monday

Plenary 1 (09:00 – 10:00) (Convention Hall)

Chair: Sydney Hall

10:15 PL05-001 **OXIDE NANOSTRUCTURES – FROM GROWTH TO NANOGENERATORS AND TO NANOPIEZOTRONICS**
Zhong Lin Wang

Oral Session 1 (10:15-12:15) (Convention Hall)

MS-16/17: New methods for structural biology

Chair/Co-chair: Isao Tanaka, Zhi-Jie Liu

10:15 O1A05-M1 **THE EFFECT OF AMINO ACIDS AND AMINO ACID DERIVATIVES ON PROTEIN CRYSTALLIZATION**
L. Ito, T. Kobayashi, K. Shiraki, T. Narukawa, A. Oosuka and H. Yamaguchi

10:40 O1A05-M2 **(NZ)CH...O CONTACTS ASSISTED CRYSTALLIZATION**
Neil Shaw, Zhongyun Cheng, Bi-Cheng Wang, Zihe Rao and Zhi-Jie Liu

11:05 O1A05-M3 **PHASING WITH IN-HOUSE SOFTER X-RAY RADIATION**
Cheng Yang, James W. Pflugrath, Joseph D. Ferrara

11:30 O1A05-M4 **LONG WAVELENGTH PHASING: CURRENT AND FUTURE CHALLENGES**
B.C. Wang, John Rose, Lirong Chen, John Ruble, James Tucker Swindell II, Zeng-Qing Albert Fu, Jim Fait, Zhongmin Jin, Andrew Horward and John Chrzas

11:55 O1A05-M5 **PSAP: PROTEIN STRUCTURE ANALYSIS PACKAGE**
K. Sekar, B.Balamurugan, M.N.A.Md.Roshan, B.Shaahul Hameed, K.Sumathi, R.Senthil Kumar, A.Udayakumar, K.H.Venkatesh Babu, M.Kalaivani, G.Sowmiya, P.Sivasankari, S.Saravanan, C.Vasuki Ranjani, K.Gopalakrishnan, K.N.Selvakumar, M.Jaikumar, T.Brindha and Daliah Michael

Oral Session 1 (10:15-12:15) (Conference Room)

MS-12: Crystallography of pharmaceuticals and natural products

Chair/Co-chair: Ian D. Williams, H. K. Fun

10:15 O1B05-M1 **CONTROL OF POLYMORPHIC TRANSITION INDUCING PREFERENTIAL ENRICHMENT BY MODIFYING MOLECULAR STRUCTURES OR ADDING SEED CRYSTALS**
Rui Tamura

10:45 O1B05-M2 **POLYMORPHISM CASE STUDIES IN THE ARTEMISININ FAMILY OF ANTI-MALARIAL DRUGS: INVOLVEMENT OF MOLECULAR SHEET MOTIFS**
Fanny L-Y. Shek, Herman H-Y. Sung, Richard K. Haynes and Ian D. Williams

11:05 O1B05-M3 **DETERMINATION OF ABSOLUTE CONFIGURATION FOR SOME NATURAL PRODUCTS FROM TRADITIONAL CHINESE MEDICINE**
Herman H-Y. Sung, Nancy Y. Ip and Ian D. Williams

11:25 O1B05-M4 **DISTINGUISHING BETWEEN NATURAL PRODUCTS AND NATURAL PRODUCT ARTIFACTS USING SINGLE CRYSTAL X-RAY STRUCTURE DETERMINATION: A CASE STUDY ON MACLURAXANTHONE, A COMPOUND CONTAINING A CHROMENE RING**
Suchada Chantrapromma, Nawong Boonnak, and Hoong-Kun Fun

11:45 O1B05-M5 **PROTEIN MEASUREMENTS ON A LABORATORY POWDER X-RAY DIFFRACTOMETER**
D. Beckers, S. Prugovečki, T. Degen, A. Stefanovic

Oral Session 1 (10:15-12:15) (Room 103)

MS-04: Advances in small angle X-ray and neutron scattering

Chair/Co-chair: Yoshiyuki Amemiya, Moonhor Ree

10:15 O1C05-M1 **QUANTITATIVE GISAXS ANALYSIS OF LAMELLAR STRUCTURES SELF-ASSEMBLED IN BRUSH POLYMER THIN FILMS**
Moonhor Ree, Jinhwan Yoon, Kyeong Sik Jin, Kyuyoung Heo, Sangwoo Jin, Jehan Kim, Kwang-Woo Kim, Tae Joo Shin

10:35 O1C05-M2 **MESO AND NANO-SCALE STRUCTURAL FORMATION OF POLYETHYLENE THIN FILMS EVALUATED BY SYNCHROTRON GRAZING-INCIDENCE SMALL-ANGLE AND WIDE-ANGLE X-RAY SCATTERING MEASUREMENTS**
Sono SASAKI, Hiroyasu MASUNAGA, Hiroo TAJIRI, Katsuaki INOUE, Hiroshi OKUDA, Atsushi TAKAHARA, Masaki TAKATA

10:55 O1C05-M3 **STRUCTURAL CHANGES IN THE MECHANICAL DEFORMATION PROCESS OF SPECIFICALLY-ORIENTED POLYETHYLENE SAMPLES AS VIEWED FROM THE SIMULTANEOUS MEASUREMENTS OF SYNCHROTRON SAXS-WAXD AND RAMAN SPECTRA**
Kohji TASHIRO, Shinichi TAKEDA, Makoto HANESAKA, Hiroyasu MASUNAGA, Sono SASAKI and Masaki TAKATA

11:15 O1C05-M4 **STRAIN-INDUCED CRYSTALLIZATION OF REINFORCED NATURAL RUBBER AS STUDIED BY SYNCHROTRON X-RAY SCATTERING**
Hyun Hoon Song, Min Kwan Kang, Hye-Jin Jeon, Gwanghoon Kwag and Hyungkyu Choi

11:35 O1C05-M5 **ANOMALOUS SMALL ANGLE X-RAY SCATTERING FOR THE DISTRIBUTION AND AGGREGATION OF THE GOLD NANOPARTICLES IN A PS-b-P4VP DIBLOCK COPOLYMER**
U-Ser Jeng, Ying-Huang Lai, Ching-Mao Huang, and Kung-Hwa Wei, Chiu-Hun Su, and Hwo-Shuenn Sheu

11:55 O1C05-M4 **CORE-SHELL MICELLAR STRUCTURES OF NOVEL TERTIARY AMINE METHACRYLATE-BASED BLOCK COPOLYMERS STUDIED BY SMALL ANGLE X-RAY SCATTERING AND DYNAMIC LIGHT SCATTERING**
Yusuf Ozcan, U-Ser Jeng, Vural Butun, Ying-Huang Lai, Chiu-Hun Su, Keng S. Liang, Semra Ide

Oral Session 2 (16:00-18:30) (Convention Hall)

MS-15: Macromolecular assemblies: proteins and nucleic acids

Chair/Co-chair: Atsushi Nakagawa, Mike Lawrence

16:00 O2A05-A1 **STRUCTURE, ASSEMBLY AND ACTION OF DODECAMERIC DPS, A STRESS RELATED FAMILY OF PROTEINS**
Siddhartha Roy, Ramachandran Saraswathi, Surbhi Gupta, K.Sekar, Dipankar Chatterji and M.Vijayan

16:25 O2A05-A2 **STRUCTURL AND FUNCTIONAL STUDY OF C. ELEGANS CELL-DEATH RELATED NUCLEASE 4 (CRN-4)**
Yu-Yuan Hsiao and Hanna S. Yuan

16:45 O2A05-A3 **CONFORMATIONAL CHANGE IN BIFUNCTIONAL REPLICATION INITIATOR PROTEIN RepE**
Akira Nakamura, Chieko Wada and Kunio Miki

17:05 O2A05-A4 **STRUCTURE OF AN IgNAR-AMA1 COMPLEX**
Victor Streltsov, Kylie Henderson, Andrew Coley, Adrian Batchelor, Robin Anders, Michael Foley, Stewart Nuttall

17:25 O2A05-A5 **STRUCTURAL AND FUNCTIONAL INSIGHTS INTO DOM34, A KEY COMPONENT OF NO-GO mRNA DECAY**
Hyung Ho Lee and Se Won Suh

17:45 O2A05-A6 **THE CRYSTAL STRUCTURE OF A VIRUS-LIKE PARTICLE FROM HYPERTHERMOPHILLIC ARCAHEON PYROCOCCUS FURIOSUS PROVIDE INSIGHT INTO THE EVOLUTION OF VIRUSES**
Fusamichi Akita, Khoon Tee Chong, Hideaki Tanaka, Eiki Yamashita, Naoyuki Miyazaki, Yuichiro Nakaishi, Kazunori Namba, Mamoru Suzuki, Tomitake Tsukihara and Atsushi Nakagawa

18:10 O2A05-A7 **HIGHER RESOLUTION STRUCTURE OF GIANT HEMOGLOBIN FROM OLIGOBRACHIA MASHIKOI**
Nobutaka Numoto, Taro Nakagawa, Akiko Kita, Yuichi Sasayama, Yoshihiro Fukumori and Kunio Miki

Oral Session 2 (16:00-18:30) (Conference Room)

MS-09: Science of inorganic materials

Chair/Co-chair: Yukio Noda, Je-Geun Park

16:00 O2B05-A1 **VISUALIZATION OF RATTILING IN PrOs4Sb12 BY SINGLE CRYSTAL NEUTRON DIFFRACTION**

Koji Kaneko, Naoto Metoki, Hiroyuki Kimura, Yukio Noda, Tatsuma D. Matsuda and Masafumi Kohgi

16:30 O2B05-A2 **SINGLE CRYSTAL NEUTRON DIFFRACTION INVESTIGATIONS OF TYPE I CLATHRATES – POTENTIAL THERMOELECTRIC MATERIAL**

Mogens Christensen, Bo B. Iversen.

16:50 O2B05-A3 **X-RAY SCATTERING STUDY OF RB_4**

Ki Bong Lee, S. Ji, C. Song, J. Koo, Y. J. Park, J. Y, Kim and B. K. Cho

17:20 O2B05-A4 **HYDROGEN BONDING PHASE TRANSITIONS IN SOME ORGANIC CRYSTALS**

Hoong-Kun Fun, Beck-Sim Lee and Suchada Chantrapromma

17:40 O2B05-A5 **DIFFRACTION STUDIES OF RELATION BETWEEN HELICITY OF CYCLOID MAGNETISM AND FERROELECTRIC POLARIZATION IN MULTIFERROIC MANGANESE OXIDES**

Taka-hisa Arima, Hajime Sagayama, Nobuyuki Abe, Koji Taniguchi, Hiroyuki Ohsumi, Masato Matsuura, Kazuma Hirota, Daisuke Okuyama, Yuichi Yamasaki, and Yoshinori Tokura

18:10 O2B05-A6 **ANOMALOUS STRUCTURAL PHASE TRANSITION ABOVE LIQUID NITROGEN TEMPERATURE IN THE MULTIFERROIC PEROVSKITE $Dy(Mn_{0.5}Fe_{0.5})O_3$**

Fu-Kuo Chiang , Fei-Ting Huang, and Ming-Wen Chu

Oral Session 2 (16:00-18:30) (Room 103)

MS-05: Electronic structure and bonding by X-ray diffraction and other techniques

Chair/Co-chair: Yu Wang, T. N. Guru Row

16:00 O2C05-A1 **SINGLE CRYSTAL STRUCUTURE ANALYSIS OF PHOTO-EXCITED STATES OF HALOGEN-BRIDGED DICOPPER(I) COMPLEXES**

Yoshiki Ozawa, Shingo Yoshida, Nobuyuki Kitayama, Minoru Mitsumi, Koshiro Toriumi, Kiyoshi Tsuge, Hiromi Araki, and Yoichi Sasaki

16:30 O2C05-A2 **INVESTIGATION OF THE PHOTOEXCITED CHARGE-TRANSFER STATE OF [AuBr(PPh_3)$_2$] BY THE MULTIPLE-EXPOSURE IP METHOD**

Manabu Hoshino, Hidehiro Uekusa, Shintaro Sonoda, Takuhiro Otsuka, Youkoh Kaizu, Yoshiki Ozawa, Koshiro Toriumi

17:00 O2C05-A3 **X-RAY ATOMIC ORBITAL ANALYSIS AND ITS APPLICATION TO RARE-EARTH CRYSTALS**

Kiyoaki Tanaka, Ryoko Makita, Shiro Funahashi, Takashi Komori, Terutoshi Sakakura

17:30 O2C05-A4 **STRUCTURES OF POLYPYRIDINE MONONUCLEAR IR(III) COMPLEXES IN THE CLOSED-SHELL SINGLET AND TRIPLET STATES**

Naokazu Yoshikawa, Shinichi Yamabe, Nobuko Kanehisa, Yasushi Kai, Hiroshi Takashima, and Keiichi Tsukahara

18:00 O2C05-A5 **APEX II ULTRA - PRECISION AND ACCURACY**

Michael Ruf, Martin Adam

November 06, Tuesday

Plenary 2 (09:00 – 10:00) (Convention Hall)

Chair: Sine Larsen

10:15 PL06-002 **BIOMOLECULAR SIGNALLING AND REGULATION; A SOLUTION SCATTERING VIEW**
Jill Trewhella

Plenary 3 (09:00 – 10:00) (Conference Room)

Chair: Shih-Lin Chang

10:15 PL06-003 **CHALLENGES IN CHARACTERIZATION OF SINGLE CRYSTALS, THIN LAYERS AND DEVICES BY HIGH RESOLUTION X-RAY DIFFRACTION AND REFLECTION TECHNIQUES**
Krishan Lal

Oral Session 3 (10:15-12:15) (Convention Hall)

MS-13: Membrane proteins - methods and structures

Chair/Co-chair: Satoshi Murakami, Che Alex Ma

10:15 O3A06-M1 **FLUORESCENCE-DETECTION SIZE EXCLUSION CHROMATOGRAPHY FOR PRECRYSTALLIZATION SCREENING OF INTEGRAL MEMBRANE PROTEINS**
Toshimitsu Kawate, Atsuko Yamashita, Jaysankar Jasti, Michael Rosconi, Paul Shaffer, Alexander Sobolevsky, Tanja Homrichhausen and Eric Gouaux

10:40 O3A06-M2 **ION BINDING AND SELECTIVITY OF THE ROTOR OF THE V-TYPE NA^+-ATPASE FROM *ENTEROCOCCUS HIRAE***
Takeshi Murata, Ichiro Yamato, Yoshimi Kakinuma, Mikako Shirouzu, John E. Walker, Shigeyuki Yokoyama and So Iwata

11:05 O3A06-M3 **NEW STRUCTURAL ASPECTS OF BOVINE HEART CYTOCHROME C OXIDASE**
H. Aoyama, T. Tsukihara and S. Yoshikawa

11:30 O3A06-M4 **STRUCTURE OF THE CYTOCHROME b_6f COMPLEX: QUINONE ANALOGUE INHIBITORS AS LIGANDS OF HEME c_n**
Eiki Yamashita, Huamin Zhang,William A. Cramer

11:50 O3A06-M5 **X-RAY STRUCTURE of EmrE SUPPORTS DUAL TOPOLOGY MODEL**

Yen-Ju Chen, Owen Pornillos, Samantha Lieu, Che Ma, Andy P. Chen, Geoffrey Chang

Oral Session 3 (10:15-12:15) (Conference Room)

MS-06: Scattering studies of novel electronic and magnetic systems

Chair/Co-chair: Donglai Feng, Yong-Qiang Cai

10:15 O3B06-M1 **MOMENTUM DEPENDENT CHARGE EXCITATIONS IN CORRELATED ELECTRON SYSTEMS STUDIED BY RESONANT INELASTIC X-RAY SCATTERING**
Kenji Ishii

10:40 O3B06-M2 **SPIN, CHARGE, AND ORBITAL ORDERING OF TRANSITION-METAL OXIDES**
Di-Jing Huang

11:05 O3B06-M3 **WIGNER CRYSTALLIZATION IN A MOLECULAR CONDUCTOR, (DI-DCNQI)2Ag**
Hiroshi Sawa, Toru Kakiuchi, Yusuke Wakabayashi, and Kazushi Kanoda

11:25 O3B06-M4 **Q-DEPENDENT DIELECTRIC FUCTION STUDIES USING INELASTIC X-RAY SCATTERING**
N. Hiraoka, H. Ishii, I. Jarrige, and Y. Q. Cai,

11:45 O3B06-M5 **CRYSTAL AND MAGNETIC STRUCTURE OF ORGANIC CONDUCTOR β'-ET2ICl2 BY USING NEUTRONS**
Yukio Noda, Masashi Watanabe, Atsushi Matsunaga, Satoshi Komiyama, HiromiTaniguchi, Atshushi Kawamoto and Yoshiya Uwatoko

12:00 O3B06-M6 **LATTICE DISTORTION AND FERROMAGNETISM IN $BaRuO_3$**
Chao-hung Du, K. J. Tseng, Y. Y. Lo, Mau-Tsu Tang

Oral Session 3 (10:15-12:15) (Room 103)

MS-02: Synchrotron, instrumentation, time-resolved technique, and remote access

Chair/Co-chair: Soichi Wakatsuki, Julian Adams

10:15 O3C06-M1 **THE AUSTRALIAN SYNCHROTRON**
Julian Adams

10:45 O3C06-M2 **AUTOMATION AT SER-CAT: TOWARDS SIGNAL BASED DATA COLLECTION**
John P. Rose, John Chrzas, James Fait, Zeng-Qing Albert Fu, Andrew Howard, John Gonczy, Zhongmin Jin and B. C. Wang

11:15 O3C06-M3 **100-PS TIME-RESOLVED X-RAY EXPERIMENTS WITH DAILY SINGLE BUNCH MODE: CURRENT STATUS OF BEAM LINE NW14A AT THE PHOTON FACTORY ADVANCED RING**
Shin-ichi Adachi

11:45 O3C06-M4 **DEVELOPMENT AND APPLICATION OF THE "PINPOINT STRUCTURE MEASUREMENT SYSTEM"**
Sub-Micron Beam and Time-Resolved Measurement at SPring-8's BL40XU
Shigeru Kimura, Nobuhiro Yasuda, Yoshimitsu Fukuyama, Jungeun Kim, Yoshihito Tanaka, Koshiro Toriumi, Yutaka Moritomo, Yoshihiro Kuroiwa, Kenichi Kato and Masaki Takata

Oral Session 4 (16:00-18:30) (Convention Hall)

MS-14: Proteins related to disease/drug discovery

Chair/Co-chair: Jennifer Martin, Andrew Wang

16:00 O4A06-A1 **ALANINE RACEMASE AS A TEMPLATE FOR DRUG DISCOVERY IN TUBERCULOSIS**

Kurt Krause , Mike Benedik, James Briggs, Milya Davlieva , Harold Kohn , Joe Longtin, Daniel Milligan , Ulrich Strych

16:30 O4A06-A2 **STRUCTURES OF ALL FOUR PHOSPHODIESTERASE-4 SUBFAMILIES PROVIDE INSIGHT INTO SUBFAMILY INHIBITOR SELECTIVITY**

Jiwen Cai, Huanchen Wang, Ming-Sheng Peng, Yi Chen, Jie Geng, Howard Robinson, Miles Houslay & Hengming Ke

17:00 O4A06-A3 **STRUCTURAL BASIS FOR RECRUITMENT OF TANDEM HOTDOG DOMAINS IN ACYL-COA THIOESTERASE 7 AND ITS ROLE IN INFLAMMATION**

Jade K. Forwood, Anil S. Thakur, Gregor Guncar, Mary Marfori, Dmitri Mouradov, Stuart Kellie, David A. Hume, Thomas Huber, Jennifer L. Martin, Bostjan Kobe

17:30 O4A06-A4 **THROUGH-PUT PROTEIN STRUCTURE DETERMINATION AND RATIONAL STRUCTURE-BASED DRUG DESIGN USING FRAGMENT-BASED APPROACH**

Tej P. Singh, Sanjit Kumar, Pradeep Sharma, Rafia Mir, Ishfaq A. Sheikh, Amit K. Singh, R. Prem Kumar, Mau Sinha, Nagendra Singh, Punit Kaur, A. Srinivasan and S. Sharma

17:50 O4A06-A5 **STRUCTURAL BASIS FOR GLUTAMATE RACEMASE INHIBITION**

Kook-Han Kim, Young-Jong Bong, Joon Kyu Park, Key-Jung Shin, Kwang Yeon Hwang and Eunice EunKyeong Kim

18:10 O4A06-A6 **CRYSTAL STRUCTURE OF ABT-737 IN COMPLEX WITH Bcl-xL**

Peter E. Czabotar, Erinna F. Lee, Brian J. Smith, Kurt Deshayes, Kerry Zobel, W. Douglas Fairlie, Peter M. Colman

Oral Session 4 (16:00-18:30) (Conference Room)

MS-07: Crystal Engineering and Supramolecular Chemistry

Chair/Co-chair: Ashwini Nangia, Jun Harada

16:00 O4B06-A1 **MOLECULAR BRICKS, PENS, GRIDS AND SPHEROIDS FROM DIHETEROAROMATIC HOSTS**
Roger Bishop, Solhe F. Alshahateet, Jason Ashmore, Donald C. Craig and Marcia L. Scudder

16:30 O4B06-A2 **ROLE OF MIXED HALOGENS (F, Br) TOWARDS CRYSTAL PACKING AND INTERMOLECULAR INTERACTIONS IN SUBSTITUTED BENZANILIDES**
Susanta K. Nayak, T. N. Guru Row

16:50 O4B06-A3 **SYNTHESIS, STRUCTURES AND MAGNETIC PROPERTIES OF A SERIES OF CYANO-BRIDGED HETEROMETALLIC COMPLEXES**
Shao-Jun Wang, Long Jiang, Wei-Xiong Zhang and Tong-Bu Lu

17:20 O4B06-A4 **WATER CLUSTERS, ISOSTRUCTURALITY AND POLYMORPHISM IN HYDROXY DERIVATIVE OF HALOBENZENE CRYSTAL STRUCTURES**
Binoy Saha

17:40 O4B06-A5 **ENGINEERING OF LUMINESCENT PROPERTIES IN MIXED LANTHANIDE CARBOXYLATE COORDINATION POLYMERS**
YuFong Yen, Samadara Thushari, Alvin Siu, Kam-Sing Wong and Ian D. Williams

18:10 O4B06-A6 **SUPRAMOLECULAR ASSEMBLIES OF MONONUCLEAR AND POLYMERIC COBALT(ii) AND NI(II) DICARBOXYLIC COMPLEXES**
Tanwawan Duangthongyou, Sutatip Siripaisarnpipat , Chris Adams

Oral Session 4 (16:00-18:30) (Room 103)

MS-08: Nano technology: structure, surface, and interface

Chair/Co-chair: Shie-Ming Peng, Isao Takahashi

16:00 O4C06-A1 **QUENCHED DISORDER EFFECTS IN TOPOLOGICALLY ORDERED NANOPORES ON THE SMECTIC PHASE TRANSITION OF 8CB**
R. Guegan, D. Morineau, R. Lefort, A. Moreac, and M. Guendouz

16:20 O4C06-A2 **AN ELECTRON DIFFRACTION METHOD FOR DETERMINING THE CHIRALITY OF CARBON NANOTUBES**
Lu-Chang Qin, Hakan Deniz, Jie Tang

16:40 O4C06-A3 **RHEED SURFACE POLE FIGURE -- A NEW IN-SITU TECHNIQUE FOR POLYCRYSTALLINE AND NANOSTRUCTURED SURFACE TEXTURE ANALYSIS**
Fu Tang, Toh-Ming Lu and Gwo-Ching Wang

17:00 O4C06-A4 **QUANTUM OSCILLATIONS AND BEATS IN X-RAY REFLECTION DURING FILM GROWTH**
Y.-R. Lee, A. Gray, J. Tischler, P. Czoschke, H. Hong, S.-L. Chang, and T.-C. Chiang

17:20 O4C06-A5 **CHARACTERIZATION OF NANOMETER SCALE GRAIN SIZED Pt ON Si AND PtSi/Si STRUCTURES DEPOSITED BY HIGH RATE MAGNETRON SPUTTERING**
V.Uma and R.Chandramani Ramu

17:40 O4C06-A6 **SYNTHESIS, STUDIES AND LUMINESCENT PROPERTIES OF TERBIUM OXIDE DOPED $LaMn_{0.9}Zn_{0.1}O_{3+d}$ NANOPEROVSKITE BY SOL-GEL METHOD**
A A Alemi, E Karimpour Nahari and H Shokri

18:00 O4C06-A7 **STUDIES OF THE NANOSTRUCTURE OF NATURAL VEGETABLE FIBERS**
Nguyen Van Tri

November 07, Wednesday

Plenary 4 (09:00 – 10:00) (Convention Hall)

Chair: Andrew H. Wang

10:15 PL07-004 **STRUCTURAL INSIGHTS INTO THE GATING CONTROL IN BACTERIAL TRANSPORTERS**
Osamu Nureki

Plenary 5 (09:00 – 10:00) (Conference Room)

Chair: Masaki Takata

10:15 PL07-005 **SYNTHESIS, CRYSTAL STRUCTURES AND PROPERTIES OF METAL SILICATES**
Kwang-Hwa Lii

Oral Session 5 (10:15-12:15) (Convention Hall)

MS-18a: Cool structures in protein crystallography I

Chair/Co-chair: Kunio Miki, T. P. Singh

10:15 O5A07-M1 **CRYSTAL STRUCTURES OF THE COMPLEXES OF C-LOBE OF LACTOFERRIN WITH NON-STEROIDAL ANTI-INFLAMMATORY DRUGS (NSAIDS) REVEAL THE BINDING PATTERN BETWEEN C-LOBE AND NSAIDS WHICH SUGGESTS A NEW THERAPY FOR MANAGEMENT OF NSAID-INDUCED GASTROPATHY**
Sujata Sharma, Rafia Mir, Mau Sinha, Nagendra Singh, and Tej P. Singh

10:40 O5A07-M2 **CRYSTAL STRUCTURES OF NATIVE BACTERIOPHAGE-ASSOCIATED HYALURONATE LYASE AND ITS COMPLXES WITH LACTOSE AND ASCORBIC ACID**
P. Mishra, V. Bhakuni, A. S. Ethayathulla, R. Prem Kumar, N. Singh, S. Sharma, P. Kaur, A. Srinivasan and T. P. Singh

11:05 O5A07-M3 **STRUCTURAL AND MUTATIONAL STUDIES OF ANTHOCYANIN MALONYLTRANSFERASES ESTABLISH THE FEATURES OF BAHD ENZYME CATALYSIS**
Hideaki Unno, Fumiko Ichimaida, Hirokazu Suzuki, Seiji Takahashi, Yoshikazu Tanaka, Atsushi Saito, Tokuzo Nishino, Toru Nakayama and Masami Kusunoki

11:30 O5A07-M4 **CRYSTAL STRUCTURE OF *N*-ACETYLGLUCOSAMINE-PHOSPHATE MUTASE, A MEMBER OF THE ALPHA-D-PHOSPHOHEXOMUTASE SUPERFAMILY**

Yuichi Nishitani, Daisuke Maruyama, Tsuyoshi Nonaka, Akiko Kita, Takaaki A. Fukami, Toshiyuki Mio, Hisafumi Yamada-Okabe, Toshiko Yamada-Okabe and Kunio Miki

11:55 O5A07-M5 **SUBSTRATE SPECIFICITY OF PHOSPHODIESTERASES, STRUCTURAL INSIGHT INTO VIAGRA FUNCTION, AND STRUCTURE-BASED DESIGN OF DRUGS FOR INFLAMMATORY DISEASES**

Hengming Ke and Huanchen Wang

Oral Session 5 (10:15-11:45) (Conference Room)

MS-10: Science of Organic Materials

Chair/Co-chair: Yoshio Nogami

10:15 O5B07-M1 **COMPLEMENTARY STUDIES OF ENZYME-RESISTANT STARCH - IMPLICATIONS FOR HUMAN HEALTH**

A. López-Rubio, M. J. Gidley, A. K. Shrestha, B.M. Flanagan, A. Htoon, H. Chanvrier, S. Uthayakumaran, I.A.M. Appelqvist, A.R. Bird, D.L. Topping, M.K. Morell and E.P. Gilbert

10:45 O5B07-M2 **CRYSTAL AND MOLECULAR STRUCTURES OF ORGANOPHOSPHORUS COMPOUNDS - CONFORMATION AND BIOLOGICAL ACTIVITY OF HETEROCYCLIC MOLECULES**

Musali Krishnaiah and Jadaprolu Radha Krishna

11:15 O5B07-M3 **IXS STUDY OF EXCITON PROPERTIES IN ORGANIC MOLECULES**

Ke Yang

Oral Session 5 (10:15-12:15) (Room 103)

MS-01: Neutron sources, instrumentation, and applications

Chair/Co-chair: Brendan Kennedy, Mahn Won Kim

10:15 O5C07-M1 **HIGH SPEED NEUTRON DIFFRACTION AT THE OPAL RESEARCH REACTOR: THE WOMBAT INSTRUMENT**

A.J. Studer, M. Avdeev, M.M. Elcombe, J.R. Hester, and V.K. Peterson

10:45 O5C07-M2 **WATER-REDISPERSIBLE SINGLE WALL CARBON NANOTUBES AND 40M SANS INSTRUMENT DEVELOPMENT AT HANARO**

Sung-Min Choi, Tae-Hwan Kim, Changwoo Doe , Young-Soo Han and Steven R Kline

11:15 O5C07-M3 **FIRST RESULTS FROM THE NEW OPAL RESEARCH REACTOR**

R. A. Robinson

11:45 O5C07-M4 **VERSATILE NEUTRON DIFFRACTOMETR AT J-PARC - IBARAKI MATERIALS DESIGN DIFFRACTOMETER -**

T. Ishigaki, A. Hoshikawa, M. Yonemura, F. Shikanai, T. Morishima, T. Kamiyama, K. Aizawa, T. Sakuma, Y. Tomota, M. Arai, M. Hayashi, K. Ebata, Y. Takano, K. Komatsuzaki, H. Asano, Y. Takano, T. Kasao

Oral Session 6 (13:30-15:30) (Convention Hall)

MS-18b: Cool structures in protein crystallography II

Chair/Co-chair: Mitchell Guss, Hanna Yuan

13:30 O6A07-A1 **TACKLING A MUNC-Y PUZZLE: STRUCTURE OF THE MUNC18C PROTEIN**
Jennifer L Martin, Shu-Hong Hu, Catherine F. Latham, Christine L. Gee, David E. James

13:55 O6A07-A2 **CRYSTAL STRUCTURE OF DSREFH, A PROTEIN ESSENTIAL FOR OXIDATION OF STORED SULFUR IN THE PURPLE SULFUR BACTERIUM ALLOCHROMATIUM VINOSUM**
Dong Hae Shin

14:20 O6A07-A3 **STRUCTURAL AND COMPUTATIONAL STUDIES ON TYPE II RIPs**
Alok Sharma, A.A. Jeyaprakash, M.J.Swamy and M.Vijayan

14:45 O6A07-A4 **STRUCTURAL STUDIES OF THE CPX PATHWAYH ACTIVATOR NLPE ON THE OUTER MEMBRANE OF ESCHERICHIA COLI**
Yu Hirano, Md. Motarab Hossain, Kazuki Takeda, Hajime Tokuda and Kunio Miki

15:10 O6A07-A5 **CRYSTAL STRUCTURE OF IL-15/IL-15RALPHA COMPLEX**
Mami Chirifu, Chiharu Hayashi, Teruya Nakamura, Sachiko Toma, Tsuyoshi Shuto, Hirofumi Kai, Yuriko Yamagata, Simon J. Davis and Shinji Ikemizu

Oral Session 6 (13:30-15:30) (Conference Room)

MS-11: Dynamic aspects of molecular crystals

Chair/Co-chair: Keiichiro Ogawa, Roger Bishop

13:30 O6B07-A1 **IXS STUDY OF EXCITATION PROPERTIES OF ORGANIC MOLECULAR CRYSTALS AND SIMPLE MOLECULES**
Binping Xie, Ke Yang, Y. Q. Cai, N. Hiraoka, Donglai Feng

13:50 O6B07-A2 **MOLECULAR DYNAMICS IN SEVERAL CHLORINE COMPOUNDS ON THE BASIS OF X-RAY THERMAL PARAMETER, IR/RAMAN AND NQR DATA**
L.Ramu and R.Chandramani.

14:10 O6B07-A3 **VAPOR INDUCED GUEST EXCHANGE OF ORGANIC INCLUSION CRYSTAL**
Hidehiro Uekusa, Yasunari Ashida, Kotaro Fujii

14:30 O6B07-A4 **CONCERTED STRUCTURAL CHANGE AND PHOTOCHROMISM OF TRANS-BIINDENILIDENEDION DERIVATIVES**
Akiko Sekine, Kumiko Aruga, Hidehiro Uekusa, Katsuya Souno and Koichi Tanaka

14:50 O6B07-A5 **CRYSTAL STRUCTURE ANALYSES OF CIS/TRANS PHOTOISOMERIZATIONS**
Jun Harada, Mayuko Harakawa and Keiichiro Ogawa

15:10 O6B07-A6 **CRYSTALLINE STATE PHOTO ISOMERIZATION OF AN ORGARNO-DIRHODIUM DITHIONITE COMPLEX**
Koshiro Toriumi, Hiroshi Kanamono, Shouichi Hashimoto, Yoshiki Ozawa, Minoru Mitsumi, Hidetaka Nakai, Yousuke Miyano, Yoshihito Hayashi, and Kiyoshi Isobe

Oral Session 6 (13:30-15:30) (Room 103)

MS-03: Advances in powder X-ray and neutron diffraction

Chair/Co-chair: Takashi Kamiyama, Andrew Studer

13:30 O6C07-A1 **STRUCTURE DETERMINATION FROM HIGH RESOLUTION SYNCHROTRON POWDER DIFFRACTION DATA**
Eiji Nishibori, Shinobu Aoyagi, and Makoto Sakata

14:00 O6C07-A2 **STRUCTURAL STUDIES EMPLOYING HIGH ENERGY POWDER DIFFRACTION**
Peter L. Lee

14:30 O6C07-A3 **EXPECTING THE UNEXPECTED. PHASE TRANSITIONS IN MANGANESE PEROVSKITES**
Brendan J Kennedy, and Zhaoming Zhang

14:50 O6C07-A4 **MORPHOTROPIC PHASE BOUNDARY LIKE CHARACTERISTIC IN A LEAD-FREE, AND NON-FERROELECTRIC SYSTEM $(1-x)NaNbO_3-xCaTiO_3$**
Saurabh Tripathi, Rajeev Ranjan, Dhananjai Pandey, Sanjay Kumar Mishra and P.S.R. Krishna

15:10 O6C07-A5 **SYNCHROTRON RADIATION X-RAY DIFFRACTION AND SPECTROSCOPIC ELLIPSOMETRY INVESTIGATION OF Si_3N_4 ON Si FOR SUB-50NM Si-IC APPLICATIONS**
Zhe Chuan Feng, Li-Chi Cheng, Chu-Wan Huang, Ying-Lang Wang, and Hwo-Shuenn Sheu

Plenary 6 (16:00 – 17:00) (Convention Hall)

Chair: Peter M. Colman

10:15 PL07-006 **MECHANISM OF PROGRAMMED CELL DEATH THROUGH STRUCTURAL BIOLOGY**
Yigong Shi

Poster Sessions

November 05, Monday

P05-001 **ENGINEERING MATERIALS DIFFRACTOMETER AT J-PARC**
Stefanus Harjo, Atsushi Moriai, Kentaro Suzuya, Kazuya Aizawa, Kaori Shirakihara, Yo Tomota, Koichi Akita, Masatoshi Arai, Yukio Morii

P05-002 **CURRENT STATUS OF IBARAKI BIOLOGICAL CRYSTAL DIFFRACTOMETER IN J-PARC**
Ichiro Tanaka, Takashi Ohhara, Kazuo Kurihara, Katsuhiro Kusaka, Takaaki Hosoya, Katsuaki Tomoyori, Nobuo Niimura, Tomoji Ozeki, Kazuya Aizawa, Masatoshi Arai, Yukio Morii, Makoto Hayashi, Kazuhiro Ebara and Yoshiki Takano

P05-003 **PROGRESS REPORT ON SUPER HIGH RESOLUTION POWDER DIFFRACTOMETER IN J-PARC**
Shuki Torii, Yasuo Kobayashi, Junichi Suzuki, Hidenori Sagehashi, Minoru Nagai, Kenichi Oikawa, Kazuhiro Mori, Masao Yonemura, Toru Ishigaki and Takashi Kamiyama

P05-014 **SHORT-RANGE ORDER PARAMETERS OF AsGeSe GLASSES**
A.H. Moharram, M. A. Hefni and A.M. Abdel-Baset

P05-015 **STRUCTURAL AND SPECTROSCOPIC STUDIES OF CATION DISORDER IN SOME BI CONTAINING PYROCHLORES**
Qingdi Zhou, Brendan J. Kennedy

P05-016 **APPLICATION OF LARGE RADIUS IMAGING PLATE CAMERA FOR SYNCHROTRON POWDER X-RAY DIFFRACTION TO STRUCTURAL PHASE TRANSITION STUDIES**
Masahiko Tanaka and Yoshio Katsuya

P05-017 **MORPHOTROPIC PHASE BOUNDARY IN (1-x)BiFeO3-xPbTiO3 : PHASE COEXISTENCE REGION AND UNUSUALLY LARGE TETRAGONALITY**
Shuvrajyoti Bhattacharjee, Saurabh Tripathi and Dhananjai Pandey

P05-018 **DISORDER OF Pb ATOM IN CUBIC PHASE OF PEROVSKITE-TYPE SOLID SOLUTIONS PZT AND PZN-PT**
Yoshihiro Terado, Chikako Moriyoshi, Yoshihiro Kuroiwa, Yasuhisa Yamamura and Makoto Iwata

P05-019 **X-RAY STRESS ANALYSIS FOR FIBER TEXTURES BASED ON SYMMETRY IN RECIPROCAL LATTICE SPACE**

Ryouichi Yokoyama, and Jimpei Harada

P05-020 **GENERALIZED METHOD OF STRUCTURE ANALYSIS FOR MICRO IMPERFECT CRYSTALS USING SR.**
Ken-ichiro Yamamoto, Yoshio Nogami, Naoshi Ikeda, Takayoshi Ito, Toru Matsuura, Taku Tsuneta, Satoshi Tanda

P05-021 **SYNTHESIS, REACTIVITY AND 3-D STRUCTURAL DETERMINATION BY POWDER DIFFRACTION ON MOLYBDOPTERIN COMPLEX**
Jey Jau Lee, Hwo-Shuenn Sheu,Keng S. Liang , Baidyanath Ghosh and Parag Sinchan Roy

P05-022 **SOLVING ZEOLITE STRUCTURES FROM POWDER DATA USING DENSITY BUILDING FUNCTIONS AND HISTOGRAM MATCHING**
Chris Gilmore and Douglas Dorset

P05-023 **BIO-MEMBRANE STRUCTURE PROBED BY THE LAMELLAR X-RAY DIFFRACTION AND THE SMALL ANGLE X-RAY SCATTERING AT NSRRC**
Ming-Tao Lee, Yu-Shan Huang, U-Ser Jeng, Ying-Huang Lai, and Ya-Sen Sun

P05-024 **ANOMALOUS X-RAY SCATTERING AND ABSORPTION SPECTROSCOPY INVESTIGATE THE MORPHOLOGY OF FePt MONOLAYER NANOPARTICLE ON SURFACE MODIFIED SUBSTRATES WITH AU OVERLAYER**
Tzu-Wen Huang, Kuan-Li Yu, Yen-Fa Liao and Chih-Hao Lee

P05-025 **SPINODAL CRYSTALLIZATION KINETICS ON SUPERCOOLED LIQUID OF POLY(TRIMETHYLENE TEREPHTHALATE)**
Wei-Tsung Chuang, Hwo-Shuenn Sheu,U-Ser Jeng, Po-Da Hong

P05-026 **AN INSTRUMENT FOR TIME RESOLVED AND ANOMALOUS SIMULTANEOUS SMALL AND WIDE ANGLE X-RAY SCATTERING (SWAXS) AT THE NSRRC**
Chiu-Hun Su, Ying-Huang Lai, Ya-Sen Sun, U-Ser Jeng, Jhih-Min Lin, Tsang-Lang Lin, Yu-Shan Huang, Hwo-Sheunn Sheu, Wei-Tsung Chuang, Chia-Hung Hsu, Ming-Tao Lee, Keng S. Liang

P05-027 **SOLUTION SAXS AND NMR ON DOMAIN ORIENTATION AND BINDING OF THE COMPONENTS OF THE HUMAN BCKD COMPLEX**
Chi-Fon Chang, Yu-Shan Huang, U-Ser Jeng

P05-028 **EXPERIMENTAL ELECTRON DENSITIES AND MOLECULAR INTERACTIONS: INTER-MOLECULAR HYDROGEN BONDING**
Azadeh Matin, Thanh Ha Nguyen, Jane Hanrahan and David Hibbs

P05-029 **EXPERIMENTAL ELECTRON DENSITIES AND MOLECULAR INTERACTIONS: INTER-MOLECULAR II-STACKING INTERACTIONS**
Thanh Ha Nguyen and David Hibbs

P05-030 **Yb-DOPING EFFECT AND TEMPERATURE DEPENDENCE IN CoSb3 SKUTTERUDITE STRUCTURE**
Atsuko Ohno, Satoshi Sasaki, Eiji Nishibori, Shinobu Aoyagi, Makoto Sakata and Bo Brummerstedt Iversen

P05-031 **SITE PREFERENCE AND DOPING EFFECT IN (Hg,Pb)(Ba,Sr)2Ca2Cu3O8+δ SUPERCONDUCTORS**
Satoshi Sasaki and Kouji Yamawaki

P05-032 **CLOSE CL···CL CONTACT: IS IT ATTRACTIVE OR REPULSIVE?**
Daisuke Hashizume

P05-033 **THEORETICAL CALCULATION OF XMCD SPECTRA AT K-EDGE Ni AND Fe SPINEL FERITE**
Koichi Ohkubo, Takeshi Toyoda

P05-034 **ELECTRONIC STRUCTURE OF MERCURIC IODIDE USING COMPTON SCATTERING TECHNIQUE**
M. Sharma, Gulzar Ahmed and B. L. Ahuja

P05-035 **CHARGE DENSITY DISTRIBUTION AND BOND CHARACTERIZATION ON COMPLEX MN(H2O)2NI(CN)4·3H2O**
Lai-Chin Wu, I-Jui Hsu, Gene-Hsiang Lee, Yu Wang

P05-036 **CHEMICAL BONDING AND INTERMOLECULAR INTERACTIONS OF A NICKEL(II) COMPLEX**
Yu-Chun Chuang, Yu Wang, Gene-Hsiang Lee, Ben-Jie Liaw, Chen-Wei Liu

P05-037 **MIXED LIGAND COPPER(I) COMPLEXES OF TRIPHENYLPHOSPHINE AND PHENYLTHAIOUREA**
Ruthairat Nimthong, Chaveng Pakawatchai, Yupa Thunyasirikul and Saowanit Saithong

P05-038 **INVESTIGATION OF ELECTRON DENSITY DISTRIBUTION IN ANATASE (TiO2) WITH- AND WITHOUT UV-IRRADIATION**
Ken-ichi Ito and Hiroki Okudera

P05-039 **CHARGE DENSITY STUDIES ON HETEROBIMETALLIC PHOSPHIDO-BRIDGED Mo AND W COMPLEXES**
Chi-Rung Lee, I-Jui Hsu, Hsiu-Mei Lin and Shin-Guang Shyu

P05-040 **EXPERIMENTAL CHARGE DENSITY STUDY ON A Fe(II) COMPLEX AT HIGH SPIN AND LOW SPIN STATES**
Chou-Fu Sheu, Che-Hsiu Shih, Szu-Miao Chen, Yu-Chun Chuang, Gene-Hsiang Lee, Yu-Shan Huang, Kuan-Li Yu, Yu Wang

P05-083 **PRELIMINARY STRUCTURAL REFINEMENTS AND A NEW SYNTHETIC ROUTE TO δ-Bi2O3-RELATED PHASES IN THE Bi-W-O, Bi-Mo-O, Bi-Ta-O AND Bi-Nb-O SYSTEMS**
Neeraj Sharma, Rene Macquart and Chris D. Ling

P05-084 **INSIGHT INTO THE STABILITY OF TETRAGONAL AND RHOMBOHEDRAL PHASES IN DOUBLE PEROVSKITES**
P. J. Saines, J. Spencer and B. J. Kennedy

P05-085 **A STUDY OF STRONTIUM, ALUMINIUM AND INDIUM TUNGSTEN BRONZES**
M. S. Rahman and A. Hussain

P05-086 **CRYSTAL STRUCTURE AND HABIT OF $CaIrO_3$**
Masahiko Sugahara, Akira Yoshiasa, Takafumi Hashimoto, Syunsuke Sakai, Akihiko Nakatsuka, Maki Okube and Akira Yoneda

P05-087 **SYNCHROTRON POWDER DIFFRACTION STUDY ON GAMMAAl2O3**
Seiichi Matsuda, Takashi Ida, Kazuhiro Asai and Hisashi Hibino

P05-088 **STRUCTURE DETERMINATION OF HYBRID STRUCTURES FOUND IN $BaTiO_3$ CRYSTAL**
Y. Yoshimura, K. Sone, H. Sumiyoshi, T. Kondo, A. Kojima, K. Tozaki

P05-089 **DIFFRACTION AND XAFS STUDY OF AgI UNDER HIGH PRESSURE AND HIGH TEMPERATURE**
Akira Yoshiasa, Hiroshi Arima, Hiroshi Fukui, Osamu Ohtaka, Maki Okube, and Yoshinori Katayama

P05-090 **CAGE SUBSTRUCTURES AND SITE OCCUPANCIES IN CLATHRATE COMPOUNDS,$La_3Pd_{20}T_6$ (T = Si And Ge)**
Y. Matsushita, A. Satoa, H. Kobayashi, A. Dönni, H. Kitazawa, F. Izumi, Y. Nemoto, T. Goto, M. Kaneko, S. Sasaki, and N. Kishimoto

P05-091 **MODULATED STRUCTURES IN THE $AMOB_2O_5$ FAMILY FROM VARIABLE TEMPERATURE X-RAY POWDER DIFFRACTION DATA**
Siegbert Schmid

P05-092 **RXMS STUDY ON A MAGNETIC HELIX OF BaTiCoFe10O19**
Maki Okube, Seiji Ohsawa, Takeshi Toyoda, Takeharu Mori, Satoshi Sasaki

P05-093 **SODIUM ARRANGEMENT IN NAXMO2 P2 STRUCTURE AS A FUNCTION OF TEMPERATURE, TRANSITION METAL TYPE, AND SODIUM STOICHIOMETRY**
Angélique Jarry, Maxim Avdeev

P05-094 **UNUSUAL SITE PREFERENCE OF BORON IN SYNTHETIC MgAl2-xBxO4 SPINEL (x = 0.11 and 0.13) UNDER HIGH PRESSURE**
Shunsuke Sakai,Akira Yoshiasa, Takafumi Hashimoto, Akihiko Nakatsuka, Kazumasa Sugiyama, Maki Okube, and Eiji Ito

P05-095 **PHOTOISOMERIZATION OF RUTHENIUM DIMETHYL SULFOXIDE COMPLEXES AND THEIR CRYSTAL STRUCTURES**
Yuji Karakane, Hidehiro Uekusa

P05-096 **CRYSTALLOGRAPHIC STUDY ON DEHYDRATION BEHAVIOR OF CHABAZITE**
Akihiko Nakatsuka, Hironao Okada, Keiko Fujiwara, Noriaki Nakayama and Tadato Mizota

P05-097 **TEMPERATURE DEPENDENCE OF CRYSTAL STRUCTURE OF PYROPE GARNET**
Mami Shimokawa, Akihiko Nakatsuka, Makio Ohkawa and Noriaki Nakayama

P05-098 **EVOLUTION OF CORUNDUM STRUCTURE AT HIGH TEMPERATURES**
S. Kondo, K. Tateishi, H. Hibino and N. Ishizawa

P05-099 **PHASE TRANSITION OF Gd_3RuO_7**
K. Okada, S. Kondo, T. Suwa and N. Ishizawa

P05-100 **ANOMALOUS STRUCTURAL PHASE TRANSITION ABOVE LIQUID NITROGEN TEMPERATURE IN THE MULTIFERROIC PEROVSKITE Dy(Mn0.5Fe0.5)O3**
Fu-Kuo Chiang , Fei-Ting Huang, and Ming-Wen Chu

P05-101 **SYNTHESIS AND STRUCTURE OF FERROMAGNETIC RUTILE**
Takashi Mochiku, Kazuhiro Yamaki, Natsumi Shimizu, Akinori Hoshikawa, Hiroki Fujii, Katsura Yamada, Shinji Itoh, Itsuhiro Kakeya, Kazuo Kadowaki and Kazuto Hirata

P05-102 **TEMPERATURE AND PRESSURE INDUCED TRANSITIONS OF PEROVSKITES ABX3 TO OTHER STRUCTURE TYPES**
Maxim Avdeev, Sergey Yakovlev

P05-103 **SYNTHESIS AND CHARACTERIZATION OF SERIES HETERMETALLIC COORDINATION POLYMER MaxMb1-x(tda)H2O (Ma, Mb=Zn, Co AND Ni, 0<x<1)**
Ming-Cheng Wu and Chi-Shen Lee

P05-104 **SYNTHESIS AND CHARACTERIZATION OF NEW QUATERNARY SELENIDE In1.91Pb4Bi4.09Se13**
Ming-Fang Wang and Chi-Shen Lee

P05-105 **MAGNETIC PROPERTIES OF DINUCLEAR ONE-DIMENSIONAL COMPLEXES WITH TRIAZOLE BASED LIGANDS**
S. M. Chen, C. F. Sheu, Y. S. Wen, and Y. Wang

P05-106 **INVESTIGATION OF THE ELECTRONIC STRUCTURE OF LANTHANIDE ZIRCONATES**
Richard Clements, Brendan Kennedy, Chris Ling, Anton Stampfl

P05-107 **STRUCTURAL PHASE TRANSITION ACCOMPANIED BY METAL-INSULATOR TRANSITION IN HOLLANDITE VANADATE**
Masahiko Isobe, Shigenori Koishi and Yutaka Ueda

P05-108 **PSEUDO-MEROHEDRAL TWINNING : HOW TO TREAT A SIX-FOLD TWIN**
Martin Adam, Anita Coetzee, Leo Straver and Rob Hooft

P05-109 **THE CRYSTAL STRUCTURE OF GUEST-REMOVED MELANOPHLOGITE**
Akihiro Ida, Kuniaki Kihara and Shuhei Fujinami

P05-110 **Structure REFINEMENT OF THE SAMPLE OBTAINED BY NASA'S STARDUST MISSION**
Kazumasa Ohsumi, Kenji Hagiya, Takashi Mikouchi and Michael Zolensky

P05-111 **CRYSTAL STRUCTURE AND PHOTO-EXCITATION ENERGY MIGRATION IN CRYSTALS OF DOUBLE-COMPLEX SALTS M[Ru(bpy)3][CrxAl1-x(ox)3] (M+ = Na+, Li+; 0≦x≦1)**
Satoshi Ishii, Tomoko Nakaguchi, Takuhiro Otsuka and Youkoh Kaizu

P05-112 **STRUCTURE AND MAGNETIC PROPERTY OF CYANIDE BRIDGE MOLECULAR SQUARE AND MOLECULAR SQUARE CHAIN**
Chin-Lin Yang, Yu Wang

P05-113 **LIGHT AND THERMAL INDUCED META-STABLE STATE STRUCTURE OF SPIN CROSSOVER COMPOUND {Fe(abpt)2[N(CN)2]2}**
C. F. Sheu, S. Pillet, S. M. Chen, Y. C. Lin, I. J. Hsu, G. H. Lee, Y. H. Liu, C. Lecomte, Y. Wang

P05-114 **STRUCTURAL STUDIES OF BIOLOGICALLY IMPORTANT HETEROCYCLIC COMPOUNDS**
Periyasamy Murugan, Munusamy Thirumavalavan, Tian-Huey Lu, Kuo Chu Hwang

P05-115 **HYDROGEN BONDING INTERACTIONS AND SHEET-LIKE STRUCTURES IN NICOTINAMIDE COMPLEXES**
S. Athimoolam and S. Natarajan

P05-116 **PYRIDOXINIUM NITRATE AND TRICHLOROACETATE**
S. Athimoolam and S. Natarajan

P05-117 **SYNTHESIS, GROWTH AND CHARACTERIZATION OF NEW ORGANIC NONLINEAR OPTICAL CHALCONE DERIVATIVES SINGLE CRYSTALS**
P. S. Patil , S. M. Dharmaprakash , G. Bhagavannarayana and Hoong-Kun Fun

P05-118 **CRYSTAL STRUCTURES OF MONO- AND DI-SUBSTITUTED FERROCENE DERIVATIVES**
Naotake Nakamura, Kazuya Hiro and Takeshi Takamatsu

P05-119 **SUPRAMOLECULAR HYDROGEN-BONDING NETWORKS IN ADENINIUM SALTS**
Balasubramanian Sridhar and Krishnan Ravikumar

P05-120 **CRYSTAL OF 6-[BIS(2-CHLOROETHYL)AMINO]-12-OXO-DIBENZO [d,g] [1,3,2]DIOXAPHOSPHOCIN 6-OXIDE**
Jadaprolu Radha Krishna, Musali Krishnaiah, Vedavati G. Puranik

P05-121 **CRYSTAL STRUCTURE OF 4-(4-CHLORO-PHENYL)-5-PHENYL ISOXAZOLE**
A.K.Balaji, J.Radha Krishna, M.Krishnaiah, Than Zaw Oo, Thetmar Win and Pho Kaung

P05-122 **MOLECULAR RECOGNITION OF 2-PHENOXYBUTANOIC ACID BY CHIRAL AROMATIC AMINES**
Ryoma Aoki, Yukio Takahashi and Isao Fujii

P05-123 **STRUCTURE DETERMINATION OF PENTACENE DERIVATIVE BY SYNCHROTRON POWDER DIFFRACTION DATA**
Hwo-Shuenn Sheu, Wei-Ju Shih, Wei-Tsung Chuang, and Yu-Tai Tao

P05-124 **PREPARATION, PROPETIES, AND STRUCTURAL STUDIES OF [MCl(diphosphine)]2 (M = Rh, Ir; diphosphine = BINAP)**
Tsuneaki Yamagata, Aika Iseki, Kazunori Hoshida, Hiromitsu Nagata, Kazuhide Tani, and Kazushi Mashima

P05-125 **HIGH RESOLUTION CRYSTAL STRUCTURE OF A BLUE COMMERININ PIGMENT**
Naohiro Matsugaki, Masaaki Shiono, and Kosaku Takeda

P05-126 **SOLID-STATE PHOTODIMERIZATION OF 6-METHYLCOUMARIN AND IT'S INCLUSION COMPLEXES, INVESTIGATED BY Ab INITIO POWDER CRYSTAL STRUCTURE ANALYSIS**
Kotaro Fujii, Hidehiro Uekusa, Shunsuke Tanigawa, Shinji Toyota, Fumio Toda

P05-127 **GUEST EXCHANGE MECHANISM OF ORGANIC INCLUSION CRYSTAL INVESTIGATED BY POWDER X-RAY DIFFRACTION ANALYSIS**
Yasunari Ashida, Hidehiro Uekusa, Natsuki Amanokura, and Masami Kaneko

P05-128 **HYDROGEN BONDING DYNAMICS OF THE STRUCTURE 4,5-DIMETHYL-N-(2-METHYL PHENYL)-2-{[(1E)-3,4,5-TRIMETHOXY PHENYLMETHYLENE] AMINO} THIOPHENE-3-CARBOXAMIDE**
Vasu,a K. A. Nirmala,b Deepak Chopra,c S. Mohand and J. Saravanan

P05-129 **THE PHICIAL PROPERTIES OF S DOPANT IN InP UNDER HIGH-PRESSURE BY ADX AND RAMAN METHDOS**
Yen-Ting Liu, Chih-Ming Lin and Hwo-Shuenn Sheu

P05-130 **DIMERIZATION IS IMPORTANT FOR THE GTPASE ACTIVITY OF CHLOROPLAST TRANSLOCON COMPONENTS ATTOC33 AND PSTOC159**
Yi-Hung Yeh, Muppuru M. Kesavulu, Hsou-min Li, Shu-Zon Wu, Yuh-Ju Sun, Emadeldin H. E. Konozy and Chwan-Deng Hsiao

P05-131 **EFFECTS OF TERMINAL SUBSTITUENTS AND SEED CRYSTALS ON THE MODE OF POLYMORPHIC TRANSITION INDUCING PREFERENTIAL ENRICHMENT**
Masahiro Horiguchi, Shinichiro Okuhara, Eiji Shimano, Daisuke Fujimoto, Hiroki Takahashi, Hirohito Tsue, and Rui Tamura

P05-132 **STRUCTURE-ASSISTED DISCOVERY OF HELICOBACTER PYLORI SHIKIMATE KINASE (HPSK) INHIBITORS**
Wen-Chi Cheng, Yen-Fu Chen, Jinn-Moon Yang and Wen-Ching Wang

P05-133 **AB INITIO STRUCTURAL DEFERMINATION OF PHARMACEUTICAL COCRYSTAL FROM POWDER X-RAY DIFFRACTION DATA**
Chihiro Itoga, Kotaro Fujii, Hidehiro Uekusa, Noriyuki Takata, Koji Shiraki

P05-134 **PROBING INTER MOLECULAR INTERACTIONS IN FUNCTIONALISED THIOPHENES**
K.A.Nirmala, Vasu

P05-135 **MOLECULAR RECOGNITION OF SYNEPHRINE BY CHIRAL ORGANIC ACIDS**
Taira Kimino, Yukio Takahashi, and Isao Fujii

P05-136 **CRYSTAL STRUCTURE OF 2-PHENYL-2,3-DIHYDRO-4H-CHROMEN-4-ONE**
Nongnaphat Khosavithitkul, Kenneth J. Haller

P05-137 **CRYSTAL STRUCTURE OF 'N-(4-METHOXYPHENYL)-2-{[(1E)-(4-METHYLPHENYL) METHYLENE]AMINO}-4,5,6,7-TETRAHYDRO-THIENO[2,3-C]PYRIDINE-3-CARBOXAMIDE'**
G. N. Anilkumar, M. K. Kokila , Puttaraja, S. Mohan and J. Saravanan

P05-138 **CRYSTAL STRUCTURE OF 'N-(4-METHOXYPHENYL)-2-{[(1E)-(4-METHYLPHENYL) METHYLENE]AMINO}-4,5,6,7-TETRAHYDRO-THIENO[2,3-C]PYRIDINE-3-CARBOXAMIDE'**
G. N. Anilkumar , M. K. Kokila, Puttaraja , S. Mohan and J. Saravanan

P05-139 **CRYSTAL CHEMISTRY OF CYCLODEXTRINS AND THEIR INCLUSION COMPOUNDS WITH BIOLOGICALLY-ACTIVE GUESTS**
Mino R Caira

P05-140 **CRYSTAL STRUCTURE OF '2-AMINO-N-(2-METHOXYPHENYL)-5,6,7,8-TETRAHYDRO-4H-CYCLOHEPTA[B]THIOPHENE-3-CARBOXAMIDE'**
K. Chandra Kumar , M. K. Kokila, Puttaraja, S. Mohan and J. Saravanan

P05-141 **HIGH RESOLUTION, HIGH THROUGHPUT X-RAY POWDER DIFFRACTION EXPERIMENTS AND DATA ANALYSIS**
A. Stefanovic, D. Beckers, T. Degen, S. Prugovečki

P05-169 **RNA DEGRADATION BY ESCHERICHIA COLI POLYNUCLEOTIDE PHOSPHORYLASE**
Zhonghao Shi, Wei-Jen Yang, Kin-Fu Chak and Hanna S. Yuan

P05-170 **UNDERSTANDING OF D-STAGGER IN COLLAGEN FIBERS BASED ON THE 7/2-HELICAL STRUCTURE AND AMINO ACID SEQUENCE**
Koichi Masakiyo, Tatsuya Kawaguchi and Kenji Okuyama

P05-171 **X-RAY CRYSTAL STRUCTURE ANALYSIS OF HEMOGLOBIN FROM DOMESTIC PIGEON (COLUMBA LIVIA) AT 1.44Å RESOLUTION**
P.Charles, K.Neelagandan, S.Sundaresan, Jürgen J. Müller ,Udo Heinemann and M.N.Ponnuswamy

P05-172 **SMALL-ANGLE X-RAY SCATTERING EXPERIMENTS TO DETERMINE THE STRUCTURAL TRANSITIONS IN THE INSULIN RECEPTOR ECTODOMAIN UPON INSULIN BINDING**
Andrew E. Whitten, Jill Trewhella, Colin W. Ward and Michael C. Lawrence

P05-173 **CRYSTAL STRUCTURE OF THE HUMAN FOXO3A-DBD/DNA COMPLEX SUGGESTS THE EFFECTS OF POST-TRANSLATIONAL MODIFICATION**
Kuang-Lei Tsai, Yuh-Ju Sun, Cheng-Yang Huang, Jer-Yen Yang, Mien-Chie Hung and Chwan-Deng Hsiao

P05-174 **CRYSTAL STRUCTURE OF HUMAN TUDOR-SN AND IMPLICATION OF ITS ROLES IN RNA INTERFERENCE**
Chia-Lung Li and Hanna S. Yuan

P05-175 **CRYSTAL STRUCTURE OF DNAC REPLICATIVE DNA HELICASE REVEALS THE MECHANISM OF HEXAMERIZATION AND POSSIBLE PROTEIN-PROTEIN INTERACTIONS NETWORK**
Cheng-Yang Huang, Kuang-Lei Tsai, Wei-Ti Chen, Chwan-Deng Hsiao

P05-176 **PYROCOCCUS HORIKOSHII ARGINYL-TRNA SYNTHETASE LACKING ADDITIONAL N-TERMINAL DOMAIN WITH AMINOACYLATION ACTIVITY**
Emiko Uchikawa, Shun-ichi Sekine, Shigeyuki Yokoyama, and Michiko Konno

P05-177 **CRYSTAL STRUCTURE OF 5-METHYLTHIORIBOSE 1-PHOSPHATE ISOMERASE PRODUCT COMPLEX FROM BACILLUS SUBTILIS: IMPLICATIONS FOR CATALYTIC MECHANISM**
Haruka Tamura, Yohtaro Saito, Hiroki Ashida, Tsuyoshi Inoue, Yasushi Kai, Akiho Yokota, and Hiroyoshi Matsumura

P05-178 **STRUCTURAL DIFFERENCE BETWEEN RICE AND RED ALGA RUBISCO COMPLEXED WITH SULFATE**
Yasuhiro Komura, Hiroyoshi Matsumura, Hiroyuki Ishida, Hiroki Ashida, Eiichi Mizohata, Tsuyoshi Inoue, Amane Makino, Tadahiko Mae, Akiho Yokota, Yasushi Kai

P05-179 **CRYSTAL STRUCTURE OF IcaR, A REPRESSOR OF THE TetR FAMILY IMPLICATED IN BIOFILM FORMATION IN STAPHYLOCOCCUS EPIDERMIDIS**
Wen-Yih Jeng, Tzu-Ping Ko, Rey-Ting Guo, Chien-Liang Liu, Chia-I Liu, Hui-Lin Shr and Andrew H.-J. Wang

P05-180 **STRUCTURAL BASIS FOR THE DISTINCTIVE SUBCHLOROPLAST LOCATION OF THREE MAIZE LEAF FERREDOXIN:NADPH OXIDOREDUCTASES**
N. Muraki, G. T. Hanke, T. Shiba, T. Hase, and G. Kurisu

P05-181 **PREPARATION, CRYSTALLIZATION AND PRELIMINARY CRYSTALLOGRAPHIC ANALYSIS OF OLD YELLOW ENZYME FROM TRYPANOSOMA CRUZ**
Naoki Okamoto, Shigeru Sugiyama, Keiji Tokuoka, Nahoko Uchiyama, Yousuke Okano, Hiroyoshi Matsumura, Yasushi Kai, Koji Inaka, Yoshihiro Urade and Tsuyoshi Inoue

P05-182 **CRYSTALLIZATION AND PRELIMINARY X-RAY ANALYSIS OF THE CERAMIDASE FROM PSEUDOMONAS AERUGINOSA**
Hiroyuki Okano,Koji Kambayashi, Nozomu Okino, Hatsumi Monjusyo, Yoshimitsu Kakuta Makoto Ito and Tsuyoshi Inoue

P05-183 **WHY DO NITRILASES NEED TO FORM HELICES TO BE ACTIVE?**
Trevor Sewell, Serah Kimani and Muhammed Sayed

P05-184 **THE PRESENT STATUS OF ACCURATE STRUCTURE REFINEMENTS FOR MACRO MOLECULES BY THE MAXIMUM ENTROPY METHOD**
Makoto Sakata, Eiji Nishibori, , TakahiroNakamura, Masanori Arimoto, Shinobu Aoyagi, Hideo Ago, Masashi Miyano and Toshikazu Ebiszaki

P05-185 **CRYSTALLIZATION OF THE COLD-ADAPTED ARABINANASE FROM PENICILLIUM CRYSOGENUM**
Kyoko Ikoma, Yuri Sogabe, Asako Yamaguchi, Tetsuko Nakaniwa, Takayoshi Kinoshita, Tatsuji Sakamoto, Hideshi Ihara and Toshiji Tada

P05-186 **RIETVELD ANALYSIS SOFTWARE FOR J-PARC**
Ryoko Oishi, Masao Yonemura, Shuki Torii, Akinori Hoshikawa, Toru Ishigaki, Yuichiro Nishimaki, Takahiro Morishima and Takashi Kamiyama

P05-187 **VISUALISING AND QUANTIFYING INTERMOLECULAR INTERACTIONS WITH HIRSHFELD SURFACES AND CRYSTALEXPLORER**
Joshua J. McKinnon, Mark A. Spackman, and Dylan Jayatilaka

P05-188 **THE EFFECT OF AMINO ACIDS AND AMINO ACID DERIVATIVES ON PROTEIN CRYSTALLIZATION**
L. Ito, T. Kobayashi, K. Shiraki, T. Narukawa, A. Oosuka and H. Yamaguchi

P05-189 **COMPUTATIONAL METHODOLOGY TO ANALYZE VARIOUS DEFECTS IN CUBIC CRYSTALS**
S. T. Nakagawa

P05-190 **DDLM: A NEW DICTIONARY LANGUAGE SUBMITTED TO COMCIFS FOR APPROVAL**

Nick Spadaccini, John Westbrook, and Syd Hall

P05-191 **MULTIPLE STRATEGIES IN HIGH-THROUGHPUT CLONING, EXPRESSION AND PRODUCTION OF RECOMBINANT PROTEINS FOR STRUCTURAL PROTEOMICS**

Hao Xu, Jin-Yi Zhu, Mervin Zhao, Quentin Florence, James Tucker Swindell II, Bret Dillard, Dayong Zhou, Angela Yang, John Rose, and Bi-Cheng Wang

November 06, Tuesday

P06-004 **PERFORMANCE OF THE HIGH-THROUGHPUT PROTEIN CRYSTALLOGRAPHY BEAMLINE BL13B1 AT THE NSRRC**
Chun-Hsiung Chao, Yuch-Chen Jean, Yu-Shan Huang, Chien-Chang Tseng, Cheng-Hung Chiang, Chun-Jung Chen, Shih-Chun Chung, Ching-Shiang Hwang, King-Long Tsang and Chien-Te Chen

P06-005 **STANDARD OPERATION SYSTEM FOR STRUCTURAL BIOLOGY BEAMLINES AT SPRING-8**
Go Ueno, Kazuya Hasegawa, Nobuo Okazaki, Kunio Hirata, Takashi Kumasaka and Masaki Yamamoto

P06-006 **HOMELABS VS. SYNCHROTRONS: THE FACTS WILL SURPRISE YOU**
Joseph D. Ferrara, Cheng Yang

P06-007 **NEXT GENERATION X-RAY DETECTOR FOR IN-HOUSE XRD SYSTEM**
Takeyoshi Taguchi, Christian Broennimann and Eric F. Eikenberry

P06-008 **STRUCTURAL BIOLOGY BEAMLINES AT SPring-8**
Masaki Yamamoto, Go Ueno, Takaaki Hikima, Atsushi Nisawa, Kunio Hirata, Tetsuya Shimizu, Nobutaka Shimizu, Masahide Kawamoto, Kazuya Hasegawa, Hisanobu Sakai, Seiki Baba, Nobuo Okazaki, Aik Hong Teh, Takashi Kumasaka

P06-009 **STATISTICAL PROPERTIES OF X-RAY INTENSITY MEASURED WITH A COUNTING SYSTEM WITH FINITE DEAD-TIME**
Takashi Ida, Akihisa Oya, Hisashi Hibino

P06-010 **MAIL-IN DATA COLLECTION AT SPRING-8 STRUCTURAL BIOLOGY BEAMLINES**
Seiki Baba, Kazuya Hasegawa, Go Ueno, Nobuo Okazaki, Hisanobu Sakai, Hironori Murakami, Takashi Kumasaka and Masaki Yamamoto

P06-011 **HIGH THROUGHPUT PROTEIN CRYSTAL EXCHANGE ROBOTS OF THE PHOTON FACTORY BEAMLINES**
Masahiko Hiraki, Shokei Watanabe, Nobuo pHonda, Yusuke Yamada, Naohiro Matsugaki, Noriyuki Igarashi, Yurii Gaponov and Soichi Wakatsuki

P06-012 **UPGRADE OF THE STRUCTURAL BIOLOGY BEAMLINES AT THE PHOTON FACTORY**
Noriyuki Igarashi, Naohiro Matsugaki, Yusuke Yamada, Masahiko Hiraki and Soichi Wakatsuki

P06-013 **THE SIDE LINE OF TAIWAN CONTRACT BEAMLINE BL12XU AT SPRING-8 FOR HIGH ENERGY PHOTOEMISSION**
Chi-Yi Huang, Ku-Ding Tsuei, Yong Q. Cai, Cheng-Chi Chen, Yen-Fang Song and Shih-Chun Chung

P06-041 **RATIOS OF ELASTIC CONSTANTS OF CDTE DERIVED FROM X-RAY THERMAL DIFFUSE SCATTERING UNDER HIGH PRESSURE**
Daisuke Ohtsu, Maki Okube, Takahiro Kuribayashi, Yasuhiro Kudoh, Taiki Nakanishi, Hiroyuki Katsuragawa, Akiko Nakao, and Satoshi Sasaki

P06-042 **SITE OCCUPANCY AND MAGNETIC STRUCTURE OF BATIMNFE10O19 HEXAFERRITE**
Taiki Nakanishi, Maki Okube, Hiroyuki Katsuragawa, Daisuke Ohtsu, Takeshi Toyoda, Akiko Nakao, and Satoshi Sasaki

P06-043 **VALENCE AND SPIN STATE OF Co IONS IN $La_{1-x}Ca_xCoO_3$**
Hiroyuki Katsuragawa, Maki Okube, Takayasu Hanashima, Taiki Nakanishi, Daisuke Ohtsu, and Satoshi Sasaki

P06-044 **MIXED-VALENCE STATES OF TRANSITION-METAL ATOMS IN A SOLID SOLUTION BETWEEN Fe3O4 AND Co3O4**
Yoshihiro Yamamoto, Norio Shimizu, Maki Okube, Atsuko Ohno and Satoshi Sasaki

P06-045 **X-RAY SCATTERING STUDY OF YTTRIUM-DOPED HfO2 THIN FILMS**
C.-H. Hsu, Z. K. Yang, K. L. Yu, M.-T. Tang, M. L. Huang, W. C. Lee, Y. J. Lee, P. Chang, M. Hong, and J. Kwo

P06-046 **STUDIES ON FERROMAGNETIC CARBONS**
Prabal Dasgupta

P06-047 **CRYSTAL STRUCTURE AND MAGNETIC PROPERTIES OF NaFe(WO4)2 AND NaCr(WO4)2**
D.Sangaa, L.Nyam-Ochir, H.Ehrenberg, D.Mikhailova, H.Fuess

P06-048 **THE METHOD OF DETERMINATION OF STRUCTURAL IN STRETCHED POLYMERS**
Aida Martirosyan

P06-049 **CRYSTAL ENGENEERING OF NEW 4,4'-BIPYRIDINES AND RELATED COMPOUNDS**
Olexii V. Gutov, Eduard B. Rusanov, Alexander N. Chernega, Mark I. Povolotskii

P06-050 **COCRYSTALS OF OXALIC ACID WITH DERIVATIVES OF TRICYCLIC QUINAZOLONE-4**
Akmal Tojiboev, Kambarali Turgunov, Bahodir Tashkhodjaev

P06-051 **CRYSTAL STRUCTURES OF TWO ALIPHATIC AMIDASES AMIE AND AMIF FROM HELICOBACTER PYLORI REVEAL A CONSERVED CATALYTIC TRIAD**
Wen-Ching Wang, Chiu-Lien Hung, Cheng-Yu Chen, and Yu-Wen Hua

P06-052 **POLYTYPE TRANSFORMATION DURING NITROGEN DOPING OF SiC CRYSTALS**
Jinli Chen and Zhe Chuan Feng

P06-053 **FoRMATION OF LARGE LANTHANIDE CLUSTER HAVING CHIRAL LIGANDS AND THEIR MOLECULAR ASSEMBLY IN THE CRYSTALLINE STATE**
Chizuko Kabuto , Kenji Omata , Kuninobu Kabuto , and Yoichi Sasaki

P06-054 **HOST FRAMEWORK OF INCLUSION CRYSTAL OF 1,1,2,2-TETRAKIS(4-CARBOXYPHENYL) ETHANE**
Michiko Iriyama, Natsumi Sakuma, Hidehiro Uekusa, Natsuki Amanokura, Masami Kaneko

P06-055 **CRYSTAL STRUCTURE ANALYSIS OF 1,1,2,2-TETRAKIS(3-METHYL-4-HYDROXYPHENYL)ETHANE INCLUSION CRYSTALS**
Kazuyuki Toyota, Hidehiro Uekusa, Natuki Amanokura, and Masami Kaneko

P06-056 **STRUCTURAL DIVERSITY OF [M(SCN)2] FRAGMENTS WITH N,N'-BISPYRIDINE-TYPE LIGANDS, 4-BPD (4-BPD = 1,4-BIS(4-PYRIDYL)-2,3-DIAZA-1,3-BUTADIENE)**
Chih-Chieh Wang, Wei-Zeng Lin, Yu-Ruei Guo, Wei-Ting Huang, Shuen-Jie Dai, Mei-Ju Ke, Gene-Hsiang Lee

P06-057 **STRUCTURAL DIVERSITY OF [M(SCN)2] FRAGMENTS WITH BPHD (BPHD = 2,5-Bis(4-pyridyl)-3,4-diaza-2,4-hexadiene)**
Chih-Chieh Wang, Yi-Tzu Lin, Yu-Hsuan Lee, Gene-Hsiang Lee

P06-058 **CRYSTAL STRUCTURE AND VIBRATIONAL SPECTRA OF m-OXO-BIS[TETRA(p-METHOXYPHENYL)PORPHYRINATOIRON(III)]**
Ratchadaporn Puntharod, Bayden Wood, Don McNaughton, and Kenneth J. Haller

P06-059 **[H2en]2+ CATION DISORDER IN A NETWORK OF VANADIUM POLYBORATE CLUSTERS**
Aungkana Chatkon, Kenneth J. Haller, and Ian D. Williams

P06-060 **A THREE-DIMENSIONAL SUPRAMOLECULAR STRUCTURE OF ZINC VANADATE: Zn(2-EtIm)2(VO3)2**
Orrasa In-noi, Samroeng Krachodnok, Kenneth J. Haller, Herman H.-Y. Sung, Fanny L.-Y. Shek and Ian D. Williams

P06-061 **LAYERED AND NETWORK STRUCTURES OF HYBRID ZINC VANADATES CONTAINING BRIDGING AZOLE LIGANDS**
Samroeng Krachodnok, Kenneth J. Haller, Herman H-Y. Sung, Fanny L-Y. Shek and Ian D. Williams

P06-062 **OPEN COPPER TARTRATE BIPYRIDINE 3D FRAMEWORKS WITH VARYING WALL CHIRALITIES**
Pokka K-C. Pang, Herman H-Y. Sung and Ian D. Williams

P06-063 **FLUX SYNTHESIS OF NEW TARTRATOBORATE POLYMERS AND CYCLIC OLIGOMERS**
Alex S-F. Au-Yeung, Herman H-Y. Sung and Ian D. Williams

P06-064 **CRYSTAL STRUCTURE OF COMPLEX BIMETALLIC SALTS OF NICKEL(II): [Ni(ter)2(H2O)4][Ni(4-CNpy)2(H2O)4].H2O AND [Ni(H2O)6] [Ni(ter)(4-CNpy)(H2O)4].(ter)**
Sanchay J. Bora and Birinchi K. Das

P06-065 **A NOVEL 3D INTERPENETRATING FRAMEWORK CONTAINING 1D LADDERS COORDINATION POLYMERS WITH MIXED ORGANIC LIGANDS: [Ni2(H2O)2(BDC)2(bpp)2]**
Chia-Her Lin and Tai-Hsing Tsao

P06-066 **HYDROTHERMAL SYNTHESIS OF METAL HYDROXIDE IMIDAZOLIDE 3D FRAMEWORK POLYMERS**
Fion T-Y. Yeong, Fanny L-Y. Shek, Herman H-Y. Sung and Ian D. Williams

P06-067 **dSNAP: NEW SOFTWARE FOR ANALYSING THE RESULTS OF CAMBRIDGE DATA BASE SEARCHES**
Chris Gilmore, Gordon Barr, Wei Dong, Andrew Parkin, Duncan Sneddon, Chick Wilson

P06-068 **AN OBSERVATION ON THE WETTING PHENOMENON OF GALLIUM NANO DROPLETS BY X-RAY DIFFRACTION**
Masanori Tanaka, Takehiro Noda, Osami Sakata, Hikaru Terauchi, and Isao Takahashi

P06-069 **BEAM COMPRESSION AND LATTICE-CONSTANT VARIATIONS IN CURVED X-RAY CAVITY**
S.-Y. Chen, Y.-Y. Chang, Y.-J. Liu, M.-T. Tang, Yu. P. Stetsko, H.-H. Wu, Y.-R. Lee, M. Yabashi, B.-Y. Shew, and S.-L. Chang

P06-070 **DETERMINATION OF LATTICE PARAMETERS OF FeSi2/Si QUANTUM DOT NANO-STRUCTURES BY X-RAY BRAGG-SURFACE DIFFRACTION**
Yi-Wei Tsai, Chia-Hung Chu , Wen-Ching Sun, and Shih-Lin Chang

P06-071 **CRYSTALLINE LAMELLAE IN THIN FILM OF BIODEGRADABLE POLYMER POLY(HYDROXYBUTYRATE) STUDIED BY SURFACE X-RAY DIFFRACTION**
Shota Mukoyama, Kazuhiro Yamasaki, Hikaru Terauchi, Harumi Sato, Yukihiro Ozaki, Isao Noda, and Isao Takahashi

P06-072 **CORE-SHELL COMPOSITION AND ITS INFLUENCES ON THE PROPERTIES OF MATERIALS**
Vo Vong , Luu Tien Hung and Michael Hietschold

P06-073 **GLASS TRANSITION TEMPERATURE OF ULTRATHIN POLYMER UNDER ULTRASLOW HEATING: AN X-RAY REFLECTIVITY STUDY ON POLYSTYRENE FILMS SUPPORTED ON Si**
Chun-Ming Yang, Hikaru Terauchi, and Isao Takahashi

P06-074 **CRYSTAL STRUCTURE OF β-LACTOGLOBULIN AND VITAMIN D COMPLEX. IDENTIFICATION OF A SECOND BINDING SITE FOR VITAMIN D: A THERMAL INDEPENDENT SITE.**
Hong -Hsiang Guan, Ming -Chi Yang, Ming -Yih Liu, Jinn -Moon Yang,Wen -Liang Chen, Simon JT Mao and Chun- Jung Chen

P06-075 **NANOSTRUCTURED FILMS CONSTITUTED OF TiO2 AND SnO2 PREPARED BY MEANS OF SPRAY PYROLYSIS**
Pham-Van Nho, Pham-Hoang Ngan, Tran-Kim Cuong

P06-076 **STRUCTURAL STUDY OF ARSENATE INCORPORATION INTO CALCIUM PHOSPHATE HYDROXYAPATITE**
Winya Dungkaew, Weenawan Somphon, Kenneth J. Haller

P06-077 **STRUCTURAL STUDY OF COPPER INCORPORATION INTO CALCIUM PHOSPHATE HYDROXYAPATITE**
Oratai Saisa-ard, Winya Dungkaew, Weenawan Somphon and Kenneth J. Haller

P06-078 **CHROMIUM AND CADMIUM IMMOBILIZATION BY PORTLAND CEMENT SOLIDIFICATION**
Weenawan Somphon, Samroeng Krachodnok, Angkana Kiatpichitpong

P06-079 **NANOCRYSTALLINE COPPER SULPHIDE: SYNTHESIS AND ITS CHARACTERIZATION**
N.Vasumathi, B.B.Nayak and B.S.Acharya

P06-080 **X-RAY DIFFRACTION STUDY ON THERMAL BEHAVIORS OF SHAPE MEMORY ALLOY $Au_{50.5}Cd_{49.5}$**
Michinori Yoshikawa, Genki Kikuma, Takuya Ohba, Hikaru Terauchi, and Isao Takahashi

P06-081 **OBSERVATION ON TRANSITIONs in SURfACE REGION OF COCOA BUTTER BY X-RAY DIFFRACTION**
Yusuke-Hayashi, Yoshihito-Uozaki, Hikaru-Terauchi, and Isao-Takahashi

P06-082 **COMPARATIVE STUDY ON THE I-V CHARACTERISICS OF METAL STRING COMPLEXES EXPERIMENT VS THEORY**
Liang-Yan Hsu, Bih-Yaw Jin, Chun-Hsien Chen. Shie-Ming Peng

P06-142 **CRYSTAL STRUCTURES OF THE CYTOSOLIC DOMAIN OF THE Mg2+ TRANSPORTER MgtE**

Yoshiki Tanaka , Motoyuki Hattori , Shuya Fukai , Ryuichiro Ishitani and Osamu Nureki

P06-143 **CRYSTAL STRUCTURE OF THE MgtE Mg2+ TRANSPORTER**

Motoyuki Hattori, Yoshiki Tanaka, Shuya Fukai , Ryuichiro Ishitani and Osamu Nureki

P06-144 **STRUCTURAL BASIS OF PROSTACYCLIN BIOSYNTHESIS**

Yi-Ching Li, Chia-Wang Chiang, Hui-Chun Yeh, Frank G. Whitby, Lee-Ho Wang, and Nei-Li Chan

P06-145 **STRUCTURAL STUDIES OF THE HUMAN PROSTACYCLIN SYNTHASE**

Chia-Wang Chiang, Hui-Chun Yeh, Lee-Ho Wang, and Nei-Li Chan

P06-146 **HIGHLY AMPHIPHILIC INTERFACE IN THE COMPLEX FORMED BETWEEN DPPIV (CD26) AND ADENOSINE DEAMINASE**

Wolfram Saenger, Wilhelm A. Weihofen, Jiango Liu, Werner Reutter, Hua Fan

P06-147 **CRYSTAL STRUCTURE OF BOVINE LACTOPEROXIDASE AT 2.3 Å RESOLUTION**

Amit Kumar Singh, Nagendra Singh, Sujata Sharma, Mau Sinha, Punit Kaur, A. Srinivasan and T. P. Singh

P06-148 **CRYSTAL STRUCTURE OF CAMEL PEPTIDOGLYCAN RECOGNITION PROTEINS AT 3.0 Å RESOLUTION**

Pradeep Sharma, Nagendra Singh, Sujata Sharma and T.P.Singh

P06-149 **CRYSTAL STRUCTURE OF THE COMPLEX OF SHEEP SIGNALING GLYCOPROTEIN WITH 2-METHYL-2,4-PENTANEDIOL AT 1.65Å RESOLUTION**

Mau Sinha, Pradeep Sharma, Nagendra Singh, Sujata Sharma, Punit Kaur and Tej P. Singh

P06-150 **CRYSTAL STRUCTURES OF COMPLEXES OF C-LOBE OF BOVINE LACTOFERRIN WITH VARIOUS SACCHARIDES AT HIGH RESOLUTIONS REVEAL A COMMON BINDING SURFACE IN THE C-LOBE**

Rafia Mir, Mau Sinha, Nagendra Singh, Vikram Gopalakrishnapillai, Sujata Sharma, Punit Kaur and Tej.P.Singh

P06-151 **CRYSTAL STRUCTURE OF GOAT LACTOPEROXIDASE AT 2.4Å RESOLUTION**

Nagendra Singh, Amit Kumar Singh, Sujata Sharma, Asha Bhushan, Punit Kaur and Tej P. Singh

P06-152 **CRYSTAL STRUCTURE OF A COMPLEX OF PHOSPHOLIPASE A2 (PLA2) WITH A NEW GRAMINE DERIVATIVE AT 2.2 Å RESOLUTION**
Sanjit Kumar, Nagendra Singh, Sujata Sharma, Tej.Pal.Singh

P06-153 **CRYSTAL STRUCTURES OF THREE ACTIVE SITE MUTANTS OF BOVINE PANCREATIC PHOSPHOLIPASE A2**
Shankar Prasad Kanaujia and Kanagaraj Sekar

P06-154 **CRYSTAL STRUCTURE OF BOVINE C-LOBE WITH RIBOSE AT 2.5 Å RESOLUTION**
G. Vikram, R. Mir, M. Sinha, N.Singh, S. Sharma, P. Kaur and T.P. Singh

P06-155 **FRAGMENT-BASED INHIBITION OF PROTEINASE K: CRYSTAL STRUCTURE OF A COMPLEX OF PROTEINASE K WITH BORONIC ACID AT 0.83 Å RESOLUTION**
R. Jain, N. Singh, M. Perbandt, C. Betzel, S. Sharma, P. Kaur, A. Srinivasan, T.P. Singh\

P06-156 **CRYSTAL STRUCTURE OF BUFFALO LACTOPEROXIDASE AT 2.8Å RESOLUTION**
Ishfaq Ahmed Sheikh, Nagendra Singh, Sujata Sharma, Asha bhushan and T.P. Singh

P06-157 **CRYSTAL STRUCTURE OF MAMMARY SECRETORY GLYCOPROTEIN FROM BUFFALO AND ITS COMPLEXES WITH OLIGO-SACCHARIDES**
Punit Kaur, A.K. Singh, Rishi Jain, N. Singh, S, Sharma and T.P. Singh

P06-158 **X-RAY CRYSTAL STRUCTURE ANALYSIS OF ERK1/IODOTUBERCIDIN COMPLEX**
Ikuyo Yoshida, Takayoshi Kinoshita, Masaki Gouda, Mamoru Matsubara, Hiroshi Ishiguro, Toshiji Tada

P06-159 **CRYSTAL STRUCTURE OF HUMAN LYN KINASE DOMAIN**
Nao Miyano, Takayoshi Kinoshita, Koichi Yokota, Hiroshi Ishiguro and Toshiji Tada

P06-160 **PROTEOMIC ANALYSIS OF MANGANESE REGULATION OF NEISSERIA GONORRHOEAE**
Hsing-Ju Wu, Kuan-Tin Pan, He-Hsuan Hsiao, Chen-Wen Yao, Alastair G. McEwan, Michael P. Jennings and Andrew H-J. Wang

P06-161 **MOLECULAR BASIS FOR RECOGNITION OF A SELECTIVE NUCLEOSIDE INHIBITOR BY PLASMODIUM FALCIPARUM S-ADENOSYL-L-HOMOCYSTEINE HYDROLASE**
Yoshio Kusakabe, Nobutada Tanaka, Ken-ichi Aoki, Masayuki Nakanishi, Yukio Kitade,d and Kazuo T. Nakamura

P06-162 **CRYSTAL STRUCTURE OF MYCOBACTERIUM TUBERCULOSIS S-ADENOSYL-L-HOMOCYSTEINE HYDROLASE**

Nobutada Tanaka, Yoshio Kusakabe, Masayuki Nakanishi, Koichi Maruyama, Takayuki Ezaki,e Yukio Kitade,b,c,d and Kazuo T. Nakamura

P06-163 **ELUCIDATION OF A CATALYTIC-CRITICAL HYDROGEN BOND NETWORK IN THE ACTIVE SITE OF ANIMAL GLUTAMINYL CYCLASES SUGGESTS AN ESSENTIAL PROTON TRANSFER PROCESS DURING CATALYSIS**

Kai-Fa Huang, Yu-Ruei Wang, En-Cheng Chang, Tsung-Lin Chou, and Andrew H.-J. Wang

P06-164 **STRUCTURAL COMPARISON STUDIES FOR 2H PHOSPHOESTERASE SUPERFAMILY PROTEINS**

Yasumitsu Sakamoto, Nobutada Tanaka, Tomomi Ichimiya, Tadashi Kurihara, and Kazuo T. Nakamura

P06-165 **CRYSTAL STRUCTURE OF PARASPORIN-2, AN ANTI-TUMOR TOXIN FROM BACILLUS THURINGIENSIS**

Toshihiko Akiba,a Yuichi Abe,b Sakae Kitada,b Yoshitomo Kusaka,b Akio Ito,b Tokio Ichimatsu,c Hideki Katayama,c Tetsuyuki Akao,c Kazuhiko Higuchi,c Eiichi Mizuki,c Michio Ohba,d Ryuta Kanai a and Kazuaki Harata

P06-166 **CRYSTAL STRUCTURE OF THE HRDC DOMAIN OF HUMAN WERNER SYNDROME PROTEIN, WRN.**

Ken Kitano, Nozomi Yoshihara and Toshio Hakoshima

P06-167 **CRYSTAL STRUCTURE OF FUSOBACTERIUM ADHESIN A (FADA): IMPLICATIONS FOR ORAL DISEASES AND PRETERM BIRTH**

Stanley Nithianantham, Minghua Xu, Mitsunori Yamada, Hongqi Liu, Jonathan Ross, Mark Durham, Hameem Kawsar, Menachem Shoham and Yiping W. Han

P06-168 **STRUCTURE-BASED DESIGN OF INHIBITORS OF HUMAN MTH1 PROTEIN I**

Teruya Nakamura, Miyuki Inazato, Sinji Ikemizu, Yusaku Nakabeppu, and Yuriko Yamagata

P06-192 **CRYSTAL STRUCTURES OF D-AMINO ACID AMIDASE FROM OCHROBACTRUM ANTHROPI SV3 AND A-AMINO-E-CAPROLACTAM RACEMASE FROM ACHROMOBACTER OBAE**

Seiji Okazaki, Atsuo Suzuki, Tsunehiro Mizushima, Hidenobu Komeda, Yasuhisa Asano, Takashi Yamane

P06-193 **XC5848, AN ORFAN PROTEIN FROM XANTHOMONAS CAMPESTRIS, ADOPTS A NOVEL VARIANT OF SM-LIKE MOTIF**

Ko-Hsin Chin, Andrew H.-J. Wang, & Shan-Ho Chou

P06-194 **THE CRYSTAL STRUCTURE OF XC1258 FROM XANTHOMONAS CAMPESTRIS: A PUTATIVE PROCARYOTIC NIT PROTEIN WITH AN ARSENIC ADDUCT IN THE ACTIVE SITE**
Ko-Hsin Chin, Andrew H.-J. Wang, & Shan-Ho Chou

P06-195 **KINETIC AND STRUCTURAL PROPERTIES OF TRIOSEPHOSPHATE ISOMERASE FROM HELICOBACTER PYLORI**
Chen-Hsi Chu, Yi-Ju Lai, and Yuh-Ju Sun

P06-196 **CARBOHYDRATE-BINDING OF THE STARCH BINDING DOMAIN OF RHIZOPUS ORYZAE GLUCOAMYLASE IN COMPLEX WITH β-CYCLODEXTRIN AND MALTOHEPTAOSE**
Jung-Yu Tung , Yen-Yi Liu, Wei-I Chou, Fang-Yu Chang, Dah-Tsyr Chang and Yuh-Ju Sun

P06-197 **ATP-DRIVEN MOTIONS OF 70-KDA HEAT SHOCK PROTEINS (HSP70S): INSIGHTS INTO STRUCTURAL DYNAMICS OF THE HSP70 POWER STROKE**
Yi-Wei Chang, Chung Wang, and Chwan-Deng Hsiao

P06-198 **CRYSTAL STRUCTURE OF PHOSPHORIBOSYLPYROPHOSPHATE BOUND NICOTINATE PHOSPHORIBOSYLTRANSFERASE FROM PYROCOCCUS FURIOSUS**
KyuBeen Sohn, Yilan Fang, Rosalind Kim, Sung-Hou Kim and Dong Hae Shin

P06-199 **STABILIZATION OF COLLAGEN TRIPLE-HELIX BY ARG IN THE Y POSITION**
Tatsuya Morimoto, Mitsuru Haga, Chizuru Hongo, Keiichi Noguchi, Kenji Okuyama and Toshiki Tanaka

P06-200 **THE STRUCTURAL ANALYSIS OF THE COLLAGEN-MODEL PEPTIDE, (Pro-Pro-Gly)4-Hyp-Asp-Gly-(Pro-Pro-Gly)4 CRYSTAL**
Tatsuya Kawaguchi, Masaki Shimura, Chizuru Hongo, Keiichi Noguchi, Kenji Okuyama, Kazunori Mizuno and Hans Peter Bachinger

P06-201 **CRYSTAL STRUCTURE OF 3D8 scFv ANTI-DNA ANTIBODY, ITS SINGLE DOMAINS, AND THE COMPLEX WITH A SMALL MOLECULE**
Suk-Yeol Park, Young-Rim Kim, Yong-Sung Kim, Myung-Hee Kwon, Jeong-Sun Kim

P06-202 **CRYSTAL STRUCTURE OF YDJA FROM ESCHERICHIA COLI**
Ji-Woo Choi, Ji-Eun Lee, Che-Hun Jung, and Jeong-Sun Kim

P06-203 **CRYSTAL STRUCTURE OF ybfF FROM ESCHERICHIA COLI**
Nishi Kosuke, Suk-Youl Park, Sang-Hak Lee, Ji-Woo Choi, Nguyen To Uyen, Ji-Eun Lee, Che-Hun Jung, and Jeong-Sun Kim

P06-204 **STRUCTURE AND FUNCTIONAL STUDY OF RICE BIFUCTIONAL ALPHA-AMYLASE/SUBTILISIN INHIBITOR FROM Oryza sativa**
Wen-Yan Peng, Yi-Hung Lin, Yen-Chieh Huang, Hong-Hsiang Guan, Ying-Cheng Hsieh, Ming-Yih Liu,Tschining Chang, and Chun-Jung Chen

P06-205 **X-RAY 3D STRUCTURE AND FUNCTION STUDY OF RICE LECTIN-LIKE COMPLEX**
Chin-Wen Wu, Yen-Chieh Huang, Hong-Hsiang Guan, Yin-Cheng Hsieh, Chia-Hao Shin, Tschining Chang, Yi-Hung Lin and Chun-Jung Chen

P06-206 **COMPLEX STRUCTURE OF XYLANASE WITH XYLO-OLIGOSACCHARIDES FROM TRICHODERMA HARZIANUM ETS323 : STRUCTURAL EVIDENCE FOR GLYCOSYL TRANSFERASE REACTION**
En-Hung Liu, Kun-Che Chang, Yuan-Lung Chiang, Ying-Cheng Hsieh, Chaur-Tsuen Lo, Yi-Hung Lin,Yen-Chieh Huang, Hong-Hsiang Guan, Kuo-Cheng Peng, Chun-Jung Chen

P06-207 **CRYSTAL STRUCTURE AND FUNCTIONAL STUDY OF THE BOWMAN-BIRK INHIBITOR FROM RICE BRAN IN TERNARY COMPLEX WITH BOVINE TRYPSIN**
Hsin-Tai Li, Yi-Hung Lin, Yen-Chieh Huang, Ying-Cheng Hsieh, Hong-Hsiang Guan, Tschining Chang, Andrew H.-J. Wang and Chun-Jung Chen

P06-208 **CRYSTAL STRUCTURE STUDY OF WILD TYPE AND MUTATED BACILLUS CEREUS NCTU2 CHITINASE**
Yin-Cheng Hsieh, Chueh-Yuan Kuo , Huei-Ju Tasi , Yi-Hsin Pan , Yaw-Kuen Li , and Chun-Jung Chen

P06-209 **CRYSTALLOGRAPHIC STUDIES OF THE C-TERMINAL DOMAIN OF DNA GYRASE**
Tung-Ju Hsieh, Hsun-Tang Chang, Te-Sheng Lin, Shu-Yun Haung, Lynn Farh, and Nei-Li Chan

P06-210 **STRUCTURAL AND FUNCTIONAL STUDIES OF THE 6-PHOSPHOGLUCONATE DEHYDROGENASE ASSOCIATED WITH PATHOGENESIS OF KLEBSIELLA PNEUMONIAE**
Ying-Yin Chen , Tzu-Ping Ko, Li-ping Lo, Chun-Hung Lin, Andrew H-J Wang

P06-211 **CRYSTALLIZATION AND STRUCTURAL ELUCIDATION OF PLASMODIUM VIVAX DIHYDROFOLATE REDUCTASE-THYMIDYLATE SYNTHASE**
Puttapol Khongsuk, Ubolsree Leartsakulpanich, Yongyuth Yuthavong and Palangpon Kongsaeree

P06-212 **THE CRYSTAL STRUCTURE OF N-TERMINAL DOMAIN OF PLANTS NADPH OXIDASE**

Takashi Oda, Kokoro Hayashi, Chojiro Kojima, Hiroshi Hashimoto, Tsutomu Kawasaki, Ko Shimamoto, Mamoru Sato, and Toshiyuki Shimizu

P06-213 **HIGHER SIGNAL, LOWER NOISE: HOW TO GET THE BEST DATA FROM YOUR CRYSTALS**

Martin Adam, Anita Coetzee, Bram Schierbeek, Cary Bauer and Rob Hooft

P06-214 **CRYSTALLOGRAPHIC CHARACTERIZATION OF THE RADIXIN FERM DOMAIN BOUND TO CYTOPLASMIC TAIL OF ADHESION MOLECULE CD44**

Tomoyuki Mori, Ken Kitano, Shin-ichi Terawaki, Ryoko Maesaki and Toshio Hakoshima

P06-215 **CRYSTALLOGRAPHIC STUDIES OF A LECTIN FROM THE OCTOCORAL**

Akiko Kita, Mitsuru Jimbo, Yukio Morimoto, Ryuichi Sakai, Hisao Kamiya, and Kunio Miki

P06-216 **CRYSTALLIZATION AND STRUCTURAL ELUCIDATION OF PLASMODIUM VIVAX DIHYDROFOLATE REDUCTASE-THYMIDYLATE SYNTHASE**

Puttapol Khongsuk, Ubolsree Leartsakulpanich, Yongyuth Yuthavong and Palangpon Kongsaeree

P06-217 **NOVEL DNA-BINDING FOLD AND DNA-RECOGNITION MODE DISCOVERED IN PABI FAMILY OF RESTRICTION ENZYMES**

Ken-ichi Miyazono, Miki Watanabe, Jan Kosinski, Ken Ishikawa, Masayuki Kamo, Tatsuya Sawasaki, Koji Nagata, Janusz M. Bujnicki, Yaeta Endo, Ichizo Kobayashi, & Masaru Tanokura

P06-218 **SINGLE MUTATIONS LEAD TO SIGNIFICANT INCREASE IN SUBSTRATE SPECIFICITY AND ACTIVITY: STRUCTURAL, ENZYME KINETICS AND MOLECULAR MODELING STUDIES FOR CYSTEINE PROTEASE FROM A TROPICAL PLANT**

Raka Ghosh, Chandana Chakrabarti, Sampa Biswas and J.K. Dattagupta

P06-219 **SYNTHESIS AND CHARACTERIZATION OF CuMPt6 (M= 3D ELEMENTS) TERNARY ALLOYS**

Ejaz Ahmed , Miwako Takahashi , Hiroshi Iwasaki and Ken-ichi Ohshima

P06-220 **X-RAY STRUCTURE OF THE SKP1-FBS1 GLYCOPROTEIN COMPLEX**

Tsunehiro Mizushima, Yukiko Yoshida, Taichi Kumanomidou, Yuko Hasegawa, Atsuo Suzuki, Takashi Yamane and Keiji Tanaka

P06-221 **X-RAY MULTIPLE-WAVE DIFFRACTION ANOMALOUS FINE STRUCTURE**
S.-C. Weng, Y.-R. Lee, Yu. P. Stetsko, W.-H. Sun, Y.-L. Soo and S.-L. Chang

P06-222 **DYNAMICAL CALCULATION FOR TWENTY-FOUR BEAM X-RAY DIFFRACTION IN A TWO-PLATE CRYSTAL CAVITY OF SILICON**
M.-S. Chiu, Yu. P. Stetsko, and S.-L. Chang

P06-223 **STRUCTURAL FEATURES OF PSYCHROPHILIC MALATE DEHYDROGENASE ADAPTING TO THE EXTREME ENVIRONMENT**
Yasuo Hata, Tomomi Fujii, Tadao Oikawa and Kenji Soda

P06-224 **GROWTH RING OF TEETH- A MICRO X-RAY DIFFRACTION STUDY**
Hejing Wang, Jian Zhou, Nan Zheng and Tingjing Xu

P06-225 **STRUCTURES OF SOME CRYSTAL SOLVATES OF N-(3-ETHYLTHIO-1,2,4-THIADIAZOL-5-YL-AMINOCARBONYLMETHYL) CYTIZINE**
U.S.Mahmudov, T.F.Ibragimov, K.K.Turgunov, B.Tashkhodjaev.

P06-226 **STRUCTURAL EVIDENCE THAT AN a-PROTEOBACTERIA IS THE OLDEST SURVIVING SPECIES**
William L. Duax, Robert Huether, Qilong Mao, Vladimir Pletnev, Timothy Umland and Charles M. Weeks

P06-227 **STRUCTURAL STUDY FOR THE ENZYME MECHANISM OF EUKARYOTIC GLUTAMINE SYNTHETASE FROM ZEA MAYS**
Takeshi Ozaki, Hideaki Unno, Toshiharu Hase, Masami Kusunoki

P06-228 **CRYSTAL SOLVATES OF N-(3-METHYLTHIO-1,2,4-THIADIAZOL-5-YL-AMINOCARBONYLMETHYL)CYTISINE**
Kambarali Turgunov, Utkur Makhmudov, Temur Ibragimov, Bakhodir Tashkodjaev

P06-229 **SYNTHESIS OF NANOCRYSTALLINE (Co,Ni)Al2O4 SPINEL POWDER BY QUASICRYSTALLINE PRECURSOR**
T.P. Yadav, N.K. Mukhopadhyay, R.S. Tiwari and O.N. Srivastava

P06-230 **PROBING LOCAL STRUCTURES AROUND Co IN FERROMAGNETIC HfO2:Co THIN FILMS USING EXAFS**
Y. L. Soo, S. C. Weng, W. H. Sun, S. L. Chang, W. C. Lee, Y. S. Chang, J. Kwo, M. Hong J. M. Ablett, C-. C. Kao, D.G. Liu, and J. F. Lee

P06-231 **CRYO-CRYSTALLIZATION OF DIETHYL OXALATE AND STUDIES ON INTERMOLECULAR INTERACTION**
T. Vijay, S. J. Prathap and T. N. Guru Row

P06-232 **CRYO-CRYSTALLIZATION OF DIETHYL OXALATE AND STUDIES ON INTERMOLECULAR INTERACTION**

T. Vijay, S. J. Prathap and T. N. Guru Row

P06-233 **CRYSALISPro's ADVANCED STRATEGY MODULE FOR CHARGE DENSITY EXPERIMENTS**

Dr. Jiwen Cai

P06-234 **NON-CONVENTIONAL SCATTERING STUDIES OF MATERIALS USING A LABORATORY IMAGE PLATE DIFFRACTOMETER**

Lynne H. Thomas, Sylvia E. McLain, Andrew Parkin, and Chick C. Wilson

P06-235 **CLASSIFYING MOLECULAR GEOMETRIES: APPLICATION OF FACTOR ANALYSIS TO CLUSTER FORMATION IN dSNAP**

Duncan Sneddon, Christopher J. Gilmore, Gordon Barr, Wei Dong, Andrew Parkin, and Chick C. Wilson

O1A05-M1

THE EFFECT OF AMINO ACIDS AND AMINO ACID DERIVATIVES ON PROTEIN CRYSTALLIZATION

L. Ito[1], T. Kobayashi[1], K. Shiraki[2], T. Narukawa[1], A. Oosuka[1] and H. Yamaguchi[1]

[1]*Sch of Sci and Tech, Univ of Kwansei Gakuin, 2-1 Gakuen, Sanda, Hyogo 669-1337,*
[2]*Inst of Appl Phys, Univ of Tsukuba, 1-1-1 Tennodai, Tsukuba, Ibaraki 305-8573*

Protein crystallography is an indispensable technique for biological, biotechnological, and pharmaceutical researches. The structure determination by X-ray crystallography has been dramatically developed by progress in sample preparation, data collection and computation. To obtain high quality single crystals, however, still remains as the great problem. The difficulty depends on the many parameters that influence protein crystallization, including protein concentration, pH, ionic strength and precipitant concentration. Recently, many researchers adopt the sparse-matrix including different mother liquors that cover many chemical factors, in order to determine the primary crystallization conditions. Single crystals suitable for X-ray diffraction experiment are not always obtained by the procedure. Such screening procedures are not effective enough.

Prevention of protein aggregation plays a key role in the formation of single crystals in the aggregation-prone solution condition. Guanidine and urea are well known as aggregation suppressors that weaken the hydrophobic intermolecular interaction of proteins. Such denaturants are contained in a commercially available additive-screen kit, but decrease the stability of the native state. Recently, amino acids and amino acid derivatives, which are non-denaturating reagents, such as arginine have been used for additives to decrease the aggregation during a refolding process and a heat treatment process. In this study, we investigated the effect of amino acids and amino acids derivatives on protein crystallization.

As a result, protein crystals were obtained in expanded concentration range of the known precipitant in the presence of some kind of these reagents. Especially, crystals were obtained from many conditions including precipitants that crystal did not appear in the absence of the reagents. For example, in the presence of arginine, HEWL crystals were obtained from ammonium sulfate solution. It is considered that the basic additive and amino acid derivatives promote the crystallization of positively charged HEWL. These results show that these reagents are very effective for crystallization and promote success ratio of it and suggests a new strategy to improve the performance of the protein crystallization by addition of amino acids.

O1A05-M2

(NZ)CH...O CONTACTS ASSISTED CRYSTALLIZATION

Neil Shaw[a], Zhongyun Cheng[a], Bi-Cheng Wang[b], Zihe Rao[a] and Zhi-Jie Liu[a]

[a] *National Laboratory of Biomacromolecules, Institute of Biophysics, Chinese Academy of Sciences, Beijing, 100101, China*

[b] *Southeast Collaboratory for Structural Genomics, Department of Biochemistry and Molecular Biology, University of Georgia, GA 30602, USA*

The successful crystallization and structure determination of a ParB nuclease by creating new designer (NZ)CH…O bonds. 44 new cohesive (NZ) CH…O contacts (3.2 – 3.7 Å) were synthesized by the addition of 2 methyl groups to the side chain amine nitrogen (NZ) of 9 lysine residues of the nuclease. The engineered contacts dramatically altered the crystallization properties of the nuclease, resulting in crystals that diffracted to 1.2 Å resolution. The structure of the ParB nuclease protein determined in this study provides new insights and direction for deciphering the events of DNA segregation at the atomic level. In addition, the generality of the engineering makes it an attractive tool for tackling crystallization problems for a broad range of protein targets.

O1A05-M3

PHASING WITH IN-HOUSE SOFTER X-RAY RADIATION

Cheng Yang, James W. Pflugrath, Joseph D. Ferrara

Rigaku Americas Corporation, The Woodlands, Texas 77381, USA

The phase problem in macromolecular crystallography has been mitigated dramatically in recent years by advances in methodology and instrumentation. SAD phasing has now become the primary *de novo* phasing method. A search of the PDB of structures released in 2006 reveals the number of structures solved by SAD phasing exceeds those solved by MAD for the first time. A number of these examples of successful S-SAD and Se-SAD phasing used Cr radiation (λ = 2.29 Å), which can double the anomalous signal of sulfur and selenium compared to Cu radiation.

This report reviews recent results from phasing with the enhanced anomalous signal provided by Cr radiation to demonstrate this longer wavelength can be used to solve *de novo* structures. Selenium, as the heavy atom, with Cr radiation can provide sufficient anomalous scattering for routine phasing. Cr radiation opens a new path to extracting the weak anomalous signal from sulfur to phase native protein data. With the addition of Cr radiation to the crystallographer's toolkit, in-house X-ray sources can routinely provide at least two wavelength options. The combination of diffraction data collected using both Cu (λ = 1.54 Å) and Cr radiation can improve the electron density tremendously. Anomalous scattering from sulfur can also assist in molecular replacement solutions. Finally, the data collected with Cr radiation can be used to refine a structure. Ultimately, this makes it possible to solve a protein structure with a single data set.

This in-house phasing approach we describe has been given the label "**know before you go**" by John Rose and B.C. Wang at the University of Georgia. This method improves the efficiency of the solution of macromolecular crystal structures and usage of the synchrotron beam time.

O1A05-M4

Long Wavelength Phasing: Current and Future Challenges

B.C. Wang[1,2], John Rose[1,2], Lirong Chen[2], John Ruble[2], James Tucker Swindell II[2], Zeng-Qing Albert Fu[1,2], Jim Fait[1,2], Zhongmin Jin[1,2], Andrew Horward[2,3] and John Chrzas[1,2]

[1]*Dept. of Biochemistry and Molecular Biology, The University of Georgia, Athens, GA, USA,* [2]*SER-CAT, Bldg. 436 B, APS, ANL, 9700 S. Cass. Ave., Argonne, IL, USA,* [3]*Biological, Chemical, and Physical Sciences Department, Illinois Institute of Technology, Chicago, IL, USA*

With the increased interest in single wavelength anomalous scattering (SAS) phasing, data collection using ~1Å X-rays has become an option, instead of a requirement. In principle, synchrotron beamlines are capable of generating X-rays with broad wavelength spectrum and theoretically there are certain advantages in collecting data using longer wavelength ($\lambda > 1.5$Å) or soft X-rays. However, in practice data collection using soft X-rays is only occasionally carried out at synchrotron sites due to various technical reasons.

At SER-CAT we have an active program in synchrotron sulfur SAS phasing and have over the past two years embarked on a program of soft X-ray beamline optimization focused on identifying and correcting instabilities in the system at low energies which can significantly contribute to noise level in the SAS data produced. In addition, software development on collecting data with enhanced signal-to-nose has also been initiated.

Progress on the optimization of both the SER-CAT undulator and bending magnet beamlines for routine, high quality soft X-ray data collection will be presented.

Work is supported in part with funds from the National Institutes of Health (GM62407), SER-CAT, The Georgia Research Alliance and The University of Georgia Research Foundation.

O1A05-M5

PSAP: PROTEIN STRUCTURE ANALYSIS PACKAGE

K. Sekar[a,b], B.Balamurugan[a], M.N.A.Md.Roshan[a], B.Shaahul Hameed[a], K.Sumathi[a], R.Senthil Kumar[a], A.Udayakumar[a], K.H.Venkatesh Babu[a], M.Kalaivani[a], G.Sowmiya[a], P.Sivasankari[a], S.Saravanan[a], C.Vasuki Ranjani[a], K.Gopalakrishnan[a], K.N.Selvakumar[a], M.Jaikumar[a], T.Brindha[a] and Daliah Michael[a]

[a]Bioinformatics Centre and [b]Supercomputer Education and Research Centre, Indian Institute of Science, Bangalore 560 012, INDIA

In the post genomic era, understanding essential knowledge hidden in a protein molecule is of considerable interest in unraveling its structural and functional behavior. In particular, identifying and visualizing various structural features is an essential component for structural biologists and practicing bioinformaticians to better understand the protein molecule. To this end, a computing engine, Protein Structure Analysis Package (PSAP), is developed to identify, calculate and display various structural features of the three-dimensional protein structures. For visualization, the free molecular graphics programs, RasMol and Jmol are deployed in the computing engine. Further, the proposed computing engine is interfaced with the up-to-date local copy of the Protein Data Bank. The users need to provide the PDB-identification code or upload the three-dimensional atomic coordinates from the client machine. The atomic coordinates are being updated every week and hence the users can access all the structures available in the Protein Data Bank. The computing engine is free and is accessible online over the World Wide Web at the URL http://iris.physics.iisc.ernet.in/psap/.

PSAP : Protein Structure Analysis Package
B.Balamurugan, M.N.A.Md.Roshan, B.Shaahul Hameed, K.Sumathi, R.Senthil Kumar, A.Udayakumar, K.H.Venkatesh Babu, M.Kalaivani, G.Sowmiya, P.Sivasankari, S.Saravanan, C.Vasuki Ranjani, K.Gopalakrishnan, K.N.Selvakumar, M.Jaikumar, T.Brindha, Daliah Michael and K.Sekar
J. APPL. CRYST. (2007). (IN PRESS).

O1B05-M1

CONTROL OF POLYMORPHIC TRANSITION INDUCING PREFERENTIAL ENRICHMENT BY MODIFYING MOLECULAR STRUCTURES OR ADDING SEED CRYSTALS

Rui Tamura

Graduate School of Human and Environmental Studies, Kyoto University, Kyoto 606-8501, Japan

Preferential Enrichment is an unusually symmetry-breaking enantiomeric resolution phenomenon that is ascribed to an event of a complexity system [1]. We have shown that Preferential Enrichment is initiated by the solvent-assisted solid-to-solid transformation of a metastable polymorphic form into a thermodynamically stable one occurring during crystallization from the supersaturated EtOH solution of a certain kind of racemic mixed crystals (i.e., solid solutions or pseudoracemates) composed of the two enantiomers, followed by partial crystal-disintegration inside the crystal lattice to release the excess enantiomer existing in the initially-formed crystal into solution (Figure 1) [1,2]. Accordingly, Preferential Enrichment is strongly affected by the surrounding conditions, such as additives (seed crystals), solvent, concentration, and temperature, as well as the molecular structure.

Here we report (i) the modes of polymorphic transition relevant to the occurrence of Preferential Enrichment and (ii) two complimentary strategies for the induction of Preferential Enrichment by controlling the mode polymorphic transition; one is the slight modification of the molecular structure so as to prevent the undesired polymorphic transition, and the other is the use of the appropriate seed crystals to induce the desired “epitaxial transition” [1,3].

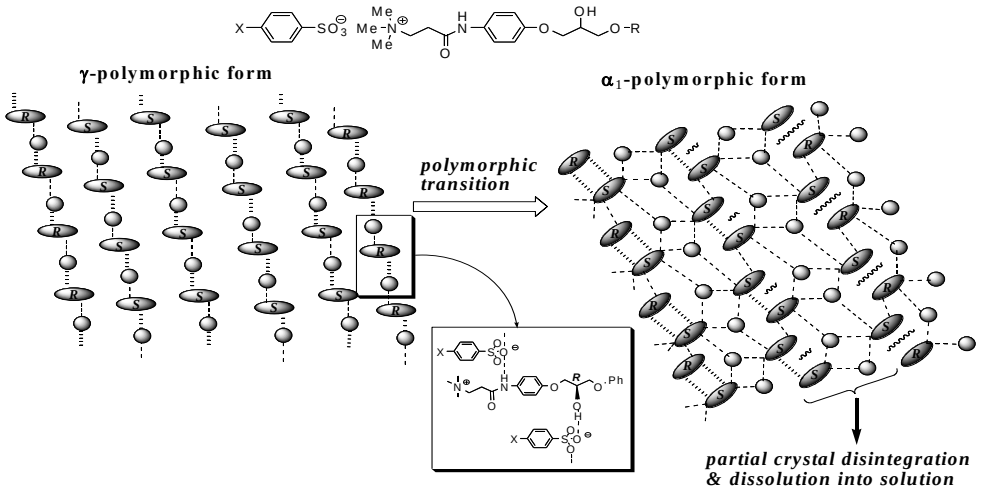

Figure 1

Reference:

[1] *Top. Curr. Chem.* **2007**, *269*, 53-82.
[2] (a) *J. Am. Chem. Soc.* **2002**, *124*, 13139-13153. (b) *Cryst. Growth Des.* **2003**, *3*, 973-979. (c) *Enantiomeric Separation: Fundamentals and Practical Methods*; Toda, F. Ed, Kluwer Academic Publishers, Dortrecht, 2004, pp. 135-163.
[3] (a) *Chem. Eur. J.* **2006**, *12*, 3515-3527. (b) *Cryst. Growth Des.*, in press.

O1B05-M2

POLYMORPHISM CASE STUDIES IN THE ARTEMISININ FAMILY OF ANTI-MALARIAL DRUGS: INVOLVEMENT OF MOLECULAR SHEET MOTIFS

Fanny L-Y. Shek, Herman H-Y. Sung, Richard K. Haynes and Ian D. Williams

Department of Chemistry, Hong Kong University of Science and Technology, Clear Water Bay, Kowloon, Hong Kong, China. Email: fanny@ust.hk

Atremisinin, a polycyclic peroxide natural product, is the component known as 'Qing Hao Su' in Traditional Chinese Medicine derived from *Artemisia annua*. Its' derivatives has been used as anti-malarial agents for a number of years. The parent compound and several related members of its family have been found to display polymorphism, of which some forms have been prepared by us through hydrothermal or sub-hydrothermal crystallization. Recently a highly effective new dervative Artemisone has been developed (R.K. Haynes et al, *Angew. Chemie*, **2006**, 45, 2082) and here we report its low temperature polymorphic phase transition. This involves rotation of one molecular sheet with respect to adjacent ones, taking a monoclinic Z' = 2 to a triclinic Z' = 4 arrangement, details below. Preserved molecular sheet motifs have also been observed in a family of 11-azaartemisinins in which arylsulphonate groups are substituted at the nitrogen. (R.K. Haynes et al, *ChemMedChem*, **2007**, in press) The 4-chlorophenyl and bromophenyl derivatives are isostructural $P2_1$, with molecular sheets which are in register, the 4-tolyl derivative is also $P2_1$ but with a doubled cell due to offset of alternate sheets along the b-axis, whilst the 4-nitrophenyl analog is orthorhombic $P2_12_12_1$ with adjacent sheets rotated by 180°, which has the effect of cancelling molecular dipoles. The relevance of such partially conserved structures to pharmaceutical polymorph searching and engineering will be discussed. We thank the HKSAR Research Grants Council and Bayer Corporation for financial support.

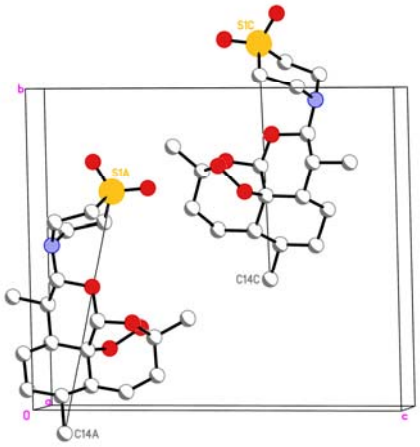

Artemisone	
100K	298K
Triclinic P1	Monoclinic $P2_1$
a = 11.1078	11.187
b= 12.385	12.501
c = 15.280	15.398
α= 90.03	90
β = 108.63	108.53
γ = 90.15	90
V = 1986.2	2041.9A^3

O1B05-M3

DETERMINATION OF ABSOLUTE CONFIGURATION FOR SOME NATURAL PRODUCTS FROM TRADITIONAL CHINESE MEDICINE

Herman H-Y. Sung, Nancy Y. Ip and Ian D. Williams

Department of Chemistry and Biotechnology Research Institute, Hong Kong University of Science and Technology, Clear Water Bay, Kowloon, Hong Kong, China.
Email: hermans@ust.hk

The determination of natural product structures continues to be dominated by multi-nuclear high field nmr spectroscopy in conjunction with high resolution mass spectrometry. However these are either indirect or inconclusive techniques and it may be hoped that the use of X-ray structure determination will become more prevalent in this field. The use of copper X-radiation from in-house diffractometers is also essential in determining the absolute configurations of the compounds involved. We herein present benchmark results of such determinations on a number of standard natural product compounds with varying degrees of oxygen and nitrogen content and using different collection times, temperatures and strategies with an Oxford Diffraction Xcalibur instrument employing a Copper Enhance Ultra source. The determinacy of the Flack parameter for high oxygen content compounds such as sucrose is compared to those from a variety of new compounds isolated from herbs used in Traditional Chinese Medicine. Examples include the diterpenoid compounds ent-isopimar-8(14), 15-dien-19-oic acid, and 5-alpha-hydroxy-ent-rosa-15-en-18-oic acid, (below) isolated from the whole herb of Sagittaria pygmaea (Liu X.T. et al, *Planta Medica*, **2007**, 73, 84)

We thank the HKSAR Research Grants Council for financial support.

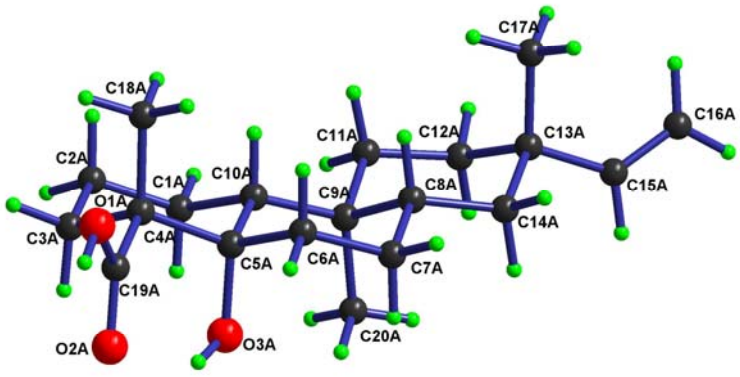

O1B05-M4

DISTINGUISHING BETWEEN NATURAL PRODUCTS AND NATURAL PRODUCT ARTIFACTS USING SINGLE CRYSTAL X-RAY STRUCTURE DETERMINATION: A CASE STUDY ON MACLURAXANTHONE, A COMPOUND CONTAINING A CHROMENE RING

Suchada Chantrapromma,[a] Nawong Boonnak,[a] and Hoong-Kun Fun[b]

[a]*Department of Chemistry, Faculty of Science, Prince of Songkla University, Hat-Yai, Songkhla 90112, Thailand.*
[b]*X-ray Crystallography Unit, School of Physics, Universiti Sains Malaysia, 11800 USM, Penang,Malaysia.*

Natural products are frequently tested for their potentials to be used as drugs, so the correct differentiation between natural products and natural product artifacts is extremely important so as not to make the wrong conclusions during the testing of these compounds for potential drug application. The distinguishing between natural products and natural product artifacts is of paramount importance and interest to researchers in natural products, pharmacology and chemistry. Besides offering the complete approach to 3-D structural analysis, single crystal X-ray structure determination also has the simple ability to differentiate easily between natural products and natural product artifacts. The distinguishing between the natural products and natural product artifacts by this technique shall be presented using as an example, a compound containing a chromene ring namely macluraxanthone (Fig. 1). This compound was isolated from *Cratoxylum formosum* subsp. *pruniflorum* (or Tui-Khon in Thai), a Thai medicinal plant. The decoction of the fresh or dried leaves from this plant has been used in traditional medicine such as tonic, stomachic and diuretic [1].

Cratoxylum formosum subsp. *pruniflorum*

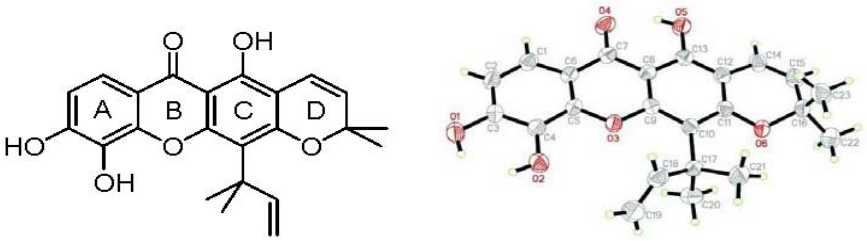

Fig. **1** The chemical diagram and X-ray structure of macluraxanthone.

Reference:

1. G. M. Kitanov, I. Assenov, Dam The Van, Pharmazie, **43**, H12 (1988).

O1B05-M5

PROTEIN MEASUREMENTS ON A LABORATORY POWDER X-RAY DIFFRACTOMETER

D. Beckers, S. Prugovečki, T. Degen, A. Stefanovic

PANalytical B.V. , Almelo, The Netherlands

The Bragg-Brentano diffractometer has been used for decades for the investigation of organic compounds as encountered, for example, in the pharmaceutical industry. In the last ten years, the introduction of new X-ray optical components and fast detection systems has widened the number of attractive configurations for laboratory X-ray diffractometers considerably. Choosing the optimum hardware for a given set of analytical problems is more difficult (and interesting!) than it was before.

In this presentation, we will show the capability of modern powder diffractometers to provide reasonable high-resolution data on weakly scattering protein samples by choosing an optimized set-up. Measurement an analysis results on different samples are shown. The data quality was good enough for indexing, space group determination and even a Rietveld refinement was reasonable. Although longer measurement times than on beam-lines are required, radiation damage is much less. The possibility of high throughput screening of proteins on X-ray powder laboratory instrumentation is also demonstrated and discussed.

O1C05-M1

QUANTITATIVE GISAXS ANALYSIS OF LAMELLAR STRUCTURES SELF-ASSEMBLED IN BRUSH POLYMER THIN FILMS

Moonhor Ree*, Jinhwan Yoon, Kyeong Sik Jin, Kyuyoung Heo, Sangwoo Jin, Jehan Kim, Kwang-Woo Kim, Tae Joo Shin

Pohang University of Science & Technology, Pohang Accelerator Laboratory,
Department of Chemistry, BK21 School of Molecular Science
Pohang 790-784, Republic of Korea ree@postech.edu

Lamellar stack structures are one of the most common morphological structures observed in polymer thin films, including those of brush polymers, and are even observed in bulk polymer samples. However, no quantitative two-dimensional grazing incidence small-angle X-ray scattering (2D GISAXS) analysis, or even transmission small-angle X-ray and neutron scattering (TSAXS and TSANS) analysis, has been performed on such lamellar stack structures in polymer thin films and bulk samples. Only limited, qualitative scattering analyses have been carried out with scattering profiles extracted along the direction of the lamellar stacking. In this study, we developed a GISAXS formula for the quantitative analysis of lamellar stack structures formed in polymer thin films, and used it to characterize 2D GISAXS patterns measured for lamellar structures in nanometer-scaled thin films of brush polymers. The 2D GISAXS measurements and a quantitative data analysis using the derived GISAXS formula provide, for the first time, the comprehensive structure and orientation details of the lamellar stacks formed in the thin films of several brush polymers, details of brush polymers that cannot be obtained by TSAXS, TSANS and microscopic methods. Furthermore, this study provides a molecular structure model and electron density profiles. This study was supported by the Korea Science & Engineering Foundation (National Research Lab for Polymer Synthesis and Physics and Center for Integrated Molecular Systems) and by the Ministry of Education (BK21 Program). Synchrotron GIXS measurements at the Pohang Accelerator Laboratory were supported by the Ministry of Science & Technology and the POSCO Company.

O1C05-M2

MESO AND NANO-SCALE STRUCTURAL FORMATION OF POLYETHYLENE THIN FILMS EVALUATED BY SYNCHROTRON GRAZING-INCIDENCE SMALL-ANGLE AND WIDE-ANGLE X-RAY SCATTERING MEASUREMENTS

Sono SASAKI[1], Hiroyasu MASUNAGA[1], Hiroo TAJIRI[1], Katsuaki INOUE[1], Hiroshi OKUDA[2], Atsushi TAKAHARA[3], Masaki TAKATA[1,4]

[1] Japan Synchrotron Radiation Research Institute (JASRI) / SPring-8, Hyogo 679-5198, Japan; [2]International Innovation Center, Kyoto University, Kyoto 606-8501 Japan; [3]Institute for Materials Chemistry and Engineering, Kyushu University, Fukuoka 812-8581, Japan; [4]The RIKEN Harima Institute / SPring-8, Hyogo 679-5198, Japan.

Polymer thin films have been used for parts of components of displays, as the insulation layer of semiconductors and as materials to coat papers for printing. To satisfy the physical properties of the thin films as materials, it is important to control their higher-order structures at meso-to-nano scales. To reveal the essential structural property of the thin films, we have developed the grazing-incidence small-angle and wide-angle X-ray scattering (GISWAXS) experimental technique at the BL40B2 in SPring-8 (Hyogo, Japan). In this study, the higher-order structures of polyethylene (PE) thin films on Si wafers in annealing and crystallization processes were investigated at molecular and lamellar scales by synchrotron GISWAXS measurements.

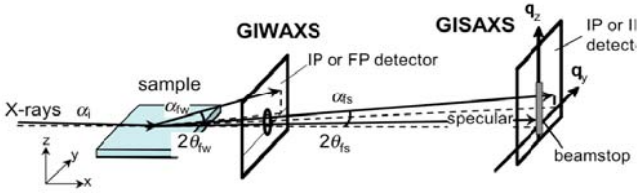

Figure 1. Experimental geometry of the GISWAXS measurements.
IP: imaging plate, FP: flat panel, II:Imaging intensifier, CCD: charge coupled device.

Figure 1 shows the experimental geometry of the GISWAXS measurements. The components of the scattering vector, **q**, parallel and perpendicular to the sample surface were defined as $\mathbf{q}_y = (2\pi/\lambda) \sin(2\theta_f) \cos(\alpha_f)$ and $\mathbf{q}_z = (2\pi/\lambda) (\sin(\alpha_i) + \sin(\alpha_f))$, respectively, for reflected scattering. Here, α_i is the incident angle of the X-ray beams near the critical angle of total external reflection, α_f is the exit angle, λ is the wavelength of the incident X-ray beams and $2\theta_f$ is the angle between the scattered beam and the plane of incidence. The subscripts s and w in Figure 1 indicate the grazing-incidence small-angle X-ray scattering (GISAXS) and the grazing-incidence

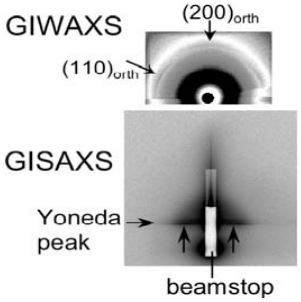

Figure 2. GISWAXS patterns measured for the PE thin films on a Si wafer at 393 K in a stepwise annealing process from 298 K. The λ was 0.15nm and the α_i was 0.13 deg.

wide-angle X-ray scattering (GIWAXS) geometries, respectively.

Figure 2 shows GISWAXS patterns measured for the PE thin films (thickness: ca. 400 nm) on a Si wafer at 393 K in a stepwise annealing process from 298 K. *In-situ* GIWAXS profiles of the PE thin film detected at the certain annealing temperatures (*Ta*) between 373 K and 393 K indicated that the *a* axis of the PE orthorhombic unit cell was relatively oriented in the perpendicular direction to the film surface. On the other hand, the GISAXS data suggested that crystalline lamellae were stacked with large disordering parallel to the film surface, and the long period became longer with the *Ta*. The crystallization behavior of polyethylene in thin films during solvent-evaporation of a droplet of its *p*-xylene solution was evaluated by time-resolved GISWAXS measurements as a technical application to the kinetic study, which will be presented and discussed.

STRUCTURAL CHANGES IN THE MECHANICAL DEFORMATION PROCESS OF SPECIFICALLY-ORIENTED POLYETHYLENE SAMPLES AS VIEWED FROM THE SIMULTANEOUS MEASUREMENTS OF SYNCHROTRON SAXS-WAXD AND RAMAN SPECTRA

Kohji TASHIRO[1], Shinichi TAKEDA[1], Makoto HANESAKA[1], Hiroyasu MASUNAGA[2], Sono SASAKI[2] and Masaki TAKATA[2, 3]

[1] *Graduate School of Engineering, Toyota Technological Institute, Tempaku Nagoya, 468-8511, Japan*
[2] *JASRI / SPring-8, Hyogo 679-5198, Japan*
[3] *The RIKEN Harima Institute / SPring-8, Hyogo, 679-5198, Japan*

Investigation of structural changes occurring in the deformation process of polymer solids subjected to the mechanical stress is essentially important for the design of new polymer materials with excellent mechanical properties. In many studies, however, the samples used were mainly unoriented and the lamellae are distributed randomly, and so the change in lamellar orientation before and after the deformation is impossible to trace. Rather it might be easier to trace the deformation procedure of lamellae when the specifically-oriented sample of already-known lamellar stacking structure is utilized in the measurement. In the present experiment the *a*-axially-oriented polyethylene sample, obtained by spinning of the molten sample, was stretched along the draw axis, during which the SAXS and WAXD patterns were measured at short intervals using the synchrotron X-ray beam in parallel with the Raman spectral measurement for the molecular characterization. This *in-situ* simultaneous measurement has been performed at the beam line 40B2 in SPring-8, Japan. Figure shows schematically the changes in the 2-dimensional patterns of WAXD and SAXS taken in the necking process of the *a*-axially-oriented linear low-density polyethylene sample. At the starting point the meridional scattering was observed in the SAXS pattern. As the sample was drawn gradually the necking phenomenon was started and the four-scattering patterns were observed to appear, indicating the transformation to the stacking structure of tilted lamellae. It should be noticed that, before an occurrence of this remarkable change in lamellar stacking structure, the “discontinuous” change of the *a*-axial orientation to the *c*-axial orientation was found to occur in the crystal lattice. By stretching the sample furthermore, the other type of meridional scatterings appeared in the SAXS pattern and it changes to the four-points scattering pattern, indicating the tilted lamellae change to the fibrillar structure. These behaviors are different each other depending on the degree of side branching in the polyethylene samples.

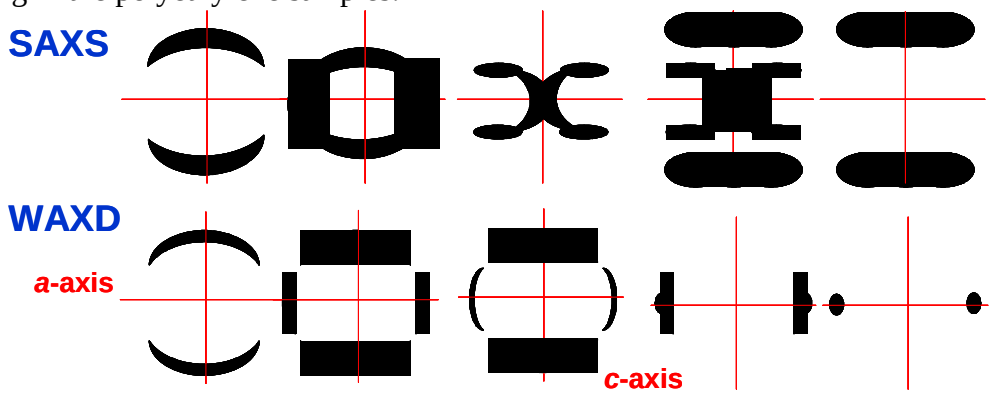

O1C05-M4

STRAIN-INDUCED CRYSTALLIZATION OF REINFORCED NATURAL RUBBER AS STUDIED BY SYNCHROTRON X-RAY SCATTERING

Hyun Hoon Song[a], Min Kwan Kang[a], Hye-Jin Jeon[a], Gwanghoon Kwag[b] and Hyungkyu Choi[b]

[a]Department of Advanced Materials, Hannam University, S. Korea; [b]R&D Center, Kumho Petrochemical Co. Ltd., S. Korea

Natural rubber is one of the most commercially utilized elastomeric polymers. Intensive studies have been carried out to improve the mechanical and physical properties including elasticity, abrasion resistance and resilience of natural rubber. Synthetic polybutadiene rubber of ultra high *cis* content has been also of particular interest in the rubber industry and intensively studied due to its properties which are superior to those of natural rubber. In rubber industry, the natural rubber/synthetic rubber blend is practically utilized. Carbon black (CB) is another traditional filler used to increase the mechanical and physical properties in rubber industry. Carbon nanotubes (CNTs) also have been identified as an excellent reinforcing material to modify mechanical, thermal and other properties of polymers.

In our recent work, strain-induced crystallization of natural rubber containing various amounts of synthetic rubber, carbon nanotubes (CNTs) and carbon black (CB) was systematically studied by synchrotron X-ray scattering. X-ray scattering intensities from the oriented rubber were decomposed into three phases; isotropic amorphous (IA), oriented noncrystalline (ON), and crystalline (Cr) phase and each phase changes were monitored upon stretching. In this presentation, the structure evolution of the orienting rubbers and the mechanical properties, in particular, the effects of the reinforcing synthetic rubbers and inorganic fillers will be discussed.

O1C05-M5

ANOMALOUS SMALL ANGLE X-RAY SCATTERING FOR THE DISTRIBUTION AND AGGREGATION OF THE GOLD NANOPARTICLES IN A PS-B-P4VP DIBLOCK COPOLYMER

U-Ser Jeng,[a] Ying-Huang Lai,[a] Ching-Mao Huang,[b] and Kung-Hwa Wei,[b] Chiu-Hun Su,[a] and Hwo-Shuenn Sheu[a]

[a] *National Synchrotron Radiation Research Center, Hsinch 30049 Taiwan.* [b] *Department of Materials Science and Engineering, National Chiao Tung University, Hsinchu, Taiwan 30049*

Using anomalous small angle X-ray scattering (ASAXS), we have studied the ordered structure formed by 2-phenylethanethiol-coated gold nanoparticles (NPs) embedded in a spherical poly(styrene-*b*-4-vinylpyridine) diblock copolymer (PS-*b*-P4VP). The SAXS image taken for the copolymer/NPs composite illustrates a powder ring in conjunction with diffraction spots distributed along the powder ring. From the diffraction peak positions and profiles, an ordering spacing of 3.5 nm and an ordering size up to 100 nm are estimated. With the X-ray energy tuned closed to the L_{III}-absorption edge of gold (11.919 keV), the diffraction peaks decreases obviously when the photon energy is changed from 11.200 keV to 11.910 keV. This result indicates clearly that the 2 nm gold nanoparticles are responsible for the highly ordered structure observed. The dissociation of the ordered gold clusters in an isothermal annealing at 170 °C is monitored by in-situ small angle X-ray scattering. The four-hour isothermal annealing disrupts the ordered gold clusters completely, while P4VP spheres develop better ordering inside the composite. With ASAXS, further, we have found that the dissociated gold NPs have relocated themselves to the surfaces of the P4VP spheres, forming NPs shells outside the P4VP cores. We discuss the mechanism of the structural evolution of the gold NPs in the

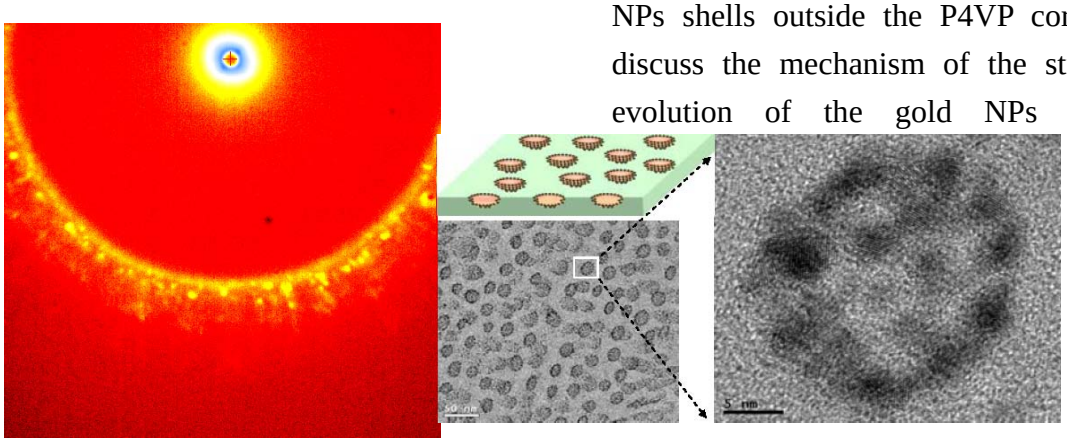

Fig. 1: SAXS and TEM images for the PS-b-P4VP/gold NPs composite before and after thermal annealing, respectively.

O1C05-M6

CORE-SHELL MICELLAR STRUCTURES OF NOVEL TERTIARY AMINE METHACRYLATE-BASED BLOCK COPOLYMERS STUDIED BY SMALL ANGLE X-RAY SCATTERING AND DYNAMICS LIGHT SCATTERING

Yusuf Ozcan,[a,b] U-Ser Jeng,[a,*] Vural Butun,[c] Ying-Huang Lai,[a] Chiu-Hun Su,[a] Keng S. Liang,[a] Semra Ide [b]

[a] *National Synchrotron Radiation Research Center, Hsinch 30049 Taiwan.* [b]*Department of Physics Engineering, Hacettepe University, 06800, Beytepe, Ankara, TURKEY.* [c]*Faculty of Arts and Science, Department of Chemistry, Eskisehir Osmangazi University, Campus of Meselik, 26480, Eskisehir, TURKEY.*

We have studied the solution structure of couple novel amphiphilic block polymers, with the same hydrophobic end of 2-(dimethylamino)ethyl methacrylate (DMA) block-copolymerized with, respectively, two polyeleclyte ends of tertiary amine methacrylate copolymers of 2-(diethylamino)ethyl methacrylate (DEA) and 2-(N-morpholino)ethyl methacrylate (MEMA). The micellization of the polyelectrolyte block copolymer is controlled by the sample concentration, temperature, and pH value. In contrast to the traditional micelles formed by small surfactant molecules, whose inverted micelle structure is achieved by selected solvents, the novel polyelectrolyte block copolymer of DEA_n-$(DMA\text{-}MEMA)_m$ can invert the micelle structure in aqueous solution simply by changing pH value from 6.7 to 8. The micelle structures, including the size, shape, aggregation number, and polydispersity, are characterized using small angle X-ray scattering and dynamic light scattering. The result indicates that a more stable micelle structure of DEA_n-DMA_m can be achieved with n:m ~ ~1:2 at 23 °C and pH= 7.7. At which condition, the narrowly disperse spherical micelles have a core-shell structure with a core radius of 54±5Å, a shell thickness of 28±3Å, and an aggregation number of 105±5. Interestingly, the volume ratio 1:2 of the hydrophobic core (DEA) to the hydrophilic shell (DMA swelled with water) is nearly the same as the ratio of n/m, and the packing parameter *p* of the micelle structure is ~0.2 which satisfies the criterion of p <1/3 for stable spherical micelles of common amphiphilic molecules.

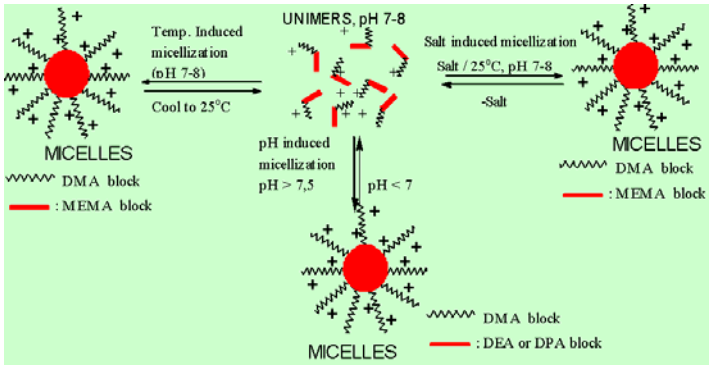

Fig. 1: Micelle formations of polyelectrolyte block copolymers in various solution conditions.

O2A05-A1

STRUCTURE, ASSEMBLY AND ACTION OF DODECAMERIC DPS, A STRESS RELATED FAMILY OF PROTEINS

Siddhartha Roy[a], Ramachandran Saraswathi[a], Surbhi Gupta[a], K.Sekar[b], Dipankar Chatterji[a] and M.Vijayan[a]

[a]*Molecular Biophysics Unit,* [b]*Bioinformatics Centre, Indian Institute of Science, Bangalore 560012, India*

DNA binding protein from stationary phase cells (Dps) is involved in protecting DNA from oxidative damage and in sequestering ferric ions during nutritional starvation. We had earlier determined the structure of a Dps molecule from *M. smegmatis* (MsDps1). Through the analysis of this structure in comparison with the known structures of Dps from other sources, among other things, the dodecameric molecule was established to be a distorted icosahedron (*J.Mol.Biol.* **339**, 1103-1113, 2004). The subsequent analysis of mutants involving the deletion of the N-terminal and C-terminal tails of the subunit demonstrated the role of the tails in dodecameric assembly, in addition to the role of the C-terminal tail in DNA binding (*J.Mol.Biol.* **370**, 752-767, 2007). We have now identified a second Dps (MsDps2) through a search of the *M. smegmatis* genome, cloned and expressed it and determined its structure. The dodecameric structure is stabler in MsDps2 than in MsDps1, substantially because the N-terminal tail is more strongly involved in holding the subunits together than the tails are in MsDps1. This N-terminal tail also appears to be involved in DNA binding. The structures of MsDps1, its N- and C-terminal mutants and MsDps2 provide insights into the nuances of the assembly, DNA binding and ferroxidase activity of the Dps family.

O2A05-A2

STRUCTURL AND FUNCTIONAL STUDY OF *C. ELEGANS* CELL-DEATH RELATED NUCLEASE 4 (CRN-4)

Yu-Yuan Hsiao [a,b] and Hanna S. Yuan [b]

[a]*Institute of Bioinformatics and Structure Biology, National Tsing Hua University*
[b]*Institute of Molecular Biology, Academia Sinica, Taipei, Taiwan*

Programmed cell death (apoptosis) is an essential biological process for development, maintenance of appropriate cell number and defense against virus infection. One of the major biochemical features of apoptosis is chromosome DNA fragmentation. Cell death related nuclease 4 (CRN-4) is one of the newly identified apoptotic nucleases in *C. elegans* involved in the sequential DNA degradation process. CRN-4 interacts with several nucleases, including CPS-6, NUC-1, CRN-1 and CRN-5, to form a multi-protein complex, named degradeosome, which promotes apoptotic DNA degradation. A DEDDh exonuclease domain is identified in the CRN-4 and therefore CRN-4 likely bears 3'-5' exonuclease activity, responsible for chromosome DNA nicking and/or exonuclease digestion.

To reveal the molecular basis for DNA fragmentation in apoptosis, we over expressed and purified recombinant CRN-4 from *E. coli.* We found that CRN-4 contains both DNase and RNase activities and prefers dsDNA over ssDNA. The crystal structure of CRN-4 was determined at a resolution of 2.5 Å by MAD method (data collected at BL12B1 in NSRRC). CRN-4 folds into a dimer with an N-terminal DEDDh exonuclease domain and a C-terminal domain with unknown function. The N-terminal catalytic domain adopts an α/β globular fold and shares similar structure and catalytic residues to those of other members of DEDDh exonucleases, such as 3'hExo and ε186. The C-terminal domain contains a novel mixed α/β fold with 7 basic residues exposing to the surface. We suggest that the C-terminal domain in CRN-4 is involved in DNA binding in a way similar to the RNA-binding SAP domain of 3'hExo. The structural comparison of dimeric CRN-4 to several nucleases further reveals that this protein likely recognizes DNA in a unique way than we had seen before in other DEDD family of nucleases.

O2C05-A3

X-RAY ATOMIC ORBITAL ANALYSIS AND ITS APPLICATION TO RARE-EARTH CRYSTALS

Kiyoaki Tanaka,[a] Ryoko Makita,[a] Shiro Funahashi,[a] Takashi Komori,[a,b] Terutoshi Sakakura[a]

[a]*Graduate school of engineering Nagoya Institute of Technology, Nagoya,Japan;* [b]*Toyota Industries Cooperation ,Kariya, Japan*

The 4f-electron density distribution in MB_6 (M=La, Ce, Sm) has been investigated successfully by the X-ray Atomic Orbital analysis (*XAO*) with the program *QNTAO*. The quantum mechanical and crystallographic framework of it are presented.

It is the method based on the atomic orbitals (AO) and all the atoms in the unit cell are divided into the groups of sub-shell electrons (s/p/d/f). Each AO in the crystal field is expressed as a linear combination of sub-shell basis functions such as d_{xy}, d_{yz} etc. The starting set of AO's are calculated for a single electron in the crystal field. The expansion coefficients are determined by the least-squares method keeping the ortho-normal relationship between the AO's. In the multi-electron system, the wave function is expressed in terms of a linear combination of the anti-symmetric Slater determinants and the system splits into atomic terms. The d^3 system in the O_h crystal field with $t_{2g}^2e_g^1$ configuration for example has ten atomic terms but the X-ray scattering factors of them always keep the contributions of the t_{2g} and e_g electrons 2 to 1. X-ray diffraction cannot specify the atomic terms. However this ensures on the sound quantum mechanical bases that the AO's calculated for the single valence electron are effective. Since the electron population on each AO cannot be measured by spectroscopy, those measured by the X-ray diffraction is very important. Each group of the electrons in the same sub-shell is treated as a pseudo-atom, which enables us to get the electron population of each AO keeping the electro-neutrality of the unit cell and trace the electron transfer among the AO's as shown in CeB_6 at low temperature.

However the XAO analysis has two limitations. First it neglects the electron correlations. The non-integer occupation number of each AO may reflect it. Second it is based on the AO models and does not explain two-center electrons which appear in the molecular orbital models. Therefore it is applied best to ionic crystals especially to the systems with highly localized d and f electrons including the compounds with a non-stoichiometric structure.

The XAO analyses for 4f-EDD have given fruitful results. In CeB_6 the electrons are transferred from Ce to B_6 at low temperature but they are back donated to Ce 5d orbitals not to 4f orbitals at 430 and 535 K accompanying the inversion of 4f energy levels, which is reflected to the obtained electron population on each AO. The 5d occupation was also found in Lab_6 and SmB_6 accompanying the change of the 4f energy levels.

O2A05-A4

STRUCTURE OF AN IGNAR-AMA1 COMPLEX

Victor Streltsov[a], Kylie Henderson[a,b,c], Andrew Coley[b,c], Adrian Batchelor[d], Robin Anders[c], Michael Foley[b,c], Stewart Nuttall[a]

[a]CSIRO Molecular and Health Technologies, Melbourne, Australia. [b]Cooperative Research Centre for Diagnostics, Brisbane, Australia. [c]School of Biochemistry, La Trobe University, Melbourne, Australia. [d]University of Maryland School of Pharmacy, Baltimore, Maryland, USA.

Apical Membrane Antigen-1 (AMA1) is essential for invasion of erythrocytes and hepatocytes by *Plasmodium* parasites and is a leading malarial vaccine candidate. While antibodies to AMA1 can prevent such invasion, extensive polymorphisms within surface-exposed loops may limit the ability of conventional AMA1-induced antibodies to protect against all parasite genotypes. Using an AMA1-specific IgNAR (Immunoglobulin New Antigen Receptors) single variable domain antibody, we performed targeted mutagenesis and selection against AMA1 from three *P. falciparum* strains. We present co-crystal structures of two antibody-AMA1 complexes, which reveal the extended IgNAR CDR3 loops penetrating deep into a hydrophobic cleft on the antigen surface, and contacting residues conserved across parasite species. Comparison of a series of affinity-enhancing mutations allowed dissection of their relative contributions to binding kinetics, and correlation with inhibition of erythrocyte invasion. These findings provide insights into mechanisms of single-domain antibody binding, and will enable design of reagents targeting otherwise cryptic epitopes in apicomplexan parasites.

O2A05-A5

STRUCTURAL AND FUNCTIONAL INSIGHTS INTO DOM34, A KEY COMPONENT OF NO-GO MRNA DECAY

Hyung Ho Lee and Se Won Suh

Department of Chemistry, College of Natural Sciences, Seoul National University, Seoul 151-747, Korea

In *Saccharomyces cerevisiae*, the two proteins Dom34 and Hbs1 play key roles in a newly identified mRNA-surveillance pathway called no-go decay, by which mRNAs with translational stalls are endonucleolytically cleaved and subsequently degraded. However, the identity of the endoribonuclease is unknown. Homologs of the yeast Dom34, called Pelota, are broadly conserved in eukaryotes and archaea. Dom34/Pelota is related to the translation termination factor eRF1.

To gain insights into the structure and function of Dom34/Pelota, we have determined the crystal structure of a representative member of the Dom34/Pelota family and investigated the ribonuclease activity of Dom34. Dom34/Pelota consists of three domains of similar sizes, with domain 1 being structurally dissimilar from domain 1 of eRF1 but resembling the RNA-binding Sm fold. The yeast Dom34 shows an endoribonuclease activity when we assayed with defined RNA substrates containing a stem-loop, suggesting that it could be responsible for the endonucleolytic cleavage of the stalled mRNA in no-go decay.

O2A05-A6

THE CRYSTAL STRUCTURE OF A VIRUS-LIKE PARTICLE FROM HYPERTHERMOPHILLIC ARCAHEON *PYROCOCCUS FURIOSUS PROVIDE INSIGHT INTO THE EVOLUTION OF VIRUSES*

Fusamichi Akita, Khoon Tee Chong, Hideaki Tanaka, Eiki Yamashita, Naoyuki Miyazaki, Yuichiro Nakaishi, Kazunori Namba, Mamoru Suzuki, Tomitake Tsukihara and Atsushi Nakagawa

Institute for Protein Research, Osaka University, Suita, Osaka, 565-0871, Japan.

Pyrococcus furiosus is a hyperthermophilic archaeal microorganism found near deep-sea thermal vents and its optimal growth temperature of 100 °C. Recently, a 38.8 kDa protein from *P. furiosus* DSM 3638 was isolated and characterized[1]. Electron microscopy revealed that this protein aggregated as spheres of approximately 30 nm in diameter, which we designated *P. furiosus* virus-like particles (PfVs).

X-ray crystallographic analysis at 3.6 Å resolution revealed that each PfV consisted of 180 copies of the 38.8-kDa protein and retained *T*=3 icosahedral symmetry, as is often the case in spherical viruses[2]. The total molecular mass of each particle was approximately 7 MDa. Although crystals diffracted to higher than 3.2 Å resolution, only 10 or fewer images could be collected from a single crystal because of radiation damage. All diffraction experiments on PfV crystals were performed using the beamline BL44XU, which is designed for biological macromolecular assembly crystallography, at SPring-8. The crystals belonged to the space group $P4_12_12$, with cell dimensions of $a = b$ =631.5, c = 351.3 Å. The crystal contained half a particle in the asymmetric unit. Initial phase calculations were performed by multiple isomorphous replacement with anomalous scattering using heavy atom clusters (SiW_{12}, Ta_6Br_{14}), and the initial phase was calculated at 10 Å resolution. To enhance the resolution, we used conventional heavy atom compounds such as LuCl6. The 4.5 Å resolution electron density map calculated by multiple isomorphous replacement with anomalous scattering using the cluster compounds LuC_{l6} and Ta_6Br_{12} was then improved by density modification, including solvent flattening, histogram mapping, and NCS averaging. An electron density map at 4-Å resolution, obtained by multiple isomorphous replacement with anomalous scattering of the heavy atom clusters SiW_{12} and Ta_6Br_{14} was used as a starting model, and the resolution was extended to 3.6 Å.

An examination of capsid structures suggested strong evolutionary links among PfV, tailed double-stranded DNA bacteriophages, and herpes viruses. The similar three-dimensional structures of the various coat proteins indicate that these viral capsids might have originated and evolved from a common ancestor. The structure of PfV provides a previously undescribed example of viral relationships across the three domains of life (Eukarya, Bacteria, and Archaea).

O2A05-A7

HIGHER RESOLUTION STRUCTURE OF GIANT HEMOGLOBIN FROM *OLIGOBRACHIA MASHIKOI*

Nobutaka Numoto,[a,b,*] Taro Nakagawa,[c] Akiko Kita,[a,d] Yuichi Sasayama,[e] Yoshihiro Fukumori[c] and Kunio Miki[a,b]

[a]*Graduate School of Science, Kyoto University;* [b]*RIKEN SPring-8 Center at Harima Institution;* [c]*Graduate School of Natural Science and Technology, Kanazawa University;* [d]*Research Reactor Institute, Kyoto University;* [e]*Institute of Nature and Environmental Technology, Kanazawa University, Japan.*

[*]*Present address; Graduate School of Natural Science and Technology, Kanazawa University.*

Siboglinid polychaetes live in sulfide rich seabed and have no mouth or gut. These animals obtain their nutrition mainly from their symbiont which is thought to be chemoautotrophic sulfur-oxidizing bacteria. One of the siboglinid polychaetes, pogonophoran beard worm has 400 kDa extracellular giant hemoglobin (Hb) which can transports oxygen and sulfide simultaneously. The symbiotic bacteria are supplied with sulfide by the giant Hb and afford host organic materials. The crystal structures of vascular and coelomic 400 kDa Hb of siboglinid polychaetes have given the insights into the mechanisms of their unique properties of oxygen binding or functions of sulfide binding, but both structures were solved with oxygenated forms at moderate resolutions. We have determined the crystal structure of 400 kDa Hb in partially ferric met state from a siboglinid polychaete *Oligobrachia mashikoi* at 1.95 Å resolution. The electron densities at higher resolution confirm the existence of an isomer of the B1 subunit. The structure showed completely lacks of electron density around distal heme pockets at the A2, B1 and B2 subunits, whereas clear peaks were observed at the A1 subunits. Because the color of the crystals were brown and absorption spectrum from the dissolved crystals were characteristic of that of met state, it was suggested that the obtained structure was in unliganded met forms at three fourth subunits of the 24mer assembly and only the A1 subunits were in oxygenated forms. Remarkable structural changes at the AB loop regions in all subunits were seen in the partially unliganded structure. These movements cause quaternary rearrangements of the dimer and the dodecamer structures, which are the common subassembly of the giant Hbs, suggesting that the ligand induced structural changes of *Oligobrachia* giant Hb is quite different from other well-studied Hbs.

We have also determined the structure of metal-binding state of *Oligobrachia* Hb beyond 1.7 Å resolution. These structures reveal that the bound metals stabilize the oxygenated form of the giant Hb.

O2B05-A1

VISUALIZATION OF RATTILING IN $PrOs_4Sb_{12}$ BY SINGLE CRYSTAL NEUTRON DIFFRACTION

Koji Kaneko,[a] Naoto Metoki,[a,b] Hiroyuki Kimura,[c] Yukio Noda,[c] Tatsuma D. Matsuda[a] and Masafumi Kohgi[d]

[a]*Advanced Science Research Center, Japan Atomic Energy Agency, Tokai, Naka, Ibaraki 319-1112, Japan;* [b]*Department of Physics, Tohoku University, Sendai 980-8578, Japan;* [c]*Institute of Multidisciplinary Research for Advanced Materials, Tohoku University, Sendai 980-8577, Japan;* [d]*Department of Physics, Tokyo Metropolitan University, Hachioji 192-0397, Japan;*

Recently, skutterudite compound $PrOs_4Sb_{12}$ was reported to be the first Pr-based heavy fermion superconductor with T_{sc}=1.85 K. Since the ground state is the non-magnetic singlet, the mechanism for the formation of heavy quasiparticles and unconventional superconductivity attracts considerable interest. The first excited triplet state close to the ground state is a suggestive of the important role of orbital degree-of-freedom in $PrOs_4Sb_{12}$, which is supported by the existence of field-induced antiferroquadrupolar ordered phase. Furthermore, since Pr ion is weakly bounded in the Sb icosahedron cage with relatively large Pr-Sb distance, the importance of *"rattling"*, large thermal vibration of Pr, and the possible existence of off-center potential minima are also discussed in connection with the emergence of superconductivity. A combination of the single crystal neutron diffraction and the analysis with using maximum entropy method (MEM) offers an ability to unveil rattling motion of Pr in $PrOs_4Sb_{12}$ without any specific model. A space-, time-averaged nuclear density distribution reflecting a thermal vibration can be obtained by a MEM analysis. The results unveil a widely spread anisotropic Pr distribution in the Sb cage at room temperature. The Pr density has a flat, trapezoidal distribution in the real space, where the width reaches roughly 0.6 Å in the full width at half maximum (FWHM). In contrast, the Pr nuclear density distribution at 8 K becomes sharp, almost isotropic and gaussian-form, although the width of 0.15 Å in FWHM is roughly twice broader than those for Os and Sb. Note that the highest density of Pr distribution at 8 K founds at the center of the cage within an experimental accuracy. These features are far from the simple harmonic model, namely, the present result suggests the strong anharmonicity for the Pr potential in the Sb cage.

O2B05-A2

SINGLE CRYSTAL NEUTRON DIFFRACTION INVESTIGATIONS OF TYPE I CLATHRATES – POTENTIAL THERMOELECTRIC MATERIAL

Mogens Christensen[1], Bo B. Iversen[2].

[1]Bragg Institute, ANSTO, Lucas Heights, Australia; [2]Department of Chemistry, University of Aarhus, Aarhus, Denmark

Inorganic clathrates with type I structure are potential thermoelectric materials. One of the key properties is an extremely low lattice thermal conductivity. Despite the perfect crystallinity of the type I clathrates they conduct heat like a glass. The low thermal conductivity can be related to guest atom inclusions in a host structure. The clathrate structure is shown in Figure 1, where the cage structure is shown by polygons.

We have investigated various clathrates type I using single crystal neutron diffraction and resonant synchrotron X-ray diffraction [1]. The guest atom siting in the host structure has been investigated. Multi-temperature diffraction data has been measured to reveal dynamic properties of the clathrates by modelling the atomic displacement parameters. The investigations have revealed a important host-guest interaction in the clathrates. The host-guest coupling appears to be responsible for off-centring of the guest atom and thereby causing disorder of the guest atom. This in turn leads to the low thermal conductivity.

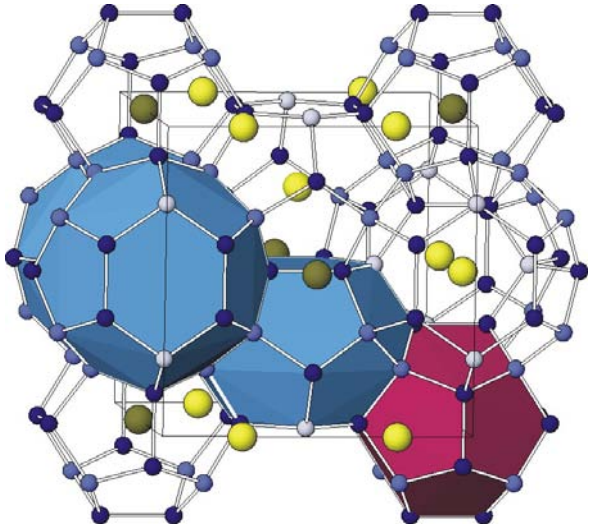

Figure 1: The clathrate type I structure.

Reference:

[1] M. Christensen, *et al.*, 2006 *J. Am. Chem. Soc.* **128** 15657-65

O2B05-A3

X-RAY SCATTERING STUDY OF RB_4

Ki Bong Lee,[a] S. Ji,[a] C. Song,[a] J. Koo,[a] Y. J. Park,[b] J. Y. Kim[c] and B. K. Cho[c]

[a]eSSC and Department of Physics; [b]Pohang Accelerator Laboratory, POSTECH, Pohang 790-784 Korea;[c]Department of Materials Science and Engineering, GIST, Gwangju 500-712 Korea

RB_4's manifest very rich interesting phenomena originating from spin-, orbital- and lattice orderings at low-temperature. Since resonant x-ray scattering (RXS) is sensitive to them, it provides a unique opportunity to study them at the same time. RXS measurements were performed on GdB_4 and DyB_4 single crystals.

GdB_4 with isotropic Gd 4*f* shells shows only antiferro-type spin orderings at low temperature while DyB_4 with anisotropic Dy 4*f* shells shows both spin- and quadrupolar orderings. From analyses of azimuthal angle dependences of RXS signals and their polarizations at different x-ray energy, we were able to identify peaks corresponding to magnetic ordering, quadrupolar ordering and structural anisotropic tensor susceptibility (ATS) scattering, which demonstrates the potential of RXS as a powerful spectroscopic probe with additional selection rules. Moreover, a coupling between quadrupolar order and strain, which has not been experimentally verified for decades, was directly demonstrated in DyB_4 by observing that the two order parameters are proportional to each other. The details of the experiments and analyses will be presented.

O2B05-A4

HYDROGEN BONDING PHASE TRANSITIONS IN SOME ORGANIC CRYSTALS

Hoong-Kun Fun,[a] Beck-Sim Lee[a] and Suchada Chantrapromma[b]

[a] *X-ray Crystallography Unit, School of Physics, Universiti Sains Malaysia, 11800 USM, Penang, Malaysia.* [b] *Department of Chemistry, Faculty of Science, Prince of Songkla University, Hat-Yai, Songkhla 90112, Thailand.*

Our study of solid state hydrogen bonding in phenol-amine adducts and benzoic acid-amine adducts has lead us to discover a new type of phase transition (Fun-Anwar-Suchada Transition or abbreviated as FAST) which we attribute to originate from hydrogen bonding. Some crystals of the phenol-amine adducts and benzoic acid-amine adducts undergo a distortive reversible temperature-dependent phase transition. In those crystals the structural phase transition is sometimes from orthorhombic-to-monoclinic ; from monoclinic-to-triclinic ; and from triclinic to triclinic. We have identified and clarified the primary order parameter of these structural phase transitions and a phenomenological Landau theory of ferroelastic phase transitions was developed which was shown to be consistent with the experimental data on the temperature dependence of the unit cell parameters [1, 2].

As is well known, the phenomenological theory, being a macroscopic theory, cannot describe the microscopic interactions causing the phase transition, although it certainly does play an important role in identifying the primary order parameter and giving insight into the overall qualitative thermodynamic behaviour of the transition.

A microscopic theory [3], formulated through a mean field calculation of the thermodynamic behaviour using a variational method, was able to explain the main features of the phase transition, in agreement with the Landau theory of ferroelastic phase transitions. The essential physical mechanism proposed in the microscopic theory is that the interactions of the hydrogen bonds with phonons induce indirect long range interactions between the hydrogen bonds. The cooperative interactions between the hydrogen bonds drive the structural phase transition.

The experimental and theoretical aspects of FAST shall be explained in this talk.

References:

1. H. -K. Fun, A. Usman, S. Chantrapromma, J. Osman, L.-H. Ong, D. R. Tilley & Y. Ishibashi. Phase transitions in hydrogen-bonded phenol-amine adducts: analysis by ferroelastic theory. Solid State Comm. 2003. 127, 677-682.

2. H. –K. Fun, Mohd Mustaqim Rosli, Beck-Sim Lee, Lye-Hock Ong, Suchada Chantrapromma. First order temperature-dependent phase transition of hexamethylenetetraminium 3,5 dinitrobenzoate hemihydrate crystal: Landau phenomenological theory approach. *Journal of Molecular Structure* 2007. 837, 132-141.

3. P. -T. How, B. -S. Lee, H. -K. Fun, I. A. Razak, S. Chantrapromma. Microscopic theory of phase transitions in hydrogen-bonded phenol-amine adducts. Phys. Rev. B. 2005. 71, 174109.

O2B05-A5

DIFFRACTION STUDIES OF RELATION BETWEEN HELICITY OF CYCLOID MAGNETISM AND FERROELECTRIC POLARIZATION IN MULTIFERROIC MANGANESE OXIDES

Taka-hisa Arima,[a,b] Hajime Sagayama,[a] Nobuyuki Abe,[a] Koji Taniguchi,[a] Hiroyuki Ohsumi,[b,c] Masato Matsuura,[d] Kazuma Hirota,[d] Daisuke Okuyama,[e] Yuichi Yamasaki,[f] and Yoshinori Tokura[e,f]

[a]Institute of Multidisciplinary Research for Advanced Materials, Tohoku University, Japan; [b]SPring-8 Center, Harima Institute, RIKEN, Japan; [c]Japan Synchrotron Radiation Research Institute, Japan; [d]Institute of Solid State Physics, University of Tokyo, Japan; [e]ERATO Multiferroic Project, Japan Science and Technology Agency, Japan; [f]Department of Applied Physics, University of Tokyo, Japan

Since Kimura et al. discovered the polarization flop in $TbMnO_3$ induced by the application of a magnetic field, the interplay between magnetic ordering and ferroelectric polarization in multiferroics has become of great interest. Extensive studies have successively indicated that the cycloid-type spin ordering should produce ferroelectric polarization through the inverse effect of Dyaloshinski-Moriya (DM) interaction. If the inverse DM effect would play an essential role in the ferroelectric polarization of such cycloid magnets, the direction of polarization should be associated with the helicity of the cycloid.

Spin-polarized neutron technique is the most powerful probe into the helicity of spiral magnets. We have carried out a spin-polarized neutron diffraction study on $TbMnO_3$ by using a triple-axis neutron spectrometer PONTA at JRR-3, Japan. The experimental result clearly demonstrates the anticipated connection between the ferroelectricity and cycloid. We also performed an x-ray magnetic scattering study at SPring8, Japan, to reveal the spin helicity in $DyMnO_3$.

O2B05-A6

ANOMALOUS STRUCTURAL PHASE TRANSITION ABOVE LIQUID NITROGEN TEMPERATURE IN THE MULTIFERROIC PEROVSKITE $Dy(Mn_{0.5}Fe_{0.5})O_3$

Fu-Kuo Chiang (蔣復國)[1,2,3], Fei-Ting Huang (黃妃婷)[1,2,4], and Ming-Wen Chu (朱明文)[1]

[1]*Center for Condensed Matter Sciences, National Taiwan University*

[2]*Taiwan International Graduated Program, Academia Sinica*

[3]*Department of Engineering and System Science, National Tsing-Hwa University*

[4]*Department of Chemistry, National Taiwan University*

Multiferroics represent a novel class of materials whose constituent electric/magnetic orders can be manipulated by external magnetic/electric fields, i.e., the magnetoelectric coupling. Potential integration of the materials into modern memory storage media would enable an electric/magnetic control of the magnetic/electric degree of freedom, thus bringing the performance and design of the devices to a new era. The representative materials reported up to date are $TbMn_2O_5$, $TbMnO_3$ and $DyMnO_3$ perovskites, and geometrically frustrated $CdCr_2S_4$ spinel, and the origin of the multiferroic properties is still of much debate. Rare-earth orthoferrites, which have been discovered in 1960~1970's, exhibit weak ferromagnetism (canted antiferromagnetism) below 600K and a spin reorientation transition at low temperature. Among them we are particularly interested in $DyFeO_3$ (space group *Pbnm*) that is the only orthoferrite undisputedly undergoing a spin transition from Γ_4 (Fz) to Γ_1 (0) at 36K. We investigate the effects of Dzyaloshinksii-Moriya interaction according to the canted antiferromagnetism in $DyFeO_3$ and incommensurate antiferromagnetism in $DyMnO_3$ (space group *Pbnm*) and report a possible ferroelectricity by a systematic substitution of Fe^{3+} in $DyFeO_3$ with Mn^{3+}.

Using the soft-chemistry method, firstly we synthesized the phase-pure and stoichiometric $Dy(Mn_{0.5}Fe_{0.5})O_3$ perovskite in the form of powders. The subsequent X-ray powder diffraction of the material at room temperature, performed on **NSRRC BL01C2**, indicates an increase (decrease) in the *b*-axis (*c*-axis) lattice parameter with respect to the parent phase. In contrast, the *a*-axis is little affected by the substitution, suggesting that the complex orbital-lattice coupling occurs principally within the *bc*-plane. The X-ray powder diffraction at low temperatures further revealed the onset of several satellite peaks at 120 ± 2 K, and the intensity of these peaks increases monotonically with the decrease in temperature, reaching the maximum at 90 ± 2 K. Below ~90 K, the intensity of these peaks decreases and

O2C05-A1

SINGLE CRYSTAL STRUCUTURE ANALYSIS OF PHOTO-EXCITED STATES OF HALOGEN-BRIDGED DICOPPER(I) COMPLEXES

Yoshiki Ozawa,[a] Shingo Yoshida,[a] Nobuyuki Kitayama,[a] Minoru Mitsumi,[a] Koshiro Toriumi,[b] Kiyoshi Tsuge, [b] Hiromi Araki, and [b] Yoichi Sasaki

[a] *Graduate School of Material Science, University of Hyogo, Hyogo, 678-1297 Japan*
[b] *Graduate School of Science, Hokkaido University, Sapporo, 060-0810 Japan.*

Photo-luminescent halogen-bridged dicopper(I) complexes $[Cu_2X_2(PPh_3)_2(L)]_\infty$ (L= 4,4'-bipyridine or pyrazine, X = I or Br) consist of $\{Cu_2X_2\}$ planer units, which are bridged by diimine (L) ligands constructing infinite 1-D chain structures [1]. The assignments of intense emission bands of these halogen-bridged oligo-cupper(I) compounds are complicate because weak interacted multi-copper centered (CC) transition states are often concurrent with common Cu(I) to ligand charge transfer (MLCT) states. We have tried to observe direct geometrical distortion of the complex by photo exited state crystallographic technique in order to figure out these emission natures. We also have made the same experiments for discrete dimeric copper(I) complexes $[CuI_2(PPh_3)_2(L')]_2$] (L' = phenylpyridine, pyrazine) having similar metal-organic frameworks which show less luminescent performance.

Single crystal X-ray diffraction experiments were performed by using the low temperature vacuum X-ray camera at SPring-8 BL02B1 beamline. Full intensity data of both under light irradiated by CW laser (442nm or 488nm) and non-irradiated conditions were collected by multiple-exposure IP method. Photo-difference Fourier syntheses for the irradiation show that a small portion of two Iodine atoms shift toward close to each other in the $\{Cu_2I_2\}$ plane. Two Cu atoms tend to shift slightly apart from each other. Results of the least-square refinements of I and Cu atom positions based on the response ratio[2] show that there are 1.1 % excited-state species in the crystal in which the I···I distance (3.82(2)Å) is contracted from the ground states (4.41(1)Å). While in the case of the discrete dimer complex $[CuI_2(PPh_3)I(pyz)_2]$, two iodine atoms tend to move out of the $\{Cu_2I_2\}$ plane with opposite direction each other. This indicates that the $\{Cu_2I_2\}$ framework rotates around an axis containing two Cu atoms. This variety of the motions of $\{Cu_2I_2\}$ frameworks will be concerned with the geometry of the frame at the ground state and solid-state luminescent properties. Details of the relationship between optical properties and excited state molecular geometries will be discussed.

Reference:

[1] H. Araki, K. Tsuge, Y. Sasaki, S. Ishizaka and N. Kitamura, *Inorg. Chem*., **2005**, *44*, 9667-9675.

[2] Y. Ozawa, M. R. Pressprich and P. Coppens, *J. Appl. Cryst.*, **1998**, *31*, 128-135.

O2C05-A2

INVESTIGATION OF THE PHOTOEXCITED CHARGE-TRANSFER STATE OF [AuBr(PPh_3)$_2$] BY THE MULTIPLE-EXPOSURE IP METHOD

Manabu Hoshino,[1] Hidehiro Uekusa,[1] Shintaro Sonoda,[1] Takuhiro Otsuka,[1] Youkoh Kaizu,[1] Yoshiki Ozawa,[2] Koshiro Toriumi[2]

[1]*Department of Chemistry and Materials Science, Tokyo Institute of Technology, Tokyo, Japan;* [2]*Graduate School of Material Science, University of Hyogo, Hyogo, Japan*

Three-coordinated gold(I) complexes, [AuX(PPh_3)$_2$] (X= Cl, Br, I), show strong uminescence, of which application to the EL materials is expected. The origin of emission is suggested to be related with molecular structural change by photoexcitation. However, three-dimensional structure in the photoexcited state of these complexes is not clear yet. In our previous study of [AuCl(PPh_3)$_2$], photo-induced structural change was observed as shrinkage of all metal – ligand bonds. In this study, the change of electron density distribution of [AuBr(PPh_3)$_2$] (scheme) by photoexcitation was investigated by using the accurate diffraction method, multiple-exposure IP method on the low-temperature vacuum X-ray camera at SPring-8 BL02B1.

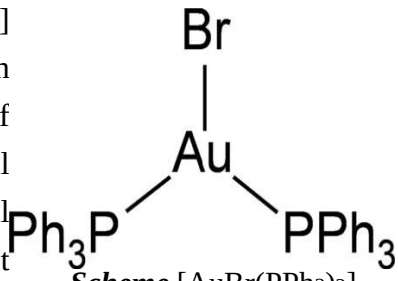

Scheme [AuBr(PPh_3)$_2$]

Diffraction intensity data at the light-on and -off stages were collected in the same IP frame by the multiple-exposure IP method. Difference Fourier synthesis on the Fo values of light-off and -on stages ($F_{o(on)} - F_{o(off)}$) showed that charge transfer from the Br atom to the Au atom (halide-to-metal charge-transfer; XMCT) was occurred by photoirradiation (shown in Figure). The results of DFT calculation on triplet excited state of [AuBr(PPh_3)$_2$] also suggest generation of the photoexcited XMCT state. Although the complexes have similar structure, the difference in the character of excited states between [AuCl(PPh_3)$_2$] (bonds shrinkage) and [AuBr(PPh_3)$_2$] (XMCT) can explain the emission color difference (λ max = 520 nm and λ max = 460 nm, respectively).

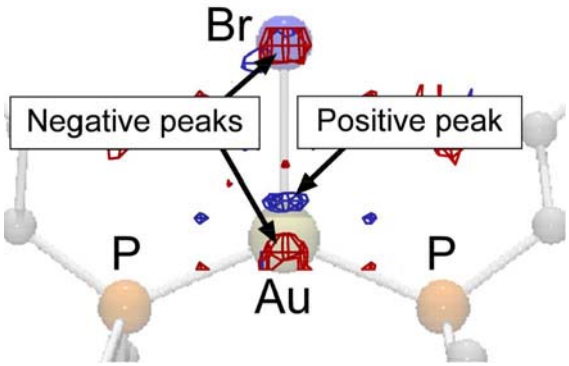

Figure $F_{o(on)} - F_{o(off)}$ map of [AuBr(PPh_3)$_2$]

O2C05-A3

X-RAY ATOMIC ORBITAL ANALYSIS AND ITS APPLICATION TO RARE-EARTH CRYSTALS

Kiyoaki Tanaka,[a] Ryoko Makita,[a] Shiro Funahashi,[a] Takashi Komori,[a,b] Terutoshi Sakakura[a]

[a]*Graduate school of engineering Nagoya Institute of Technology, Nagoya, Japan;* [b]*Toyota Industries Cooperation, Kariya, Japan*

The 4f-electron density distribution in MB_6 (M=La, Ce, Sm) has been investigated successfully by the X-ray Atomic Orbital analysis (*XAO*) with the program *QNTAO*. The quantum mechanical and crystallographic framework of it are presented.

It is the method based on the atomic orbitals (AO) and all the atoms in the unit cell are divided into the groups of sub-shell electrons (s/p/d/f). Each AO in the crystal field is expressed as a linear combination of sub-shell basis functions such as d_{xy}, d_{yz} etc. The starting set of AO's are calculated for a single electron in the crystal field. The expansion coefficients are determined by the least-squares method keeping the ortho-normal relationship between the AO's. In the multi-electron system, the wave function is expressed in terms of a linear combination of the anti-symmetric Slater determinants and the system splits into atomic terms. The d^3 system in the O_h crystal field with $t_{2g}^2e_g^1$ configuration for example has ten atomic terms but the X-ray scattering factors of them always keep the contributions of the t_{2g} and e_g electrons 2 to 1. X-ray diffraction cannot specify the atomic terms. However this ensures on the sound quantum mechanical bases that the AO's calculated for the single valence electron are effective. Since the electron population on each AO cannot be measured by spectroscopy, those measured by the X-ray diffraction is very important. Each group of the electrons in the same sub-shell is treated as a pseudo-atom, which enables us to get the electron population of each AO keeping the electro-neutrality of the unit cell and trace the electron transfer among the AO's as shown in CeB_6 at low temperature.

However the XAO analysis has two limitations. First it neglects the electron correlations. The non-integer occupation number of each AO may reflect it. Second it is based on the AO models and does not explain two-center electrons which appear in the molecular orbital models. Therefore it is applied best to ionic crystals especially to the systems with highly localized d and f electrons including the compounds with a non-stoichiometric structure.

The XAO analyses for 4f-EDD have given fruitful results. In CeB_6 the electrons are transferred from Ce to B_6 at low temperature but they are back donated to Ce 5d orbitals not to 4f orbitals at 430 and 535 K accompanying the inversion of 4f energy levels, which is reflected to the obtained electron population on each AO. The 5d occupation was also found in Lab_6 and SmB_6 accompanying the change of the 4f energy levels.

O2C05-A4

STRUCTURES OF POLYPYRIDINE MONONUCLEAR IR(III) COMPLEXES IN THE CLOSED-SHELL SINGLET AND TRIPLET STATES

Naokazu Yoshikawa,[a] Shinichi Yamabe,[b] Nobuko Kanehisa,[c] Yasushi Kai,[d] Hiroshi Takashima,[a] and Keiichi Tsukahara[a]

[a]Department of Chemistry, Nara Women's University; [b] Department of Chemistry, Nara University of Education y; [c]Division of Electrical, Electronic and Information Engineering, Osaka University.[d]Department of Environmental and Biotechnological Future Engineering, Fukui University of Technology

Structures of eight Ir^{3+} centered polypyridine complexes were determined by density functional theory calculations. The crystal structure of $[IrCl(bpy)(terpy)](PF_6)_2$ was obtained by the X-ray diffraction study, where bpy is 2, 2'- bipyridine and terpy is 2,2':6',2"-terpyridine. The computed geometries are in good agreement with the experimental ones. Those in the triplet biradical states were also determined to evaluate the singlet–triplet energy differences. These differences correlate well with wavelengths of the emission spectra. The geometric changes, free tolyl ligand → the Ir^{3+} complexed ligand → the ligand in the triplet biradical, were examined. It was found that one not two large-conjugated polypyridine ligand with spin delocalizable substituents may give efficient phosphorescence to explore the LED device.

O2C05-A5

APEX II ULTRA - PRECISION AND ACCURACY

Michael Ruf[a], Martin Adam[b],

[a]Bruker AXS Inc., 5465 East Cheryl Parkway, Madison,WI, USA,.[b]Bruker AXS B.V, Oostsingel 209, 2612 HL Delft, The Netherlands.

The APEX II ULTRA is Bruker's top of line crystallographic instrumentation for chemical crystallography. The system combines the most sensitive CCD detector with the brightest Molybdenum source and the most advanced multilayer optics available in a very compact format.

The rotating anode is so compact that it can be mounted on the goniometer, setting new standards in ease and stability of alignment. A very small focal spot combined with the HELIOS optics produce a small high flux beam of only 150 micrometer which can increase integrated intensities from small crystals by a factor of 60 compared to standard sealed tube systems. The APEX II ULTRA's ingenious design allows for a variable beam size with constant flux which allows changing the beam size to 360 micrometer within minutes without changing expensive component.

This presentation will introduce the instrumentation and present examples of charge density studies, data collected on very small crystals and powder diffraction experiments focusing on aspects of precision and accuracy in crystallographic experiments.

O3A06-M1

FLUORESCENCE-DETECTION SIZE EXCLUSION CHROMATOGRAPHY FOR PRECRYSTALLIZATION SCREENING OF INTEGRAL MEMBRANE PROTEINS

Toshimitsu Kawate[a], Atsuko Yamashita[b], Jaysankar Jasti[a], Michael Rosconi[a], Paul Shaffer[a], Alexander Sobolevsky[a], Tanja Homrichhausen[a] and Eric Gouaux[a,c]

[a]The Vollum Institute at Oregon Health and Science University, Portland, USA ;[b]Structural Physiology Research Group, RIKEN Spring-8 Center, Japan ;[c]Howard Hughes Medical Institute, USA.

Formation of well ordered crystals of membrane proteins is a bottleneck for structure determination by x-ray crystallography. Nevertheless, one can increase the probability of successful crystallization by precrystallization screening, a process by which one analyzes the monodispersity and stability of the protein-detergent complex. Traditionally, this has required microgram to milligram quantities of purified protein and a concomitant investment of time and resources. Here we show a rapid and efficient precrystallization screening strategy in which the target protein is covalently fused to green fluorescent protein (GFP) and the resulting unpurified protein is analyzed by fluorescent-detection size exclusion chromatography (FSEC). This strategy requires only nanogram quantities of unpurified protein and allows one to evaluate localization and expression level, degree of monodispersity, and approximate molecular mass. We have applied this screening strategy to six different integral membrane proteins and found promising target proteins for crystallization. We find that the probability of obtaining a well-behaved protein is about one in twenty, and most importantly, all of such "hits" have been successfully crystallized. In this talk, I show the application of this precrystallization screening to integral membrane proteins derived from prokaryotic or eukaryotic organisms.

O3A06-M2

ION BINDING AND SELECTIVITY OF THE ROTOR OF THE V-TYPE NA^+-ATPASE FROM *ENTEROCOCCUS HIRAE*

Takeshi Murata[1,2,3], Ichiro Yamato[4], Yoshimi Kakinuma[5], Mikako Shirouzu[3], John E. Walker[6], Shigeyuki Yokoyama[3] and So Iwata[1,2,3]

[1]Department of Cell Biology, Faculty of Medicine, Kyoto University, Japan, [2]Japan Science and Technology Agency, ERATO, Iwata Human Receptor Crystallography Project, Kyoto, Japan, [3]Protein Research Group, RIKEN Genomic Sciences Center, Yokohama, Japan, [4]Department of Biological Science and Technology, Tokyo University of Science, Noda, Japan, [5]Faculty of Agriculture, Ehime University, Matsuyama, Japan, [6]Medical Research Council Dunn Human Nutrition Unit, Hills Road, Cambridge, United Kingdom

In eukaryotic cells, vital processes such as protein trafficking, endocytosis, neurotransmitter release and intracellular pH regulation, depend on the movement of ions across membranes by vacuolar- or V-ATPases, multisubunit complexes related to the F-ATPases (ATP synthetases) found in eubacteria, mitochondria and chloroplasts. Both classes have globular catalytic domains, V_1 and F_1, where ATP is hydrolysed (or synthesized), attached by central and peripheral stalks to intrinsic membrane domains, V_o and F_o, where ions are pumped across the membrane. ATP hydrolysis generates rotation of the central stalk and an attached membrane ring of hydrophobic subunits. Ions are pumped through a pathway in the interface between the rotating c ring and subunit a as a static membrane component, which is linked to the outside of the V_1 or F_1 domain by the peripheral stalk.

V-type Na^+-ATPase of *Enterococcus hirae* transports Na^+ as well as Li^+ ions rather than protons under physiological conditions. Here, we report ion binding/release properties of the rotor ring of this enzyme. The purified K-ring in detergent bound one Na^+ ion per K-monomer with high affinity ($K_{D(Na^+)}$ = 12 μM). The $^{22}Na^+$ binding to K-ring was inhibited by Li^+ (K_i = 48 μM) or H^+ (K_i = 3.4 μM: pH 5.5) competitively but not by K^+, Tl^+, Rb^+, Cs^+, Mg^{2+} or Ca^{2+}, suggesting that the ion binding pocket in the K-ring accommodates only Na^+, Li^+ or H^+. The structure of the K-ring in the presence of Li^+ resolved at 2.8 Å suggested that Li^+ ion is bound to the specific binding pocket surrounded by five oxygen atoms like as Na^+ in the Na^+ bound K-ring structure (T. Murata *et al*., 2005, Science, 308, 654-659) with slight different distances between the cation and oxygens. Association and dissociation rates of the $^{22}Na^+$ to and from the rotor ring were extremely slow (k_{on} = 1 x 10^2 [$M^{-1}S^{-1}$], k_{off} = 1 x 10^{-3} [S^{-1}]) when compared with the rates of enzyme activity of the purified whole complex in detergent, consistent with the model that Na^+ binding/release reaction for transport of the V-ATPase is accomplished at the interface between I-subunit and K-ring during rotation. From these results, we discuss about ion selectivity and ion transport mechanism of the *E. hirae* V-ATPase.

O3A06-M3

X-ray structure of bovine heart cytochrome c oxidase

H. Aoyama[a*], T. Tsukihara[b] and S. Yoshikawa[c]
[a]Graduate School of Pharmaceutical Sciences, *Osaka University,*
[b]*Institute for Protein Research, Osaka University*,
[c]*Department of Life Science, University of Hyogo.*

Cytochrome c oxidase is the terminal oxidase of the cell respiration which reduces molecular oxygen(O2) to water, in a reaction coupled with a proton pumping process. Elucidation of the reaction mechanism of this enzyme is one of the most intriguing subjects in the field of bioenergetics. A mobile proton-donor functional group within a membrane protein can function as a redox-driven proton pumping site if it encounters a change in pKa and alternates accessibility between two different aqueous phases. A change in the oxidation state of a protein site can induce this alternating accessibility. These pKa and accessibility changes could be readily induced by conformational changes affecting the environment of the proton pumping site. Reliable methods other than X-ray structural analysis are not presently available for identification of these conformational changes. In other words, a high resolution X-ray structure of the enzyme is prerequisite for elucidation of the reaction mechanism. In this talk, recent progress in investigations of X-ray structure of the enzyme will be presented.

O3A06-M4

STRUCTURE OF THE CYTOCHROME b_6f COMPLEX: QUINONE ANALOGUE INHIBITORS AS LIGANDS OF HEME c_n

Eiki Yamashita[a,b], Huamin Zhang[a, c], William A. Cramer[a]

[a]*Department of Biological Sciences, Purdue University;* [c]*Aptuit, Inc., West Lafayette, IN, USA;*
[b]*Institute for Protein Research, Osaka University, Suita, Japan*

The integral-membrane cytochrome *b*6*f* complex mediates electron transfer between the photosystem II and photosystem I reaction center complexes. The electron transfer is linked to proton translocation across the membrane. Crystal structures of the b6f complex from the thermophilic cyanobacterium, *M. laminosus* [1] and the green alga, *C. reinhardtii* [2] were solved in 2003. In the crystal structures, a unique covalently bound heme, heme c_n, was found very close to heme b_n on the electrochemically negative side of the complex. Heme c_n has no amino acid side chain as an axial ligand, but has an axial H_2O that bridges heme c_n and the propionate of heme b_n. The function of heme c_n is still not understood.

The native crystal grown in the presence of Cd^{2+} of the cytochrome b6f complex from *M. laminosus* resulted in an improvement of the native structure from 3.4 Å [1] to 3.0 Å [3]. In the native structure with Cd^{2+}, two Cd^{2+} binding sites are located in each monomer. Binding sites of quinone analogue inhibitors, tridecyl-stigmatellin (TDS) and 2n-nonyl-4-hydroxy-quinoline-N-oxide (NQNO), were sought to map the transfer pathway of the lipophilic quinone across the complex [3]. Two sites were found for the chromone ring of the TDS quinone analogue inhibitor, one near the *p*-side [2Fe-2S] cluster. A second TDS site was found on the n-side of the complex facing the quinone exchange cavity as an axial ligand of heme c_n. A similar binding site as an axial ligand to heme c_n was found for the *n*-side quinone analogue inhibitor, NQNO. Binding of NQNO and TDS as axial ligands to heme c_n implies that this heme utilizes plastoquinone as a natural ligand, thus defining an *n*-side electron transfer complex consisting of hemes b_n, c_n, and plastoquinone (PQ) in the reduction pathway of the PQ pool.

Reference:

[1] Kurisu *et al.*, Science, 2003

[2] Stroebel *et al*., Nature, 2003

[3] Yamashita *et al.*, JMB, 2007

O3A06-M5

X-RAY STRUCTURE OF EmrE SUPPORTS DUAL TOPOLOGY MODEL

Yen-Ju Chen, Owen Pornillos, Samantha Lieu, Che Ma, Andy P. Chen, Geoffrey Chang

Genomics Research Center of Academia Sinica, Taiwan

EmrE, a multidrug transporter from *Escherichia coli*, functions as a homodimer of a small four-transmembrane protein. The membrane insertion topology of the two monomers is controversial. Although the EmrE protein was reported to have a unique orientation in the membrane, models based on electron microscopy (EM) and now defunct x-ray structures, as well as recent biochemical studies posit an antiparallel dimer. We have now reanalyzed our x-ray data on EmrE. The corrected structures in complex with a transport substrate are highly similar to the EM structure. The first three transmembrane helices from each monomer surround the substrate-binding chamber, whereas the fourth helices participate only in dimer formation. Selenomethionine markers clearly indicate an antiparallel orientation for the monomers, supporting a “dual topology” model.

O3B06-M1

MOMENTUM DEPENDENT CHARGE EXCITATIONS IN CORRELATED ELECTRON SYSTEMS STUDIED BY RESONANT INELASTIC X-RAY SCATTERING

Kenji Ishii

Synchrotron Radiation Research Unit (SPring-8), .Japan Atomic Energy Agency, Hyogo 679-5148, Japan

Resonant inelastic x-ray scattering (RIXS) in the hard x-ray regime is a developing experiment technique to measure charge excitations utilizing brilliant synchrotron radiation x-rays. It has a great advantage that the momentum dependence of electronic excitations can be measured unlike conventional optical method. In addition, RIXS gives element-selective excitation spectra by tuning the incident photon energy to an absorption edge of the element. There has been much activity in recent years using this technique, especially at the transition metal K-edge to study transition metal oxides.

We have applied RIXS technique to correlated electron systems, such as cuprates and manganites, in order to understand their electronic structure and underlying correlation effects. In particular, electronic structure of correlated metals is in the focus of our RIXS study, because interesting phenomena, e.g. high-Tc superconductivity in cuprates and colossal magneto resistance in manganites, occur in the vicinity of metal-insulator transition by carrier doping.

Here I would like to present our recent RIXS studies on high-Tc cuprates and related materials which were performed in close collaboration with theorists. Momentum and carrier-doping dependence of an interband excitation across the Mott gap and an intraband excitation below the gap will be discussed.

O3B06-M2

SPIN, CHARGE, AND ORBITAL ORDERING OF TRANSITION-METAL OXIDES INVESTIGATED BY RESONANT SOFT X-RAY SCATTERING

Di-Jing Huang

National Synchrotron Radiation Research Center, Hsinchu, Taiwan
Department of Physics, National Tsing Hua University, Hsinchu, Taiwan

Many phase transitions of correlated-electron materials are closely related to spin, charge, and orbital ordering. In this talk, we will present our recent studies of soft x-ray scattering on spin, charge, and orbital ordering associated with metal-insulator transition, multiferroicity, and dimensional crossover of antiferromagnetism in transition-metal oxides.

We will first address the long-lasting debate on the existence of charge ordering of Fe_3O_4 which exhibits a classic example of phase transition known as the Verwey transition. Such a transition was originally interpreted as a charge order-disorder transition. Despite intensive investigations over 60 years, the existence of charge ordering in magnetite remains controversial. Using measurements of resonant soft x-ray scattering, we report direct experimental evidence for the existence of charge-orbital ordering in magnetite [1] and the data corroborate the LDA+U prediction [2].

We will also cover antiferromagnetism and multiferroicity of $TbMn_2O_5$. Recent discovery of giant magetoelectric effects offers new opportunities of multiferroic applications. However, the lack of direct scattering evidence for the multiferroicity has limited the understanding of the microscopic mechanism behind such giant cross-coupling effects. We proffer scattering evidence for multiferroicity and a new pathway for understanding the intricate coupling between antiferromagnetism and ferroelectricity in frustrated magnets [3]. Our results set fundamental symmetry constraints on the microscopic mechanism of multiferroicity in frustrated magnets.

The final subject is dimensional crossover of antiferromagnetism in $La_{0.5}Sr_{1.5}MnO_4$ [4]. We for the first time observed quasi-2D incommensurate AF order existing at temperatures above the Neel temperature (T_N). As the temperature cools across T_N, on top of the dimensional crossover, the 2D incommensurate AF order collapses to stabilize the 3D commensurate AF order. Our results show that the spin correlation follows the same exponential growth in inverse temperature as those observed in quantum Heisenberg antiferromagnets.

Reference

[1] D. J. Huang *et al.*, Phys. Rev. Lett. **96**, 096401 (2006).
[2] H. T. Jeng, G. Y. Guo, and D. J. Huang, Phys. Rev. Lett. **93**, 156403 (2004).
[3] J. Okamoto *et al.*, Phys. Rev. Lett. **98**, 157202 (2007).
[4] K. S. Chao *et al.*, submitted to Phys. Rev. Lett.

O3B06-M3

WIGNER CRYSTALLIZATION IN A MOLECULAR CONDUCTOR, $(DI\text{-}DCNQI)_2Ag$

Hiroshi Sawa [a], Toru Kakiuchi [a], Yusuke Wakabayashi [a], and Kazushi Kanoda[b]

[a]*Photon Factory, High Energy Accelerator Research Organization (KEK), Tsukuba,*
[b]*Department of Applied Physics, the University of Tokyo, Tokyo, Japan*

Rarefied electron gas system at high temperature is homogeneous due to the large kinetic energy compared to the Coulomb repulsion among electrons. At extreme low temperatures, the system will tend to condense and make uneven lumps, as theoretically predicted in the early 1930's. Since these lumps carry a negative charge, they form a structure where they try to avoid each other in the spatial positioning. We call this phenomenon the Wigner crystallization.

A molecular conductor $(DI\text{-}DCNQI)_2Ag$ is insulating even at room temperature. Planar DCNQI molecules are piled up at even intervals along the *c* direction, composing 1D columns. Since Ag is a monovalent ion having a closed shell, they construct a quarter-filled 1D-electron band. Below 220 K, Hiraki *et al*. suggested that the $4k_F$ Wigner crystal type of charge order (CO) on DCNQI molecules arose in the low-temperature phase by NMR technique. This CO ground state was theoretically predicted by Seo *et al*. It is very interesting whether (or how) the electron crystal is stable in the real solid.

Single crystal x-ray diffraction measurements using synchrotron radiation were performed on a large warped imaging plate camera installed on beam lines BL-1A at PF, KEK. According to the result of the structural analysis, two-fold structure in ground state consists of not only charge ordering columns but also monotonic charge dimerized columns caused by geometrical frustration among DCNQI columns. This charge ordered structure is regarded as a Wigner crystal caused by inter-column Coulomb repulsion (Fig.1)[1].

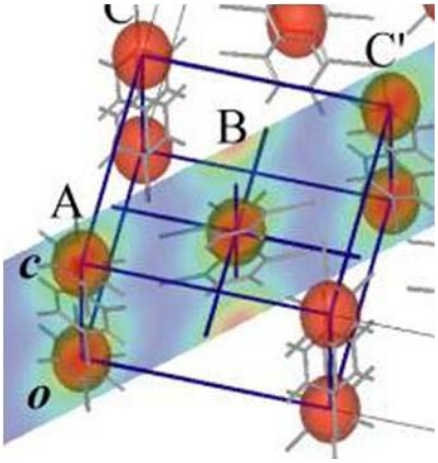

Figure.1. Three-dimensional view of the Wigner crystal-type charge arrangement and the molecules. Charge-rich areas are shown by red ellipses, forming a body-centered tetragonal lattice drawn by the blue lines.

Reference:

[1] T. Kakiuchi, et al., *Phys. Rev. Lett.*, **98** (2007) 066402.

O3B06-M4

Q-DEPENDENT DIELECTRIC FUCTION STUDIES USING INELASTIC X-RAY SCATTERING

N. Hiraoka, H. Ishii, I. Jarrige, and Y. Q. Cai,

National Synchrotron Radiation Research Center, Hsinchu, Taiwan, 300, R.O.C.

Inelastic x-ray scattering (IXS) probes the excited states of materials, like optical absorption using visible or ultraviolet photons. Optical absorption observes the excitations at the limit of zero momentum transfer ($q \rightarrow 0$), while IXS investigates the excitations as a function of q. (Non-resonant) IXS is a similar experiment to electron energy loss spectroscopy (EELS) in this sense, but it has advantages of (i) small effects of multiple scattering and (ii) a wide q range, covering several Brillouin zones. However, the scattering cross-section of non-resonant IXS is extremely small, and thus it is not a very popular method at the moment, compared with EELS or resonant IXS (RIXS). Nevertheless, it is possible to extract important information in understanding the electronic structures of solids using non-resonant IXS if one combines a high-brilliance synchrotron radiation source and optimized x-ray optics. We will discuss the following two examples.

1. **Semi-metal, graphite**: The graphite is semi-metal and only has a Fermi surface along the K-H line in the Brillouin zone (Fermi line). This fact is well-known but there are very few reports that have clearly observed the semi-metallic features. The IXS spectra that we have obtained show clear semi-metallic features, exhibiting that the energy gap repeats the opening and closing as a function of q.

2. **Strongly correlated system, NiO**: NiO is still extensively studied by various experimentalists and theorists because it is a prototype of strongly correlated systems, which still present many challenges to theoretical modelling. The IXS spectra show characteristic q-dependences of the intensities of dd (intratomic) excitations and charge transfers, corresponding to the spatial extent of these excitations.

O3B06-M5

CRYSTAL AND MAGNETIC STRUCTURE OF ORGANIC CONDUCTOR β'-ET_2ICl_2 BY USING NEUTRONS

Yukio Noda,[a] Masashi Watanabe,[a] Atsushi Matsunaga,[a] Satoshi Komiyama,[a] HiromiTaniguchi,[b] Atshushi Kawamoto[c] and Yoshiya Uwatoko[d]

[a] Institute of Multidisciplinary Research for Advanced Materials, Tohoku University, Sendai, Japan; [b] Faculty of Science, Saitama University, Saitama, Japan; [c] Graduate School of Science, Hokkaido University, Sapporo, Japan; [d] The Institute of Solid State Physics, The University of Tokyo, Kashiwa, Japan

The organic conductor β'-ET2ICl2 (here ET stands for bis(ethylenedithio)tetrathiaful-valenecoherent) transforms to a magnetically ordered phase at about 22K, presumably due to the antiferromagnetic spin ordering of π-electrons in an organic ET molecule. The characteristics of electric conductivity is semiconducting. We have performed crystal and magnetic structure analyses of β'-ET2ICl2 by using neutrons to reveal the magnetic structure. Special interest is the distribution of magnetic moment, which directly reflects the distribution of π-electrons.

A four-circle diffractometer named FONDER installed at T22 beam port of Japan Atomic Energy Agency reactor JRR3M was used. Wavelength was 1.24A and maximum 2θ angle was 115degree. For the magnetic scattering, we also used 2.40A neutrons. We have used several samples whose crystal sizes were about 1.2 x 1.6 x 10.1 mm^3 for dutarated one and 2 x 3 x 5 mm^3 for hydrogen sample. Data were taken at 12K. For the comparison, we also performed x-ray crystal structure analyses using Mo kα1 x-rays at 12K and maximum 2θ angle was 72degree. Crystal structure data are followings; T=12K, C20D16S16ICl2 , P-1, a=12.777(2), b=9.555(1), c=6.584(1), α=97.53(1), β=101.35(1), γ=87.09(1), Z=2, R(F)=0.033 for x-ray, R(F)=0.020 for neutron. Hydrogen sample gave almost the same results.

We found relatively strong new reflections at (0.5 0.5 0), (0.5 -0.5 0) and very weak ones at (0.5 1.5 0), (-0.5 1.5 0), (1.5 0.5 0) and (-1.5 0.5 0) at 7.6K. The intensity shows an order parameter behavior and vanishes at TN=23K. There were no peaks at (0.5 0 0) and (0 0.5 0). From the information of the above extinction rule, we can conclude the antiferomagnetic spin order pattern. The result is antiparallel order along [100] and [010] direction and parallel order along [110] direction. Because we performed crystal structure analysis under the same configuration and the same crystal, we had the scale factor. Thus the magnetic structure factors are taken as absolute numbers. We performed Fourier transformation to obtain the magnetic moment and π-electron distribution. The size is 10.3A along [1 -1 0] and 12.9A along [1 1 0], and this size of distribution is almost comparable with the unit cell size. We believe that the imaging of π-electron in an organic conductor might be the first case.

O3B06-M6

LATTICE DISTORTION AND FERROMAGNETISM IN $BaRuO_3$

Chao-hung Du,[a*] K. J. Tseng,[a] Y. Y. Lo, [a] Mau-Tsu Tang [b]

[a] *Department of Physics, Tamkang University, Tamsui 251, Taiwan.*

[b] *National Synchrotron Radiation Research Center, Hsinchu 300, Taiwan.*

[*] *E-mail: chd@mail.tku.edu.tw*

Studies of perovskites have stimulated research into a wide variety of unusual transition metal oxides, since the discovery of high T_C superconductors and CMR materials. It has been demonstrated that the interplay between the different degrees of freedom in perovskites can result in a very reach phase diagram, including the unusual conductivity and magnetism, charge/spin stripes, or even the phase separation phenomenon. The recently discovered layered ruthenate compounds have also been the subject of considerable study, especially for the discovery of superconductivity in Sr_2RuO_4. However, the mechanism the superconductivity in strontium ruthenates is still not clear, for example, the correlation between the dimensionality and the local moment. $BaRuO_3$ is chemically related to $SrRuO_3$, but displays different crystallographic forms. Therefore, it can be the model for understanding these issues. $BaRuO_3$ has been reported to show the unusual electrical and magnetic properties, and the pseudogap and charge-density waves (CDWs) were suggested to be the causes. The pseudogap has been observed using optical spectra, but the existence of CDWs was questioned because of lack of the experimental evidence. Using the x-ray *in-vacuum* camera on a high quality single crystal $BaRuO_3$, we located some weak spots at T= 30 K along the *c**-axis which doubles the *c**-axis of the unit cell. Further study using x-ray scattering, by measuring the peak profiles as a function of temperature, we observed that the CDW satellite reflections display a step-like transition at T≈ 80 and 50 K where the former is correspond to the formation of CDW, and the later could be caused by the lattice distortion which is related to a weak ferromagnetic transition as confirmed from susceptibility measurement.

O3C06-M1

THE AUSTRALIAN SYNCHROTRON

Julian Adams

Principal Beamline Scientist
Protein Crystallography
Australian Synchrotron

The Australian Synchrotron is a new 3rd generation synchrotron source. The initial funding covered the construction of the machine and nine beamlines.

Details of the construction, commissioning, user operations of the beamlines will be presented.

O3C06-M2

AUTOMATION AT SER-CAT: TOWARDS SIGNAL BASED DATA COLLECTION

John P. Rose[1,2], John Chrzas[1,2], James Fait[1,2], Zeng-Qing Albert Fu[1,2], Andrew Howard[2,3], John Gonczy[1,2], Zhongmin Jin[1,2] and B. C. Wang[1,2]

[1]Dept. of Biochemistry and Molecular Biology, The University of Georgia, Athens, GA, USA, [2]SER-CAT, Advanced Photon Source, Argonne National Laboratory, USA. [3]Biological, Chemical, and Physical Sciences Department, Illinois Institute of Technology, Chicago, IL, USA

With the highly optimized X-ray flux and beam quality now available at 3rd generation synchrotron sources, future improvements in overall throughput must now be directed to improving the flow and logistics of conducting crystallographic experiments and data acquisition themselves.

At SER-CAT, beamline setup, sample handling, sample alignment, data collection strategy, data collection, data reduction, structure solution and data archive have all been automated or are in the process of being automated. Building on these technologies a new data collection paradigm we term Signal Based Data Collection (SBDC) is being developed aimed at increasing the success rate of structure determination and overall beamline efficiency. The SBDC approach monitors the anomalous scattering signal present in the data (SAS or MAD), as it is being collected, to ensure that an interpretable electron map (i.e. the structure) can be produced. This approach differs from traditional data collection in that there is direct feedback from the data reduction and structure determination process to the data collection process.

The project is a partnership between structural biologists at the University of Georgia and the excellent technical staff at SER-CAT; it builds on the methodology and technology developed at both institutions over the past seven years, which if successful, could in a very real sense change the way that synchrotron X-ray diffraction data is collected, increase the productivity and cost-effectiveness of beamline operation, resulting in more and better science being produced.

Details of the implementation of various aspects of the SBDC approach will be presented.

Work is supported in part with funds from SER-CAT, the Georgia Research Alliance, the National Institutes of Health (GM62407) and the University of Georgia Research Foundation.

O3C06-M3

100-PS TIME-RESOLVED X-RAY EXPERIMENTS WITH DAILY SINGLE BUNCH MODE: CURRENT STATUS OF BEAM LINE NW14A AT THE PHOTON FACTORY ADVANCED RING

Shin-ichi Adachi[1,2], Shunsuke Nozawa[2], Ryoko Tazaki[2], Tokushi Sato[3], Ayana Tomita[3], Matthieu Chollet[3], Laurent Guérin[1], Kouhei Ichiyanagi[1], Hirohiko Ichikawa[2], Masahiro Daimon[2], Hiroshi Sawa[1], Hiroshi Kawata[1], and Shin-ya Koshihara[2,3]

[1]*Photon Factory, KEK, Japan*
[2]*Non-equilibrium Dynamics Project, ERATO, JST, Japan*
[3]*Frontier Collaborative Research Center & Department of Materials Science, Tokyo Institute of Technology, Japan*

Time-resolved X-ray experiments using synchrotron radiation sources are becoming general and powerful tools to explore structural dynamics of condensed matters in materials and biological science. NW14A is a newly constructed undulator beam line for 100-ps time-resolved X-ray experiments at the Photon Factory Advanced Ring, KEK [1]. This beam line was designed to conduct a wide variety of time-resolved X-ray measurements, such as time-resolved diffraction, scattering and X-ray absorption fine structure. Its versatility is allowed by various instruments, including two undulators, three diffractometers, two pulse laser systems and an X-ray chopper. The current status of the beam line will be presented.

Reference:

[1] Nozawa et al. (2007) *J. Synchrotron Rad.* **14**, 313-319.

O3C06-M4

DEVELOPMENT AND APPLICATION OF THE "PINPOINT STRUCTURE MEASUREMENT SYSTEM"

SUB-MICRON BEAM AND TIME-RESOLVED MEASUREMENT AT SPring-8's BL40XU

Shigeru Kimura[a,f], Nobuhiro Yasuda[a,f], Yoshimitsu Fukuyama[a,f], Jungeun Kim[a,f], Yoshihito Tanaka[b,f], Koshiro Toriumi[c,f], Yutaka Moritomo[d,f], Yoshihiro Kuroiwa[e,f], Kenichi Kato[a,b,f] and Masaki Takata[a,b,f]

[a]*JASRI/SPring-8, Hyogo 679-5198, Japan;* [b]*RIKEN SPring-8 Center, Hyogo 679-5198, Japan;* [c]*University of Hyogo;* [d]*Tsukuba University;* [e]*Hiroshima University;*[f]*CREST-JST, Saitama 332-0012, Japan*

The "X-ray Pinpoint Structure Measurement" project is a part of the CREST projects (2004-2008) funded by the Japan Science and Technology Agency (JST). It is our key project to promote the research utilization for the chemical reactions of nanomaterials and the behavior of nano-devices in operation at SPring-8. The project's architecture, basic design, and overall strategy were previously reported with the technical achievement status at the AsCA06 conference. In the report, we acknowledged the importance and difficulty of coincidentally measuring the timing and area of a structure, simultaneously with the challenge of measuring the physical and/or chemical properties in reaction, such as optical reflectivity, absorption, electric conductivity, dielectric property and etc. In addition, of particular importance is gaining a higher S/N ratio of measured data. In our presentation, we will report the progress in the application of the time-resolved diffraction experiments and its upgrading by combining with the sub-micron diffraction technique.

For photo-irradiation experiments, it has proved difficult to accurately measure the signal from the photo-induced phase due to the quite few volume ratio of pump laser penetration region compared to the entire crystallite. The sub-micron single crystal structure analysis technique, performed by applying high brilliance, focused X-ray microbeam, will overcome this limitation because the penetration depth of laser light is typically at the micrometer order. With the 100% volume penetration of the laser light, we can eliminate ambiguity over the volume ratio in photo-induced reaction. This technique also provides a breakthrough by enabling single crystal structure analysis from a single grain of powder sample.

To date, we have achieved sub-micron single crystal structure analysis with a focused X-ray microbeam and time resolved "pump and probe" experiment with 40 ps time resolution. In our presentation, we will review the present status of the project with results of the flagship research subject, the "time resolved structure analysis of crystal-amorphous phase change in DVD optical memory material".

O4A06-A1

ALANINE RACEMASE AS A TEMPLATE FOR DRUG DISCOVERY IN TUBERCULOSIS

Kurt Krause [a], Mike Benedik[b], James Briggs[c], Milya Davlieva [c], Harold Kohn [d], Joe Longtin[c], Daniel Milligan [a], Ulrich Strych [c]

[a]Department of Biochemistry, University of Otago, [b]Department of Biology and Biochemistry, University of Houston, [c]Department of Biology, Texas A&M University, [d]School of Pharmacy, University of North Carolina

Tuberculosis is the leading cause of death from infectious diseases worldwide, yet few new agents have been developed to treat it over the past two decades. As a result, academic laboratories around the world are working to accelerate anti-tuberculosis drug development. We present progress from an academic based structure-aided drug design program that is focused on the design of inhibitors of alanine racemase in *M. tuberculosis*, Because of the broad importance of alanine racemase as a prokaryotic drug target, its inhibitors would prove useful in the development of antibiotics for tuberculosis, including MDR strains, as well as other for the treatment of other pathogenic bacteria.

We will present results from recent work relating to proving the essential nature of alanine racemase in mycobacteria. We will also present data on three alanine racemase crystal structure determinations and analyze them in terms of pharmacophore development. We will review the creation of pharmacophore models that incorporate the results of molecular dynamics simulations. These pharmacophore models have been used to survey, *in silico,* chemical databases for racemase inhibitors. In our medicinal chemistry effort, the structure of cycloserine and its analogs have been used as a starting platform for structure-aided design efforts. In our drug design project we encountered first-hand the difficulties of designing inhibitors for enzymes with restricted entryways into the active sites. Possible ways to overcome this problem will be presented.

O4A06-A2

STRUCTURES OF ALL FOUR PHOSPHODIESTERASE-4 SUBFAMILIES PROVIDE INSIGHT INTO SUBFAMILY INHIBITOR SELECTIVITY

Jiwen Cai[1], Huanchen Wang[2], Ming-Sheng Peng[1], Yi Chen[1], Jie Geng[2], Howard Robinson[3], Miles Houslay[4] & Hengming Ke[2]

[1]*Structural Biology Centre, School of Pharmaceutical Sciences, Sun Yat-Sen University, Guangzhou, 510080, China*

[2] *Department of Biochemistry and Biophysics and Lineberger Comprehensive Cancer Center, The University of North Carolina, Chapel Hill, NC 27599-7260, USA.*

[3] *Biology Department, Brookhaven National Laboratory, Upton, NY 11973-5000, USA.*

[4] *Molecular Pharmacology Group, Wolfson Building, Division of Biochemistry and Molecular Biology, Institute of Biomedical and Life Sciences, University of Glasgow, Glasgow G12 8QQ, Scotland, UK.*

Phosphodiesterase-4 (PDE4) selective inhibitors have attracted much attention as potential therapeutics for treatment of both depression and major inflammatory diseases, but their practical application has been compromised by side effects. A possible cause for the side effects is similar inhibition of current inhibitors to all PDE4 subfamilies. The development of PDE4 subfamily-selective inhibitors has been hampered by lack of structure information. Here we rectify this by providing the crystal structures of the catalytic domains of PDE4A, PDE4B and PDE4D in complex with the PDE4D-selective inhibitor NVP as well as the unliganded PDE4C structure. NVP binds in the same conformation to the deep substrate pocket and interacts with the same residues. However, detailed structural comparison reveals significant conformation differences. While the active sites of PDE4B and PDE4D are mostly comparable, PDE4A shows significant displacements of the residues next to the invariant glutamine that is critical for substrate and inhibitor binding. PDE4C appears to be more distal from other PDE4 subfamilies with certain key residues being disordered. Our analyses provide novel mechanistic insight into the feasibility of developing PDE4 subfamily-selective inhibitors.

* Jiwen Cai's current affiliation is Oxford Diffraction (Hong Kong) Ltd. Rm 1303, 13/F, Kwai Hung Holdings Centre, 89 King's Rd. North Point, Hong Kong.

O4A06-A3

STRUCTURAL BASIS FOR RECRUITMENT OF TANDEM HOTDOG DOMAINS IN ACYL-COA THIOESTERASE 7 AND ITS ROLE IN INFLAMMATION

Jade K. Forwood, Anil S. Thakur, Gregor Guncar, Mary Marfori, Dmitri Mouradov, Stuart Kellie, David A. Hume, Thomas Huber, Jennifer L. Martin, Bostjan Kobe

School of Molecular and Microbial Sciences and Institute for Molecular Bioscience, University of Queensland, Brisbane, Australia.

As part of our program on high-throughput crystallography of macrophage proteins, we have carried out a comprehensive structural and functional characterisation of mouse acyl-CoA thioesterase 7 (Acot7). Acots catalyse the hydrolysis of fatty acyl-CoA to free fatty acid and coenzyme A and thereby regulate lipid metabolism and cellular signalling. While prokaryotic homologues possess a single thioesterase domain, mammalian Acot7 contains a pair of domains in tandem. We determined the crystal structures of both the N- and C-terminal domains (1.8 and 2.5 Å resolution, respectively) of the mouse enzyme, and the structure of the full-length enzyme using a combination of chemical crosslinking, mass spectrometry, and molecular modelling. The novel quaternary arrangement features a trimer of hotdog fold dimers. We show that both domains of Acot7 are required for activity, that only one of two possible active sites in the dimer is functional, and identify Asn24 and Asp213 (from N- and C-domains, respectively) as the catalytic residues through site-directed mutagenesis. We also designed an enzyme with higher activity than wild-type Acot7 by mutating the residues in the non-functional active site. Because Acot7 shows the highest activity towards arachidonoyl-CoA (a precursor of eicosanoids), is highly expressed in macrophages and upregulated by pro-inflammatory factors, and its over-expression in macrophages alters the production of prostaglandins D2 and E2, we propose a role in inflammatory processes. Together, our results provide a foundation to relate the molecular and cellular functions of Acot7 in macrophages and other mammalian tissues.

Forwood JK, Thakur AS, Guncar G, Marfori M, Mouradov D, Meng W, Robinson J, Huber T, Kellie S, Martin JL, Hume DA and Kobe B (2007). Structural basis for recruitment of tandem hotdog domains in acyl-CoA thioesterase 7 and its role in inflammation. Proc Natl Acad Sci USA 104: 10382-10387

O4A06-A4

THROUGH-PUT PROTEIN STRUCTURE DETERMINATION AND RATIONAL STRUCTURE-BASED DRUG DESIGN USING FRAGMENT-BASED APPROACH

Tej P. Singh, Sanjit Kumar, Pradeep Sharma, Rafia Mir, Ishfaq A. Sheikh, Amit K. Singh, R. Prem Kumar, Mau Sinha, Nagendra Singh, Punit Kaur, A. Srinivasan and S. Sharma

Department of Biophysics, All India Institute of Medical Sciences, New Delhi-110 029, India (tps_aiims@hotmail.com)

Discovering and developing new medicines is a long and expensive process. Any new compound must not only produce the desired response with minimal side effects but also be demonstrably better than existing therapies. The conventional methods are slow, expensive and full of uncertainties. The conceptual breakthrough that a drug may have a specific target at the macromolecular level has benefited the drug development process profoundly. The recent phase in drug design has utilized the knowledge of the three-dimensional structures of the target molecules. In order to develop potent anti-inflammatory agents, we have used three potential macromolecular targets of the inflammatory pathway. Phospholipase A_2 (PLA_2), cyclooxygenase (COX-1 and COX-2) and lipoxygenase (LOX) are the three main enzymes that catalyze the cascade which produces pro-inflammatory compounds. From the experimental observations at the atomic level of how inhibitors bind to these targets, specific interactions that are important in molecular recognition were inferred. We have determined the crystal structures of several isoforms of native enzymes, their complexes with substrate analogues, natural ligands, known anti-inflammatory agents and designed compounds. In order to obtain potent drugs by keeping in mind the Lipinsky's rule of five, we have designed more than one ligand (fragments) to saturate the binding sites of these targets. The structures of ternary complexes with two different ligands occupying the non-overlapping sites in the substrate binding domain have shown that the potential of fragment-based design is enormous. Since every tight inhibitor due to its size may not be a drug, the combination of smaller fragments should be a better choice.

O4A06-A5

D- STRUCTURAL BASIS FOR GLUTAMATE RACEMASE INHIBITION

Kook-Han Kim[a], Young-Jong Bong[a], Joon Kyu Park[a], Key-Jung Shin[a], Kwang Yeon Hwang[b] and Eunice EunKyeong Kim[a]

[a]Life Sciences Division, Korea Institute of Science and Technology, 39-1 Hawolkok-dong, Sungbuk-gu, Seoul 136-791, Korea; [b], College of Life Sciences and Biotechnology, Korea University, Seoul, Korea

Glutamic acid is a required biosynthetic building block for peptidoglycan, and the enzyme glutamate racemase(GluR) catalyzes the inter-conversion of D- and L-glutamate enantiomers. Therefore, GluR is considered as an attractive target for the design of new antibacterial drugs. Here we report the crystal structures of GluR from *Streptococcus pyogenes* in both inhibitor free and inhibitor bound forms. The inhibitor free GluR crystallized in two different forms and they diffracted to 2.25 Å and 2.5 Å resolution, while the inhibitor bound crystal diffracted to 2.5 Å resolution. GluR is composed of two domains of α/β protein that are related by pseudo-2-fold symmetry and the active site is located at the domain interface. The inhibitor, γ-2-naphthylmethyl-D-glutamate, which was reported earlier as a novel potent competitive inhibitor, makes several hydrogen bonds with protein atoms, and the naphthyl moiety is located in the hydrophobic pocket. The inhibitor binding induces a disorder in one of the loops near the active site. In both crystal forms GluR exists as a dimer and the interactions seen at the dimer interface are almost identical. This agrees well with the results from gel filtration and dynamic light scattering.

O4A06-A6

CRYSTAL STRUCTURE OF ABT-737 IN COMPLEX WITH Bcl-x_L

Peter E. Czabotar[1], Erinna F. Lee[1], Brian J. Smith[1], Kurt Deshayes[2], Kerry Zobel[2], W. Douglas Fairlie[1], Peter M. Colman[1]

[1]The Walter and Eliza Hall Institute of Medical Research, Melbourne, Australia; [2]Genentech Inc, San Francisco, USA

ABT-737 is a recently described compound that has commanded interest as a potential cancer therapeutic. Discovered by Abbott laboratories, it targets pro-survival members of the Bcl-2 family of proteins, specifically Bcl-x_L, Bcl-w and Bcl-2, but does not bind to Mcl-1. These proteins inhibit programmed cell death and are over expressed in many cancer cells thus making them refractory to established cancer therapeutics. Inhibition of these proteins by ABT-737, or a similarly acting compound, is seen as a promising strategy for enhanced killing of cancer cells.

We have solved the crystal structure of ABT-737 in complex with Bcl-x_L. Although a number of NMR-derived structures have been described, this is the first reported x-ray structure for any Bcl-2 family member in complex with an organic ligand. The structure demonstrates that ABT-737 targets a hydrophobic groove on the surface of Bcl-x_L. The biological ligands for this groove are the BH3 domains of the pro-apoptotic members of the Bcl-2 family, for example Bim. We have performed saturation mutagenesis on the residues of Bim that are mimicked by ABT-737. In conjunction with our structure these data provide important insights into the design of BH3 mimetics with selective binding profiles for the Bcl-2 family of proteins.

O4B06-A1

MOLECULAR BRICKS, PENS, GRIDS AND SPHEROIDS FROM DIHETEROAROMATIC HOSTS

Roger Bishop, Solhe F. Alshahateet, Jason Ashmore, Donald C. Craig and Marcia L. Scudder

School of Chemistry, The University of New South Wales, Sydney, Australia

.

Halogenated diheteroaromatic molecules are V-shaped compounds designed to behave as lattice inclusion hosts that lack the ability to use strong hydrogen bonding in their crystal structures [1]. Consequently, their host-guest self-assembly employs a wide variety of weaker intermolecular interactions. This presentation describes the varied methods by which *endo-endo* facial interactions can occur between groups of such host molecules in their crystal structures.

Novel molecular brick, pen, grid and spheroid structures are obtained. The X-ray crystal structures of these building blocks will be compared and contrasted in crystal engineering terms.

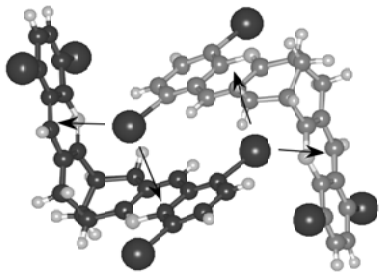

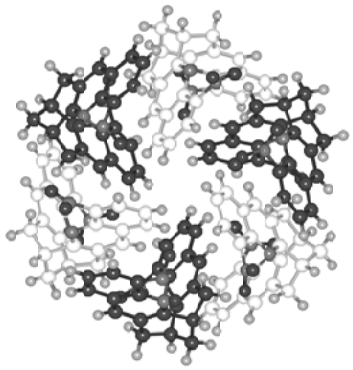

Reference:

[1] R. Bishop, *Crystal Engineering of Halogenated Heteroaromatic Clathrate Systems*, Chapter 5, pages 91-116, *Frontiers in Crystal Engineering*, Editors: E.R.T. Tiekink and J.J. Vittal, J. Wiley & Sons (Chichester), 2006.

O4B06-A2

ROLE OF MIXED HALOGENS (F, Br) TOWARDS CRYSTAL PACKING AND INTERMOLECULAR INTERACTIONS IN SUBSTITUTED BENZANILIDES

Susanta K. Nayak, T. N. Guru Row*.

Solid State and Structural Chemistry Unit, Indian Institute of Science, Bangalore-560012. India.

Crystal structures of differently substituted benzanilides (Fluoro and bromo derivatives) have been analysed to evaluate the influence of halogen bonding, appearance of weak intermolecular interactions and hydrogen bonding on the features of crystal packing. Five compounds (Scheme-1) namely 4-fluoro-N-(2-bromophenyl) benzamide, 2-fluoro-N-(2-bromophenyl) benzamide, 3-fluoro-N-(2-bromophenyl) benzamide, 3-fluoro-N-(4-bromophenyl) benzamide and 4-fluoro-N-(4-bromophenyl) benzamide have been studied by single crystal x-ray diffraction and the intra- and inter-molecular interactions have been analyzed for halogen bonding features.

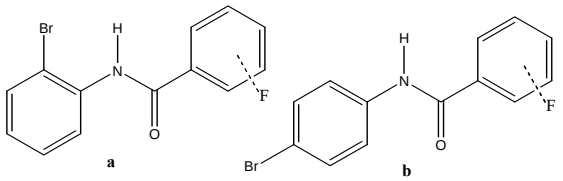

Scheme-1

These studies clearly point out that if an intra-molecular H bond is involved with the carbonyl moiety, the possibility of halogen…oxygen bonding is remote. This implies that the orientation and presence of lone pairs on the oxygen atom is a prerequisite for halogen bonding. Even though several halogen…halogen contacts have been observed in these structures all such contacts except one contact [Br…F], are with disordered positions of halogens. Thus a systematic study of mixed halogen (Br and F) substituted benzanilides brings out the fact that the propensity of formation of halogen…halogen bonding is sparse in these molecules.

O4B06-A3

SYNTHESIS, STRUCTURES AND MAGNETIC PROPERTIES OF A SERIES OF CYANO-BRIDGED HETEROMETALLIC COMPLEXES

Shao-Jun Wang, Long Jiang, Wei-Xiong Zhang and Tong-Bu Lu

MOE Key Laboratory of Bioinorganic and Synthetic Chemistry / State Key Laboratory of Optoelectronic Materials and Technologies / School of Chemistry and Chemical Engineering, Sun Yat-Sen University, Guangzhou 510275, China

Cyano-bridged clusters and coordination polymers have been extensively investigated in the field of molecular magnetism since cyano-bridge can be efficient propagation for magnetic coupling. In this report, we will present a series of cyano-bridged heterometallic chains with different structures and magnetic properties.

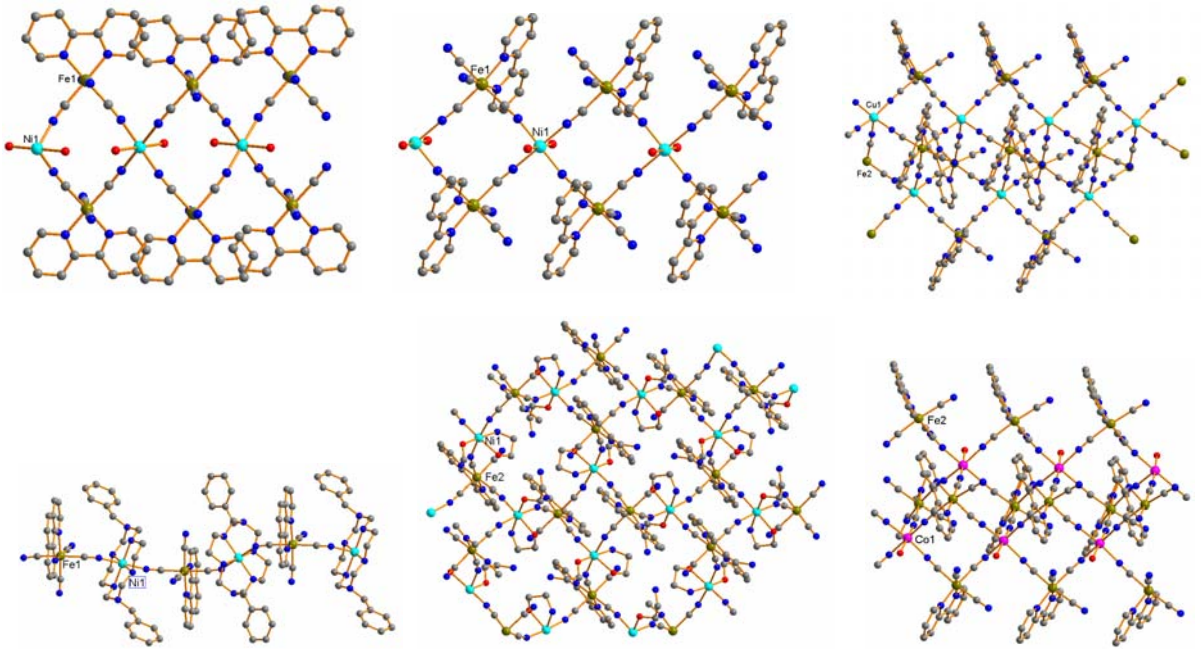

O4B06-A4

WATER CLUSTERS, ISOSTRUCTURALITY AND POLYMORPHISM IN HYDROXY DERIVATIVE OF HALOBENZENE CRYSTAL STRUCTURES

Binoy Krishna Saha

Department of Chemistry, Pondicherry University, Puducherry-605014, India

Water helices surrounding the nano-column of trichlorophloroglucinol and tribromophloroglucinol hosts have different handedness, *PMPMPM* and *PPPMMM* (*P* = right-handed and *M* = left-handed) depending upon the halogen···halogen interactions. Trichlorophloroglucinol host lattice shows zeolite like behavior.

A T6(2) tape of hydrogen bonded water molecules in boat cyclohexane conformation is trapped in the channel structure of the dibromophloroglucinol host; water escapes at 40-90 °C to transform to the anhydrous form but is readily reabsorbed from air to regain the hydrated structure.

Triiodophloroglucinol, triiodoresorcinol, triiodophenol, triiodobenzene, tribromobenzene and trichlorobenzene are isostructural. Triiodophloroglucinol and triiodoresorcinol are dimorphic and their second forms are also themselves isostructural. Solid solutions are formed between isostructural compounds.

O4B06-A5

ENGINEERING OF LUMINESCENT PROPERTIES IN MIXED LANTHANIDE CARBOXYLATE COORDINATION POLYMERS

YuFong Yen, Samadara Thushari, Alvin Siu, Kam-Sing Wong and Ian D. Williams

a) Department of Chemistry, Western Connecticut State University, Danbury CT, U.S.A. b) Department of Chemistry and Physics, Hong Kong University of Science and Technology, Clear Water Bay, Kowloon, Hong Kong, China.

The engineering of luminescence as a function of composition and structure has been carried out for several families of crystalline lanthanide coordination polymers. Luminescence for the 1D chain polymer [Ln_2(2,2-biphenate)$_3$(H_2O)$_2$] and 3D network polymer [Ln(trimesate)] prepared from hydrothermal synthesis is strong for Tb and Eu homopolymers, weak for Sm and Dy, whilst Gd is non-emissive as a metal center. When the 50:50 mixed metal polymers were prepared and tested some striking results were found. Both Gd and Tb act as sensitizers and enhance the luminescence of Eu, Sm and Dy. Efficient energy transfer appears to be possible between metal centers in these polymers, since typically only emission from one metal is observed. Other families such as [Ln_2(L-TAR)$_3$(H_2O)$_2$] have different properties for the mixed-lanthanide polymers, for example both Tb and Eu emissions are clearly seen together in the Tb-Eu compound. This polymer has a carboxylate bridge, but no bridging O atom commonly shared. The structural features affecting the emissive behaviour and energy transfer process will be summarized. The Research Grants Council (HKSAR) is thanked for financial support of this work (603306).

O4B06-A6

SUPRAMOLECULAR ASSEMBLIES OF MONONUCLEAR AND POLYMERIC COBALT(II) AND NI(II) DICARBOXYLIC COMPLEXES

Tanwawan Duangthongyou,[a] Sutatip Siripaisarnpipat [a], Chris Adams [b]

[a]*Department of Chemistry, Faculty of Science, Kasetsart University, Bangkok Thailand;* [b] *The School of Chemistry, University of Bristol, Bristol BS8 1TS, UK*

Self – assembly based on metal ligand coordination bonds, π-π stacking interactions and hydrogen bonds provide an efficient route to supramolecular architectures with specific topologies. Dicarboxylic acid ligands are excellent spacers to constitute 1D, 2D and 3D structures. The structural framework of Ni^{II} and Co^{II} metal center, involving dicarboxylic acids of varying chain length and *N*-donor ligands have been studied to understand the conformational flexibility of dicarboxylic acids, and the various modes of network that can be created by manipulating the *N*–donor ligand, for example in the figure below.

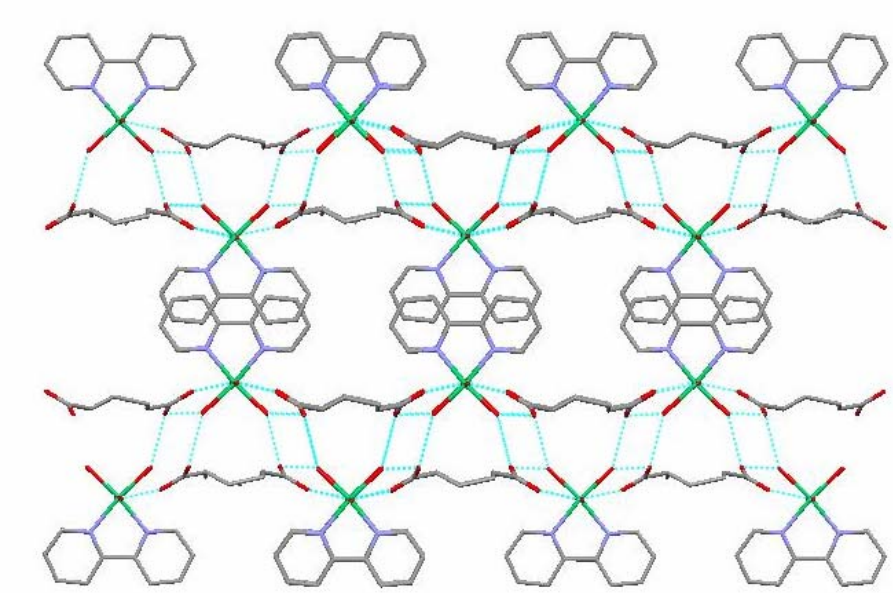

View of crystal structure of $[Ni(H_2O)_4(2,2'\text{-bipyridine})](C_6H_8O_4)(H_2O)$. The hydrogen atoms and the sovent molecules (water) have been omitted.

O4B06-A7

ENGINEERING OF LUMINESCENT PROPERTIES IN MIXED LANTHANIDE CARBOXYLATE COORDINATION POLYMERS

YuFong Yen, Samadara Thushari, Alvin Siu, Kam-Sing Wong and Ian D. Williams

a) Department of Chemistry, Western Connecticut State University, Danbury CT, U.S.A.
b) Department of Chemistry and Physics, Hong Kong University of Science and Technology, Clear Water Bay, Kowloon, Hong Kong, China.

The engineering of luminescence as a function of composition and structure has been carried out for several families of crystalline lanthanide coordination polymers. Luminescence for the 1D chain polymer $[Ln_2(2,2\text{-biphenate})_3(H_2O)_2]$ and 3D network polymer [Ln(trimesate)] prepared from hydrothermal synthesis is strong for Tb and Eu homopolymers, weak for Sm and Dy, whilst Gd is non-emissive as a metal center. When the 50:50 mixed metal polymers were prepared and tested some striking results were found. Both Gd and Tb act as sensitizers and enhance the luminescence of Eu, Sm and Dy. Efficient energy transfer appears to be possible between metal centers in these polymers, since typically only emission from one metal is observed. Other families such as $[Ln_2(L\text{-TAR})_3(H_2O)_2]$ have different properties for the mixed-lanthanide polymers, for example both Tb and Eu emissions are clearly seen together in the Tb-Eu compound. This polymer has a carboxylate bridge, but no bridging O atom commonly shared. The structural features affecting the emissive behaviour and energy transfer process will be summarized. The Research Grants Council (HKSAR) is thanked for financial support of this work (603306).

O4C06-A1

QUENCHED DISORDER EFFECTS IN TOPOLOGICALLY ORDERED NANOPORES ON THE SMECTIC PHASE TRANSITION OF 8CB

R. Guegan,[a,b] D. Morineau,[a] R. Lefort,[a] A. Moreac,[a] and M. Guendouz[c]

[a]*Groupe Matière Condensée et Matériaux, Université de Rennes 1, Rennes, France,* [b]*Institute of Industrial Science, University of Tokyo, Meguro-ku, Tokyo, Japan,* [c]*Laboratoire d'Optronique, ENSSAT, Université de Rennes 1, Lannion, France*

The advancement of nanotechnologies in an increasing number of fields –including microfluidics, biotechnology, nanoelectronics, supports the growing interest of the scientific community in the understanding of the peculiar properties of systems of nanometer scale dimensions. A subject of current matter concerns the effects of confinement of molecular phases in mesoporous materials. The question of the phase behavior of fluids in restricted geometries is especially rich, leading to the occurrence of new phases or modifying the nature of the transition (order or critical scaling). Liquid crystals have been commonly used as model systems in statistical mechanics and soft matter physics. Experiments on phase transitions in liquid crystals have provided many of the most detailed tests of the modern theories of critical phenomena., Several studies have recently shown the effects of the quenched disorder imposed by random porous media on the continuous smectic transition. Isotropic porous aerogels and aerosil dispersions are the two prototype systems that induce such conditions experimentally [1, 2].

In this contribution, we have introduced porous silicon (PS) as a way to control some conditions of confinement that provide an unique opportunity to check the effect or quenched disorder in strongly anisotropic geometry.. PS displays a well-defined geometry with a preferential alignment (1D) of nanochannels (diameter: 100-200 Å, length: 30 m). The confinement of 4-n-octyl-4-cyanobiphenyl (8CB) liquid crystal in PS shows interesting novel features related to a striking behavior of the Nematic-Smectic A transition. Various experimental techniques (neutron scattering, micro-Raman spectroscopy and spectroscopic ellipsometry), demonstrated a preferential alignment of the molecules into the channels and the destruction of the quasi-long range order of the Smectic A phase. The transition is replaced by a progressive short range ordering on an extended temperature range (60K below Tc). This result has been successfully interpreted in the theoretical context of random fields, according to the strongly disordering nature of the inner pore surface of PS [3].

Reference:

[1] T. Bellini, L. Radzihovsky, J. Toner, N. A. Clark, Science, 294 1074-1079 (2001)

[2] R.L. Leheny, et al, *Phys Rev E*, 011708-1-13 (2003)

[3] R. Guégan**,** D. Morineau, C. Loverdo, W. Béziel, M. Guendouz, *Phys. Rev.* E, **73**, 011707 (2006).

O4C06-A2

AN ELECTRON DIFFRACTION METHOD FOR DETERMINING THE CHIRALITY OF CARBON NANOTUBES

Lu-Chang Qin,[a] Hakan Deniz,[a] Jie Tang [b]

[a]*W.M. Keck Laboratory for Atomic Imaging and Manipulation, Department of Physics and Astronomy, University of North Carolina at Chapel Hill, Chapel Hill, NC 27599-3255, USA*

[b]*National Institute for Materials Science, Tsukuba, Ibaraki 305-0047, Japan*

Email: lcqin@physics.unc.edu

The knowledge of the chirality of a carbon nanotube (defined by the chirial indices (*n*,*m*) that specify the perimeter of the nanotube) is crucial for the understanding, predictions, and investigations of the structure-property relationships of the nanotube and it has been a challenging task to obtain the chirality (diameter and helicity) of carbon nanotubes, in particular multiwalled carbon nanotubes, where the chiral indices of each and every shell are required for a complete determination of the chirality of the nanotube.

Electron diffraction from a carbon nanotube of chiral indices (*n*,*m*) can be expressed analytically in closed form [1]. The chiral indices (*n*,*m*) of a single-shell carbon nanotube can be measured directly from the scattering intensities I_{l1} , I_{l2}, and I_{l3} on the principal layer lines l_1, l_2, and l_3 formed by the primary graphene reflections [2-3]. An alternative relationship relating the chiral indices (*n*,*m*) and the principal layer line spacings D_1 and D_2, $m/n = (2D_2 - D_1)/(2D_1 - D_2)$, is also most useful for the determination of the chirality of carbon nanotubes [4-6].

These relationships have enabled us to establish a systematic procedure to obtain the chiral indices of carbon nanotubes unambiguously with a high accuracy. Examples of application of this method to the determination of the chirality of single-walled, doubule-walled, few-walled, and multiwalled carbon nanotubes will also be presented.

Reference:

[1] L.-C. Qin, J. Mater. Res. 9, 2450 (1994).

[2] L.-C. Qin, Chem. Phys. Lett. 297, 23 (1998).

[3] Z. Liu and L.-C. Qin, Chem. Phys. Lett. 408, 75 (2005).

[4] Z. Liu, Q. Zhang, and L.-C. Qin, Appl. Phys. Lett. 86, 191903 (2005).

[5] L.-C. Qin, Rep. Prog. Phys. 69, 2761 (2006).

[6] L.-C. Qin, Phys. Chem. Chem. Phys. 9, 31 (2007).

O4C06-A3

RHEED SURFACE POLE FIGURE -- A NEW *IN-SITU* TECHNIQUE FOR POLYCRYSTALLINE AND NANOSTRUCTURED SURFACE TEXTURE ANALYSIS

Fu Tang, Toh-Ming Lu and Gwo-Ching Wang

Dept. of Physics, Rensselaer Polytechnic Institute, 110 8th Street, Troy, New York 12180-3590

The preferred crystalline orientation, or texture, is a fundamental property of polycrystalline film and it directly controls many important physical properties such as optical, magnetic, mechanical, and electrical properties of the films. Texture formation is a very complex phenomenon. To date, the fundamental understanding of the atomistic mechanisms on the texture evolution still remains as a challenging subject. We demonstrated that it is possible to construct a reflection high-energy electron diffraction (RHEED) pole figure of a polycrystalline film by recording multiple RHEED patterns as we rotate the substrate around the surface normal. Since electrons have limited penetration depth (nm range), the pole figure constructed is a *surface* pole figure. It is in contrast with the conventional x-ray pole figure which gives an average texture information of the entire film and substrate. Examples of i*n situ* study of biaxial texture evolution of unusual Mg nanoblades grown by oblique angle vapor deposition using this RHEED surface pole figure technique will be given. Figures 1(a) and 1(b) show SEM images viewed 90_o from incident flux direction and facing the incident flux direction, respectively. The figure 2 below shows the development of normalized $(10\bar{1}1)$ RHEED pole figures at Mg deposition times (a) 0.5 min (~22 nm thick), (b) 8.5 min (~365 nm thick), (c) 24.5 min (~1.05 μm thick) and (d) 34.7 min (~1.49 μm thick). The positions of poles in the figures move towards the incident vapor flux as the film grows. The center of circle is the geometrical position of the [0001] axis. We will show that very rich information on the texture evolution can be obtained quantitatively from this pole figure analysis.

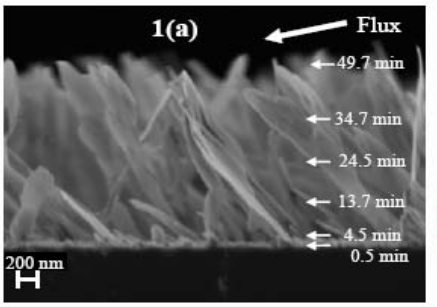
1(a)
Flux
49.7 min
34.7 min
24.5 min
13.7 min
4.5 min
0.5 min
200 nm

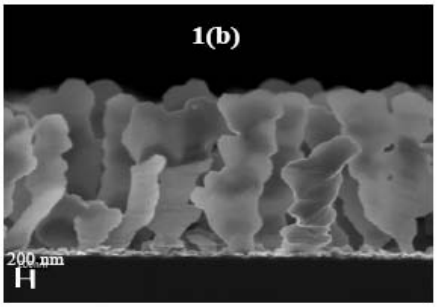
1(b)
200 nm

Figure 2

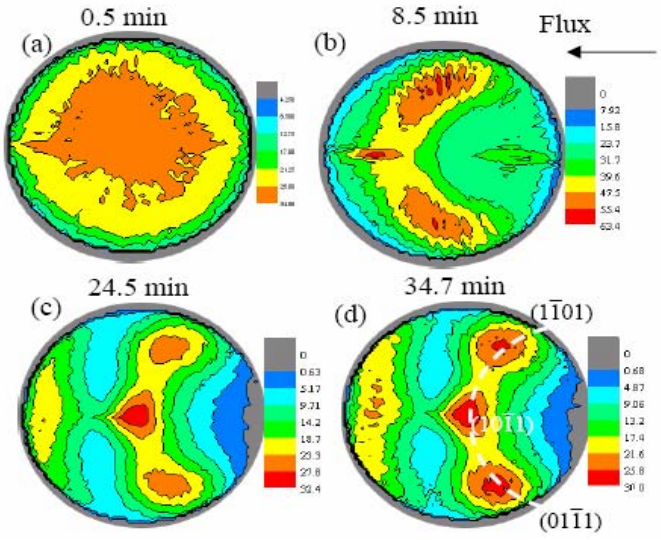
0.5 min
(a)
8.5 min
(b)
Flux
24.5 min
(c)
34.7 min
(d)
(1$\bar{1}$01)
(10$\bar{1}$1)
(01$\bar{1}$1)

O4C06-A4

QUANTUM OSCILLATIONS AND BEATS IN X-RAY REFLECTION DURING FILM GROWTH

Y.-R. Lee,[1,2,3] A. Gray,[1,2] J. Tischler,[4] P. Czoschke,[5] H. Hong,[1] S.-L. Chang,[3] and T.-C. Chiang[1,2*]

[1]*Department of Physics, University of Illinois at Urbana-Champaign, 1110 West Green Street, Urbana, Illinois 61801-3080, USA*

[2]*Frederick Seitz Materials Research Laboratory, University of Illinois at Urbana-Champaign, 104 South Goodwin Avenue, Urbana, Illinois, 61801-2902, USA*

[3]*National Tsing Hua University, 101, Section 2, Kuang Fu Road, Hsinchu, Taiwan 30013, Republic of China*

[4]*Division of Materials Science and Technology, Oak Ridge National Laboratory, Oak Ridge, Tennessee 37831, USA*

[5]*Seagate Technology, 7801 Computer Avenue South, Bloomington, MN 55435-5412*

X-ray reflection from a growing film at an anti-Bragg position, where reflection amplitudes from two adjacent atomic layers are out of phase and cancel each other, should exhibit bilayer oscillations caused by interference. In an experiment of TiN growth by laser ablation onto a sapphire substrate, an unexpected beating envelope function is found to modulate the oscillations. The successive nodes and antinodes in the envelope function are identified with the development of new growth domains separated by one atomic layer in thickness. This effect allows atomic layer counting of the film thickness distribution (roughness), and its observation implies that the growth is not characterized by a continuum stochastic process, as usually assumed.

O4C06-A5

CHARACTERIZATION OF NANOMETER SCALE GRAIN SIZED Pt ON Si AND PtSi/Si STRUCTURES DEPOSITED BY HIGH RATE MAGNETRON SPUTTERING

V.Uma[1] and R.Chandramani[2,]Ramu[2]

1. Mount Carmel College, Bangalore. umaa12342001@yahoo.co.in
2.Department of Physics, Bangalore University, rchandramani@rediffmail.com*,Bangalore,INDIA.*

Thin film silicides become increasingly important with the progress of very large-scale integrated (VLSI) and ULSI technology. Formation of low-resistance contact, low sheet resistance diffused region, and interconnection line is crucial for the VLSI circuit performance. Despite the potential applications of Pt and PtSi materials, the electronic and atomic structures of platinum silicide (PtSi) films grown on Si surfaces have not been heavily studied. So an attempt has been made to deposit metal with low substrate temperature in high vacuum at high rates. Among the various methods in preparing metallic nano particles, the most successful method for refractory metals is the high rate magnetron R.F sputtering. Low substrate temperature, high productivity, and high current densities are salient features of high rate sputtering deposition technique. Platinum with sheet resistance 3.40Ω was deposited on Si using High rate Magnetron Sputtering system. The deposited film was heated to550^{o}C in the Nitrogen atmosphere to get platinum silicide (PtSi). Samples were subjected to XRD, AFM and Spectroscopic Ellipsometry**.**

The XRD and AFM studies revealed the films Pt on Si are nano grain sized The XRD pattern of the platinum shows the cubic (111) phase whereas PtSi is neither orthorhombic nor monoclinic.

Sample	Rp in nm	r.m.s roughness	Shape	Grain size XRD	Grain size AFM
Pt/Si	10.73	1.7954nm	Plate like surface	11.3nm	11-12 nm
PtSi	6.398	1.235 nm	Pin hole free shape	~55 nm	50-60nm

Spectroscopy ellipsometry analysis revealed that optical constants value Nano Pt on Si shows little variation from the standard .The values have increased in PtSi samples due to the annealing effects, decrease in roughness, less oxidation. The optical band gap or Activation energy was found to be 0.8eV and 1.4eV for Pt on Si and PtSi respectively.

Any device based on metal –Semiconductor contacts can either form an active rectifying contact or an ohmic contact. I-V characteristics on Pt on Si confirm that the structure exhibits Schottky-rectifying characteristics. The PtSi/Si structure exhibited the ohmic behavior.

Sample	Knee Voltage	Reverse saturation current	Barrier height	Ideality factor
Pt /Si	0.8V	0.04473μA	0.371342eV	2.277
PtSi/Si	-	0.74473nA	0.13eV	2.903

It can be concluded that contact characteristics are controlled by **Fermi level pinning** due to the interface states.

O4C06-A6

SYNTHESIS, STUDIES AND LUMINESCENT PROPERTIES OF TERBIUM OXIDE DOPED $LaMn_{0.9}Zn_{0.1}O_{3+d}$ NANOPEROVSKITE BY SOL-GEL METHOD

A A Alemi, E Karimpour Nahari and H Shokri

Department of Inorganic Chemistry, Faculty of Chemistry, University of Tabriz, Tabriz Iran.

In this research we report the characterization of $La_{1-x}Tb_xMn_{0.9}Zn_{0.1}O_{3+d}$ (LTMZ) ($0.0 \leq x \leq 0.32$) nano particles with high surface area were synthesized by the polymerized complex (PC) method based on the Pechini-type reaction. High-quality nanopowders with controlled stiochiometry and microstructure were prepared at temperature rang of 700-800^{0}C for 6 h, with mean particle sizes of approximately 18.35 nm.

The synthesized materials were characterized by X-ray powder diffraction (XRD), fourier transform infrared spectrum (FTIR) and Photoluminescence(PL). Photoluminescence measurements showed Tb^{3+} ions characteristic green emission in crystalline LTMZ powders due to the $^5D_4 \rightarrow {}^7F_J$ transitions of the 4f electrons of Tb^{3+} ions. The structure, homogeneity and particle size of the obtained compounds during different stages were investigated by scanning electron microscopy (SEM).

Key words: Lanthanum; Manganese; Terbium; Perovskite; Sol–gel; Luminescence.

O4C06-A7

STUDIES OF THE NANOSTRUCTURE OF NATURAL VEGETABLE FIBERS

Nguyen Van Tri

Institute of Engineering Physics, Hanoi University of Technology, Hanoi, Vietnam.

Vegetable fiber is a wonder of the nature, a most important and widespread natural organic polymer. An effective, modern and intelligential use of full advantage of this gigantic and precious raw material source will only can be attained when the inside structure of the fiber and its relationship to specific fiber features are sufficiently known.

The chemical structure of the native cellulose, a basic component of the vegetable fiber, as a linear β-1,4 - Glucose chain is well accepted newsdays. However, the physical structure of the vegetable fiber, i.e. the other key component and the bonding structure between the cellulose chains to create the wonderful fibred network of the supermolecular order is not yet completely clear.

From our experiments with ESR, especially with the called "ESR Spectroscopy - Tomography", in combination with some other methods (X-ray diffraction, SEM, SPM, ...) on different genera of vegetable fibers (such as cotton, jute, pineapple, sisal, bamboo), we have to the first time discovered that the inside structure of the vegetable fiber is constituted not only by polysaccharide cellulose, but also by an another very important component consists of fivefold [2Fe-2S] super-exchange metallo-organic combinations. These persist in the form of the composite aperiodic Nanostructures linking diagonally the cellulose macromolecule chains creating an elementary fiber.

A visible "macroscopic practical fiber" is constituted by a lot of the elementary fibers spiraling together about an axis by a sloping angle Θ_O= 54.7°. This spiral angle is of a deep significance on the statistic quantum electronic dynamics and the biophysical function of the fibers in the nature.

This fivefold metallo-organic composite Nanostructure plays a decisive role in the specific features of vegetable fibers (such as the strength, the torsional module, the conductivity, the radiation response). On the basis of these achieved results, some physical and biological treatment techniques to improve fiber properties have been elaborated and examined.

This research was supported by the National Research Program "New Materials", the National Basic Research Program in Natural Sciences and the Textile Research Institute of the Ministry for Industry.

O5A07-M1

CRYSTAL STRUCTURES OF THE COMPLEXES OF C-LOBE OF LACTOFERRIN WITH NON-STEROIDAL ANTI-INFLAMMATORY DRUGS (NSAIDS) REVEAL THE BINDING PATTERN BETWEEN C-LOBE AND NSAIDS WHICH SUGGESTS A NEW THERAPY FOR MANAGEMENT OF NSAID-INDUCED GASTROPATHY

Sujata Sharma, Rafia Mir, Mau Sinha, Nagendra Singh, and Tej P. Singh

Department of Biophysics, All India Institute of Medical Sciences, New Delhi-110 029, India (lactotransferrin@yahoo.com)

Lactoferrin is a bilobal 80 kDa glycoprotein comprising of a single polypeptide chain folded into two homologous N- and C-lobes. Each lobe is made up of two domains N1, N2 and C1, C2 respectively with iron binding sites situated in the interdomain clefts. Non-steroidal anti-inflammatory drugs (NSAIDs) are most commonly prescribed drugs for arthritis and inflammatory conditions. Because of their widespread use, NSAID-related gastrointestinal complications are recognized as the most prevalent drug toxicity in the world. This drug toxicity comprises of bleeding and perforation in the esophagus, stomach, and duodenum due to NSAID effects on platelets and on other mucosal lesions. Though previous studies have shown that orally administered human lactoferrin is effective at preventing NSAID-induced intestinal injury, however, its mechanism of action was not clear. In the present study, the structures of C-terminal molecular half (C-lobe) of bovine lactoferrin with four NSAIDS ; indomethacin, diclofenac, aspirin and paracetamol have been determined. The C-lobe of lactoferrin was produced proteolytically with Proteinase K. The structures of the complexes of C-lobe with These structures have revealed a new site for the binding of NSAIDS in the C2 domain The structures of C-lobes also revealed a new role for the N-terminal residues of C-lobe which were involved in the interactions with N-lobe at the interface in the intact lactoferrin. These structures reveal the mechanism by which lactoferrin is effective at preventing NSAID-induced intestinal injury.

O5A07-M2

CRYSTAL STRUCTURES OF NATIVE BACTERIOPHAGE-ASSOCIATED HYALURONATE LYASE AND ITS COMPLXES WITH LACTOSE AND ASCORBIC ACID

P. Mishra[1], V. Bhakuni[1], A. S. Ethayathulla[2], R. Prem Kumar[2], N. Singh[2], S. Sharma[2], P. Kaur[2], A. Srinivasan[2] and T. P. Singh[2]

[1]Division of Molecular and Structural Biology, Central Drug Research Institute, Lucknow-226001, India [2]Department of Biophysics, All India Institute of Medical Sciences, New Delhi-110029, India

Hyaluronate lyases (HylP2) are a class of endoglycosaminidase enzymes with considerable complexity and heterogeneity. Their function is to degrade hyaluronan, the main polysaccharide component of the host connective tissues into unsaturated disaccharide units as the final product. Crystal structures of the cloned native enzyme and its complexes with lactose and ascorbic acid have been determined. The protein crystallized in hexagonal space group with cell dimensions of a = b = 58.5Å, c = 583.5Å. The structure of HylP2 is composed of three intertwined polypeptides centered on a crystallographic three-fold axis. The N-terminal forms a mixed globular α/β capping region that is followed by a coiled region. The central core of HylP2 forms a cylindrical arrangement with alternating β strands from each of the three polypeptides. The external faces are shaped with depressions so as to allow the ligand binding. The C-terminal region of the structure does not have intertwined β strands but interdigitating strands. The end is concluded with α helical nose. Both lactose and ascorbic acid have three binding sites in the central concave part of the molecule. The protein residues that are involved in the interactions with ligands are Glu 167 and Lys 179 at site 1, Asn 182, Asn 202, Arg 216 and Glu 214 at site 2 while Gly 223, Asn 241, Gln 261, Tyr 264 and Asn 226 are involved at site 3. At each site, there at least six hydrogen bonded interactions indicating specific mode of binding of these ligands resulting in the inhibition of enzyme activity.

O5A07-M3

STRUCTURAL AND MUTATIONAL STUDIES OF ANTHOCYANIN MALONYLTRANSFERASES ESTABLISH THE FEATURES OF BAHD ENZYME CATALYSIS

Hideaki Unno[a], Fumiko Ichimaida[b], Hirokazu Suzuki[b], Seiji Takahashi[b], Yoshikazu Tanaka[c], Atsushi Saito[b], Tokuzo Nishino[b], Toru Nakayama[b] and Masami Kusunoki[d]

[a] Faculy of Engineering, Nagasaki University; [c] Department of Biomolecular Engineering, Graduate School of Engineering, Tohoku University; [c] Suntory Research Center; [d] Institute for Protein Research, Osaka University, 3-2 Yamada-oka, Suita, Osaka 565-0871,

The BAHD family is a class of acyl-CoA-dependent acyltransferases which are involved in plant secondary metabolism and shows a diverse range of specificities for acyl acceptors. Anthocyanin acyltransferases make up an important class of the BAHD family and catalyze the acylation of anthocyanins that are responsible for most of the red-to-blue colors of flowers. Here, we describe crystallographic and mutational studies of three similar anthocyanin malonyltransferases from red chrysanthemum petals: anthocyanidin 3-*O*-glucoside-6"-*O*-malonyltransferase (Dm3MaT1), anthocyanidin 3-*O*-glucoside-3",6"-*O*-dimalonyltransferase (Dm3MaT2), and a homolog (Dm3MaT3). Mutational analyses revealed that seven amino acid residues in the N- and C-terminal regions are important for the differential acyl-acceptor specificity between Dm3MaT1 and Dm3MaT2. The SeMet structure of Dm3MaT3 has been determined by the MAD method and the free and complex structures of Dm3MaT3 was refined at 2.2 Å and 2.1 Å resolution, respectively. Crystallographic studies of Dm3MaT3 provided the first structure of a BAHD member, in complex with acyl-CoA, showing the detailed interactions between the enzyme and acyl-CoA molecules. The structure, combined with the results of mutational analyses, allowed us to identify the acyl-acceptor binding site of anthocyanin malonyltransferases, which is structurally different from the corresponding portion of vinorine synthase, another BAHD member, thus permitting the diversity of the acyl-acceptor specificity of BAHD family to be understood.

O5A07-M4

CRYSTAL STRUCTURE OF *N*-ACETYLGLUCOSAMINE-PHOSPHATE MUTASE, A MEMBER OF THE ALPHA-D-PHOSPHOHEXOMUTASE SUPERFAMILY

Yuichi Nishitani,[a] Daisuke Maruyama,[a] Tsuyoshi Nonaka,[a] Akiko Kita,[a] Takaaki A. Fukami,[b] Toshiyuki Mio,[b] Hisafumi Yamada-Okabe,[b] Toshiko Yamada-Okabe[c] and Kunio Miki[a, d]

[a]Department of Chemistry, Graduate School of Science, Kyoto University, Sakyo-ku, Kyoto 606-8502, Japan, [b]Kamakura Research Laboratory, Chugai Pharmaceutical Company Ltd., 200 Kajiwara, Kamakura, Kanagawa, 247-8530 Japan, [c]Department of Hygiene, School of Medicine, Yokohama City University, 3-9, Fukuura, Kanazawa, Yokohama 236-0004, Japan, [d]RIKEN SPring-8 Center at Harima Institute, Koto 1-1-1, Sayo, Hyogo 679-5148, Japan

N-acetylglucosamine-phosphate mutase (AGM1) is an essential enzyme in the synthetic process of UDP-*N*-acetylglucosamine (UDP-GlcNAc). UDP-GlcNAc is a UDP sugar that serves as a biosynthetic precursor of glycoproteins, mucopolysaccharides, and the cell wall of bacteria. Thus, a specific inhibitor of AGM1 from pathogenetic fungi could be a new candidate for an antifungal reagent that inhibits cell wall synthesis. AGM1 catalyzes the conversion of *N*-acetylglucosamine 6-phosphate (GlcNAc-6-P) into *N*-acetylglucosamine 1-phosphate (GlcNAc-1-P). This enzyme is a member of the alpha-D-phosphohexomutase superfamily, which catalyzes the intramolecular phosphoryl transfer of sugar substrates. Here we report the crystal structures of AGM1 from *Candida albicans* for the first time, both in the apoform and in the complex forms with the substrate and the product, and discuss its catalytic mechanism.

The structure of AGM1 consists of four domains, of which three domains have essentially the same fold. The overall structure is similar to those of phosphohexomutases; however, there are two additional beta-strands in domain 4, and a circular permutation occurs in domain 1. The catalytic cleft is formed by four loops from each domain. The *N*-acetyl group of the substrate is recognized by Val-370 and Asn-389 in domain 3, from which the substrate specificity arises. By comparing the substrate and product complexes, it is suggested that the substrate rotates about 180° on the axis linking C-4 and the midpoint of the C-5—O-5 bond in the reaction.

O5A07-M5

SUBSTRATE SPECIFICITY OF PHOSPHODIESTERASES, STRUCTURAL INSIGHT INTO VIAGRA FUNCTION, AND STRUCTURE-BASED DESIGN OF DRUGS FOR INFLAMMATORY DISEASES

Hengming Ke and Huanchen Wang,

Department of Biochemistry and Biophysics, University of North Carolina, Chapel Hill, NC 27599, USA

Cyclic nucleotide phosphodiesterases (PDEs) are key enzymes controlling cellular concentrations of the second messengers cAMP and cGMP. Family selective PDE inhibitors have been widely studied as therapeutics for treatment of various human diseases. For example, PDE4 inhibitors have been studied for treatment of inflammatory diseases such as asthma and chronic obstructive pulmonary diseases (COPD) and PDE10 inhibitors for psychosis. The most successful example of this drug class is the PDE5 inhibitor sildenafil (Viagra) that has been used for treatment of male erectile dysfunction and pulmonary hypertension. Human genome encodes 21 PDE genes that have been grouped into 11 families. Alternative splicing of the 21 genes produces over hundred of PDE isoforms that contain a variable regulatory domain and a conserved catalytic domain. Individual families of PDEs specifically recognize substrates cAMP and cGMP and possess their selective inhibitors. However, the basic issues of substrate specificity and inhibitor selectivity of the enzyme have not been extensively illustrated.

To elucidate the substrate specificity, the crystal structures of PDE10 and PDE4 in complex with the substrates cAMP and cGMP have been determined at high resolution. The PDE10 structures show that cAMP and cGMP bind in different conformations, suggesting that the substrates are recognized by different orientations and interactions. The PDE4 structure reveals only one hydrogen bond between substrate cAMP and the invariant glutamine and therefore provides direct evidence against the widely circulated mechanism of “glutamine switch”. To study the inhibitor selectivity, the structures of PDE5 in complex with various inhibitors have been determined. These structures reveal multiple conformations of the H-loop at the active site of PDE5 upon binding of the inhibitors IBMX, icarisid II, sildenefil, and vardenafil (Levitra), in addition to the different configurations of two drugs vardenafil and sildenafil that have similar chemical formulae. These studies provide structure bases for the different physiological behaviors of the inhibitors. The structure-based drug design has led to discovery of a novel type of PDE4 selective inhibitors that are very potent in anti-inflammation activity. The best one inhibits the TNFα release in human peripheral blood mononuclear cell system with IC50 of 40 nM, at least 10-fold more potent than cilomilast that is a GSK drug-lead in phase III clinic trial for treatment of COPD.

O5B07-M1

COMPLEMENTARY STUDIES OF ENZYME-RESISTANT STARCH - IMPLICATIONS FOR HUMAN HEALTH

A. López-Rubio[a], M. J. Gidley[b], A. K. Shrestha[b], B.M. Flanagan[b], A. Htoon[c,d], H. Chanvrier[c,d], S. Uthayakumaran[c,d], I.A.M. Appelqvist[c,d], A.R. Bird[c,e], D.L. Topping[c,e], M.K. Morell[c] and E.P. Gilbert[a]

[a]*Bragg Institute, Australian Nuclear Science and Technology Organisation, Menai, NSW*
[b]*Centre for Nutrition and Food Sciences, University of Queensland, St Lucia, QLD 4072, Australia*
[c]*Commonwealth Scientific and Industrial Research Organisation, Food Futures Flagship, Riverside Corporate Park, North Ryde, NSW, Australia*
[d]*Food Science Australia, Riverside Corporate Park, North Ryde, NSW, Australia*
[e]*Food Science Australia, PO Box 10041, Adelaide, SA 5000*

Resistant starch (RS) has been defined as the fraction of starch that escapes digestion in the small intestine of healthy individuals, reaching the large bowel where it is fermented into short-chain fatty acids (SCFA) by colonic bacteria. The beneficial health effects derived from increasing the amount of SCFA delivery in the colon (such as reduced glycaemic load, apoptosis in colo-rectal cancer cells) have lead to a general interest in understanding the different types of RS, aimed at designing food products with increased contents of these fractions. Whilst hindering the access of the enzymes to the starch molecules is one of the mechanisms preventing hydrolysis in, for example, RS types I and IV (physically inaccessible and chemically modified starch respectively), processed starches, constituting the bulk of ingested starches in many diets, have a different mechanism of RS formation. Several studies have focussed on the description of RS fractions from processed starches (RSIII), but little attention has been paid to the digestion process itself, which from the present *in vitro* work, is suggested to play a key role.

In this work, a novel approach has been used to investigate the origin of RSIII using a combination of small-angle X-ray scattering and X-ray diffraction, microscopy, chromatography and NMR. High-amylose maize starch samples extruded under two different processing conditions were characterised at different stages of amylase digestion under conditions shown to be representative of *in vivo* digestion, and compared with control samples which were kept in the digestion solution without enzyme. From the results a comprehensive picture of the changes occurring during amylase digestion is gained, providing the rationale behind the “resistance-to-digestion” mechanism of processed high-amylose starches.

O5B07-M2

CRYSTAL AND MOLECULAR STRUCTURES OF ORGANOPHOSPHORUS COMPOUNDS - CONFORMATION AND BIOLOGICAL ACTIVITY OF HETEROCYCLIC MOLECULES

Musali Krishnaiah and Jadaprolu Radha Krishna

Department of Physics, Sri Venkateswara University, Tirupati-517502-India.

Structure and conformational studies of organophosphorus heterocycles have drawn much interest in recent years, because of their applications as insecticides, bactericides, fungicides, flame retardants, lubricants, pesticides, antioxidents, antitumor agents and stabilizers in polymers and oils. The structure determination on a series of organophosphorus compounds have been carried out, to understand the influence of the substituents on the conformation and molecular geometry of the heterocyclic ring of different sizes and their relation to biological activity.

Structures of oxazaphosphorine derivatives reveal that six membered ring exhibits boat, screw-boat and in between intermediate sofa and half chair conformation, where as benzodioxaphosphorine ring adopts a boat form with different orientations of the substituents. Substituted benzo and dibenzo-dioxaphosphepine derivatives (seven membered) show twist-chair and distorted boat form and similar conformation has been found in eight membered dibenzo substituted dioxaphosphocin derivatives. The most common geometrical observation is that the equality in P-O bond lengths with homogeneous substituents and considerable variation depending on electronegativity of the fourth substituent at phosphorus.

It is interesting to observe the conformation changes when substituents are common but differs with ring size and also with different substituents on the same ring. These structural features are correlated and discussed in terms of their biological activities, useful for industrial applications.

O5B07-M3

INELASTIC X-RAY SCATTERING STUDY OF EXCITON PROPERTIES IN AN ORGANIC MOLECULAR CRYSTAL

Ke Yang

JASRI/SPring-8, 1-1-1 Kouto, Mikazuki-cho, Sayo-gun, Hyogo 679-5198, Japan

Excitons in a complex organic molecular crystal were studied by inelastic x-ray scattering (IXS) for the first time. The dynamic dielectric response function is measured over a large momentum transfer region, from which an exciton dispersion of 130 meV is observed. Semiempirical quantum chemical calculations reproduce well the momentum dependence of the measured dynamic dielectric responses, and thus unambiguously indicate that the lowest Frenkel exciton is confined within a fraction of the complex molecule. Our results demonstrate that IXS is a powerful tool for studying excitons in complex organic molecular systems. Besides the energy position, the IXS spectra provide a stringent test on the validity of the theoretically calculated exciton wave functions.

O5C07-M1

HIGH SPEED NEUTRON DIFFRACTION AT THE OPAL RESEARCH REACTOR: THE WOMBAT INSTRUMENT

A.J. Studer, M. Avdeev, M.M. Elcombe, J.R. Hester, and V.K. Peterson

Bragg Institute, ANSTO, RMB 1, Menai 2234, NSW Australia

Wombat is an instrument designed for high speed powder diffraction at the OPAL research reactor in Australia. It combines a high flux at the sample with a high speed detector. The instrument is located along a 300mm high neutron guide which begins at the edge of the reactor core. Combined with a variable vertical focus monochromator, this enables the high flux at the sample. The detector is a compact, curved, continuous 120^{o} design with two dimensional area detection. It has very high throughput, easily capable of handling a million events per second.

Wombat achieved “first neutrons” in February 2007, During its commissioning it has demonstrated its power in rapid real time pattern acquisition. Measurements have been made in both “one shot” mode, where a dynamically changing system is measured in real time, and “stroboscopic” mode, where a rapidly cycling system is measured repeatedly to built up statistics.

As well as high speed powder diffraction, Wombat is useful for single crystal applications such as measuring diffuse scattering. The combination of high flux and a detector with a large solid angle allow large regions of reciprocal space to be mapped with great efficiency.

O5C07-M2

WATER-REDISPERSIBLE SINGLE WALL CARBON NANOTUBES AND 40M SANS INSTRUMENT DEVELOPMENT AT HANARO

Sung-Min Choi,[a] Tae-Hwan Kim [a], Changwoo Doe [a], Young-Soo Han[b] and Steven R Kline[c]

[a]Department of Nuclear and Quantum Engineering, Korea Advanced Institute of Science and Technology, Daejeon, Korea;Physics,; [b]HANARO Research Center, Korea Atomic Energy Research Institute, Daejeon, Korea; [c]NIST Center for Neutron Research, Gaithersburg MD USA

Part I: Single-wall carbon nanotubes (SWNTs) have remarkable properties that have a wide range of potential applications. In many cases, however, insolubility and bundling of SWNTs in aqueous solution due to their strong hydrophobicity and van der Waals attraction, respectively, are problematic for various practical applications. Here, we report a new type of non-covalently (no covalent bonding between the dispersants and SWNTs) functionalized and individually isolated SWNTs (*p*-SWNT) that are readily re-dispersible (by only 10 minutes of mild vortex mixing) in water even after freeze-drying and stable for months long time period. This was achieved by 1) dispersing SWNTs in water using cationic surfactants, Cetyltrimethylammonium 4-vinylbenzoate (CTVB), which have polymerizable counterions (VB- ions), and 2) permanently fixing the surfactant layer on the SWNTs by polymerizing the counterions. The dispersion quality and surfactant encapsulation structure of p-SWNTs are characterized by SANS, AFM and UV-vis NIR. Unlike the previous SWNT dispersions, the *p*-SWNT does not form any aggregates or networks at the concentrations investigated in this study.

Part II: A 40m small angle neutron scattering instrument is being developed at HANARO, Korea. The current progress and some details of design of the 40m SANS will be presented.

O5C07-M3

FIRST RESULTS FROM THE NEW OPAL RESEARCH REACTOR

R. A. Robinson

Bragg Institute, Australian Nuclear Science and Technology Organisation, Menai, NSW 2234, Australia.

Australian science is entering a new "golden age", with the startup of bright new neutron and photon sources in Sydney and Melbourne, in 2006 and 2007 respectively. The OPAL reactor and the Australian Synchrotron can be considered the greatest single investment in scientific infrastructure in Australia's history. They will essentially be "sister" facilities, with a common open user ethos, and a vision to play a major role in international science. Fuel was loaded into the OPAL reactor in August 2006, and full power (20MW) achieved in November 2006. The formal user program commences in mid 2007, and some commissioning experiments have already taken place well before then. The first three instruments in operation are a high-resolution powder diffractometer (for materials discovery), high-intensity powder diffractometer (for kinetic studies) and a strain scanner (for mechanical engineering and industrial applications). These will be closely followed by four more instruments with broad application in materials science, physics, chemistry, biology, engineering and the earth sciences. Instrument performance will be competitive with the best research-reactor facilities anywhere. To date there is committed funding for 9 instruments, with a capacity to install a total of ~18 beamlines. An update will be given on the status of OPAL, its thermal and cold neutron sources, its instruments and the first data.

O5C07-M4

VERSATILE NEUTRON DIFFRACTOMETR AT J-PARC - IBARAKI MATERIALS DESIGN DIFFRACTOMETER -

T. Ishigaki,[a] A. Hoshikawa,[b] M. Yonemura,[c] F. Shikanai [d] T. Morishima, [d] T. Kamiyama,[d] K. Aizawa,[b] T. Sakuma,[b] Y. Tomota,[b] M. Arai,[b] M. Hayashi,[e] K. Ebata,[e] Y. Takano,[e] K. Komatsuzaki,[e] H. Asano,[e] Y. Takano,[e] T. Kasao[e]

[a]Division of Research & Development of Ibaraki Beam Line, Ibaraki University, 4-12-1 Nakanarusawa, Hitachi, 316-8511 Ibaraki, Japan; [b]J-PARC Center, Japan Atomic Energy Agency, 2-4 Shirakata Shirane, Tokai, 319-1195 Ibaraki, Japan; [c]Institute of Applied Beam Science, Ibaraki University, 4-12-1 Nakanarusawa, Hitachi, 316-8511 Ibaraki, Japan; [c]Neutron Science Laboratory, KEK, 1-1 Oho, Tsukuba, 305-0801 Ibaraki, Japan; [e]Ibaraki Prefecture, 978-6 Kasahara, Mito, 310-8555 Ibaraki, Japan

Ibaraki prefecture, the local government of the area for J-PARC site, was decided to build a versatile neutron diffractometer (IBARAKI Materials Design Diffractometer) to promote an industrial application for neutron beam in J-PARC. This diffractometer is planned to be a high throughput diffractometer so that materials engineers and scientists can use it like the chemical analytical instruments in their materials development process. It covers in d range $0.18 < d\ (Å) < 5$ with $\Delta d/d = 0.16$ % at high resolution bank, and covers $5 < d\ (Å) < 800$ with gradually changing resolution at three detector bank (90 degree, low angle and small angle). Typical measuring time to obtain a 'Rietveld-quality' data is several minutes with the sample size of laboratory X-ray diffractometer. To promote industrial application, a utilization system for this diffractometer is required. We will establish a support system for both academic and industrial users who are willing to use neutron but have not been familiar with neutron diffraction. The analysis software is also very important for powder diffraction, we will also prepare a software package consisting of combination of several powder-diffraction software, structural databases and visualization. The construction of this instrument was already begun and will be completed in the beginning of 2008, as one of day-one instruments for J-PARC. The current status for this instrument also will be reported.

O6A07-A1

TACKLING A MUNC-Y PUZZLE: STRUCTURE OF THE MUNC18C PROTEIN

Jennifer L Martin[1], Shu-Hong Hu[1], Catherine F. Latham[1], Christine L. Gee[1], David E. James[2]

1 Institute for Molecular Bioscience, University of Queensland, Brisbane, QLD, Australia
2 Garvan Institute, Sydney, NSW, Australia

Sec1p/Munc18 (SM) proteins bind to SNARE (Soluble NSF-attachment protein receptors) proteins and play an essential role in membrane fusion. Divergent modes of regulation have been proposed for different SM proteins indicating that they can either promote or inhibit SNARE assembly. This is in part due to discrete modes of binding that have been described for various SM/SNARE complexes. One mode suggests that SM proteins bind only to Syntaxins, preventing SNARE assembly, whereas in another they facilitate SNARE assembly and bind to SNARE complexes.

The mammalian cell surface SM protein Munc18c binds to an N-peptide in Sytaxin4 and this is compatible with its interaction with SNARE complexes. We determined the crystal structure of Munc18c in complex with the Syntaxin N-peptide. This structure shows remarkable similarity with a yeast complex indicating that the mode of binding, which can accommodate SNARE complexes, is highly conserved throughout evolution. Modelling reveals that the N-peptide binding mode is present in most but not all yeast and mammalian SM/Syntaxin pairs suggesting that it has co-evolved to fulfill a specific regulatory function. The likely regulatory function will be discussed.

O6A07-A2

CRYSTAL STRUCTURE OF DsrEFH, A PROTEIN ESSENTIAL FOR OXIDATION OF STORED SULFUR IN THE PURPLE SULFUR BACTERIUM *ALLOCHROMATIUM VINOSUM*

Dong Hae Shin[1*]

[1]*College of Pharmacy, Ewha Womans University, Seoul 120-750, Korea*

[*]*Corresponding author*

In the purple sulfur bacterium *Allochromatium vinosum*, the *dsrEFH* genes are part of the *dsr* operon the products of which are involved in the oxidation of sulfur stored in intracellular sulfur globules. We proved the essential role of DsrEFH in this process with an *A. vinosum* Δ*dsrE* mutant unable to oxidize accumulated sulfur. To assist functional assignment in detail, we also determined the crystal structure of the soluble $\alpha_2\beta_2\gamma_2$-structured *A. vinosum* DsrEFH at 2.5 Å resolution. Each of DsrE, DsrF, and DsrH has a single domain with the YchN fold. Structural comparison revealed that the conserved cysteine 78 of *A. vinosum* DsrE corresponds to the active site cysteines of *E. coli* YchN and TusD. The putative active site in DsrE is formed between interfaces of DsrE and DsrF with a depth of ~11 Å and a width of ~ 6Å x 14 Å. Based on a structural comparison with *E. coli* TusBCD, a sulfur transfer activity of DsrE through Cys78 has been suggested. A big cleft with a depth of ~11 Å and a width of about ~ 10 Å x 30 Å is apparent on the surface of DsrFH. Since the highly conserved residues Cys20, His5 and Trp101 of DsrH are constellated in this pocket, this cleft probably constitutes another active site. Amino acid sequence comparisons and phylogenetic analyses indicate that the presence of two different types of putative active sites in DsrE and DsrH is a common and unique trait of DsrEFH proteins from sulfur-oxidizing organisms.

O6A07-A3

STRUCTURAL AND COMPUTATIONAL STUDIES ON TYPE II RIPs

Alok Sharma,[a] A.A. Jeyaprakash,[a] M.J.Swamy [b] and M.Vijayan [a]

[a]*Molecular Biophysics Unit, Indian Institute of Science, Bangalore, India.* [b]*School of Chemistry University of Hyderabad, Hyderabad, India.*

The crystal structures of six type II Ribosome Inactivating Proteins (RIPs) have been reported. Each structure consists of a catalytic domain and a lectin domain made up of two β-trefoils. Each trefoil involves one sugar binding site. Among the RIPs of known structure, four are toxic. One is non-toxic on account of defect in carbohydrate binding. The rough structure of another non-toxic type II RIP is also available, although the reason for the absence of toxicity has not been elucidated. Here we report the structure of a non-toxic type II RIP from Snake gourd (*Trichosanthes anguina*) at 2.4 Å resolution. A detailed analysis of the structure and its interactions indicates that a combination of changes in the active site in the catalytic domain and alterations in carbohydrate binding is responsible for the abolition of toxicity. An exhaustive search of sequence data led to the identification of close to thirty non-redundant type II RIPs. The three-dimensional structures of some of them are already known. Homology models were constructed for representatives from the remaining RIPs. A comparison of these structures and models provides further insights into the molecular basis of the toxicity and the absence of it in some cases, of type II RIPs.

O6A07-A4

STRUCTURAL STUDIES OF THE CPX PATHWAYH ACTIVATOR NLPE ON THE OUTER MEMBRANE OF *ESCHERICHIA COLI*

Yu Hirano,[a] Md. Motarab Hossain,[b] Kazuki Takeda,[a,c] Hajime Tokuda[b] and Kunio Miki[a,c]

a Department of Chemistry, Graduate School of Science, Kyoto University, Kyoto, Japan; b Institute of Molecular and Cellular Biosciences, University of Tokyo, Tokyo, Japan; c RIKEN SPring-8 Center at Harima Institute, Hyogo, Japan.

NlpE is an outer membrane lipoprotein widely found in Gram-negative bacteria. NlpE is anchored on the periplasimc side of the outer membrane with three acyl chains at the N-terminal cysteine residue. During envelope stress responses, NlpE functions as an activator of the Cpx signal transduction pathway. In *Escherichia coli*, adhesion to abiotic surfaces has been reported to activate the Cpx pathway in an NlpE-dependent manner. External copper ions are also thought to activate the Cpx pathway mediated by NlpE. Based on the properties of the Cpx pathway, the activating signals are probably related to the accumulation of misfolded or mislocated proteins in the envelope. We determined the crystal structure of NlpE from *E. coli* at 2.6 Å resolution. The structure showed that NlpE consists of two β-barrel domains. The N-terminal domain resembles the bacterial lipocalin Blc, and the C-terminal domain has an oligonucleotide/oligosaccharide binding (OB) fold. NlpE from *E. coli* possesses characteristic sequence motifs, such as the Cys-X-X-Cys (CXXC) motif (31-CADC) and the serine protease inhibitor signature (99-MLDREGNPIESQFNYTL). The four conserved cysteine residues of NlpE were investigated by both biochemical analyses and the crystal structure. Deducing from these studies, the cysteine residues in the CXXC motif may be chemically active. Furthermore, two monomers in the asymmetric unit form an unusual 3D domain-swapped dimer. One of the strands of each N-terminal β-barrel is made of an alternative chain in the asymmetric unit. These structural features suggest that NlpE can easily unfold at the β-strand of the N-terminal β-barrel. The unfolding of the single strand at the β-barrel has a notable similarity to the loss of donor strand complementation in PapE causing activation of the Cpx pathway. These findings indicate that tertiary and/or quaternary structural instability of NlpE may be responsible for Cpx pathway activation.

O6A07-A5

CRYSTAL STRUCTURE OF IL-15/IL-15RALPHA COMPLEX

Mami Chirifu[1], Chiharu Hayashi[1], Teruya Nakamura[1], Sachiko Toma[2], Tsuyoshi Shuto[1], Hirofumi Kai[1], Yuriko Yamagata[1], Simon J. Davis[3] and Shinji Ikemizu[1]

1Graduate School of Pharmaceutical Sciences, Kumamoto University, Kumamoto, Japan, 2Graduate School of Pharmaceutical Sciences, The University of Tokyo, Tokyo, Japan, 3Nuffield Department of Clinical Medicine and MRC Human Immunology Unit, The University of Oxford, Oxford, Oxford UK

Interleukin (IL)-15 contributes to $CD8^+$ T-cell memory acquisition and natural killer cell generation, whereas IL-2 has a pivotal role in the expansion and functions of regulatory and activated effector T cells. The IL-15 and IL-2 receptors belong to the common γ cytokine receptor class and share signal-transducing β and γ. subunits. Within the γ-chain class, the IL-15 and IL-2 receptors are unique insofar as specificity is provided by a third, higher affinity “private” receptor α-subunit. Whereas the private IL-2Rα subunit is co-expressed with β and γ on T- and B-cells ostensibly to allow cell-autonomous signaling, IL-15Rα is expressed *in trans* on antigen-presenting cells. The 1.85Å crystal structure of the human IL-15/IL-15Rα complex accounts for the specificity of cytokine recognition, highlighting the high degree of electrostatic and geometric complementarity between the acidic receptor-binding surface of IL-15 and the basic ligand-binding region of IL-15Rα, and the essential role of binding-site waters in forming this very high affinity complex (K_d = 38 pM). In spite of very low IL-15/IL-2 sequence homology and the distinct architectures of the cytokine-binding “sushi” domains of each receptor, the receptor binding foot-prints of each cytokine, and therefore the topologies of both the IL-15/IL-15Rα and IL-2/IL-2Rα complexes, are remarkably similar. Overall, there appear to be no structural obstacles to the *in trans* presentation of either cytokine. Our findings suggest that antigen-experienced $IL\text{-}2R\alpha^+$ T cells could, in principle, enhance $IL\text{-}2R\alpha^-$ T cells responses *via* the direct presentation of IL-2.

O6B07-A1

IXS STUDY OF EXCITATION PROPERTIES OF ORGANIC MOLECULAR CRYSTALS AND SIMPLE MOLECULES

Binping Xie,[a] Ke Yang,[a] Y. Q. Cai,[b] N. Hiraoka,[b] Donglai Feng[a]

[a]Department of Physics, and Applied Surface Physics state Key Laboratory, Fudan University, Shanghai 200433, China; [b]National Synchrotron Radiation Research Center, Hsinchu 30076, Taiwan, Republic of China.

Inelastic x-ray scattering (IXS) has proven to be a powerful tool for investigating the electronic excitations in inorganic systems. For example, IXS data have helped our understanding of the metal-insulator transition, Plasmon excitations, and band gap. IXS is a clean and direct probe of the dynamic structure factor S(q, ω), which is proportional to $q^2 \mathrm{Im}(\quad^{-1})$, being the dynamic dielectric function. In comparison with high energy electron-energy-loss spectroscopy (EELS), IXS is almost free from multiple scattering effects, and it can generate reliable information at high momentum transfer q. Therefore, IXS is particularly advantageous for studying electronic excitations that are more constrained in space in organic molecular crystals and simple molecules.

Our group developed a new method to study excitons in a complex organic molecular crystal by IXS. The dynamic dielectric response function is measured over a large momentum transfer region, from which an exciton dispersion of 130meV is observed. We further developed this method to study other interesting system like C_{60} and gas molecules. Good results are obtained, which will be presented and discussed.

O6B07-A2

MOLECULAR DYNAMICS IN SEVERAL CHLORINE COMPOUNDS ON THE BASIS OF X-RAY THERMAL PARAMETER, IR/RAMAN AND NQR DATA

L. Ramu and R. Chandramani.
E-mail - sarasaramu76@hotmail.com
Phone – +91 -09880047250

Department of Physics, Bangalore University. Bangalore, INDIA.560056

Molecular dynamics (Torsional frequencies-f_T) in several organic and inorganic chlorine compounds have been evaluated on the basis of X-ray thermal parameters,IR/Raman and NQR data. NQR Studies gives useful information about the molecular dynamics and phase transitions in solids. Usually the f_T obtained through NQR data are compared with FT IR/Raman data. Here an approach has been made to evaluate f_T at room temperature using available data on X-ray thermal parameters.

Temperature factor of an atom for any set of lattice planes (hkl) depends on the inter planar spacing and on the magnitude of vibration perpendicular to the planes. There is an expression, which relates general temperature factor, the reciprocal lattice parameters and thermal parameters (U_{ij}) expressed in terms of mean square amplitudes ($<\theta^2>$) of vibration in Pm^2. The NQR motional averaging has been shown to arise from temperature dependent tilting of the z-axis of the EFG tensor. One can therefore estimate $<\theta^2>$ for various C-Cl bond directions, which define the respective z-axis of the EFG tensor using the X-ray thermal parameters.

The f_T at T=300K in the following compounds has been done:

(1) Barium Chlorate monohydrate.

(2) Bismuth Trichloride.

(3) 1-chloro 2,4 -dinitrobenzene.

(4).4-Chlorophenoxyacetic acid.

(5).2, 4- Dichlorophenoxyacetic acid.

(6).Monochloroacetic acid.

The f_T obtained by X-ray thermal parameters, IR/Raman and by NQR data have been compared. The values obtained in all the three cases are in good agreement. The above approach is a good illustration of the supplementary nature of the data from X-ray studies in relation to NQR studies of compounds in solid state. It is also interesting to compare this value with Raman data and Infrared data**.**

Reference:

1).L.Ramu, R.Banu, S.Rani and R.Chandramani. *ACTA PHYSICA POLONICA-A,* 775,Vol-**109**(2006).

O6B07-A3

VAPOR INDUCED GUEST EXCHANGE OF ORGANIC INCLUSION CRYSTAL

Hidehiro Uekusa, Yasunari Ashida, Kotaro Fujii

Department of Chemistry and Materials Science, Tokyo Institute of Technology, Japan

Among many characteristics of organic host-guest crystal, guest releasing and absorbing ability is one of the most attracting ones. By using this kind of crystal, controlled release of functional materials such as pharmaceuticals or chemicals is realized. In usual, the guest releasing is achieved by heating or mechanical crushing; however, it is also possible by applying vapor to crystal and sometimes the guest exchange occur.

In this study, some examples of the guest releasing or exchange phenomena by vapor application and their crystal structure change are presented. As the organic host framework is rather soft and it has guest induced structure, the single crystalline form of the organic inclusion compound often corrupted after guest release or exchange. In that case, crystal structure determination from powder diffraction data (SDPD) is very powerful technique and well utilized in this study.

By application of water vapor, pyromellitic acid di-methanol solvates crystal lost methanol molecules and new dihydrate crystal was grown as powder crystalline form. Also, the methanol and water guests were lost in ambient condition or by heating to form dehydrated powder crystal. The crystal structure analysis was successfully performed by SDPD technique. In di-methanol and dihydrate form, there are large channels, through which guest molecules are easily in and out. In dehydrate form; the channel is closed by small displacement of hosts and hydrogen bonds are formed, so the absorption of water molecule to recover the dihydrate form proceeds slowly. The reverse process (hydrate to methanol solvate) was not observed because the methanol solvate is rather unstable in the air.

Reversible guest exchange process by vapor application was observed between 1,1,2,2-tetrakis (4-hydroxyphenyl) ethane methanol and water solvates. Also in this case, crystal structures share common solvent channel feature and similar hydrogen bonding pattern, which should be the keys for guest exchange phenomena.

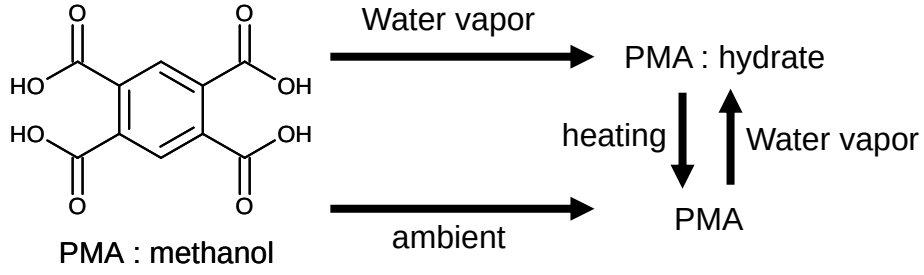

O6B07-A4

CONCERTED STRUCTURAL CHANGE AND PHOTOCHROMISM OF TRANS-BIINDENILIDENEDION DERIVATIVES

Akiko Sekine,[a] Kumiko Aruga,[a] Hidehiro Uekusa,[a] Katsuya Souno [b] and Koichi Tanaka [b]

[a]*Department of Chemistry and Materials Science, Tokyo Institute of Technology, Tokyo 152-8551, Japan,* [b]*Department of Applied Chemistry,, Kansai University, Osaka 564-8680, Japan*

Crystals of trans-biindenylidenedione (TBID) derivatives show photochromism and the color changes from yellow to red upon irradiation with UV and visible light [1]. In our previous study, crystal structure determination of several derivatives and their pseudo-polymorphs was performed in order to reveal the photochromic reaction mechanism. The crystal structures after irradiated with UV light (red form) were analyzed to show both the reactant (**1a**) and the photoproduct (**1b**) were located as a disordered structure, indicating that the photochromism is caused by an intramolecular (Norrish Type II) hydrogen transfer reaction.

In this study, the relationship between the crystal structures of TBD and their photochromic properties is presented. From the comparison of the crystal structures and the life-time of red-colored photoproduct, it is elucidated that the following three factors are important for photochromism; (1) molecular conformation of the initial crystal, (2) cavity size around the reactive part of the molecule, and (3) cooperative movement of the solvent molecules in the crystal.

For example, both of the crystal of TBID with Ar=4-F-Ph and its toluene solvate have Z'>1 and they show a very long photoproduct lifetime of more than 200 hrs. A careful investigation of their crystal structures revealed that only the molecule which has the most favorable conformation is photo-reactive and the occupancy of the corresponding photoproduct is very high. Moreover, the molecules surrounding the photo-reacting molecule are slightly shifted in position to allow the generation of photoproduct molecules. Thus, it is concluded that this kind of concerted crystal structure change would stabilize the red-colored photo-product and realize exceptional long-life photochromic specie.

Reference:

[1] Koichi Tanaka et al., CryslEngComm., 2004, **6**(2), 1-4

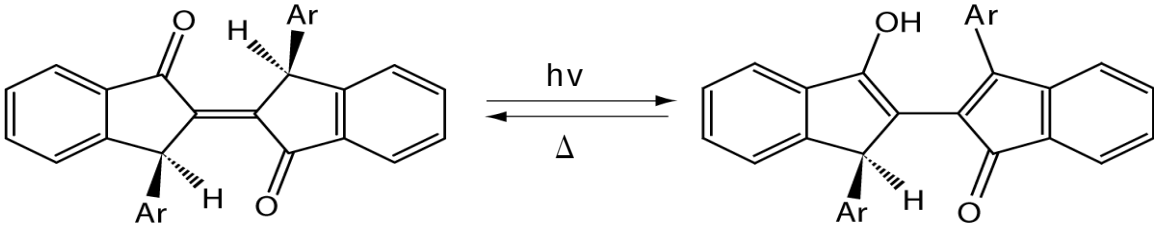

1a **1b**

O6B07-A5

CRYSTAL STRUCTURE ANALYSES OF CIS/TRANS PHOTOISOMERIZATIONS

Jun Harada, Mayuko Harakawa and Keiichiro Ogawa

Graduate School of Arts and Sciences, The University of Tokyo, Komaba

Cis-trans photoisomerization is one of the most important types of photoreactions, and innumerable studies on the subject have been carried out. The photoisomerization in the solid state, however, has generally been considered difficult to take place, and only a limited number of studies have been reported. In this study, we investigated the solid-state photoreactions of 2-(9-anthrylmethylene)-1-indanone and its derivatives. We have found that some of the compounds photoisomerize in their crystals. We succeeded in observing the crystal structural changes accompanying the isomerizations using X-ray diffraction analysis. The results showed that the solid-state photoisomerizations of these compounds proceed through the one bond flip of the isomerizing double bonds, and that the shapes of the molecules do not change so much before and after the reactions.

O6B07-A6

CRYSTALLINE STATE PHOTO ISOMERIZATION OF AN ORGARNO-DIRHODIUM DITHIONITE COMPLEX

Koshiro Toriumi,[a] Hiroshi Kanamono,[a] Shouichi Hashimoto,[a] Yoshiki Ozawa,[a] Minoru Mitsumi,[a] Hidetaka Nakai,[b] Yousuke Miyano,[b] Yoshihito Hayashi,[b] and Kiyoshi Isobe.[b]

[a]*Graduate School of Material Science, University of Hyogo, Hyogo 678-1297, Japan;*
[b]*Graduate School of Natural Science and Technology, Kanazawa University, Kanazawa 920-1192, Japan.*

An orgarno-dirhodium dithionite complex [{Rh(η^5-C_5Me_5)}2(μ-CH_2)$_2$(μ-O_2SSO_2)] (1)shows fully reversible photochromism in which one of four terminal oxygen atoms in the side-on type dithionite μ-O_2SSO_2 moiety is converted to a bridged one to produce geometrical isomer form μ-$OSOSO_2$ by visible light irradiation in crystalline-state [1,2].

An analogous dirhodium complex [{Rh(η^5-C_5Me_4Et)}2(μ-CH_2)$_2$(μ-O_2SSO_2)] (2) which has η^5-C_5Me_4Et instead of η^5-C_5Me_5 is isostructure to (1), and both the crystals belong to the same space group $P2_1/n$ and have almost the same cell parameters. We have tried to analyze the photo-isomerization process of the dirhodium complex (2) in crystalline state by X-ray structure analyses. The photo-irradiation time and light intensity dependencies of the photo-generated isomer ratio were measured for (2). As a result, it was revealed that kind of the main product of photo-generated isomers and their total ratio for (2) were different to the case for (1). Sum of the ratios of the photo-generated isomers for (2) was about 30% for the low intensity irradiation case but about 90% for the high intensity case. These phenomena seem to suggest that the photo-isomerization processes in crystalline states occur stereoselectively depend on reaction cavity and also an increase in crystal mosaicity owing to photo irradiation.

Reference:

1) H. Nakai, M. Mizuno, T. Nishioka, N. Koga, K. Shiomi, Y. Miyano, M. Irie, B. K. Breedlove, I. Kinoshita, Y. Hayashi, Y. Ozawa, T. Yonezawa, K. Toriumi, and K. Isobe, *Angew. Chem. Int. Ed.*, **2006**, *45*, 6473-6476.

2) Y. Ozawa, T. Yonezawa, T. Yokoyama, M. Mitsumi, K. Toriumi, H. Nakai, Y. Hayashi, and K. Isobe, *AsCA* 06*/CrSJ*, Tsukuba, Japan, 2006/11.

O6C07-A1

STRUCTURE DETEMINATION FROM HIGH RESOLUTION SYNCHROTRON POWDER DIFFRACTION DATA

EIji Nishibori,[a] Shinobu Aoyagi,[a] and Makoto Sakata[a]

[a]*Department of Applied Physics, Nagoya University*

The crystal structure determination from powder diffraction (SDPD) has attracted wide interests for its huge potential to accelerate a design, synthesis, and characterization of the materials in the fields of nano- and bio- technologies. During past decade, many studies of SDPD have been reported on the methodology, the software, and also the actual ab initio structural determinations. Presently, the structure of small molecule with less than 30 atoms and approximately 10 degree of freedoms can routinely solve by the several software on single personal computer from powder data of laboratory X-ray source. The SDPD for large systems such as medium-sized pharmaceuticals are still difficult task due to a large number of degree of freedoms. High resolution powder data and additional techniques for structure solution have been normally required for SDPD in these cases. In the present study, we have performed SDPD for medium-sized pharmaceutical, Prednisolone Succinate, using high resolution synchrotron X-ray powder diffraction data.

The data used in the present study are collected at BL02B2, SPring-8. The d-spacing range of the data is d>1.0Å, which is much wider than that of laboratory data, d>2.0-1.4Å. The structure determination has been carried by the original Genetic Algorithm (GA) system. The number of degree of freedoms in the GA analysis is 25. In the refinement process, the Maximum Entropy Method (MEM) analysis has played a crucial role to have a better structure model. The reliability factors, R_{wp} and R_I, of the final structure analysis by the Rietveld refinement reach less than 3% and 5%, respectively. The reasonable structure including hydrogen atoms of medium-sized pharmaceutical with no check-cif Alert relating to the fundamental structure such as inter-atomic distances and bond angles has been determined in the present study.

O6C07-A2

STRUCTURAL STUDIES EMPLOYING HIGH ENERGY POWDER DIFFRACTION

Peter L. Lee

Advanced Photon Source, Argonne National Laboratory, Argonne, IL 60439, U. S. A.

The structural information is crucial for all materials research projects. The increasing complex materials process critically needed the timely feed back of the structural information during the initial discovery stage. However, most of the materials being studied do not have a single crystal form suitable for the routine crystal structure determination. Powder diffraction becomes a critical tool that can determine the structure or follow structural changes parametrically.

The high energy third generation synchrotron sources such as Advanced Photon Source are capable of producing extremely intense high-energy x-rays has opened a wide variety of important structural research opportunities. Combining advanced specialized undulators and optics designed can produce unprecedented brilliance and photon flux for the high energy x-rays. The use of high x-ray energies for powder diffraction largely eliminates the absorption and extinction effects, opening the possibility to study many materials containing high-Z elements. The ability to penetrate through bulk materials and/or environmental cell enables us to examine the insight dynamically under extreme and carefully controlled conditions. The short wavelengths also allow the measurement of very high Q data, providing more structure detail and satisfying the requirement of the Pair Distribution Function analysis.

Recent development of high energy powder diffraction at the Advanced Photon Source will be presented including the advancement of instrumentation and new research opportunities.

Use of the Advanced Photon Source was supported by the U. S. Department of Energy, Office of Science, Office of Basic Energy Sciences, under Contract No. DE-AC02-06CH11357.

O6C07-A3

EXPECTING THE UNEXPECTED. PHASE TRANSITIONS IN MANGANESE PEROVSKITES

Brendan J Kennedy,[a] and Zhaoming Zhang,[b]

[a] *School of Chemistry, The University of Sydney, Sydney Australia;* [b] *Institute for Materials and Engineering, ANSTO, Australia*

Manganese perovskites, have the general formula $AMnO_3$, and exhibit a rich and diverse range of structures, the precise structure depending on the oxidation state of the manganese, both Mn^{3+} (d^4) and Mn^{4+} (d^{3+}) are found in perovskite type oxides, the size of the A-type cation and the presence of any vacancies in the lattice. Following the discovery of colossal magnetoresistance in $LaMnO_3$ considerable effort has been made towards understanding the complex interplay between orbital ordering associated with the Jahn-Tellar active Mn^{3+} ions and the tilting of the MnO_6 polyhedra associated with the relative sizes of the cations.

The present work describes structural studies, using a combination of high resolution synchrotron X-ray and neutron diffraction, of three series of manganese perovskites; namely the Mn^{4+} containing oxides of the type $Ca_{1-x}Sr_xMnO_3$; and the mixed valence $Mn^{3+/4+}$ oxides $Sr_{1-x}Ce_xMnO_3$ $0.075 < x < 0.4$ and $Sr_{0.9-x}Ca_xCe_{0.1}MnO_3$ $0.0 < x < 0.9$. In the first series the progressive replacement of the Ca^{2+} by the smaller Sr^{2+} cation induces a first order orthorhombic (*Pnma*) to tetragonal (*I*4/*mcm*) transition associated with tilting of the octahedra. Introducing Mn^{3+} into the structure, by partially replacing Sr^{2+} with Ce^{3+}, results in a large Jahn-Tellar induced tetragonal distortion of the MnO_6 octahedra and the formation of a second orthorhombic phase in *Imma*. Progressive replacement of Sr by Ca in $Sr_{0.9-x}Ca_xCe_{0.1}MnO_3$ results in a reduction in the distortion of the unit cell, but an increase in the distortion of the MnO_6 octahedra. We present the clearest evidence to date for the independence of the orbital ordering and octahedral titling in these oxides.

O6C07-A4

MORPHOTROPIC PHASE BOUNDARY LIKE CHARACTERISTIC IN A LEAD-FREE, AND NON-FERROELECTRIC SYSTEM $(1-x)NaNbO_3$-$xCaTiO_3$

Saurabh Tripathi[a], Rajeev Ranjan[a], Dhananjai Pandey[a], Sanjay Kumar Mishra[b] and P.S.R. Krishna[b]

[a]*School of Materials Science and Technology, Institute of Technology, Banaras Hindu University, Varanasi-221005, India;* [b]*Solid State Physics Division, Bhabha Atomic Research Centre, Trombay, Mumbai-400085, India.*

The phase diagrams of several mixed solid solutions of the ABO_3 type perovskites contain a nearly vertical morphotropic phase boundary (MPB) separating tetragonal and rhombohedral phase fields. The MPB composition has been found to be of special technological significance for numerous sensor and actuator devices, as several physical properties like dielectric permittivity, electromechanical coupling coefficients and piezoelectric strain coefficients are maximized around this composition. In the well known commercial MPB systems, like $Pb(Zr_xTi_{(1-x)})O_3$(PZT), (1-x)[$Pb(Mg_{(1/3)}Nb_{(2/3)})O_3$]-$xPbTiO_3$(PMN-xPT) and (1-x)[$Pb(Zn_{(1/3)}Nb_{(2/3)}O_3$]-$xPbTiO_3$(PZN-xPT), this peak in the composition dependence of dielectric and piezoelectric properties around the MPB has been linked with the change of crystal structure from tetragonal to rhombohedral through a narrow range of stability of monoclinic phases. The toxicity of lead oxide and its high vapour pressure during processing of these MPB ceramics have led to the search for alternative environmentally friendly materials free from lead. The MPB systems discovered so far, be it lead-based or non-lead based, have at least one component, which is ferroelectric in nature (e.g. $PbTiO_3$, $KNbO_3$, LiNbO3). We present here MPB like characteristic in a new lead free system, (1-x)$NaNbO_3$-$xCaTiO_3$ (NN-xCT), in which the end members $NaNbO_3$ and $CaTiO_3$ are well known antiferroelectric and paraelectric materials, respectively, under ambient conditions. At low temperatures, antiferroelectric $NaNbO_3$ transforms to a ferroelectric phase while $CaTiO_3$ exhibits quantum paraelectric behaviour. The composition dependence of the room temperature dielectric permittivity of this mixed system exhibits a sharp rise in the composition range $0.10<x<0.20$ with a peak at $x\approx0.16$. This anomalous rise in the dielectric permittivity is shown to be linked with a change of crystal structure from an orthorhombic structure in the Pbma space group for $x\leq0.10$ to another orthorhombic structure but in the Pbnm space group for $x\geq0.20$. This behavior is reminiscent of a similar rise in the dielectric permittivity near the MPB composition of the technologically important PZT and PMN-xPT ceramics due to a change of crystal structure from tetragonal to rhombohedral. Further, the composition dependence of the (+) and (-) tilt angles due to M and R point phonon instability with wave vectors ($^1/_2{}^1/_2{}^1/_2$) and ($^1/_2{}^1/_20$) of the cubic brillouin zone have been discussed in detail. Bond lengths and bond angles have been calculated to show the nature of the octahedral distortion. To the best of our knowledge, the NN-xCT ceramics are the first example of a non-ferroelectric and non-piezoelectric MPB system in contrast to the well known MPB systems which are all ferroelectric and piezoelectric.

O6C07-A5

SYNCHROTRON RADIATION X-RAY DIFFRACTION AND SPECTROSCOPIC ELLIPSOMETRY INVESTIGATION OF Si_3N_4 ON Si FOR SUB-50NM Si-IC APPLICATIONS

Zhe Chuan Feng[a,*] , Li-Chi Cheng [a], Chu-Wan Huang [a], Ying-Lang Wang [b], and Hwo-Shuenn Sheu [c]

[a] *Institute of Photonics & Optoelectronics and Department of Electrical Engineering, National Taiwan University, Taipei, Taiwan 106-17, ROC;*

[b] *Taiwan Semiconductor Manufacturing Company, Tainan, 741-44 Taiwan, ROC;*

[c] *National Synchrotron Radiation Research Center, Hsinchu, 300-76 Taiwan, ROC.*

** E-mail: zcfeng@cc.ee.ntu.edu.tw*

Silicon nitride (Si_3N_4) is an advanced material and has the potential to be used in various applications due to good performance in mechanical, chemical, electronic, and thermal properties. On the other hand, its high doping concentration, and chemical stabilities are similar to the III–N compounds such as GaN and AlN, which are used to grow quantum well structures for obtaining blue laser. They play an important role in the electronics industry, especially in Si-based large-scale integration circuit technology and possibly in optoelectronics. The sample is constructed from 50 nm Si_3N_4 thin film grown on 12” silicon substrate by chemical vapor deposition (CVD) process which is from our collaborator-Taiwan Semiconductor Manufacturing Company (TSMC) company. We have performed the synchrotron radiation X-ray diffraction (SR-XRD) experiments on Si_3N_4 using a short wavelength (~0.443Å) in National Synchrotron Radiation Research Center (NSRRC). The thickness, reflectance index and extinction coefficient of Si_3N_4 thin film were also determined using variable angle spectroscopic ellipsometer (VASE). By the using of superior experimental instruments, we found from the XRD pattern that there is a mixture state of α- and β- Si_3N_4 and other impurities present in the samples. We are going to plan another set of synchrotron XRD measurements using another energy synchrotron source to have different wavelengths excitation XRD data on the samples. This will benefit to analyze the studied materials and lead to better understand materials properties.

P05-001

ENGINEERING MATERIALS DIFFRACTOMETER AT J-PARC

Stefanus Harjo[a], Atsushi Moriai[a], Kentaro Suzuya[a], Kazuya Aizawa[a], Kaori Shirakihara[b], Yo Tomota[c], Koichi Akita[d], Masatoshi Arai[a], Yukio Morii[e]

[a]J-PARC Center, Japan Atomic Energy Agency, Tokai, Ibaraki, Japan; [b]Department of Mechanical Engineering, Suzuka National College of Technology, Suzuka, Mie, Japan; [c]Institute of Applied Beam Science, Ibaraki University, Hitachi, Ibaraki, Japan; [d]Department of Mechanical System Engineering, Musashi Institute of Technology, Tokyo, Japan; [e]Quantum Beam Science Directorate, Japan Atomic Energy Agency, Tokai, Ibaraki, Japan.

The Engineering Materials Diffractometer TAKUMI is now being developed at J-PARC project. TAKUMI is one of the prospective instruments to promote industrial users at J-PARC, and has main specifications as follows. A high intensity to realize short measuring times that are particularly necessary for in situ measurements, a high resolution to assure high accuracies on stresses measurements and microscopic strains measurements, an enough wavelength bandwidth to assure many reflections for analyzes of anisotropic deformation behaviors and textures in bulk engineering materials, etc.

TAKUMI views a decoupled-poisoned liquid H_2 moderator, having the primary and the secondary flight paths of 40m and 2.0m, respectively. It will have the 90 degree scattering detector banks with $75° < 2\theta < 105°$ and off angle of ±20°, and a curved supermirror neutron guide with focusing-vertically tapered at the tail part. From a Monte Carlo simulation, an appropriate resolution of about 0.15% in $\Delta d/d$ has been confirmed at a high resolution mode. TAKUMI has an effective wavelength bandwidth of about 3.5Å at a 25Hz disk chopper operation (similar to pulse repetition rate), that gives more than 15 reflections including the lowest index for steel samples. Details of the designs and the construction progresses are presented.

P05-002

CURRENT STATUS OF IBARAKI BIOLOGICAL CRYSTAL DIFFRACTOMETER IN J-PARC

Ichiro Tanaka,[a] Takashi Ohhara,[b] Kazuo Kurihara, [b] Katsuhiro Kusaka, [c] Takaaki Hosoya, [c] Katsuaki Tomoyori, [d] Nobuo Niimura, [d] Tomoji Ozeki, [e] Kazuya Aizawa, [c] Masatoshi Arai, [c] Yukio Morii, [b] Makoto Hayashi, [f] Kazuhiro Ebara [f] and Yoshiki Takano [f]

[a]Dept. Biomol. Func. Eng., Ibaraki Univ.; [b]Quantum Beam Sci., Japan Atomic Energy Agency, Tokai, Ibaraki 319-1195, Japan; [c]J-PARC Center, Japan Atomic Energy Agency; [d]Inst. Appl. Beam Sci., Ibaraki Univ.; [e]Dept. Chem. Mat. Sci., Tokyo Institute of Technology; [f]Ibaraki Prefectural Government.

IBARAKI Biological Crystal Diffractometer is a new single-crystal neutron diffractometer for biological and chemical crystallography, and is now being constructed at J-PARC by Ibaraki Prefectural Government in Japan. This diffractometer is designed for the protein crystals with the cell dimension up to 135Å. The measurement efficiency is more than 50 times larger than the present neutron diffractometer, BIX-3/BIX-4 in JRR-3 reactor at JAEA. To achieve this performance, we've selected a coupled moderator, and worked out the optimisation of the neutron guide tube. For the detector, a new wavelength-shifting-fiber type scintillation area detector system with high spatial (0.5-1.0mm) and time (1μs-) resolution are in development.

P05-003

PROGRESS REPORT ON SUPER HIGH RESOLUTION POWDER DIFFRACTOMETER IN J-PARC

Shuki Torii[a], Yasuo Kobayashi[a], Junichi Suzuki[a], Hidenori Sagehashi[a], Minoru Nagai[a], Kenichi Oikawa[b], Kazuhiro Mori[c], Masao Yonemura[d], Toru Ishigaki[d] and Takashi Kamiyama[a]

[a] *High Energy Accelerator Research Organization; Oho Tsukuba, Ibaraki 305-0801, Japan*
[b] *Japan Atomic Energy Agency; Tokai-mura, Naka-gun, Ibaraki 319-1195, Japan*
[c] *Kyoto University Research Reactor Institute; Kumatori-cho, Sennan-gun, Osaka 590-0494, Japan*
[d] *Ibaraki University; Nakanarusawa-cho, Hitachi, Ibaraki 316-8511, Japan*

Neutron Science Division of High Energy Accelerator Research Organization (KEK) is constructing a Super High Resolution Powder Diffractometer (SHRPD) at a Materials and Life Science Experimental Facility (MLF) in Japan Proton Accelerator Research Complex (J-PARC). SHRPD is designed to have the world best resolution with $\Delta d/d = 0.03\%$ in $0.5 < d$ [Å] < 4 and covers $4 < d$ [Å] < 45 with gradually changing resolution. The combination of the high quality data from SHRPD and their high-precision analysis gives us information on tiny structural changes that have been overlooked previously. SHRPD is located at 100 m from a thin side of a decoupled poisoned moderator, which has been developed to produce a high-resolution & good S/N data to achieve the 0.03 % resolution within 100 m flight path. SHRPD has a 32 m curved guide and 50 m straight guide section between the instrument and the moderator. A beam line building with 50 m length and an annex experimental hall with 7 m (H) x 10 m (W) x 13 m (L) for the SHRPD instrument are under construction in the east side of MLF experimental hall. The first beam is scheduled to be delivered on May 2008.

P05-014

SHORT-RANGE ORDER PARAMETERS OF AsGeSe GLASSES

A.H. Moharram, M. A. Hefni and A.M. Abdel-Baset

Physics Department, Assiut University, Assiut, Egypt

Short range order (SRO) parameters of the bulk $As_xGe_{40-x}Se_{60}$ (with x = 0, 10 & 20 at.%) alloys have been determined using the x-ray Cu(Kα) radiation in the wave vector interval $0.28 \leq K \leq 6.5$ Å^{-1}. The radial distribution functions, $RDF(r)$, have been obtained either by Monte-Carlo simulation or by Fourier transformation of the experimental data (conventional method). The Monte Carlo method used to generate the numerical radial density function, $g(r)$, and randomly modified until the corresponding interference structure factor $I(K)$ fit with the experimental data for all the investigated glasses. Gaussian analyses of the first four peaks in the total correlation function shows that $Ge_2(Se_{1/2})_6$ and $Ge_2(Se_{1/2})_4$ molecular units are the basic structural units for the binary and ternary alloys, respectively. Insignificant structural changes have occurred as a result of replacing Ge atoms by As atoms in the ternary glasses.

P05-015

STRUCTURAL AND SPECTROSCOPIC STUDIES OF CATION DISORDER IN SOME Bi CONTAINING PYROCHLORES

Qingdi Zhou, Brendan J. Kennedy

Centre for Structural Biology and Structural Chemistry and Centre for Heavy Metals Research, School of Chemistry, The University of Sydney, Sydney, NSW, 2006, Australia

Metal oxides displaying the pyrochlore type structure have been extensively studied as they possess important electronic and magnetic properties. These properties are strongly dependent on the nature and bonding of the *B*-site cations as well as disorder of *A*-site cations from the ideal position. To be better understanding the A-site disorder in pyrochlore oxide, a number of bismuth or lead containing pyrochlores based on Bi_2CrNbO_7 and $Pb_2TiNbO_{6.5}$ together with the *A*-site substituted $(Bi_{1-x}Y_x)_2(Z_{1-x}Nb_x)_2O_{7-\delta}$ (Y = Pb, Na, K; Z = Cr, Ti) oxides have been investigated using room-temperature powder neutron and synchrotron X-ray diffraction methods. Also bismuth and lead *L*-edge X-ray absorption fine structure (XAFS) experiments were performed in the solid state at low temperature (10 K) to investigate the local structure of the *A*-site cations. All samples exhibited an $A_2B_2O_7$ pyrochlore like cubic structure. Precise local structures for the Bi and Pb cations were obtained from single- and multiple-scattering fits to the XAFS data.

P05-016

APPLICATION OF LARGE RADIUS IMAGING PLATE CAMERA FOR SYNCHROTRON POWDER X-RAY DIFFRACTION TO STRUCTURAL PHASE TRANSITION STUDIES

Masahiko Tanaka[a] and Yoshio Katsuya[b]

[a]*BL15XU /SPring8, National Institute for Materials Science, Kouto, Sayo, Hyogo, Japan;* [b]*SPring8 Service Co. Ltd. Kouto, Sayo, Hyogo, Japan*

A newly developed large radius imaging plate (IP) camera system for the diffractometer of BL15XU, which is an undulator beamline of synchrotron facility, SPring-8, was applied for powder diffraction studies altering sample condition.

We have developed a new large radius imaging plate camera system for high angular resolution and high throughput synchrotron X-ray powder diffraction. The new IP camera system consists of a cylindrical shape IP cassette installed on the 2-theta arm of the diffractometer of BL15XU. Powder diffraction data were recorded on an IP by multiple exposures changing 2-theta setting angles and separately collected diffraction data can be provided for various powder crystal-structure analysis methods after data processing such as data format conversion, connection and correction. The sample-to-IP distance of this camera was designed to be 954.9mm and the large sample-to-IP distance brings high angular resolution. The angular resolution of this IP camera was evaluated by the FWHM of NBS-Si 111 peak and the observed FWHM value was smaller than that of a powder diffractometer with Ge(111) analyzer at a bending magnet beamline of 2nd generation synchrotron. An exposure time was less than 120 seconds for most samples, thus a total measurement time for one powder diffraction pattern was less than 20 minutes. This new system has achieved twenty-times faster powder diffraction improving the high resolution of current synchrotron powder diffractometer. The high angular resolution and high throughput realized by this newly developed IP camera is suitable for diffraction experiment altering the sample conditions diversely, such as the detailed observation of structural phase transition and the determination of thermal expansion coefficient. We will demonstrate the application experiments of this camera to such experiments of inorganic crystal powder samples.

P05-017

MORPHOTROPIC PHASE BOUNDARY IN (1-x)$BiFeO_3$-x$PbTiO_3$: PHASE COEXISTENCE REGION AND UNUSUALLY LARGE TETRAGONALITY

Shuvrajyoti Bhattacharjee, Saurabh Tripathi and Dhananjai Pandey

School of Materials Science and Technology, Institute of Technology, Banaras Hindu University Varanasi – 221005, India.

Multiferroics are promising materials for technological exploitation in actuator, sensor and data storage devices. Perovskite $BiFeO_3$ (BF), in bulk form, is ferroelectric, antiferromagnetic and ferroelastic multiferroic material with antiferromagnetic (T_N ~ 643 K), ferroelectric (T_C ~ 1103 K), and structural ordering temperatures well above room temperature. It shows weak magnetism at room temperature due to canted spin arrangements in G-type antiferromagnetic structure (with an incommensurate spiral magnetic ordering). It has a rhombohedrally distorted perovskite structure in the R3c space group with $a^-a^-a^-$ tilt system in which the neighbouring oxygen octahedra of the elementary perovskite cells are rotated anti-clockwise about the [111] direction due to a ferroelastic transition involving R(q =1/2 1/2 1/2) point phonon. $BiFeO_3$ forms a continuous solid solution with $PbTiO_3$ (PT) and shows a morphotropic phase boundary (MPB) similar to the MPBs in the well known $Pb(Zr_xTi_{1-x})O_3$ (PZT) and (1-x)$Pb(Mg_{1/3}Nb_{2/3})O_3$-x$PbTiO_3$ (PMN-xPT) ceramics. There is considerable controversy about the location and width of the MPB in the (1-x)$BiFeO_3$-x$PbTiO_3$ (BF-xPT) system. For example, the tetragonal phase is reported to be stable upto compositions (x_T) in the range $0.3<x_T\leq0.4$. In the MPB region, the tetragonal and rhombohedral phases coexist over a composition range $x_R<x_{MPB}<x_T$, where x_R marks the onset of the stability of single phase rhombohedral region. The width (x_T- x_R) of the MPB region is still unsettled, as values as small as ~0.06 and as high as 0.10 have been reported in the literature. The existing controversy about the stability field of the room temperature tetragonal structure of multiferroic BF-xPT and width of the morphotropic phase boundary are settled using powder x-ray diffraction data. It is shown that BF-xPT shows pure tetragonal structure upto x_T = 0.31 and rhombohedral structure for $x_R \leq 0.27$. In the intermediate composition range ($0.27<x_{MPB}<0.31$), the two phases are found to coexist. The composition width, $\Delta x \sim 0.03$, for the MPB observed by us is the narrowest reported so far in the literature for this system. We have carried out Rietveld refinement of the pure tetragonal composition (x = 0.31) closest to the MPB showing the highest c/a ratio of 1.18739(2). Results of Rietveld refinement of the powder x-ray diffraction data for BF-0.31PT provide some structural insight into the unusually large tetragonality of this composition.

P05-018

DISORDER OF Pb ATOM IN CUBIC PHASE OF PEROVSKITE-TYPE SOLID SOLUTIONS PZT AND PZN-PT

Yoshihiro Terado,[a] Chikako Moriyoshi,[a] Yoshihiro Kuroiwa,[a,d] Yasuhisa Yamamura[b] and Makoto Iwata[c]

[a]*Department of Physical Science, Hiroshima University, Kagamiyama, Higashi-Hiroshima 739-8526, Japan;* [b]*Department of Chemistry, University of Tukuba, Tennodai, Tsukuba 305-8571, Japan;* [c]*Department of Engineering Physics, Electronics and Mechanics, Nagoya Institute of Technology, Showa-ku, Nagoya 466-8555, Japan;* [d]*CREST, Japan Science and Technology Agency, Honmachi, Kawaguchi 332-0012, Japan*

Ferroelectric properties of perovskite-type oxides with the chemical formula ABO_3 are enormously influenced by substituting the other atoms for the *A* and/or *B* atoms. A lot of promising materials have been discovered by taking advantages of this substitution effects. Among them, Pb-based perovskite-type solid solutions $PbZr_{1-x}Ti_xO_3$ (PZT) are well known as piezoelectric ceramics for the industrial applications due to their high electromechanical coupling constant and piezoelectric constant. All PZT do not show the high piezoelectric performance. A PZT with a morphotropic phase boundary (MPB) composition possesses the high piezoelectric properties. In $(1-x)Pb(Zn_{1/3}Nb_{2/3})O_3–xPbTiO_3$ (PZN–PT) and $(1-x)Pb(Mg_{1/3}Nb_{2/3})O_3–xPbTiO_3$ (PMN–PT) systems, the prominent properties are also reported around their MPB compositions. Hence, it is essential to understand the formation mechanism of MPB for designing new piezoelectric ceramics nowadays.

The aim of the present study is to investigate the relationship between the crystal structure of the Pb-based perovskite-type solid solutions in the cubic phase and the appearance of MPB that separates the ferroelectric phase by the vertical phase boundary. High-energy synchrotron-radiation powder-diffraction experiments for PZT ($0 \leq x \leq 1$, MPB at $x \sim 0.5$) and PZN–PT ($0 \leq x \leq 0.3$, MPB at $x \sim 0.1$) in the cubic phase were performed at BL02B2 in SPring-8.

Thus far, every crystal structure of the paraelectric phase has generally been considered to be isomorphous to the classical perovskite with a cubic symmetry, where Pb and *B*-site atoms are settled at the cubic corner and body center, respectively, and O atoms at the face centers. Our precise Rietveld analyses for PZT and PZN-PT with various compositions have showed clear evidence that the Pb atom is disordered around the cubic corner site and the thermal motions significantly change near the MPB composition, while no anomaly on the thermal parameter is revealed for the *B*-site atoms. Hence, we considered that the appearance of MPB is strongly related to the changes in local environment around the Pb atom caused by the *B*-site substitution.

P05-019

X-RAY STRESS ANALYSIS FOR FIBER TEXTURES BASED ON SYMMETRY IN RECIPROCAL LATTICE SPACE

Ryouichi Yokoyama, and Jimpei Harada

Rigaku Corporation, Tokyo, Japan

A technique to derive analytical formulae is shown in obtaining residual stress of poly-crystalline materials with fiber textures from the XRD measurement of a strain component. The relation between the strain measured by XRD, $<\varepsilon^{L}_{33}>$, and stress, σ_{kl}, in a specimen for Reuss model is given by

$$<\varepsilon^{L}_{33}> = \omega_{3i}\omega_{3j} <\boldsymbol{S}^{P}_{ijkl}> \sigma_{kl}$$

where $<\boldsymbol{S}^{P}_{ijkl}>$ is the elastic compliance constants defined in Specimen coordinate and $\omega_{3i}\omega_{3j}$ the transformation matrices from Specimen coordinate to Laboratory coordinate and the superscripts L and P represent the Laboratory and Specimen coordinates, respectively.

The key point is how to calculate average elastic compliance constants $<\boldsymbol{S}^{P}_{ijkl}>$ for specimen with fiber texture in terms of the well known elastic compliance constants defined for a constituent single crystallite. For such calculation it is very advantageous to take into account symmetry, Laue symmetry, of the intensity distribution in reciprocal lattice space, for the constituent micro crystallite in specimen. By taking up a stress state of $\sigma_{13}=\sigma_{23}=\sigma_{33}=0$, which is so-called non-equi-biaxial state, for the [111] cubic fiber texture as an example, relations between strain measured and stress are given for both Reuss and Voigt models. When this technique is applied to the equi-biaxial state, that is, $\sigma_{11}=\sigma_{22}=\sigma$ in addition to the above stress state, the resultant equation for Reuss model is in agreement with that for Voigt model, indicating the approval of the present derivation.

P05-020

GENERALIZED METHOD OF STRUCTURE ANALYSIS FOR MICRO IMPERFECT CRYSTALS USING SR.

Ken-ichiro Yamamoto,[a] Yoshio Nogami,[a] Naoshi Ikeda,[a] Takayoshi Ito,[b] Toru Matsuura,[c] Taku Tsuneta,[c] Satoshi Tanda[c]

[a]*Department of Physics, Okayama University, Japan;* [b]*Japan Synchrotron Radiation Research Institute SPring-8, Japan;* [b] *Department of Applied Physics, Hokkaido University, Japan.*

For many years, to determine the atomic coordinate for imperfect crystals was particular difficult. For perfect single crystals, one can use well-defined structure analysis method with Direct method, least square method and the UB matrix obtained by the k-space positions of Bragg reflections. On the other hand, one can use powder crystal method using perfect powder crystals without preferred orientation.

Recently, S. Tanda *et al.* found that the instability against deformation of thin whisker crystal of quasi one-dimensional conductor $NbSe_3$ results in several new crystal forms with folded structures named topological crystals[1]. Surprisingly, the new crystal forms are *seamless* ring (cylinder, tube), *seamless* Möbius strip and *seamless* figure of eight strip, all few tens of micrometers.

Determination of atomic arrangement in the topological crystal was also very difficult owing to the curved shape. In other words, the orientation of each crystallite composing a topological crystal has positional dependence reflecting its shape. Thereby, we abandoned single crystal method applicable only to a perfect crystal with constant crystal orientation. On the other hand, powder crystal method also faced the difficulty of strong positional variation of the crystal orientation depending the curved shape. If we divide or crash a topological crystal to average its crystal orientation and to obtain good powder crystal, we may lose important structural information originated from its bound and twisted shape.

Bearing this difficulty in our mind, we determined to develop new camera and analysis method to solve the structure of the topological crystal *without any sample treatment.* For the suppression of preferred orientation, we get some hint from traditional Gandolfi camera and developed new two-axis sample rotator. The original Gandolfi camera with the two-axis rotator was used in the mineralogy for qualitative analysis of constituting elements. However, their rotations were not independent nor incommensurate, because of the geared transmission between the two axis rotation.

Reference:

[1] S. Tanda and T. Tsuneta et al. Nature 417 (2002) 397.

P05-021

SYNTHESIS, REACTIVITY AND 3-D STRUCTURAL DETERMINATION BY POWDER DIFFRACTION ON MOLYBDOPTERIN COMPLEX

Jey Jau Lee*[a], Hwo-Shuenn Sheu[a],Keng S. Liang[a] , Baidyanath Ghosh[b] and Parag Sinchan Roy[b]

[a]*National Synchrotron Radiation Research Center Hsinchu 30076, Taiwan R.O.C.* [b]*. Department of Chemistry, University of North Bengal, Dist.- Darjeeling – 734013, India.*

The biological function of Molybdenum has been known to be contained in more than 30 distinct enzymes. The molybdenum-cofactor (Mo-co) consists of a mononuclear molybdenum ion coordinated by one or two molybdopterin ligands. Crystallographic results are very rare because of the crystal are very hard to grow up. The few results have demonstrated that the molybdopterin ligands are tricyclic and nonplanar, and that they coordinate the metal through their dithiolene sulfurs.

The molybdopterin ligand may participate in the various electron transfer reactions associated with the catalytic mechanism of these proteins, as suggested by both oxidation state-dependent changes in the metal coordination environment and the molybdopterin structure, and by the interaction of the molybdopterin with other redox groups within Mo-co-containing enzymes. In here the 2-pivaloylamino-6-acetonyl- isoxanthopterin (**1**, H_2L) has been reacted with Na_2MoO_4 $2H_2O$ under suitable conditions in presence of cysteine and Ph_4PBr for synthesizing the new compound $(Ph_4P)_2[Mo^{IV}(L)(cys)_2].0.5CH_3OH$. Synchrotron powder diffraction studies throw light on its structural aspect. Here we report the 3-D structure determination of bio-mimic molybdenum coordination compounds from synchrotron powder diffraction data. The asymmetric unit contains more than 400 atoms. The synthesis, reactivity and structure determination from synchrotron radiation powder diffraction will be shown and discussed.

P05-022

SOLVING ZEOLITE STRUCTURES FROM POWDER DATA USING DENSITY BUILDING FUNCTIONS AND HISTOGRAM MATCHING

Chris Gilmore[a] and Douglas Dorset[b]

[a]*WESTCHEM, Department of Chemistry, Unversity of Glasgow, Glasgow G12 8QQ, UK*
[b]*Advanced Characterization, ExxonMobil Research and Engineering Co.,1545 Route 22 East, Annandale, New Jersey 08801, USA.*

Recently we have applied techniques that use density building functions and density histogram matching methods coupled with entropy maximisation and likelihood analysis to solve a number of structures *ab initio* using electron diffraction data in 2- and 3-dimensions.

The same methodology can be used with powder diffraction:

1. A low resolution structure is generated using non-overlapped low resolution structure factors combined with the origin defining rules of direct methods [1].
2. New reflections are given permuted phase angles (and intensities if overlapped) and analysed using density building functions [2].
3. The optimal phase sets are subjected to entropy maximisation [3].
4. Likelihood and density histograms are used to select the optimal phase set.

Applications to a number of varied zeolite systems will be presented.

Reference:

[1] Rogers, D. (1980) *Theory and Practice of Direct Methods in Crystallography* edited by M.F.C. Ladd & R.A. Palmer pp. 23-92. New York: Plenum Press.

[2] Gilmore, C.J., Bricogne, G & Bannister, C. (1990). *Acta Cryst.* **A46,** 297-308.

[3] Bricogne, G & Gilmore, C.J. (1990). *Acta Cryst.* **A46**, 284-297.

P05-023

BIO-MEMBRANE STRUCTURE PROBED BY THE LAMELLAR X-RAY DIFFRACTION AND THE SMALL ANGLE X-RAY SCATTERING AT NSRRC

Ming-Tao Lee, Yu-Shan Huang, U-Ser Jeng, Ying-Huang Lai, and Ya-Sen Sun

National Synchrotron Radiation Research Center, Hsinchu, Taiwan, 300, R.O.C.

The bio-membrane structure has long been an interesting issue in life science. Various techniques, including X-ray diffraction, small-angle scattering and nuclear magnetic resonance (NMR), have often been introduced in revealing bio-membrane structures under various humilities and temperatures as well as interactions with proteins. In this study, the lamellar X-ray diffraction (LXD) and small angle X-ray scattering (SAXS) are used to determine the membrane structures under various environments. Temperature- and humility-dependent LXD experiments for a multilamellar membrane on a plane substrate were conducted with 12keV photons of the BL13A beamline at the National Synchrotron Radiation Research Center (NSRRC). The electron density profile and thickness of membrane are extracted from the data fitting. Furthermore, temperature-dependent SAXS experiments for unilamellar vesicles in an aqueous solution were measured with 10.5keV photon of the BL17B3 beamline, NSRRC. Combining model fitting and SAXS data, the membrane thickness of vesicles in the solution has been determined.

P05-024

ANOMALOUS X-RAY SCATTERING AND ABSORPTION SPECTROSCOPY INVESTIGATE THE MORPHOLOGY OF FePt MONOLAYER NANOPARTICLE ON SURFACE MODIFIED SUBSTRATES WITH AU OVERLAYER

Tzu-Wen Huang,[a,b], Kuan-Li Yu,[c], Yen-Fa Liao,[a] and Chih-Hao Lee[a]

[a]Department of Engineering and System Science, National Tsing Hua University, Hsinchu, Taiwan; [b]Institute of Physics, Academia Sinica, Taipei, Taiwan; [c]National Synchrotron Radiation Research Center, Hsinchu, Taiwan.

The anomalous grazing incidence small angle scattering was used to verify the intact of FePt nanoparticles under the Au overlayer during the anneal temperature at 800 C. The structural stability of self-assembled FePt monolayer nanoparticles on functional substrate with the Au overlayer during the annealing were studied. To deposit a monolayer of particles under control, the functional substrates such as polyethylenimine (PEI) or [3-(2-aminoethlyamino)ropyl] trimethoxysilane (APTS) modified silicon wafers were used to capture the FePt nanoparticles coated with oleic acids. With the X-ray diffraction, anomalous X-ray absorption spectroscopy and the anomalous grazing incidence small angle x-ray scattering techniques, the FePt nanoparticles monolayer were found to be free from coalescence and convert into ordered alloy under the annealing process after 5-10 nm of Au overlayer deposited on the top of FePt nanoparticles. The result indicates that the particle size 4.5±0.5 nm is typically unchanged, but the distance between particles is reduced from 7.5±1.5 nm to 5.5±1.1 nm after annealing. The results suggest that the 5 nm Au coverlayer is an effective diffusing barrier layer to prevent the FePt nanoparticles from sintering during the annealing process. The ordered FePt(001) diffraction peak was obscured under the strong Au background, but its spectrum of diffraction anomalous X-ray absorption fine structure at FePt(111) shows an order FePt structure was formed.

P05-025

SPINODAL CRYSTALLIZATION KINETICS ON SUPERCOOLED LIQUID OF POLY(TRIMETHYLENE TEREPHTHALATE)

Wei-Tsung Chuang[a], Hwo-Shuenn Sheu[a],U-Ser Jeng[a], Po-Da Hong[b]

[a]*National Synchrotron Radiation Research Center, Hsinchu,300 Taiwan.*

[b]*Department of Polymer Engineering, National Taiwan University of Science and Technology, Taipei 106, Taiwan*

Polytrimethylene terephthalate (PTT) is a promising material for engineering plastic and textile fiber, and in particular it combines many advantages of nylons and other polyesters. Resently, we found that crystallization of supercooling liquid strongly influences process of PTT. However, crystallization from supercooling liquid, which is the metastable state, is very poor understood in polymeric crystallization. We have systematically investigated the crystallization kinetics on the supercooled liquid of poly(trimethylene terephthalate) using small-angle X-ray scattering (SAXS), wide-angle X-ray scattering (WAXS), and small-angle light scattering (SALS) measurements. The superstructure of PTT crystallization from supercooling liquid is composed of the few adjacent chains come together with parallel orientation to form a fringed-micelle /or bundle-like crystallite probed by atomic force microscopy (AFM) and transmission electron microscopy (TEM). However, in the early stage of PTT crystallization, we find that the logarithm of SAXS intensity was increased linearly, corresponding to spinodal kinetics proposed by Cahn. This phenomenon indicates that the precursory mesophase induce density fluctuations by spinodal decomposition before fringed-micelle crystallites. This mechanism is different from common crystallization associated with nucleation and growth.

.

P05-026

AN INSTRUMENT FOR TIME RESOLVED AND ANOMALOUS SIMULTANEOUS SMALL AND WIDE ANGLE X-RAY SCATTERING (SWAXS) AT THE NSRRC

Chiu-Hun Su,[a] Ying-Huang Lai,[a] Ya-Sen Sun,[a] U-Ser Jeng,[a,*] Jhih-Min Lin,[b] Tsang-Lang Lin,[b] Yu-Shan Huang,[a] Hwo-Sheunn Sheu,[a] Wei-Tsung Chuang,[a] Chia-Hung Hsu,[a] Ming-Tao Lee,[a] Keng S. Liang[a]

[a] *National Synchrotron Radiation Research Center, Hsinch 30049 Taiwan.* [b]*Department of Engineering and System Science, National Tsing Hua University, Hsinchu 30013, Taiwan.*

A SWAXS (small- and wide-angle X-ray scattering) instrument was recently installed at the wiggler beamline BL17B3 of the National Synchrotron Radiation Research Center (NSRRC), Taiwan. The instrument which is designed for studies of static and dynamic nanostructures and correlations between the nano (or meso) structure (SAXS) and crystalline structure (WAXS) provides a flux of 10^{10} - 10^{11} photon/s at the sample at energies between 5 and 14 keV. With a SAXS area detector (MarCCD165 or Gabriel-type gas detector) and a WAXS linear detector connected to two data acquisition systems operated in master-slave mode the instrument allows one to perform synchronized SAXS/WAXS for time-resolved measurements. Data reduction algorithms have been developed for rapid processing of the large SWAXS data sets collected during time-resolved measurements. The performance of the instrument is illustrated by examples taken from different classes of ongoing projects: (1) time-resolved SAXS/WAXS/differential scanning calorimetry (DSC) with a time resolution of 60s on a semi-crystalline syndiotactic polystyrene sample, (2) anomalous SAXS/WAXS measurements on a nanoparticulate Pt-Ru catalyst and (3) grazing-incidence SAXS of a monolayer of oriented semiconductor quantum wires and humidity-controlled ordering of Alamethicin peptides embedded in an oriented lipid membrane.

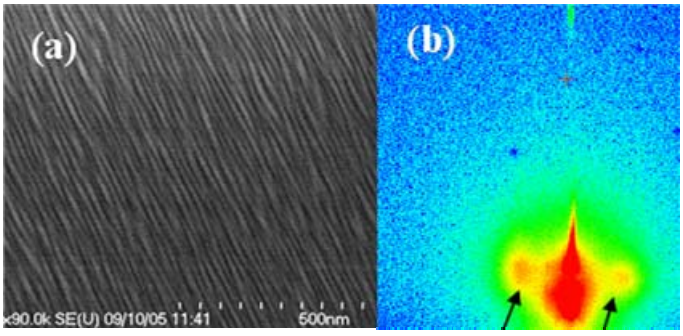

Fig. 1: Scanning electron microscope (SEM) image of the oriented GaSb quantum wires (a). GISAXS pattern of the *oriented* quantum wires recorded with the area detector (b).

P05-027

SOLUTION SAXS AND NMR ON DOMAIN ORIENTATION AND BINDING OF THE COMPONENTS OF THE HUMAN BCKD COMPLEX

Chi-Fon Chang,[a,*] Yu-Shan Huang,[b,*] U-Ser Jeng[b]

[a]*Institute of Biomedical Sciences, Academic Sinica, Taipei, 11529, Taiwan,* [b]*National Synchrotron Radiation Research Center, Hsinch 30049 Taiwan.*

The mammalian mitochondrial branched-chain-α-ketoacid dehydrogenase (BCKD) complex, containing E1, E2, and E3 domains, catalyzes the oxidative decarboxylation of branched-chain-α-ketoacids derived from leucine, isoleucine, and valine, hence, gives rise to branched-chain acyl-CoAs. The transacylase subunit (E2) of BCKD complex carries three independently folded domains linked together by flexible loops: the hbLBD (a.a. 1-84), hbSBD (a.a. 104-152), and di-domain (hbDD) comprising residues 1–168 of E2. With multidimensional heteronuclear NMR techniques, the structures and dynamics of the three truncated fragments were determined, respectively. For the quaternary structure, solution small angle X-ray scattering (SAXS) result reveals a linear-like arrangement of the sub-complex of hbLBD linked with hbSBD (DD) by the flexible chains, based on a rigid body refinement of the two individual structures of LBD and SBD determined by NMR. Furthermore, from the changes of the SAXS profile of the E1 component of BCKD, upon the binding of the DD sub-complex, most likely, the DD sub-complex keeps a free LBD end after the binding to the E1 domain.

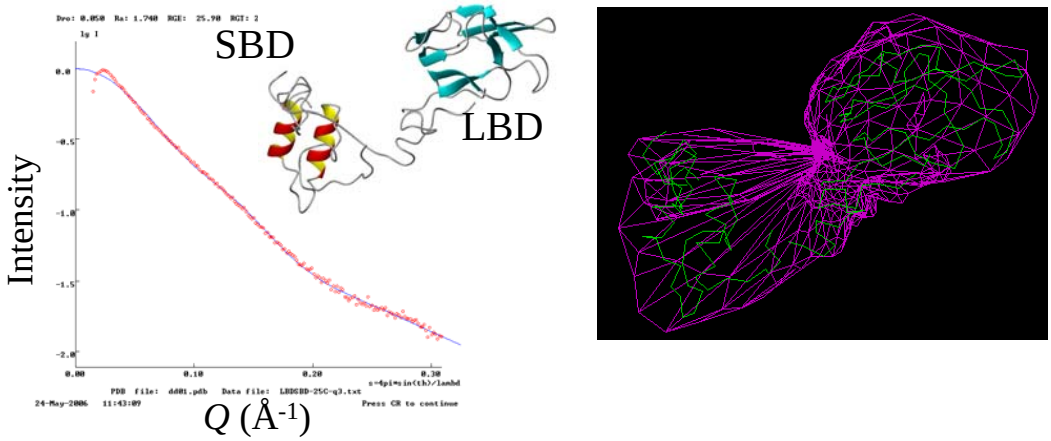

Fig. 1: A quaternary model and the protein envelope deduced from the SAXS data for the sub-complex DD (LBS+SBD) of BCKD, using rigid body refinement with the PDB data of each component.

P05-028

EXPERIMENTAL ELECTRON DENSITIES AND MOLECULAR INTERACTIONS: *INTER*-MOLECULAR HYDROGEN BONDING.

Azadeh Matin, Thanh Ha Nguyen, Jane Hanrahan and David Hibbs

Faculty of Pharmacy, University of Sydney, Sydney, Australia

The successful practice of materials and medicinal chemistry is crucially dependent upon an understanding of the principles of intermolecular interactions and becomes of paramount importance when investigating the mechanisms of molecular recognition.

The solid state offers the opportunity to study the structure of co-crystallized complexes in detail; and if high-resolution, low-temperature X-ray data can be obtained, then quantitative aspects of electrostatic interactions and hydrogen bonding can be analyzed in even greater detail using experimental charge density methods.

To this end, we are investigating the design and synthesis of co-crystal systems that mimic biological macromolecular host-guest complexes, with a view to carrying out such charge density experiments. The syntheses of receptor mimics have been completed, and the co-crystallization of the receptor mimic with dicarboxylic acid (glutaric and adipic acid) followed by high-resolution X-ray studies has been accomplished (Figure 1).

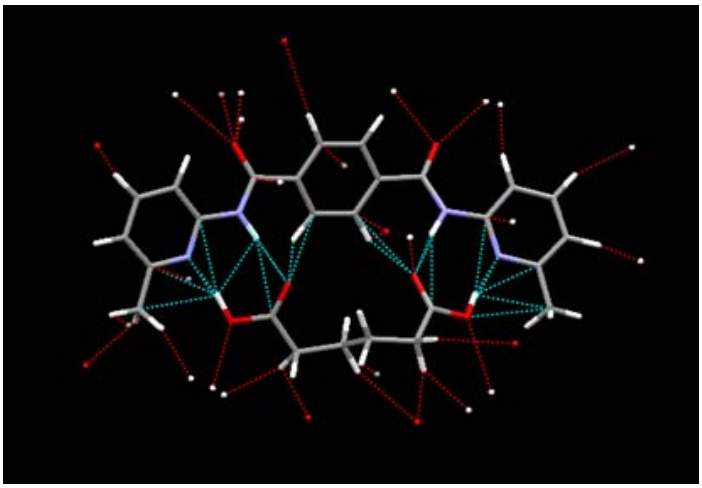

Figure 1:Intermolecular interaction in the receptor complex

The combination of theoretical and experimental data on hydrogen bonding provides a unique insight into the nature of weak intermolecular interactions.

P05-029

EXPERIMENTAL ELECTRON DENSITIES AND MOLECULAR INTERACTIONS: *INTER*-MOLECULAR II-STACKING INTERACTIONS.

Thanh Ha Nguyen and David Hibbs

Faculty of Pharmacy, University of Sydney, Sydney, Australia

π-π interactions in aromatic systems have been studied extensively in the past two decades by many theoretical methods as they play an important role in chemistry and biology. Despite the many reviews that deal with intermolecular interactions in π-stacked systems, there are still relatively few practical applications of these ideas.

The topological analysis of the electron density deduced from theoretical calculations as devised by R. F. W. Bader is well documented and has shown to be a useful tool in obtaining valuable information about chemical bonding and the properties of atoms in molecules. These studies have recently been extended to experimental electron densities obtained by X-ray diffraction.

Currently, we have investigated the crystal electron density of π-systems on the basis of the collected X-ray diffraction data and from quantum chemical calculations (Figure 1). The combination of theoretical and experimental data for these systems provides a unique insight into the nature of aromatic π-π stacking.

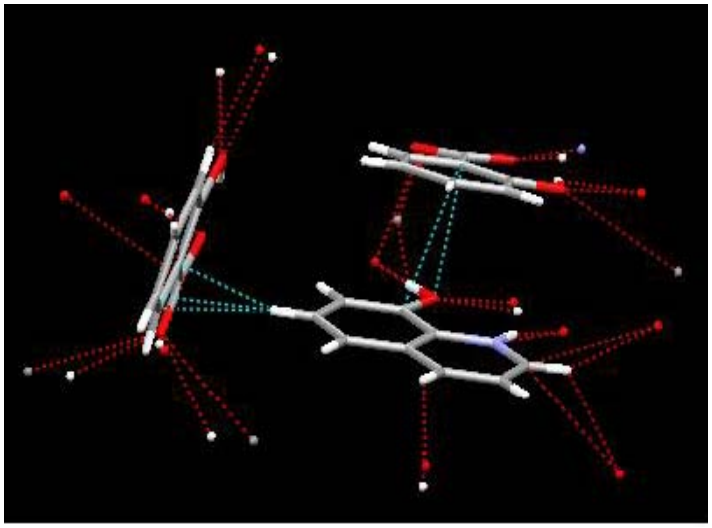

Figure 1:π-π interactions in an aromatic complex

P05-030

Yb-DOPING EFFECT AND TEMPERATURE DEPENDENCE IN $CoSb_3$ SKUTTERUDITE STRUCTURE

Atsuko Ohno,[a] Satoshi Sasaki,[a] Eiji Nishibori,[b] Shinobu Aoyagi,[b] Makoto Sakata[b] and Bo Brummerstedt Iversen[c]

[a]*Materials and Structures Laboratory, Tokyo Institute of Technology, Yokohama, 206-8503, Japan;*
[b]*Department of Applied Physics, Nagoya University, Nagoya 464-8603, Japan;*
[c]*Department of Chemistry, University of Aarhus, Aarhus, 8000, Denmark*

Metal-doped $CoSb_3$ skutterudite is known as a good candidate for thermoelectric materials with high-electrical and low-thermal conductivities. A rattling effect of the doped atoms in the cages can reduce the lattice thermal conductivity. It is important to study how the doped Yb atom affects the host framework of the skutterudite structure. By using the high-resolution powder diffraction data, we have analyzed the crystal structure of Yb-doped $CoSb_3$ in comparison with non-doped one.

Synchrotron X-ray powder diffraction experiments were carried out at the beamline BL02B2 of the SPring-8. The wavelength used in this study was λ = 0.43081 Å. The diffraction data were collected at an interval of 0.01º step within the 2θ range from 3º to 74º, corresponding to the d spacing up to 0.36 Å. Rietveld refinements were carried out with software named as Synchrotron-Powder (SP). The structural parameters of Yb-doped $CoSb_3$ were determined within temperature ranges from T = 90 to 700 K. The structural parameters of non-doped $CoSb_3$ were also determined within temperature ranges from T = 10 to 300 K. Lattice constants for Yb-doped and non-doped $CoSb_3$ are a = 9.04095(1) Å and 9.03246(1) Å at room temperature, respectively. The lattice constants increase as a function of temperature for both crystals. Yb-doped skutterudite has a lattice constant change of 0.01510 Å within the temperature range from T = 90 to 300 K. On the other hand, the change for non-doped skutterudite is 0.01377 Å within the temperature range from T = 80 to 300 K. In $CoSb_3$ skutterudite structure, there are three types of crystallographically different bond, which are a Co-Sb and two Sb-Sb bonds. The interatomic distances for Yb-doped and non-doped $CoSb_3$ were calculated from the structure parameters finally refined. The presentation will discuss the rattling and doping effects in the structural aspects such as the change of inter-atomic distances in the cages and host framework.

P05-031

SITE PREFERENCE AND DOPING EFFECT IN $(Hg,Pb)(Ba,Sr)_2Ca_2Cu_3O_{8+\delta}$ SUPERCONDUCTORS

Satoshi Sasaki[a] and Kouji Yamawaki[a]

[a]*Materials and Structures Laboratory, Tokyo Institute of Technology, Yokohama, 226-8503, Japan*

Hg-1223 superconductor has the highest critical temperature of T_c = 135 K for samples synthesized at an atmospheric pressure, which is a layered perovskite having a structural unit sequence of -HgO-BaO-CuO-Ca- along the *c*-axis. The substitution of mercury by lead can enhance the stability of the Hg-1223 phase. The doping effect into the mercury layers is deeply related to an interstitial oxygen defect and cation substitution. In order to synthesize high-quality superconductors, the substitution of barium by strontium is one of the most important factors to improve such properties as the hole doping of CuO_2 planes.

Single crystals with various strontium contents were grown at T = 1130 K by the encapsulation method. EDX and SQUID experiments were carried out to measure the chemical composition and magnetic property, respectively. The single-crystal intensity measurements were first made using a conventional Rigaku AFC-5 four-circle diffractometer with Mo $K\alpha$ radiation. The integrated intensity data were collected up to 2θ = 110° in the ω-2θ scan mode at a scan speed of 1°/min. The absorption correction was made by the grid-integration method for the arbitrary-shape crystal. Site-occupancy experiments were performed with the synchrotron radiation at BL-10A of the Photon Factory. A vertical-type four-circle diffractometer was used with wavelengths of λ = 1.3906 and 1.0191 Å, which is 0.01 Å longer than Cu *K* and Hg L_{III} absorption edges, respectively. Atomic coordinates and anisotropic temperature factors were first refined with the Mo *K*a data. Then, site-occupancy parameters were determined with the anomalous scattering effect. Final *R* factors range from 6.4 to 6.7 % in the Mo $K\alpha$ refinements.

The cation distribution among mercury, lead and copper in the Hg sites was determined the two-wavelengths anomalous dispersion (TWAD) method using the diffraction data at Cu *K* and Hg L_{III} edges. The minimum residual factors in the analyses indicated that no copper exists in the Hg sites for all samples. The occupancy parameters for the Ba sites were also determined from the Mo $K\alpha$ diffraction data and compared with the chemical composition of starting materials. The presentation will discuss the site preference and structural change in the aspects of strontium content, superconductivity transition temperature, concentration of holes and so on.

P05-032

CLOSE CL···CL CONTACT: IS IT ATTRACTIVE OR REPULSIVE?

Daisuke Hashizume

Molecular Characterization Team, RIKEN, Saitama 351-0198, JAPAN

Cl…Cl contact is frequently found in organic crystals. Because of their strong directionality, the contact has been used for designing the structure of crystal and supramolecular aggregate. The nature of the contact, however, has not been characterized experimentally. The aim of the study is characterize the nature of the contact from electron density distribution, which is obtainable from X-ray diffraction data.

In the crystal of 3,4-dichlorophenol, there are different directional Cl…Cl contacts. Since the different directional contacts can be compared in the same crystal, the crystal is suitable to examine the nature of the contacts. Single crystal diffraction data were collected at BL04B2 beam line of SPring-8. The electron density distribution was refined applying pseudo atom models. Topological analysis for total electron density reveals that bond paths and bond critical points are found for each of the Cl…Cl contacts. The outer shell electrons on the Cl atoms deformed. Nevertheless, the different directionalities of the Cl…Cl contacts, the electrons distribute similar way between Cl atoms in contacts. The outer shell electron concentrate regions direct toward electron deficient regions.

In conclusion, the Cl…Cl contact is an interaction between electron donor and accepter even if the directionality of the contact is different.

P05-033

THEORETICAL CALCULATION OF XMCD SPECTRA AT K-EDGE Ni AND Fe SPINEL FERITE

Koichi Ohkubo[a], Takeshi Toyoda[b]

[a] *Earth Appraisal Co,LTD , Tokyo 101-0063, Japan*
[b] *Industrial Research Institute of Ishikawa, Kanazawa, 920-8203, Japan*

Spinel ferrites are well known as materials which consist of Fe with various transition-metal cations in A (tetrahedral Td) and B(octahedral Oh) sites of the crystal structure. The physical property of the ferrites depends on the site occupancy of such ions. Therefore, specific information on the site as electronic and magnetic properties of Ni ferrite together with the other transition-metal ferrites have been examined by means of X-ray absorption experiments along with theoretical calculations.

Theoretical XMCD (X-ray Magnetic Circular Dichroism) studies were performed to focus the ferric ions surrounded by oxygen atoms. The XMCD spectra provided the local information on magnetic ions within the investigated molecular systems.

In the numerical calculation based on the expansion on perturbation in electro-magnetic fields showed a good agreement between the XMCD measurements and numerical calculations on inverse type Ni ferrite. In this study, other effect (e.g. ligand field) is discussed by theoretical calculation.

P05-034

ELECTRONIC STRUCTURE OF MERCURIC IODIDE USING COMPTON SCATTERING TECHNIQUE

*M. Sharma, Gulzar Ahmed and B. L. Ahuja

** Department of Physics, Arya College of Engg. and I. T., Kukas, Jaipur – 303 001*
Department of Physics, Univ. College of Science, M. L. Sukhadia University, Udaipur – 313 001

In this paper, we report the experimental Compton profile of mercuric iodide using our 20 Ci ^{137}Cs [1] and 100 mCi ^{241}Am [2] Compton spectrometers, at the instrumental resolutions 0.38 a.u. and 0.55 a.u., respectively. We have also computed theoretical Compton profile along with energy bands and density of states within the framework of Linear Combination of Atomic Orbital (LCAO) scheme as employed in CRYSTAL03 code of Tornio group [3]. The experimental Compton profiles of both measurements have been compared with the pseudopotential scheme within the Hartree Fock (HF) and density functional schemes. It is observed that the density functional calculations are in better agreement the experimental data.

Reference:

1. B. L. Ahuja, M. Sharma and S. Mathur
Nucl. Instrum. and Meths. **B244**, 419 (2006).
2. B. L. Ahuja and N. L. Heda
Z. Naturforsch. **A61**, 364 (2006).
3. R. Dovesi, V.R. Saunders, C. Roetti, R. Orlando, C. M. Zicovich-Wilson, F. Pascale, B. Civalleri, K. Doll, N.M. Harrison, I.J. Bush, Ph. D'Arco, M. Llunell
CRYSTAL03 ***User's Manual***, University of Torino, Torino, 2003

P05-035

CHARGE DENSITY DISTRIBUTION AND BOND CHARACTERIZATION ON COMPLEX $MN(H_2O)_2NI(CN)_4 \cdot 3H_2O$

Lai-Chin Wu,[a] I-Jui Hsu,[a] Gene-Hsiang Lee,[b] Yu Wang.[a]

[a]*Department of Chemistry, National Taiwan University, Taipei, Taiwan, R.O.C.,*
[b]*Instrumental Center National Taiwan University Taipei, Taiwan, R.O.C.*

The title compound is a bimetallic complex bridging by cyanide groups. It is crystalized in space group Pnma with cell dimension a=12.0791(9), b=14.071(2), c= 7.308(2). The local coordination geometry of manganese is octahedral with four nitrogen atoms of cyanide group in horizontal positions and two water molecules at axial positions. The nickel is coordinated with four carbon atoms of cyanide group in a square planar geometry. However, there is an unusual short distance 2.657(1) Å between Ni and O of water in the axial direction of Ni. The $MnNi(\mu\text{-}CN)_4$ unit forms 2-D layer and the three non-coordinated water molecules are pack between layers. Each water molecule is H-bonded to three nearest water molecules. The contact short distances between these oxygen atoms of water molecules are 2.786(1) Å to 2.849(1) Å. In order to characterize all the chemical bonds as well as the weak interactions such as hydrogen bonds etc., X-ray diffraction data was collected at 100K with resolution up to 0.36 Å ($\sin\theta/\lambda$~1.38). The deformation density, Laplacian of the total electron density in terms of multipole model is applied to investigate the bonding character. Topological properties associated with bond critical points, energy density, etc. based on AIM theory will be presented.

P05-036

CHEMICAL BONDING AND INTERMOLECULAR INTERACTIONS OF A NICKEL(II) COMPLEX

Yu-Chun Chuang[a], Yu Wang[a], Gene-Hsiang Lee[b], Ben-Jie Liaw[c], Chen-Wei Liu[c]

[a]Department of Chemistry, National Taiwan University, Taipei, Taiwan, bInstrumentation Center, National Taiwan University, [c]National Dong-Hwa University

A Nickel(II) complex, bis-(di-isopropyl-diseleno-phosphato)-Nickel(II), is a square planar complex, where Ni ion is bonded to four Se ligand. The electron density distribution is investigated by single crystal x-ray diffraction at 100K using Mo Kα on a Kappa CCD diffractometer. It crystallized in space group is P-1, the inter-set agreement index, R_{int}, is 0.033, (total # reflections/unique reflection = 75997/11924) with the max resolution $(\sin\theta/\lambda)_{max}$ of 1.08 $Å^{-1}$. The nickel atom is located at the inversion center. There are two different Ni-Se distances: one at 2.3615(6)Å and the other at 2.3294(6)Å. Interestingly, there is a short Se-Se contact of 3.294 Å between the neighboring molecules; which is roughly the same as intra molecular Se---Se contact distance. Thus there is a Se square network throughout the crystal. The aim of this study is not only looking into the chemical bonding interactions of this Ni complex but also search for the interesting intermolecular interactions through short contact of Se---Se interaction. The experimental electron density will be produced with multipole model. The electron density distribution of metal ligand and Se---Se interactions will be presented in terms of deformation density and respective Laplacian of density. The topological properties associated with bond critical points will also be discussed.

P05-037

MIXED LIGAND COPPER(I) COMPLEXES OF TRIPHENYLPHOSPHINE AND PHENYLTHAIOUREA

Ruthairat Nimthong[a], Chaveng Pakawatchai[a], Yupa Thunyasirikul[a] and Saowanit Saithong[a]

[a]*Department of Chemistry, Faculty of Science,Prince of Songkla University, Hatyai, Songkhla, 90112 Thailand.*

Copper(I) halide complexes (CuX; X= Cl, Br, I) containing triphenylphosphine(PPh_3) and *N*-phenylthiourea (ptu) ligands have been synthesized and characterized by elemental analysis, X-ray fluorescence spectrometry, Fourier transform nuclear magnetic resonance spectroscopy and Fourier transform infrared spectroscopy. The complexes obtained by the addition of ptu ligand to a CuX-PPh_3 adduct in solution. The molecular structures of $[CuCl(PPh_3)_2(ptu)]$(1), $[CuBr(PPh_3)_2(ptu)]$(2), $[CuI(PPh_3)_2(ptu)]$(3) have been established by single-crystal X-ray diffraction. The complex(1) is isomorphous and isostructural with complex(2), crystallize in triclinic system space group $P\bar{1}$, Z = 2 with cell parameters a = 10.5226(1), b = 11.3035(2), c = 17.1848(2) Å, α = 97.605(1), β = 103.508(1), γ = 103.605(1)° and a = 10.6236(4), b = 11.2135(4), c = 17.1481(7) Å, α = 97.957(1), β = 102.424(1), γ = 102.994(1)° for complex(1) and complex (2), respectively. Complex (3), crystallizes in space group $P\bar{1}$ Z = 2 with cell parameters a = 10.9505(9), b = 18.7294(15), c = 21.3731(18) Å, α = 67.4220(10), β = 77.2150(10), γ = 73.2240(10)°. Each of these structures features a distorted tetrahedral copper(I) center coordinated to two phosphorus atoms from two triphenylphosphine molecules, one sulfur atom of phenylthiourea molecule and one halide atom.

P05-038

INVESTIGATION OF ELECTRON DENSITY DISTRIBUTION IN ANATASE (TiO_2) WITH- AND WITHOUT UV-IRRADIATION

Ken-ichi Ito and Hiroki Okudera

Division of Earth and Environmental Science, Graduate School of Natural Science & Techology, Kanazawa University, Kanazawa, 920-1192 Japan

Anatase-phase TiO_2 is widely recognized as an effective photocatalyst for the degradation of organic pollutants in air and water. This photocatalytic activity is due to a formation of OH radical on the surface, and transition of electrons from valence band to conduction band by UV irradiation is ascribed to the formation of hole and electron on the surface. Electron density distribution in anatase, however, has not been well established.

Electron density distribution was examined by means of single crystal X-ray diffractometry. Natural single crystal of anatase (Tisey, Norway) was spherically ground in 200 μm in diameter and used for the experiments. Trace amounts of Fe and Nb were found as impurities. A Rigaku AFC-5S four-circle diffractometer was used (radiation: Mo*K*α). Three sets of diffraction intensities were collected; set 1 was collected under no light, set 2 under UV (λ = 253.6 nm: 4.9 eV) plus fluorescent light, and set 3, again, under no light. Results of Fourier syntheses were compared with each other to estimate an amount of experimental uncertainty ($\rho_{3\text{-}1} = \rho_{set3} - \rho_{set1}$) and extract difference in electron density with- and without UV irradiation ($\rho_{2\text{-}1} = \rho_{set2} - \rho_{set1}$). Residual density ($eÅ^{-3}$) was in the range -0.16 ~ 0.17 on $\rho_{3\text{-}1}$ and -0.22 ~ 0.43 on $\rho_{2\text{-}1}$ in *YZ* plane (x = 1/2), and -0.13 ~ 0.17 on $\rho_{3\text{-}1}$ and -0.13 ~ 0.30 on $\rho_{2\text{-}1}$ in *XY* plane (z = 0).

Conventional difference Fourier maps commonly showed electron densities which can be ascribed to Ti-O bonding orbitals among three data sets. On the other hand, $\rho_{2\text{-}1}$ maps showed weak concentration of positive density in the vicinity of Ti (8*a*) site, one is found on the line along longer Ti-O bond and the other on <110> where there is no Ti-O bond. The latter density may be ascribed to electron density transferred from non-conductive bonding orbital to antibonding Ti $t_{2g}(d_{xy})$ orbital, while the former does not match antibonding Ti e_g orbital which requires higher activation energy. Change in electron configuration with- and without UV irradiation and mechanism of photocatalytic activity will be discussed based on the results.

P05-039

CHARGE DENSITY STUDIES ON HETEROBIMETALLIC PHOSPHIDO-BRIDGED Mo AND W COMPLEXES

Chi-Rung Lee,[a] I-Jui Hsu,[b] Hsiu-Mei Lin[c] and Shin-Guang Shyu[d]

[a]*Department of Chemical Engineering, Minghsin University of Science and Technology, Taiwan.* [b]*Department of Chemistry, National Taiwan University, Taiwan.* [c]*Institute of Bioscience and Biotechnology, National Taiwan Ocean University, Taiwan.* [d]*Institute of Chemistry, Academia Sinica, Taiwan*

The heterobimetallic phosphido-bridged complexes, $CpW(CO)_2(\mu\text{-}PPh_2)Mo(CO)_5$ (**1**) with W-Mo distance 3.1723(4) Å and $CpW(CO)_3(\mu\text{-}PPh_2)Mo(CO)_5$ (**2**) with W-Mo distance 4.510(4) Å have been reported with special chemical reaction properties because of the interaction between W and Mo. For example, complex **2** will be converted into **1** after irradiation with UV or heating at reflux temperature. In order to realize how chemical bonds influence the reaction properties in complex **1** and **2**, the X-ray diffraction data of both complexes at 100 K are collected and the experimental electron density in terms of multipole model are used to investigate the electron density distribution and chemical bonds. All chemical bonds will be quantified based on atoms in molecule (AIM) theory to elucidate the nature of those interactions. All interactions are verified by the location of the bond critical point and its associated topological properties, such as local density, Laplacian, and energy density at bond critical points. Moreover, the isovalue surface of Laplacian charge density distribution and the detailed atomic graph around each atomic site will reveal the shape of the valence-shell charge concentration and provide a reasonable interpretation of the bonding in each atom. All extracted chemical bonding characters from experimental charge density will be further compared with the density functional theory calculation and give out a reasonable explanation related to the different chemical reaction properties between **1** and **2**.

P05-040

EXPERIMENTAL CHARGE DENSITY STUDY ON A Fe(II) COMPLEX AT HIGH SPIN AND LOW SPIN STATES

Chou-Fu Sheu[1], Che-Hsiu Shih[1], Szu-Miao Chen[1], Yu-Chun Chuang[1], Gene-Hsiang Lee[1], Yu-Shan Huang[2], Kuan-Li Yu[2], Yu Wang*[1]

[1]*Department of Chemistry, National Taiwan University, Taipei 106, Taiwan*
[2]*National Synchrotron Radiation Research Center, Hsinchu 30077, Taiwan*

Charge density study, on polymorph D of a spin crossover complex, [t-Fe(abpt)$_2$(NCS)$_2$] (abpt = 4-amino-3,5 bis(pyridine-2-yl)-1,2,4-triazole), is undertaken. It crystallizes in monoclinic space group $P2_1/c$ with two crystallographic independent mononuclear molecules in the unit cell. Out of two unique iron sites, only one iron (Fe) undergoes a thermal spin transition from high spin (HS) to low spin (LS) state at 162 K, while the other site (Fe') remains in HS state in the temperature range studied. The aim of this study is to probe the electron density distributions in HS and LS state of Fe(II) with exact same coordination geometry within a single sample at 100K. The electron density distributions around the two iron sites are expected to be very different due to the distinct electronic configurations in HS (e_g^2)(t_{2g}^4) and LS (e_g^0)(t_{2g}^6) state. Two diffraction data were collected at 100 K; one with an in-house kappa CCD using MoKα radiation and the other with synchrotron radiation using the wavelength of 0.5 Å (25 KeV). The results in terms of multipole model from two sets of data are comparable. The detail of necessary correction on the CCD detector will be discussed. The apparent difference in electron density distribution of Fe at HS and at LS will be demonstrated in terms of deformation density and Laplacian of density. Topological properties associated with the bond critical points will be discussed. A DFT calculated charge density will also be presented for comparison. d-Orbital populations at HS and LS states are as expected.

P05-083

PRELIMINARY STRUCTURAL REFINEMENTS AND A NEW SYNTHETIC ROUTE TO δ-Bi_2O_3-RELATED PHASES IN THE Bi-W-O, Bi-Mo-O, Bi-Ta-O AND Bi-Nb-O SYSTEMS

Neeraj Sharma[a], Rene Macquart[a] and Chris D. Ling[a,b]

[a]*School of Chemistry, University of Sydney, Sydney, Australia*

[b]*Bragg Institute, Australian Nuclear Science and Technology Organisation, Menai, Australia*

The floating zone image furnace is an ideal tool to grow micrometre to millimetre sized metal-oxide crystals. During crystal growth there is no contact with crucibles or quartz/platinum tubes, minimising the formation of impurities. The rapid cooling of the melt produces quenching conditions, allowing synthesis of crystals that do not form with slow cooling; e.g. crystals within the solid-solution range. Here we report the use of the floating zone image furnace technique to grow single crystals of the δ-Bi_2O_3-related solid-solution phases of nominal composition $Bi_8Nb_2O_{17}$, $Bi_{5.6}WO_{11.4}$, $Bi_{16}Ta_2O_{19}$ and $Bi_{38}Mo_7O_{78}$. The $Bi_{5.6}WO_{11.4}$ and line phase $Bi_{38}Mo_7O_{78}$ single crystals were analysed with synchrotron and laboratory based X-ray diffraction to determine metal cation positions and neutron diffraction to determine the oxygen anion positions. The diffraction methods are also applied to the 3-D incommensurately modulated structures of $Bi_8Nb_2O_{17}$ and $Bi_{16}Ta_2O_{19}$. There are challenges encountered in these latter complicated structures; e.g. integration of the collected '6-D' data and subsequent refinements. Each sample studied presents different methods of approaching the structural solutions. The ability to grow single crystals of the Bi-rich transition-metal oxides and solve these structures, highlight the potential for the exploration of phase diagrams by the use of the floating zone technique.

P05-084

INSIGHT INTO THE STABILITY OF TETRAGONAL AND RHOMBOHEDRAL PHASES IN DOUBLE PEROVSKITES

P. J. Saines, J. Spencer and B. J. Kennedy

School of Chemistry, The University of Sydney, Sydney, New South Wales, 2006, Australia.

The precise structure adopted by double perovskites is known to have a significant influence on the interesting and useful properties displayed by these materials such as magnetism, ferroelectricity and colossal magneto-resistance. It is therefore important to understand why apparently similar perovskite systems adopt different structures. An example of this is the significantly different structures adopted by members of the series of double perovskites of the type $Ba_2LnB'O_6$ (Ln = lanthanide and B' = Nb^{5+}, Ta^{5+} or Sb^{5+}). It has recently been established that members of the Nb^{5+} series adopt *I*4/*m* tetragonal symmetry while Sb^{5+} adopts $R\bar{3}$ rhombohedral symmetry as intermediate phases between the *I*2/*m* monoclinic and the $Fm\bar{3}m$ cubic phase. The cause of the difference in the intermediate phase adopted in these two similar systems is still not certain.

In order to develop an understanding of why changes to the pentavalent cation influence the symmetry of the intermediate phase we have studied the structures of the Ba_2LnTaO_6 series using a combination of synchrotron X-ray and neutron powder diffraction. The majority of oxides adopting the intermediate symmetry at room temperature exhibited the same tetragonal intermediate phase seen in the niobates. Ba_2LaTaO_6 however adopts the rhombohedral intermediate seen in the antimonates. This prompted us to examine the phase transitions of other members of the tantalate and niobate series using variable temperature X-ray diffraction. This indicated that where Ln^{3+} = La^{3+} or Pr^{3+} rhombohedral symmetry is adopted while in all other cases examined the intermediate symmetry was found to be tetragonal. That some tantalates and niobates exhibit rhombohedral symmetry while others exhibit tetragonal symmetry indicates that the factors causing the difference in symmetry adopted are particularly subtle and that the systems are finely balanced between these two possibilities. This paper will examine the results in these and other related compounds and attempt to explain the relative stability of the rhombohedral and tetragonal symmetries in this context.

P05-085

A STUDY OF STRONTIUM, ALUMINIUM AND INDIUM TUNGSTEN BRONZES

M. S. Rahman and A. Hussain

Department of Chemistry, University of Dhaka, Dhaka – 1000, Bangladesh

The tungsten bronzes and bronze type compounds have received much attention over the years because of their interesting physical and chemical properties such as intense colour, electronic conductivity and chemical inertness. Tungsten bronzes, M_xWO_3, are non-stoichiometric oxides where M is generally an electropositive metal in the range $0< x <1$. There are many reports available in literatures on the alkali metal tungsten bronzes but very few reports are there on alkaline earth metal and also on aluminium group metal tungsten bronzes.

Attempts were made to prepare Sr_xWO_3, Al_xWO_3 and In_xWO_3 with $0 < x \leq 0.25$ at a temperature 800 ^{0}C and in ambient pressure by conventional solid-state method using appropriate amount of $M_2(WO_4)_3$, WO_3 and WO_2 in evacuated sealed silica tubes. However, the starting material for strontium bronzes was $SrCO_3$ instead of $SrWO_4$. Optical microscopic study shows that the colour of the products becomes more intense with increasing x. In most cases, the X-ray analysis of the samples shows a mixture of various bronze phases. A detailed phase analysis of these systems will be presented in the conference.

P05-086

CRYSTAL STRUCTURE AND HABIT OF $CaIrO_3$

Masahiko Sugahara[a], Akira Yoshiasa[a], Takafumi Hashimoto[a], Syunsuke Sakai[a], Akihiko Nakatsuka[b], Maki Okube[c] and Akira Yoneda[d]

[a]*Graduate School of Science and Technology, Kumamoto University;* [b]*Faculty of Engineering, Yamaguchi University;* [c]*Tokyo Institute of Technology;* [d]*Institute for Study of the Earth's Interior, Okayama University.*

The $CaIrO_3$-type post-perovsike structure of $MgSiO_3$ has been shown experimentally and theoretically to occur at the temperature and pressure conditions of D'' layer of the lowest Earth's mantle extend to 2700~2900 km depth. The discovery of a post-perovskite phase has attracted considerable attention because of its potential relevance to the D'' layer. The $CaIrO_3$ type structure is closely related to the Earth's lower mantle. Similar pressure-induced phase transition to the $CaIrO_3$-type structure has been reported in other familiar compounds including $MgGeO_3$, $MnGeO_3$, Fe_2O_3 and Al_2O_3. $CaIrO_3$ type phases of these compounds are unquenchable to ambient conditions. Detailed knowledge of the structure is, therefore, important not only for understanding the Earth's mantle but also for high-temperature and high-pressure crystal chemistry.

Single crystals of $CaIrO_3$ were prepared via flux growth. Precise crystal structural parameters, including the anisotropic displacement parameters, are determined based on a single-crystal X-ray diffraction experiment. Cell dimensions: a=3.147(2), b=9.866(6), c=7.302(5) (Å). The structure is actually a three-dimensional dense structure with small vacant spaces. The IrO_6 octahedra are distorted greatly. The O-O distances for the shared faces and edges among polyhedra are shorter than other non-shared edge distances. These effects are explained by Pauling's rules and occur to decrease the repulsion between the cations. Thermal vibration of all atoms is significantly anisotropic. The large anisotropy and amplitude of thermal displacements for Ca and Ir atoms are observed toward the *b*-axis while that for O(1) and O(2) atoms are observed toward the *c*-axis. Thermal vibrations of Ca and Ir atoms are restricted toward the shared face, shared edges and shortest cation-cation directions. Moreover, a component of thermal vibration toward the vacant space is added because the $CaIrO_3$ structure is highly dense structure. The single-crystal experiment shows that $CaIrO_3$ crystal grows toward the *a*-axis and that it has a prism- or needle-shaped crystal habit. Strongly preferred orientation of such prism shaped $CaIrO_3$ type post perovskite $MgSiO_3$ crystals may develop under the share flow in Earth's mantle.

P05-087

SYNCHROTRON POWDER DIFFRACTION STUDY ON GAMMA-Al2O3

Seiichi Matsuda, Takashi Ida, Kazuhiro Asai and Hisashi Hibino

Ceramics Research Laboratory,Nagoya Institute of Technology;Asahigaoka 10-6-29, Tajimi, Gifu ,Japan

1,Introduction

Many studies on the structure of gamma-Al2O3 have assumed that it has a defect spinel structure, while a tetragonal structure model has also been proposed based on neutron diffraction and NMR experiments (Paglia et al., 2003). However, both indexing and evaluation of integrated intensity from X-ray diffraction data of gamma-Al2O3 are generally quite difficult because of intrinsically broad width of diffraction peaks. In this study, the diffraction intensity profile of gamma-Al2O3 measured with a synchrotron powder diffractometer has been analyzed by deconvolution and profile fitting methods to extract maximum information about the structure from the X-ray diffraction data.

2,Experimental

Alumina samples were prepared by treatment of chemically synthesized boehmite powder at 780, 840, 900, 960, 1020, 1080, 1140, 1200, 1260 K for 8 hours. The diffraction intensity data were collected with a synchrotron powder diffractometer (multiple-detector-system; MDS) on the beam-line BL-4B2 at the Photon Factory in Tsukuba. Apparent asymmetric deformation of peak profile caused by optical aberration and spectroscopic distribution of the source X-ray was removed by an originally developed deconvolution method.

3,Results

The observed diffraction patterns of samples treated at 780~960 K were similar to the typical pattern reported for gamma-Al2O3. Significant narrowing and splitting of overlapped peaks have been observed for the samples treated at temperatures higher than 960 K. The diffraction patterns of the samples treated at 960~1200 K were almost identical to that reported as delta-phase. The splitting of pseudo-cubic {400}-reflections is systematically enlarged on elevating the treatment temperature in the range from 1020 to 1260 K. When the tetragonal deformation of the pseudo-cubic unit cell is assumed, the observed change in the {400} peak profile can be explained by shift of 400 and 040 peaks to the lower angle side and 004 peak to the higher angle side at higher treatment temperatures, which correspond to expansion of a axis and shrinkage of c axis, respectively. The change of profile observed for the {440} reflections was also consistent with the above tendency, while the change in {311} reflections could not be fully explained by the tetragonal deformation of a pseudo-cubic structure. More detailed profile analysis has been conducted aiming at evaluation of coherent domain size along each crystallographic directions.

P05-088

STRUCTURE DETERMINATION OF HYBRID STRUCTURES FOUND IN $BaTiO_3$ CRYSTAL

Y. Yoshimura,[a] K. Sone,[a] H. Sumiyoshi,[a] T. Kondo,[a] A. Kojima,[b] K. Tozaki[c]

[a] *Faculty of Science and Engineering, Ritsumeikan University, Shiga 525-8577, Japan*

[b] *Department of Materials Science, University of Shiga Prefecture, Shiga 522-8533, Japan*

[c] *Department of Physics, Faculty of Education, Chiba University, Chiba 263-8522, Japan*

$BaTiO_3$ crystal is known to have four phases: for convenience we call here α-phase (P_α), β-phase (P_β), γ-phase (P_γ) and δ-phase (P_δ) from high to low temperatures, undergoing three phase transitions at approximately 403 K (T_1), 283 K (T_2) and 183 K (T_3). As for the crystal system of P_β, we have reported very recently that the single crystals reveal a notable feature [1]: different from the commonly accepted notion, $BaTiO_3$ changes its structure on cooling from the cubic to a coherent hybrid structure composed of tetragonal and monoclinic forms, having the tetragonal $(\bar{1}01)_T$ lattice plane in common. In P_γ between T_2 and T_3, the crystal also has a coherent hybrid structure composed of tetragonal and monoclinic forms sharing the tetragonal $(\bar{1}01)_T$ lattice plane in common but it is different from another coherent hybrid structure in the room temperature β-phase [2]. In P_δ below T_3, it reveals a tetragonal structure very close to a cubic system [2].

Accordingly, we tried to analyze the crystal structure of each phase. Before the crystal structure analyses, we examined possible crystal structure models explaining the X-ray diffraction data fairly well. We show that the relations between the reciprocal lattices of the tetragonal and monoclinic forms of the hybrid structure play an important role to a uniquely determined space group and a provable crystal structure model for both forms. The details about the analytical procedures and the results will be presented and discussed.

P05-089

DIFFRACTION AND XAFS STUDY OF AgI UNDER HIGH PRESSURE AND HIGH TEMPERATURE

Akira Yoshiasa[a], Hiroshi Arima[b], Hiroshi Fukui[b], Osamu Ohtaka[b], Maki Okube[c], and Yoshinori Katayama[d]

[a]Graduate School of Scienc, Kumamoto University, Kumamoto 860-8555, Japan; [b]Graduate School of Science, Osaka University, Toyonaka 560-0043, Japan; [c]Materials and Structures Laboratory, Tokyo Institute of Technology, Yokohama 226-850 Japan; [d]Japan Atomic Energy Agency , Hyogo 679-5198, Japan

Using multi-anvil high-pressure devices and synchrotron radiation at BK11XU and BL14B1 beam lines in Spring-8, Japan, extended x-ray absorption fine structure (EXAFS) and angular dispersive X-ray diffraction observations of AgI up to 6.0 GPa and 1000K have been performed to investigate the phase relations, precise structure and effective potentials in various phases. The melting curve of α-AgI has a temperature maximum at 1.0 GPa, which indicates the existence of dense liquid phase above this pressure. The three phases of α-AgI disordered rock salt type, and liquid meet in a triple point at 823K and 1.3 GPa. X-ray absorption near edge structure spectra are quite sensitive to the three-dimensional atomic configuration around X-ray absorbing atoms, they are useful for phase study under high temperature and high pressure. α-AgI and disordered rock-salt type phase have super-ionic conduction behaviors. Ag ions occupy both octahedral and tetrahedral sites in the disordered phase and twenty percent of Ag ions occupy the tetrahedral site as a maximum value at 2GPa. The transition between the rock salt type and disordered rock salt type phases is a broad and diffuse disorder type within the same structure. Some sudden changes are recognized near the phase transition point. EXAFS provides the useful information about thermal vibration of local structure under pressure. In EXAFS analysis, we have directly carried out the numerical integration of EXAFS function. The anharmonic effective pair potentials, $V(u)=\mathbf{a}u^2/2+\mathbf{b}u^3/3!$ for I-Ag bond have been determined under pressures. The potential parameter **a** for α-AgI at 1 GPa is 2.5(1) eV/A^2. The potential parameter **a** for rock-salt type is 1.7(1) eV/A^2 at 1.0 GPa and which increases to 1.9(1) eV/A^2 at 6.0 GPa. The extent of anharmonicity is larger in α-AgI than in rock salt type AgI. Pressure influences greatly the effective pair potential of anti-bonding side and anharmonicity decreases with increasing pressure. The phonon energies can be estimated using the potential parameter **a** by calculating the dynamical matrix. Analysis of EXAFS Debye-Waller factor is useful because the force constant can be decided directly even at high pressure and high temperature.

P05-090

CAGE SUBSTRUCTURES AND SITE OCCUPANCIES IN CLATHRATE COMPOUNDS,$La_3Pd_{20}T_6$ (T = Si And Ge)

Y. Matsushita[a], A. Sato[a], H. Kobayashi[b], A. Dönni[a], H. Kitazawa[a], F. Izumi[a], Y. Nemoto[b], T. Goto[b], M. Kaneko[b], S. Sasaki[b], and N. Kishimoto[a]

[a]*National Institute for Material Science, Tsukuba, Ibaraki, Japan* [b]*Niigata University, Niigata, Japan*

$Ln_3Pd_{20}T_6$ (Ln = Lanthanoids, T = Si and Ge) system shows various kinds of interesting unusual physics under low temperature. For example, Ce compounds show metallic Kondo-lattice antiferromagnetic behaviour, and $Ln_3Pd_{20}Ge_6$ (Ln = Nd, Dy and Tb) show successive antiferromagnetic orderings. These interesting physical properties may be due to the existence of the following specific crystallographic characters. In the system, all of compounds belong to C_6Cr_{23}-type structure (Fm3m). The crystal structures have two kinds of crystallographically independent lanthanoid sites, and the sites locate in cage substructures formed by Pd-Pd and Pd-T like a clathrate compound. Site-occupancy information of each sites and crystallochemical natures of these Pd-Pd and Pd-T, are also indispensable knowledge to understand the interesting properties, because the elements forming cage substructure give direct influence to the center lanthanoid. Our target La compounds are important compounds to clearly show the contrast between La compounds and other lanthanoid compounds to understand the physical properties because La takes trivalent without any 4*f* electrons as valence electrons.

The $La_3Pd_{20}T_6$ crystals are grown by floating zone method with high purity elements. Intensity measurements are carried out Bruker Smart-1000 CCD diffractometer (MoKα) at room temperature. Final R1-values are 2.23 % for Si and 2.34 % for Ge, respectively. In both compounds, all of sites are fully occupied without any disordering behaviour. In the structures there are five crystallographic independent sites, two lanthanum, two paradium and one T elements. La1 is located at centre of non-polar Pd_{12} cluster formed by Pd_1, and T is connected to each of Pd_4 square plane of the cluster as the second neighbour. On the other hand, La2 is located in more complex cluster formed by Pd and T. The first neighbour around La2 is polar Pd_{16} cluster formed by Pd_1 and Pd_2, and T connects to triangle plane by two Pd2 and one Pd1 as second neighbour of the cluster.

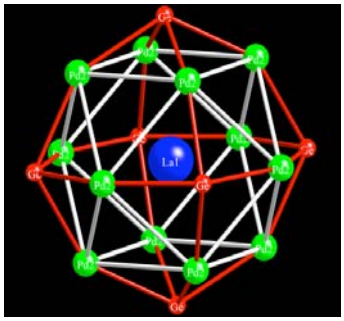

a) La1 cluster

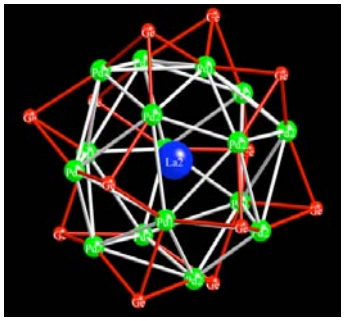

b) La2 cluster

P05-091

MODULATED STRUCTURES IN THE A*M*OB_2O_5 FAMILY FROM VARIABLE TEMPERATURE X-RAY POWDER DIFFRACTION DATA

Siegbert Schmid

School of Chemistry, The University of Sydney, Sydney NSW 2006, Australia

Non-centrosymmetric oxo pyroborates, A*M*OB_2O_5 (A = K, Rb, Cs, Tl; *M* = Nb, Ta), have attracted considerable interest owing to their potential use as non-linear optical materials. All members of the family possess a common underlying average structure. In addition most exhibit superstructures of varying multiplicities (2, 5 and 8) along the *b* axis (corresponding to the $Pmn2_1$ setting of $CsNbOB_2O_5$).

The structures of $RbNbOB_2O_5$ and $RbNbOB_2O_5$ have been refined previously using a super space approach. While for $RbNbOB_2O_5$ the structure is incommensurately modulated, despite the apparent value of the modulation wave vector of 2/5 **b*** exactly, the structure of $KNbOB_2O_5$ refined significantly better as commensurate modulated structure and was therefore reported as a superstructure.

Given the ambiguity in deciding whether a structure is commensurately or incommensurately modulated using metrics alone, a variability of the magnitude of the modulation wave vector with composition (e.g. for solid solutions) or temperature is usually taken as a means to make an informed decision.

Variable temperature X-ray powder diffraction data were collected for both $RbNbOB_2O_5$ and $KNbOB_2O_5$ at the Australian National Beamline Facility, Photon Factory, Tsukuba, Japan. Diffraction patterns were collected at RT and from 150 °C to 800 °C in 25 °C steps. The results of the analysis of these data, which supports the previously suggested reason for the modulation, will be presented here.

P05-092

RXMS STUDY ON A MAGNETIC HELIX OF $BaTiCoFe_{10}O_{19}$

Maki Okube,[a] Seiji Ohsawa,[a] Takeshi Toyoda,[b] Takeharu Mori,[c] Satoshi Sasaki[a]

[a]*Materials and Structures Laboratory, Tokyo Institute of Technology, Yokohama, 226-8503;*
[b]*Industrial Research Institute of Ishikawa, Kanazawa, 920-8203, Japan;*
[c]*Photon Factory, Institute of Materials Structure Science, KEK, Tsukuba, 305-0801*

Barium hexaferrite $BaFe_{12}O_{19}$ is ferrimagnetic and has the strong uniaxial magnetic anisotropy. The M-type ferrite has a spin collinear structure, in which all the magnetic moments in five independent iron sites are ordered parallel or antiparallel to *c* axis. It is known that the substitution of Fe^{3+} by a pair of Ti^{4+} and Co^{2+} causes a magnetic helix propagated along the hexagonal *c* axis and results the reduction of the anisotropy. Resonant X-ray magnetic scattering (RXMS), which has the selectivity between iron and cobalt atoms, is a useful tool to determine the structure and electronic state of the magnetic helix. Therefore, we investigate the magnetic structure of $BaTiCoFe_{10}O_{19}$ by RXMS at the Fe *K* absorption edge.

RXMS experiments were carried out at the BL-3A/6C of Photon Factory. X-rays monochromatized by Si(111) crystals were guided into a transmitted-type phase retarder to produce the circular polarization near the 111 Bragg condition of diamond in the asymmetric Laue case. Diffraction profiles were measured at wavelengths of λ = 1.7406 and 1.7390 Å, using a four-circle/triple-axes diffractometer. An ω step-scan technique was applied for single crystals in the weak magnetic filed. Low-temperature experiments at T = 100 K were performed with the Oxford Cryostream Cooler, where cold and dry nitrogen gas is directly blown onto the crystal.

The crystal structure with spin orientation can be determined based on the difference between observed and calculated asymmetry ratios. The observed asymmetrical ratio ΔR_{obs} was obtained for 32 Bragg reflections through the RXMS measurements. The ΔR_{calc} was estimated from the crystal structure factors related to charge, anomalous, magnetic and resonant magnetic scattering terms, based on the structural model. The canting angles of spins were estimated with residual factors of $\Sigma(\Delta R_{obs} - \Delta R_{calc})^2$, where each iron sites had a minimum for the multiplicity. The relation between the substitution of Fe^{3+} and the magnetic helix structure was obtained from the estimation of the degree of the spin canting. In the presentation, the magnetic structure and magnetic anisotropy will be discussed in comparison with the results of $BaFe_{12}O_{19}$ and $BaTiCoFe_{10}O_{19}$.

P05-093

SODIUM ARRANGEMENT IN NA_XMO_2 P2 STRUCTURE AS A FUNCTION OF TEMPERATURE, TRANSITION METAL TYPE, AND SODIUM STOICHIOMETRY

Angélique Jarry[a], Maxim Avdeev[b]

[a]*Magistère Materiaux, university of Rennes 1, France*

[b]*The Bragg Institute, Australian Nuclear Science and Technology Organisation, Sydney, Australia*

Recently renewed research interest in Na_xMO_2 compounds (M=transition metal) has revealed a range of interesting properties of this system. Due to its potential for thermoelectric applications and superconductivity in the hydrated form, Na_xCoO_2 has been subjected to extensive study.

The γ-Na_xCoO_2, or P2 in Hagenmuller's notation [1], structure type is built of hexagonal layers $[MO_2]^{2\infty}$ with Na ions sandwiched between planes of edge sharing MO_6 octahedra. Sodium ions can occupy two different types of trigonal prisms sharing either edges or faces with MO_6 octahedra. Due to the repulsion between sodium and transition metal M, the latter type of prisms is less electrostatically favorable. Delicate balance between sodium-sodium and sodium-transition metal interactions results in various arrangements of Na^+ in the interlayer space [3].

We extend previous theoretical and experimental studies of sodium clustering in sodium cobaltate by investigating sodium arrangement in P2 structure type as a function of transition metal type M, sodium content x, and temperature using X-ray and neutron powder diffraction.

References:

[1] C. Delmas et al, Physica 99B (1980) 81-85

[2] P. Zhang et al, Phys. Rev B 71 (2005) 153102

[3] M. Roger et al, Nature 445 (2007) 631.

P05-094

UNUSUAL SITE PREFERENCE OF BORON IN SYNTHETIC $MgAl_{2-x}B_xO_4$ SPINEL (x = 0.11 and 0.13) UNDER HIGH PRESSURE

Shunsuke Sakai,[a] Akira Yoshiasa,[a] Takafumi Hashimoto,[a] Akihiko Nakatsuka,[b] Kazumasa Sugiyama,[c] Maki Okube,[d] and Eiji Ito[e]

[a] *Graduate School of Science and Technology, Kumamoto University, Kumamoto 860-8555, Japan*

[b] *Department of Advanced Material and Engineering, Faculty of Engineering, Yamaguchi University, Ube 755-8611, Japan*

c Institute for Materials Research, Tohoku University, Sendai 980-8577, Japan

[d] *Materials and structure laboratory, Tokyo Institute of Technology, Yokohama 226-8503, Japan*

[e] *Institute for study of the Earth's Interior, Okayama University, Tottori 682-0193, Japan*

Using "6-8" type uniaxial split-sphere apparatus Single crystals of $MgAl_{2-x}B_xO_4$ (x = 0.11 and 0.13) spinel were synthesized of 9GPa and 11GPa at 1000℃. Site preference of Boron and structural variation in $MgAl_{2-x}B_xO_4$ spinel solid solution, have been investigated by single crystal X-ray diffraction technique. The intensity data of X-ray diffraction were measured at room temperature using Rigaku AFC-5S four-circle diffractometer with graphite-monochromatized MoKα radiation (λ = 0.71069 Å; 40KeV, 30mA). The crystal structure refinements using single-crystal X-ray diffraction method were carried out to determine the site preference of B, Mg and Al atoms. The crystals were ascertained to satisfy the systematic absence of space group Fd3m from precession photographs. Structural refinements were carried out using the full-matrix least-square program RADY92. The R factors for x = 0.0, x = 0.11 and x = 0.13 were reached 2.25 %, 2.97 % and 2.52 %, repetitively. All B^{3+} occupy the octahedral site. Based on the site preference refinements and observed bond length of each site, the chemical formula of B-bearling spinels are $(Mg_{0.63}, Al_{0.37})[Mg_{0.37}, Al_{1.50}, B_{0.13}]O_4$ and $(Mg_{0.63}, Al_{0.37})[Mg_{0.37}, Al_{1.50}, B_{0.13}]O_4$, respectively. These results are very important; the small B ion dose not occupying the small tetrahedral site, but it occupies the largely octahedral site. When we compare the pure $MgAl_2O_4$ spinel, disordernes of cation site preference is increase with Boron contents. It is well known that spinel structure wih higher symmetry has a peculiar site preference. The octahedral sites in spinel are proffered by smaller Al ion than larger Mg ion. More ever, the smallest B ion gives priority to the octahedral site most in the Mg-Al-B systems. The site preference depends greatly on the structure of host crystal.

P05-095

PHOTOISOMERIZATION OF RUTHENIUM DIMETHYL SULFOXIDE COMPLEXES AND THEIR CRYSTAL STRUCTURES

Yuji Karakane, Hidehiro Uekusa

Department of Chemistry and Materials Science, Tokyo Institute of Technology, JAPAN

Ruthenium DMSO complex (Fig.1) shows photochromism from orange to red by irradiation of UV light. It is suggsted that the color change is caused by photoisomerization of DMSO ligand (from Ru-S=O(S-form) to Ru-O=S(O-form)) from spectroscopic studies. However, the relationship between the photo-reactivity and molecular/crystal structure was not discussed well. In this study, geometrical features in the crystal structure that characterize the photoisomerization process are investigated by X-ray single crystal analysis. In order to modify the crystal structure and reaction cavity around DMSO group (Fig.2) from known $[Ru(bpy)(tpy)(DMSO)](OTf)_2$ crystal, $[Ru(bpy)(tpy)(DMSO)](PF_6)_2$ was synthesized by literature method, and crystal structure was determined.

The change of UV/VIS specta and powder diffraction pattern after UV irradiation indicated that the photoisomerization reaction was occurred in solid-state. Also, the reaction rate of $[Ru(bpy)(tpy)(DMSO)](OTf)_2$ was faster than $[Ru(bpy)(tpy)(DMSO)](PF_6)_2$. The reaction cavity volume calculation indicated that $[Ru(bpy)(tpy)(DMSO)](OTf)_2$ crystal ($14.8Å^3$) has larger cavity than $[Ru(bpy)(tpy)(DMSO)](PF_6)_2$ crystal ($14.2Å^3$) and it may contribute to the lower energy barrier of photoisomerization.

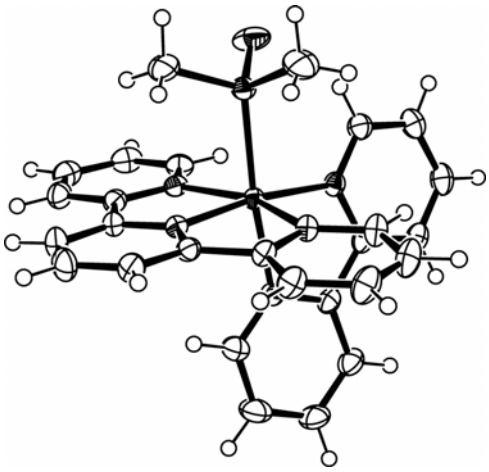

Fig.1 $[Ru(bpy)(tpy)(DMSO)]^{2+}$

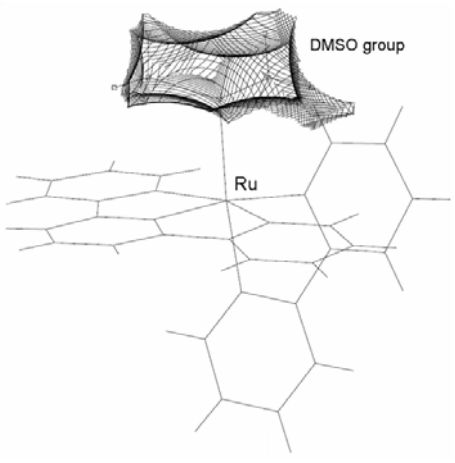

Fig.2 $[Ru(bpy)(tpy)(DMSO)](OTf)_2$ reaction cavity

P05-096

CRYSTALLOGRAPHIC STUDY ON DEHYDRATION BEHAVIOR OF CHABAZITE

Akihiko Nakatsuka, Hironao Okada, Keiko Fujiwara, Noriaki Nakayama and Tadato Mizota

Graduate School of Science and Engineering, Yamaguchi University, Ube, Yamaguchi 755-8611, Japan

Chabazite [idealized formula $Ca_2(Al_4Si_8)O_{24}\cdot 12H_2O$], one of the most widespread natural zeolites, is a promising heat absorbent for the zeolite-water heat pump system because of its high heat-exchange abilities at low temperatures. The heat-exchange abilities of zeolites are closely related to their thermodynamic hydration-dehydration process, and hence can depend on the strengths of the interactions between water molecules and their neighbors (framework atoms and exchangeable cations). Therefore, investigation of the dehydration behaviors of water sites in chabazites is important for elucidating their properties as heat absorbents. However, the dehydration behaviors of water sites in chabazites have been unknown to date owing to the uncertainty of positions of water molecules and exchangeable cations. In the present study, we carry out single-crystal X-ray diffraction study of fully hydrated and partially dehydrated chabazites to examine the dehydration behaviors of water sites.

Single crystals of a natural chabazite [$Ca_{1.57}Na_{0.49}(Al_{3.39}Si_{8.55})O_{24}\cdot 12.47H_2O$] from Komuro, Oh-hito, Shizuoka Prefecture, Japan, were used in the present study. Selected crystals were put into silica-glass capillaries, attached to a vacuum line, and dehydrated by heating at 100, 150 and 200 °C for 1 hour under 5×10^{-5} Torr. After that, the capillaries were sealed and slowly cooled to room temperature.

The present structure analyses have revealed the presence of five partially-occupied water sites and four partially-occupied exchangeable-cation sites. The final structure refinements converged to R = 0.0280–0.0303 and R_w = 0.0276–0.0302 for each sample. From the resulting occupancies of the water sites, we confirmed that the prepared dehydrated-samples have different water contents. The present results show that exchangeable cations migrate to the exchangeable-cation sites located near the 6-ring windows with dehydration. Moreover, the dehydration behaviors of the water sites will be discussed with attention to the interactions between water molecules and their neighbors (framework atoms and exchangeable cations).

P05-097

TEMPERATURE DEPENDENCE OF CRYSTAL STRUCTURE OF PYROPE GARNET

Mami Shimokawa,[a] Akihiko Nakatsuka,[a] Makio Ohkawa[b] and Noriaki Nakayama[a]

[a]*Graduate School of Science and Engineering, Yamaguchi University, Ube, Yamaguchi 755-8611, Japan;*[b]*Graduate School of Science, Hiroshima University, Higashi-Hiroshima, Hiroshima 739-8526, Japan*

Pyrope garnet ($Mg_3Al_2Si_3O_{12}$) is an important mineral as constituents in the Earth's upper mantle. In this garnet, Mg, Al and Si occupy dodecahedral, octahedral and tetrahedral sites, respectively. Since the dodecahedral cavity size is too large for the ionic radius of Mg, which would fit better into an octahedral coordinated site, Mg in pyrope has a geometrical anomaly. The large difference between the dodecahedral cavity size and the ionic radius of Mg suggests that positional disorder of Mg could occur together with its strong vibrational motion. Indeed, it is well known that the displacement parameter of Mg in pyrope is much larger than those in other silicate garnets. However, conclusive evidence for the positional disorder of Mg has not been obtained to date, although efforts to solve this problem have been made by several researchers. In the present study, to examine the possibility of positional disorder of Mg, we investigate the temperature dependence of crystal structure of pyrope, with attention to temperature dependence of displacement parameter.

Single crystals of pyrope were synthesized at 8 GPa and 1600 °C. X-ray diffraction intensities of a selected crystal were measured in the temperature range of 88–473 K using a four circle diffractometer. The structure refinements at each temperature converged to R = 0.0198–0.0291 and R_w = 0.0126–0.0234.

The present result shows that the isotropic equivalent displacement parameter of Mg [B_{eq}(Mg)] decreases linearly with decreasing temperature. The possibility of positional disorder of Mg will be discussed from the extrapolation of the displacement parameter to 0 K. Moreover, the residual electron density distribution around the dodecahedral site obtained from the difference Fourier synthesis will be also discussed to clear whether or not there is the positional disorder of Mg.

P05-098

EVOLUTION OF CORUNDUM STRUCTURE AT HIGH TEMPERATURES

S. Kondo, K. Tateishi, H. Hibino and N. Ishizawa

Nagoya Institute of Technology, Tajimi, Japan.

The evolution of corundum (α-Al_2O_3) structure was investigated at 297, 573, 873 and 1173K using single-crystal X-ray diffraction method and molecular dynamics simulation. The results were smoothly extrapolated to the previous high-temperature data of the compound at 2170 K [1], revealing a significant shift of fractional coordinate *z* of the Al atom as a function of temperature. The Al atom shift indicates that the Al-Al repulsion force across a pair of face-sharing octahedra becomes conspicuous over the other interatomic forces at high temperatures. The increasing Al-Al repulsion is relieved by both the preferential expansion of the unit cell along the *c* axis and the change in the *z* coordinate of Al atom. The molecular dynamics simulation experiments qualitatively agreed with the X-ray results. The thermal expansion of the crystal was well described by the quadratic functions, $a = 4.75385\ (1.0 + 5.05841\times10^{-6}\ T + 1.69084\times10^{-9}\ T^2)$ Å, and $c = 12.9782\ (1.0 + 4.61344\times10^{-6}\ T + 2.63802\times10^{-9}\ T^2)$ Å. The thermal expansion data of corundum in the literature [2-4] will be discussed.

Reference:

1) N. Ishizawa, T. Miyata, I. Minato, F. Marumo and S. Iwai : Acta Cryst. B36 (1980) 228-230.

2) W. M. Yim & R. J. Paff: J. Appl. Phys. 45. (1974) 1456-1457.

3) Yu. V. Shvy'ko, M. Lucht, E. Gerdau, M. Lerche, E. E. Alp, W. Sturhahn, J. Sutter & T. S. Toellner: J. Synchrotron Rad. **9**. (2002) 17-23.

4) M. Lucht, M. Lerche, H.-C. Wille, Yu. V. Shvyd'ko, H. D. Rutter, E. Gerdau & P. Becker: J. Appl. Cryst. **36**. (2003) 1075-1081.

P05-099

PHASE TRANSITION OF Gd_3RuO_7

K. Okada, S. Kondo, T. Suwa and N. Ishizawa

Nagoya Institute of Technology, Tajimi, Japan.

The series of Ln_3MO_7 crystals composed of trivalent lanthanide (Ln) and pentavalent transition metal (M=Ru, Os) oxides are expected to possess quasi one-dimensional electric conduction properties along the MO_6 octahedral single-chains. The series shows a polymorphism. A noncentrosymmetric orthorhombic $P2_1nb$ modification has been recently found for Gd_3RuO_7 [1] in addition to the centrosymmetric *Cmcm*. The present study shows that Gd_3RuO_7 undergoes a phase transition at approximately 382 K from $P2_1nb$ to centrosymmetric *Cmcm*.

Crystals were grown by cooling the $SrCl_2$-RuO_2-Gd_2O_3 solution at the rate of 5 $Kmin^{-1}$ from 1373 K. Data were collected in nitrogen atmosphere by the CCD single crystal diffractometer (Smart Apex II, Bruker) equipped with a heating apparatus. The structure was determined at 297, 423, 773 and 1173 K. The structure at 297 K was confirmed to be $P2_1nb$ while those at 423, 773 and 1173 K were *Cmcm* with halved *b*-length. Changes of the cell dimensions and superstructure reflection intensities were examined in the temperature range between 296 and 523 K at the interval of 20 K. The anomalies were observed in both *b* and *c* cell dimensions while not clear in *a*. The superstructure reflections associated with the $P2_1nb$ modifications were gradually weakened with increasing temperature and disappeared between 363 and 383 K. A reverse change occurred with decreasing temperature. The transition observed by the present X-ray diffraction study presumably corresponds to the anomaly at 382 K reported from the specific heat measurement [2].

The phase transition between the $P2_1nb$ and *Cmcm* modifications can be structurally characterized by an additional tilt about *a* which occurs in the low temperature form ($P2_1nb$) for the half of the RuO_6 octahedra. A reduction of coordination number from 8 (*Cmcm*) to 7 ($P2_1nb$) also occurs for some Gd atoms bridging the adjacent RuO_6 single-chains. A positional disorder reported for several Ln atom sites in the $P2_1nb$ modifications [3] was also observed in the *Cmcm* modification, suggesting that the phase transition is not the origin of the positional disorder of Ln atoms.

References:

1) N. Ishizawa et al., Acta Cryst., **E62**, i13-i16 (2006).

2) D. Harada and Y. Hinatsu, J. Solid State Chem. 164, 163-168 (2002).

3) N. Ishizawa et al., Acta Cryst. **C63**, i43-i46 (2007); Acta Cryst. **E63**, i163 (2007).

P05-100

STRUCTURE OF $SrTiO_3$-DOPED $LaAlO_3$ PEROVSKITE

N. Ishizawa [a], Y. Inagaki [a], T. Shimada [b], I. Kagomiya [a], K. Kakimoto [a], and H. Ohsato [a]

[a] *Nagoya Institute of Technology, Nagoya, Japan.* [b] *Hitachi Metals, Ltd. Japan*

Recently the sintered samples of $(La_{1-x}Sr_x)(Al_{1-x}Ti_x)O_3$ perovskite-type solid solution are found to have higher quality factors than that of $LaAlO_3$, peaking Qf=165THz at x~0.2 [1]. Single crystals of x=0.05 and 0.20 were grown by the floating-zone method [2], and the former showed much improved Qf. The crystals, however, possessed very weak intensities at the reciprocal lattice points forbidden for the space group $R\bar{3}c$ which is commonly assumed for the rhombohedral distortion of the ideal perovskite ($Pm\bar{3}m$). The present study reveals that the $(La_{1-x}Sr_x)(Al_{1-x}Ti_x)O_3$ perovskite-type crystals (x=0.05 and 0.2) belongs to $R\bar{3}$ which accommodates two crystallographically independent octahedral sites for Al(Ti). Ti atoms are preferentially concentrated on the larger octahedron. The ordered distribution of Ti could explain the property that the $SrTiO_3$-doped compounds have higher Qf than pure $LaAlO_3$. Discussion will be given on the reasons why the symmetry of $SrTiO_3$-doped crystals differs from the pure $LaAlO_3$ [3-4], the end member of the 'solid solution'.

Reference:

1) T. Shimada et al., J. Euro. Ceram. Soc. **26**, 2017-21 (2006)
2) Y. Inagaki et al., J. European Ceram. Soc. **27**, 2861-64(2007)
3) C. J. Howard et al., J. Phys.: Cond. Mat. **12** 349-65 (2000).
4) H. Lehnert et al., Z. Kristallogr. **215** 536-41 (2000).

completely vanishes at 10 ± 2 K. The careful Rietveld refinements of the low-temperature XRD patterns indicated that these peaks arise from the *tripling* of the lattice parameter along *c*-axis. Noted that in the material there exists no driving force for this structural phase transition, neither ionic (should have taken place at room temperature) nor charge ordering. It is, therefore, most likely that a new magnetic ordering onsets and couples to the lattice degree of freedom in the temperature window, 10 ~ 120 K. Measurements of the physical properties, magnetization and heat capacity, show the anomaly around 120K indicating the spin-lattice coupling at the phase transition temperature. Dielectric constants measurement also shows a change at liquid nitrogen temperature revealing the magnetoelectric effect of $Dy(Mn_{0.5}Fe_{0.5})O_3$ and further detailed measurements are underway.

P05-101

SYNTHESIS AND STRUCTURE OF FERROMAGNETIC RUTILE

Takashi Mochiku,[a] Kazuhiro Yamaki,[b] Natsumi Shimizu,[b] Akinori Hoshikawa,[c] Hiroki Fujii,[a] Katsura Yamada,[a] Shinji Itoh,[a] Itsuhiro Kakeya,[b] Kazuo Kadowaki[b] and Kazuto Hirata[a]

[a]National Institute for Materials Science, Tsukuba, Ibaraki 305-0047, Japan; [b]University of Tsukuba, Tsukuba, Ibaraki 305-8573; [c]Japan Atomic Energy Agency, Tokai, Naka, Ibaraki 319-1195, Japan

There were many reports that ferromagnetism at room temperature was observed in TiO2 (rutile and anatase) doped with 3d transition metals. However, these samples were synthesized by the thin film growth techniques under thermally nonequilibrium conditions. We have succeeded in the single crystal growth of rutile doped with 3d transition metals by floating zone method from the melt in equilibrium conditions to investigate the mechanism of ferromagnetism at room temperature.

The crystals doped with 1 at.% Co and 0.5 at.% Ni exhibit ferromagnetism at room temperature when those are grown in reduced atmosphere. The magnetic properties of the doped crystals are strongly dependent on the oxygen deficiency. Ferromagnetism was not observed in the crystals annealed in air or oxygen atmosphere. The crystal lattice is enlarged by doping and is compressed by annealing in spite of low doping concentration of Co and Ni. These support that the doped elements are situated at the substitutional locations and the oxygen deficiency is important for exhibiting ferromagnetism.

P05-102

TEMPERATURE AND PRESSURE INDUCED TRANSITIONS OF PEROVSKITES ABX_3 TO OTHER STRUCTURE TYPES

Maxim Avdeev[a], Sergey Yakovlev[a]

[a]*Bragg Institute, Australian Nuclear Science and Technology Organisation*

Using empirical approach based on polyhedral volume ratios and *ab initio* DFT calculations we identified a number of perovskites ABX_3 close to the boundaries of perovskite structure type stability. Experimental results obtained during following *in situ* X-ray powder diffraction studies at high temperature or high pressure combined with the analysis of crystal chemical information accumulated in the Inorganic Crystal Structure Database (ICSD) allowed us to establish quantitative parameters defining stability of ABX_3 compositions in perovskite, post-perovskite ($CaIrO_3$), or ilmenite structure type. Rare cases when high pressure results in amorphisation of ABX_3 materials rather than phase transition will also be discussed in this context.

P05-103

SYNTHESIS AND CHARACTERIZATION OF SERIES HETERMETALLIC COORDINATION POLYMER $Ma_xMb_{1-x}(tda)H_2O$ (Ma, Mb=Zn, Co AND Ni, 0<x<1)

Ming-Cheng Wu and Chi-Shen Lee*

Department of chemistry and Institute of Molecular Science, National Chiao Tung University, Hsinchu, Taiwan, 300, R.O.C.

A series of two dimensional coordination polymer of mixed metal thiodiacetate $M_{ax}M_{b1-x}(tda)H_2O$(M=Zn, Co, and Ni, 1>x>0, thiodiactate=tda) were synthesis under hydrothermal condition. The structural of these compounds features a 2-dimensional metal-oxygen network connected through edge or corner sharing of the MO_5S polyhedra. These MM'-tda-H_2O have similar structure (e.g. $Zn_{0.5}Co_{0.5}$-tda-H_2O: $P2_1$ monoclinic a =15.561(10)Å b =5.187(3)Å c =17.391(11)Å β=114.571(11)°). With different transition metal as central ion, $M_{ax}M_{b1-x}(tda)H_2O$ exhibits many interesting properties due to excitation of d-d transition orbital and unpaired electron. Zn-tda-H_2O is needle shapes colorless crystal, but Co series show pink color and Ni series are green. Such physical properties measurements revealed that the optic and magnetic properties could be controlled by tuning the compositions of metal ions in $M_{ax}M_{b1-x}(tda)H_2O$. Besides, the crystal structures of $M_{ax}M_{b1-x}(tda)H_2O$ with different doping concentration were analyzed by using high-resolution powder X-ray diffractions with synchrotron radiation. The thermo-behavior of $M_{ax}M_{b1-x}(tda)H_2O$ were characterized by TGA and temperature-dependent powder X-ray diffractions indicate these compounds are stable till 300°C.

P05-104

SYNTHESIS AND CHARACTERIZATION OF NEW QUATERNARY SELENIDE $In_{1.91}Pb_4Bi_{4.09}Se_{13}$

Ming-Fang Wang and Chi-Shen Lee*

Department of Applied Chemistry and Institute of Molecular Science, National Chiao Tung University, Hsinchu, Taiwan, 300, R.O.C.

The new quaternary compound of $In_{1.91}Pb_4Bi_{4.09}Se_{13}$ was synthesized by direct combination of the In:Pb:Bi:Se = 1.91:4:4.09:13 at temperature at 1023 K. The structure was determined by single-crystal X-ray diffraction. The compound crystallized in the orthorhombic space group *Pbam* with a = 22.29(2) Å、b = 27.52 (2) Å、c = 4.144(2) Å、V = 2542(3) $Å^3$、Z = 4. The final R values are R_1 = 0.0322, wR_2 = 0.0706 and GOF = 1.04. The structure of $In_{1.91}Pb_4Bi_{4.09}Se_{13}$ features three-dimensional framework containing building blocks of wide rectangular NaCl-[100] type infinite rod type unit and corner-shared infinite one-dimensional [$InSe_4$] chains running parallel to the c-axis. Band structure calculation based on the model $In_{1.91}Pb_4Bi_{4.09}Se_{13}$ suggests that the material is a narrow band gap semiconductor. Four probe electroconductivity measurements in temperature range between 30-800 K show declines of the resistivity with increase of temperature. Thermopower of $In_{1.91}Pb_4Bi_{4.09}Se_{13}$ is ~ -200-300 μV/K over temperature range between 300 and 550 K, which indicates n-type semi-conducting property. The room temperature power factor of $In_{1.91}Pb_4Bi_{4.09}Se_{13}$ is 0.67 $\mu W/cmK^2$.

P05-105

MAGNETIC PROPERTIES OF DINUCLEAR ONE-DIMENSIONAL COMPLEXES WITH TRIAZOLE BASED LIGANDS

S. M. Chen,[a] C. F. Sheu,[a] Y. S. Wen,[b] and Y. Wang*[a]

[a] *Department of Chemistry, National Taiwan University, Taipei, Taiwan*

[b] *Institute of Chemistry, Academia Sinica, Taipei, Taiwan*

[{Fe^{II}(μ-bpt)(NCS)}$_2$L] (bpt = 3,5-bis(pyridin-2-yl)-1,2,4-triazole), L = pyrazine(**1**), 4,4'-bipy(**2**) have been synthesized by one-step solvo-thermal syntheses; both exhibit an abrupt spin transition at 130 and 156K respectively. The Fe^{II} centers are connected with two bi-dentate ligands "bpt" equatorially and bridged axially by linking ligand of "pyrazine" or "4,4'-bipy" to form an one-dimensional dinuclear zigzag chain. There is only one unique Fe site in the structure due to the center of symmetry at the center of the dinuclear species. When the temperature is cooling down through the phase transition temperature, the spin state of Fe centers will change from high spin state to low spin state, namely a [LS–LS] pair of **1** and [HS-LS] of **2** dinuclear complexes. The typical change of ~0.2 Å in Fe-N bond lengths is observed associated with the spin transition.

The another dinuclear Fe(II) complex, **[Fe_2(μ-bpt)$_2$($C_6H_4NO_2$)$_2$ • H_2O]**, with the Fe^{II} centers connected with bpt and isonicotinic acid is an one-dimemsional flexuous chain of dinuclear Fe^{II} complex. It is also synthesized by solvo-thermal synthesis and characterized by x-ray diffraction. The bond lengths of Fe-N are 2.331(1) Å, 2.130(1) Å, 2.233(1) Å, 2.126(1) Å and Fe-O are 2.057(1) Å, 2.093(1) Å at 300 K which are characteristic high spin state of Fe^{II} centers. This chain complex shows distinct ferromagnetic interaction between the Fe^{II} centers. The comparison between these dinuclear complexes and other similar structures will be presented.

Keywords: spin crossover, ferromagnetic interaction, dinuclear complex

P05-106

INVESTIGATION OF THE ELECTRONIC STRUCTURE OF LANTHANIDE ZIRCONATES

Richard Clements[a,b], Brendan Kennedy[a], Chris Ling[a,b], Anton Stampfl[b]

[a]School of Chemistry, The University of Sydney, New South Wales, 2006, Australia; [b]Bragg Institute, Australian Nuclear Science and Technology Organisation, PMB 1, Menai, New South Wales, 2234, Australia.

The lanthanide zirconates are of interest for potential use in inert matrix fuels and nuclear wasteforms. To determine the suitability of a material as an inert matrix or wasteform, the material's structure must be resistant to radiation damage and its thermal, thermodynamic and mechanical properties must be known. The structure's ability to incorporate an actinide host into the lattice vacancy must also be known. These properties may be better understood by investigating the *f*-electronic structure, which has historically proved troublesome to model.

We have undertaken a synthesis of the full range of lanthanide zirconate series using solid state techniques. We have obtained powder laboratory X-ray diffraction and synchrotron powder XRD patterns on a selection of the series. These results will be presented, along with details of the analysis and synthetic techniques used.

P05-107

STRUCTURAL PHASE TRANSITION ACCOMPANIED BY METAL-INSULATOR TRANSITION IN HOLLANDITE VANADATE

Masahiko Isobe, Shigenori Koishi and Yutaka Ueda

Institute for Solid State Physics, The University of Tokyo, Kashiwanoha 5-1-5, Kashiwa, Chiba 277-8581, Japan.

$K_2V_8O_{16}$ have a hollandite structure with space group *I*4/*m* at room temperature. In the crystal structure, the double rutile-type chains of VO_6 octahedra share corners with the neighboring chains to form a V_8O_{16} stoichiometry framework that encloses large four-sided tunnels. The K^+ cations are located in the tunnels. $K_2V_8O_{16}$ is a mixed-valence compound, since the crystallographic site of the vanadium atom is unique. The formal oxidation of the vanadium is +3.75. We reported a metal-insulator transition in $K_2V_8O_{16}$ for the first time last year [1]. This transition was accompanied by structural change from a tetragonal to a monoclinic structure.

Recently we have prepared a new hollandite vanadate $Rb_2V_8O_{16}$ and observed a similar metal-insulator transition. Also the solid solutions $K_{2-x}Rb_xV_8O_{16}$ and $K_2V_{8-y}Ti_yO_{16}$ have been prepared successfully. These structural changes at the transition have been investigated by using powder X-ray diffraction.

The metal-insulator transition of $Rb_2V_8O_{16}$ was accompanied by structural change from a tetragonal to another tetragonal structure, which is different from that of $K_2V_8O_{16}$. In the solid solutions $K_{2-x}Rb_xV_8O_{16}$, $K_{1.6}Rb_{0.4}V_8O_{16}$ showed two structural transitions. At the first transition, we observed the structural change from a tetragonal to another tetragonal structure. At lower temperature the second transition from the tetragonal to a monoclinic structure was observed. The first transition seems to correspond to the metal-insulator transition. In contract, at the second transition the magnetic susceptibility did not show any anomaly. The second transition disappears with increasing Rb contents. In $K_2V_{8-y}Ti_yO_{16}$ system, similar two structural transitions were also observed. However the both transitions disappear with increasing Ti contents rapidly.

Reference:

[1] M. Isobe, S. Koishi, N. Kouno, J. Yamaura, T. Yamauchi, H. Ueda, H. Gotou, T. Yagi and Y. Ueda, J. Phys. Soc. Jpn. **75**, 073801 (2006)

P05-108

PSEUDO-MEROHEDRAL TWINNING : HOW TO TREAT A SIX-FOLD TWIN

Martin Adam, Anita Coetzee, Leo Straver and Rob Hooft

Bruker AXS, Oostsingel 209, NL 2612 HL Delft, The Netherlands

The introduction of two dimensional detectors for single crystal diffraction has made it possible to easily collect data of pseodo-merohedral twins, incommensurate structures and structures including diffuse scatter. Many programs exist, e.g. GEMINI, CELL_NOW and DIRAX, with which these more complex matrices can be indexed.

A common problem with pseudo-merohedral twinning is cell refinement due to closely overlapping spots. Careful selection of trusted areas to refine the cell in, will improve the reliability of the cell parameters.

Recent versions of integration programs, such as SAINT and EvalCC utilize the different orientation matrices and can integrate the entire intensity of every reflection labeling them as overlapping or not. One of the pitfalls during integration of data from pseudo-merohedral twins is that the spot shape changes continuously due to the systematic overlap of areas of adjacent spots. Special care has to be taken when setting up the integration parameters.

Most semi-empirical scaling and absorption correction programs are not able to handle datasets of such complexity. The program TWINABS was developed specifically to carry out absorption correction and scaling on datasets which contain reflections from different domains. Resultant data files distinguish between non-overlapping and overlapping reflections and can be seamlessly used for structure refinement.

The approach is illustrated using a six-fold twin that shows a reversible transition to single crystal state.

P05-109

THE CRYSTAL STRUCTURE OF GUEST-REMOVED MELANOPHLOGITE

Akihiro Ida[a], Kuniaki Kihara[a] and Shuhei Fujinami[b]

[a]*Graduate School of Natural Sciences and Technology, Kanazawa University;* [b]*Department of Chemistry, Faculty of Science, Kanazawa University, Kakuma, Kanazawa, 920-1122, Japan*

Melanophlogite (MEP), $23SiO_2 \cdot M^{12} \cdot 3M^{14}$ (Z = 8 for low MEP and 2 for high MEP), is a silica clathrate mineral, containing small molecules such as CO_2, CH_4, N_2 and so on in two kinds of cage-like voids, which are represented by M^{12} and M^{14} in the formula. These molecules, hereafter called as guest-molecules, would be held in the cage via van der Waals contact with the framework atoms. According to Liu *et al*. (1997), the guest-molecules are perfectly removed from a natural MEP by heating treatment above 950 °C for 6 hours. The knowledge of the temperature dependences of structural data in a guest-removed MEP (GR-MEP) would be important to clarify the correlation between the guest-molecules and the SiO2 framework , or further to assess the stability of natural MEP.

The sample crystals of GR-MEP were obtained in heating natural MEP from Mt. Hamilton, California, USA at 950 or 1000 °C for 6 hours. The originally colorless and transparent crystals became jet black-deep brown, after the heat treatment, likely in previous reports. The crystal structure of GR-MEP was investigated with least-squares refinement based on the single-crystal X-ray diffraction data at four different temperatures. The integrated intensities were measured on CCD diffractometer (Rigaku Mercury) at -50 and 23 °C, and on 4-circle diffractometor (Rigaku AFC7S) at 23, 100 and 200 °C. An optical observation under polarization microscope at room temperature suggested that the specimen was optically isotropic. Intensity-relationship among reflections, which are to be, equivalent in the expected cubic symmetry, i.e., $m\bar{3}m$, indicated no sign of departure from that symmetry. This applies to all the measurements at the 4 temperatures, apparently being inconsistent with Liu *et al*. (1997), who found possibilities of two phase-transitions at 140 and 60 °C in NMR experiments. The space group of our GR-MEP is $Pm\bar{3}n$, the same as high MEP with a = 13.4482(12) Å at room temperature. The unit cell volume of GR-MEP slightly expanded approximately 0.9 % compared to that of natural MEP. This is another inconsistency to Liu *et al*. (1997). Difference-Fourier maps obviously indicated that residual electron densities appeared in the cages, (proved to be 32.3 % in M^{12} and 84.8 % in M^{14} in the least-squres refinement). The refinements confirmed that the original framework structure is retained with nominal Si-O bond lengths and Si-O-Si angles only insignificantly changed.

The harmonic least-squares refinements showed that mean-square displacements (MSD) for all atoms except O3 and O4 decreased with increasing temperature. Such peculiar behaviors are known in some temperature ranges above the phase-transition points in high MEP and β-quartz. A generalized probability density function (PDF) analysis showed the PDF contours on O1 and O2 to be of a tendency of splitting. The contour shape of O1 changes from unimodal to bimodal with decreasing temperature. The same is also applicable to the PDF of O2, but with a clearer splitting. The symmetry breaking from $Pm\bar{3}n$ to and $Pm\bar{3}$ will occur at lower temperature, than the present temperature in our specimen, if any.

P05-110

STRUCTURE REFINEMENT OF THE SAMPLE OBTAINED BY NASA'S STARDUST MISSION

Kazumasa Ohsumi,[a] Kenji Hagiya,[b] Takashi Mikouchi[c] and Michael Zolensky[a]

[a]NASA/Johnson Space Center; [b]Graduate School of Life Science, Univ. of Hyogo; [c]Graduate School of Science, Univ. of Tokyo

Many tiny samples from the comet named Wild2 were obtained by the NASA's Stardust Mission in January of 2006. We reported the results of the structure refinements of olivine and orthopyroxen included in the track of C2054,0,35,4 of cometary materials at AsCA'06/CrSJ in Tsukuba in the last November. These results showed the site occupancies (Mg/[Mg+Fe]) of octahedral sites of olivine and orthopyroxene as 0.905(4), 0.894(4) and 0.98(6), 0.81(9), respectively.

Olivine in the other track of C2067,1,111,4 was newly refined as follows. The Laue pattern of this sample was obtained by 120 min. exposure with the ring operation of 2.5 GeV. All of the Laue spots were indexed base on cell dimension of olivine. Although more than 200 spots were indexed, integrated intensities of 124 spots were used for structure refinement by taking into account of absorption effect. It becomes serious at the wavelength emitted at more than 1.5 A.

After several cycles of least-square refinement of the structure, the refinement including site occupancies was carried out, and showed the site occupancies [Mg/(Fe+Mg)] of octahedral sites as 0.72(2) and 0.69(2). Although these values are different from our previous results, they are acceptable considering the obtaining knowledge of Wild2 materials.

P05-111

CRYSTAL STRUCTURE AND PHOTO-EXCITATION ENERGY MIGRATION IN CRYSTALS OF DOUBLE-COMPLEX SALTS $M[Ru(bpy)_3][Cr_xAl_{1-x}(ox)_3]$ ($M^+ = Na^+, Li^+$; $0 \leqq x \leqq 1$)

Satoshi Ishii, Tomoko Nakaguchi, Takuhiro Otsuka and Youkoh Kaizu

Department of Chemistry, Tokyo Institute of Technology; Tokyo, Japan

Double complex salts of $M_I[Ru(bpy)_3][M_{II}(ox)_3]$ ($M_I^+ = Li^+, Na^+, K^+$; $M_{II}^{3+} = Cr^{3+}, Al^{3+}$) are obtained by mixing $[Ru(bpy)_3]Cl_2$ and $M_I[M_{II}(ox)_3]$ solutions. $Na[Ru(bpy)_3][M_{II}(ox)_3]$ (= Na salt) and $Li[Ru(bpy)_3][M_{II}(ox)_3]$ (= Li salt) are the same crystal structure except for the lattice constant. In the crystals, $[M_I(ox)_3]^{3-}$ constructs three-dimensional network structure (3D-network) linked by the alkali cations. $[Ru(bpy)_3]^{2+}$ is located in the space of the 3D-network of $[M_I(ox)_3]^{3-}$. However, crystal structure of $K[Ru(bpy)_3][M_{II}(ox)_3]$ is different from the Na and Li salts; $[M_I(ox)_3]^{3-}$ does not construct the 3D-network in the crystal.

We have studied one-step excitation energy-transfer from $[Ru(N\text{-}N)_3]^{2+}$ (N-N = bpy, phen) to $[Cr(CN)_6]^{3-}$ in crystals of double complex salts $[Ru(N\text{-}N)_3]_2[Cr(CN)_6]Cl$.[1), 2)] The energy transfer is much effected by relative-orientation between $[Ru(N\text{-}N)_3]^{2+}$ and $[Cr(CN)_6]^{3-}$ rather than distance and spectral overlap between them.[2)]

In this work, we focus on the different types of crystal structures composed of $[Ru(bpy)_3]^{2+}$ and $[Cr(ox)_3]^{3-}$ in order to investigate multi-step energy transfer which is called energy-migration among $[Ru(bpy)_3]^{2+}$. When visible light is irradiated to $M_I[Ru(bpy)_3]$-$[Al(ox)_3]$, $[Ru(bpy)_3]^{2+}$ absorbs the radiation light. Then, the photo-excitation energy transfers to the neighboring $[Ru(bpy)_3]^{2+}$. This energy-transfer occurs repeatedly, which is called energy migration. If Cr(III) complexes co-exists as an quencher in the crystal, the excitation-energy is finally transferred to the Cr(III) complexes. At 77K, luminescence from Cr(III) complexes can be observed.

We evaluated the energy-migration rate-constants with luminescence lifetime by changing the concentration of Cr(III) complexes in the double complex salts from 4.2 K to 300 K. We discuss the effect of lattice size and crystal structure on the energy migration.

Reference:

[1)] Otsuka, Takuhiro; Takahashi, Naoto; Fujigasaki, Naoki; Sekine, Akiko; Ohashi, Yuji; Kaizu, Youkoh. Inorganic Chemistry (1999), 38(6), 1340-1347.

[2)] Otsuka, Takuhiro; Sekine, Akiko; Fujigasaki, Naoki; Ohashi, Yuji; Kaizu, Youkoh. Inorganic Chemistry (2001), 40(14), 3406-3412.

P05-112

STRUCTURE AND MAGNETIC PROPERTY OF CYANIDE BRIDGE MOLECULAR SQUARE AND MOLECULAR SQUARE CHAIN

Chin-Lin Yang, Yu Wang

[a]*Department of Chemistry, National Taiwan University; Taiwan, 300, R.O.C.*

Poly-nuclear metal complexes often exhibit interesting photo-physical and magnetic property. For example, Prussian blue related compounds do give interesting magnetic property as being magnet at room temperature or exhibit photo-magnetic property due to charge transfer induced spin transition(CTIST). Two metal ions bridged by cyanide ligand normally show interesting magnetic coupling between them since the CN bridge makes two metal centers apart for about 5Å, which is an efficient distance for magnetic coupling and the metal coordinated by carbon and nitrogen atom is often in its low spin (LS) and high spin (HS) state respectively.

Two kinds of tetra-nuclear molecular square complexes were synthesized by the hydrothermal method: one is $Fe_4(phen)_4(CN)_4Cl_4*3H_2O$ (**1**) and the other is $[Fe_2Co_4(phen)_6(CN)_9Cl_4][FeCl_4]$ $*CH_3OH$ (**2**). The former one has a square unit of formed by two unique Fe ions linked by cyanide with a center of inversion at the center of the square, Fe_4: the Fe(1) is six-coordinated with two CN and two bi-dentate phen ligands; Fe(2) is four-coordinated with two NC groups and two chlorides. The latter one is the molecular square formed by two types of square unit: one is formed by two Fe ions and two Co ions linked by cyanide, Fe_2Co_2, the Fe(1) is again tetra-coordinated with two NC and two chlorides, whereas Co(1) is six-coordinated with four CN and one bi-dentate phen ligand; the other type of square unit is formed by four Co ions linked by cyanide, Co_4.: two Co(1) ions are shared by the Fe_2Co_2 square two Co(2) is six-coordinated with two NC and two bi-dentate phen ligands. Thus a chain like squares are formed throughout the crystal. The counter anion here is $FeCl_4^-$

From magnetic measurement, both of compounds (**1**) and (**2**) show antiferromagnetic interaction between metal centers. XmT value of compound (**1**) at room temperature, is about 6.4 , which is slightly larger than the spin only value (~6) based on two Fe^{2+} in HS state at T_d and two Fe^{2+} in LS at O_h. XmT value decreases smoothly to 5.5 at 15K and then decrease sharply to 3.5 at 2K. In compound (**2**) XmT value is 16.5 at 300K which is a slightly larger than spin only value of 14.12 XmT value decreases graduately to 9.3 at 2K. Detail distribution of the unpaired electron will be discussed. The geometries and magnetic properties in these two compounds will be presented.

P05-113

LIGHT AND THERMAL INDUCED META-STABLE STATE STRUCTURE OF SPIN CROSSOVER COMPOUND $\{Fe(abpt)_2[N(CN)_2]_2\}$

C. F. Sheu[1], S. Pillet[2], S. M. Chen[1], Y. C. Lin[1], I. J. Hsu[1], G. H. Lee[1], Y. H. Liu[1], C. Lecomte[2], Y. Wang[1*]

[1]*Department of Chemistry, National Taiwan University, Taipei 106, Taiwan*

[2]*LCM3B, UMR CNRS 7036, Université Henri Poincaré, BP 239, 54506 Vandœuvre-lès-Nancy Cédex, France*

$\{Fe(abpt)_2[N(CN)_2]_2\}$ is an intriguing spin crossover system which crystallizes in two separate phases. The crystal structure of polymorph A has one unique iron center, which has been first investigated by Moliner *et al.*[1], while that of polymorph B consists of two crystallographic independent iron centers. Magnetic measurements indicate polymorph A is paramagnetic in the range of 2-300 K and polymorph B undergoes an incomplete two-step spin transition with $T_{1/2}$ = 86 K. There are around 37% of HS molecules trapped in the low-temperature region (below 50 K) when standard cooling or warming modes (2K / min) are used. By rapid thermal quenching from room temperature to 5 K, a residual HS fraction of nearly 50 % was achieved. After warming to 52 K, it induces HS -> LS relaxation; relatively fewer HS residue is found compared to the standard cooling or warming modes. To understanding the magneto-structural relationship, the crystal structures of $\{Fe(abpt)_2[N(CN)_2]_2\}$ polymorph B in particular conditions corresponding to the different spin states are characterized, including (1) room temperature at pure HS state, (2) close to the step in the thermal transition at T = 87 K, (3) 52 K by standard cooling mode, (4) 15 K thermally quenched (5) 15 K photo-induced and (6) also the thermally relaxed state at 52 K. A unique order-disorder phase transition was observed for the first time for spin transition compounds, induced either by laser light irradiation or through rapid thermal quenching.

Reference:

[1] Moliner N., Gaspar A. B., Munoz M. C., Niel V., Cano J. & Real J. A. *Inorg. Chem*. **40**, 3986, (2001).

P05-114

STRUCTURAL STUDIES OF BIOLOGICALLY IMPORTANT HETEROCYCLIC COMPOUNDS

Periyasamy Murugan[a], Munusamy Thirumavalavan[a], Tian-Huey Lu[b], Kuo Chu Hwang[a]

[a]Department of Chemistry, [b]Department of Physics, National Tsing Hua University, Hsinchu, Taiwan, 300, R.O.C.

Synthesis of three heterocyclic compounds viz. diethyl-3,4-dimethyl thieno [2,3-b]thiophen-2,5-dicarboxylate (compound **I**), diethyl-4-(phenyl ethynyl)-2,6-pyridinedicarboxylate (compound **II**) and 3-(4-fluorophenyl)-2-(4-pyridine N-oxide) -1-phenyl-2-propene-1-one (compound **III**) and their X-ray structural and mass and NMR spectral studies will be reported. We shall present the facile synthetic routes of biologically important heterocyclic compounds **I**, **II** and **III** and the structural identification using various spectroscopic measurements, including mass, IR, NMR, and X-ray crystallography.

The M^+ peaks in the mass spectra match with the expected values for compounds **I**, **II**, and **III**. The ^1H NMR spectra show that the thiophene and pyridine rings exhibit modest de-shielding effects on the moieties which are directly chemical bound to the aromatic rings. The X-ray crystallographic measurements un-ambiguously confirmed the structures of the compounds **I**, **II**, and **III.** Selected bond lengths will be compared with those of the existing structures. The π-π interactions between the intermolecular rings will be indicated in figures.

P05-115

HYDROGEN BONDING INTERACTIONS AND SHEET-LIKE STRUCTURES IN NICOTINAMIDE COMPLEXES

S. Athimoolam and S. Natarajan

Department of Physics, Madurai Kamaraj University, Madurai - 625 021. India.
e-mail id: xrdsopmku@yahoo.com

The phenomenon of hydrogen bonding has significance in the areas of molecular recognition, crystal-engineering and organic synthons for supramolecular research. Carboxylic acids and amides are two commonly used functional groups in crystal engineering, because they generally form robust architectures via O-H...O and N-H...O hydrogen-bonded dimers. The present investigation is concerned with the X-ray analyses of crystalline complexes involving one of B vitamins (nicotinamide) with inorganic/organic acids. Nicotinamide was reacted with the inorganic/organic acids, and the single crystals of the following complexes were grown, viz., Nicotinamidium perchlorate, $C_6H_7N_2O^+.ClO_4^-$ (NAP), Nicotinamidium hydrogen oxalate, $C_6H_7N_2O^+.C_2HO_4^-$ (NAOX), Bis(nicotinamidium) bis[(2R,3R)-tartrate] 1.25 hydrate, $2(C_6H_7N_2O)^+.2(C_4H_5O_6)^-.1.25(H_2O)$ (NATAR) and nicotinamidium trifluoroacetate, $C_6H_7N_2O^+.C_2O_2F_3^-$ (NATFA). In all the four complexes, the carboxamide plane is twisted from the plane of the protonated pyridine ring. The magnitude of the twisting is measured from the dihedral angle between the planes of pyridine ring and carboxamide which have the values of 7.4(2)° in NAP, 6.3(1)° in NAOX, 22.4(6) and 8.83(8)° for the two nicotinamidium residues in NATAR and 16.3(8)° for NATFA, respectively. Protonation on the N atom is confirmed by the C-N bond distances and C-N-C bond angles. One of the characteristic features, viz., outrage of N atom from the pyridine ring, is observed in all the four structures with the slightly larger C-N-C bond angle (>120°). Lamellar or sheet like structures are observed through N—H···O and O—H···O hydrogen bonded motifs of cations and anions in NAP, NAOX and NATFA complexes. These sheets are aggregated through the chain motifs of C(4), C(5) and C(4) in NAP, NAOX and NATFA, respectively. In NATFA, the sheets are found to have distorted or corrugated lamellar features. Ring motifs of $R_1^2(4)$ in NAP and $R_1^2(5)$ in NAOX are observed through pyridine-anion bifurcated N—H···O interactions. In NAOX, carboxamide group form N—H···O dimers around the inversion centres of the unit cell with the ring motif of $R_2^2(8)$. A 2_1 screw related helical or ribbon like structure along the b axis is seen in NAOX through the carboxamide and pyridinium N—H···O hydrogen bonds with the oxalate anions. In NATAR, the anions are forming ring motifs (or) assembly of hydrogen bonded arrays through O—H···O hydrogen bonds and the cations are sandwiched within these arrays of assembly.

P05-116

PYRIDOXINIUM NITRATE AND TRICHLOROACETATE

S. Athimoolam and S. Natarajan

Department of Physics, Madurai Kamaraj University, Madurai - 625 021. India.
e-mail id: xrdsopmku@yahoo.com

Vitamin B6, a water-soluble vitamin, is also known as pyridoxine. It is essential for both mental and physical health. Other forms of vitamin B6 include pyridoxal and pyridoxamine. Pyridoxine is involved in the production of antibodies, which protect humans against bacterial diseases. Also, the combination of pyridoxine with immunosuppressive drugs improves the efficiency of that therapy. Pyridoxine has been found to play an essential role in the nervous system and aids in the metabolism of fats, carbohydrates and proteins. In the present investigation, Pyridoxine was reacted with nitric and trichloroacetic acids and the single crystals of pyridoxinium nitrate, $C_8H_{12}NO_3^+$, NO_3^- (PYN) and pyridoxinium trichloroacetate, $C_8H_{12}NO_3^+$, $C_2O_2Cl_3^-$ (PYTCA) were obtained. In contrast to many of the vitamin B6 structures so far determined which exist as zwitterions in which the phenolic group is deprotonated and pyridine N atom is protonated (a form found in metal-pyridoxine complexes), the present complexes are found to have protonated cations. The asymmetric part of the unit cell of PYTCA, contains a pyridoxinium cation and a trichloroacetate anion in which one of the $-CH_2OH$ groups of the cation, is disordered over two positions. As a characteristic feature of pyridoxine complexes, twisting of the $-CH_2OH$ group is observed in both the structures. The twisting is measured by the dihedral angles between the planes of pyridinium ring and $-C-CH_2OH$ group which have the values: 16.2(4)° and 11.6(3)° in PYN and 10.0(7)° [21.1(8)° for the minor disordered component] and 0.7(5)° in PYTCA. In PYN, the cations and anions are oriented nearly parallel to each other, the angle between the pyridinium and nitrate planes being only 2.52(1)°. In PYTCA, the $-CH_2OH$ groups decrease the overall planarity of the cation (r.m.s. deviation is 0.044 Å), particularly in comparison with that of the pyridinium ring for which the r.m.s. deviation is only 0.0072 Å. Another characterestic feature, viz., intramolecular hydrogen bond between the phenol OH and the $-CH_2OH$ group is seen through the S(6) motif in both the complexes. The zig-zag chain $C_2^2(11)$ motifs are observed through the hydrogen bonding interactions of the cations and anions in both the complexes. In PYN, planar cations and planar anions are arranged in column-like structures leading to aggregation of the cations and anions, forming a sheet-like structure parallel to the $(\bar{8}08)$ and $(80\bar{8})$ planes. In PYTCA, the pyridoxinium cation is linked by the anion and forms a closed ring structure through N-H...O and O-H...O hydrogen bonds around the inversion centres of the unit cell leading to the graph-set motif of $R_2^4(16)$.

P05-117

SYNTHESIS, GROWTH AND CHARACTERIZATION OF NEW ORGANIC NONLINEAR OPTICAL CHALCONE DERIVATIVES SINGLE CRYSTALS

P. S. Patil [a], S. M. Dharmaprakash [a], G. Bhagavannarayana [b] and Hoong-Kun Fun [c]

[a]*Department of Studies in Physics, Mangalore University, Mangalagangotri, 574 199, India;*
[b]*Materials Characterization Division, National Physical Laboratory, New Delhi, 110 012, India;*
[c]*X-ray Crystallography Unit, School of Physics, Universiti Sains Malaysia, 11800 USM, Penang, Malaysia.*

From the viewpoint of applications to optical devices, organic materials have several distinguishing features; processability, cost effectiveness, high damage threshold, large nonlinearity, and the ease with which large crystals of high optical quality can be grown and fabricated into desired shapes. For NLO materials with large second-order nonlinearities, noncentrosymmetry at both the molecular and the macroscopic level is a prerequisite for nonvanishing molecular hyperpolarizabilities β and macroscopic susceptibilities $\chi^{(2)}$. Unfortunately, only a few molecules with large β values crystallize in noncentrosymmetric structure, and fewer of them are useful for NLO materials. Recently, it has been noted that, among many organic compounds reported for their second harmonic generation, chalcone derivatives are known for their excellent blue light transmittance and good crystallizability. In these materials, the C = O bond acts as the electron withdrawing group, and electron-rich substituents on the aromatic rings serve as the electron-donating group, forming a so-called D–π–A type molecule.

Eight derivatives of chalcone were synthesized by Claisen – Schmidt condensation and evaluated their conversion efficiency of optical second- harmonic generation (SHG), UV – VIS transmission range and thermal stability. All the materials exhibit SHG efficiency higher than that of urea and also excellent UV – VIS transparency. Among them, 1-(3-methoxyphenyl)-3-(4-methoxyphenyl) prop-2-en-1-one (3MMC) has SHG activity 10.7 times as large as urea. We have also determined structures of these compounds by single crystal X – ray diffraction. All these materials crystallize in noncentrosymmetric space group. Among these, single crystals of four SHG derivatives chalcone viz., DMMC, MCC, MNC, and Ci3NC were grown by a slow evaporation solution growth technique (SEST) at room temperature. The crystalline perfection was evaluated for the grown crystals by high resolution X-ray diffractometry (HRXRD). Though the crystals contain low angle boundaries, the relatively low angular spread of the diffraction curves and the low FWHM values show that the crystalline perfections are reasonably good.

P05-118

CRYSTAL STRUCTURES OF MONO- AND DI-SUBSTITUTED FERROCENE DERIVATIVES

Naotake Nakamura, Kazuya Hiro and Takeshi Takamatsu

Department of Applied Chemistry, Ritsumeikan University, Kusatsu, 525-8577, Japan

A few mono- and di-substituted ferrocene derivatives were designed and synthesized in our laboratory in order to obtain liquid crystals containing transition metal such as ion atom. Some of them showed indeed liquid crystallinity.

In 2005, one of the present authors (N.N.) reported the crystal structure of 1,1'-bis[2-[4-(4-methoxyphenoxycarbonyl)phenoxy]ethoxycarbonyl]ferrocene, one of the di-substituted ferrocene derivatives (abbreviated hereafter as bMAF-2). The "S" shaped and "U" shaped structures of bMAF-*n*, where *n* is number of the methylene chain in the derivatives, were known already except bMAF-2, then. However, bMAF-2 assumed to novel structure as shown in Figure 1. The substituents of bMAF-2 had *gauche* conformation around the methylene chain, and it was named "Z" shaped structure by the authors. This derivative, bMAF-2, didn't show liquid crystallinity. The reason why may be considered that an aspect ratio of bMAF-2 is not large enough to show liquid crystallinity.

Crystal structure analysis of mono-substituted ferrocene derivative, 2-[4-(4-methoxyphenoxycarbonyl)phenoxy]ethoycarbonylferrocene, (abbreviated hereafter as mMAF-2), of which substituent is the same as that of bMAF-2, was carried out using X-ray diffraction method in the present study. The molecular structure obtained is shown in Figure 2. This is also included *gauche* conformation around the methylene chain, and it is almost the same as a half of bMAF-2 structure as easily understand from Figure 2. The derivative, mMAF-2, didn't show liquid crystallinity. The reason why may be considered that the molecular shape vary considerably from rod like one which is advantageous to show liquid crystallinity.

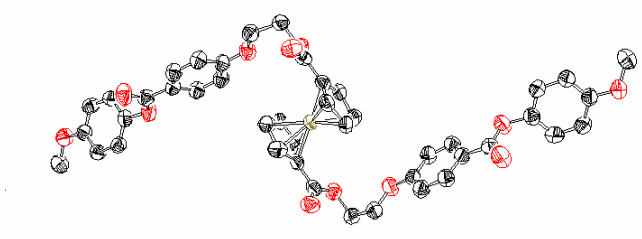

Figure 1. Molecular structure of bMAF-2. (N.Nakamura & M.Nishikawa)

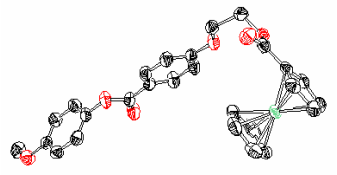

Figure 2. Molecular structure of mMAF-2. (This work)

The details will be presented and discussed at the conference.

P05-119

SUPRAMOLECULAR HYDROGEN-BONDING NETWORKS IN ADENINIUM SALTS

Balasubramanian Sridhar and Krishnan Ravikumar

Laboratory of X-ray Crystallography, Indian Institute of Chemical Technology, Hyderabad – 500007, India.
Email : sshiya@yahoo.com

Adenine is one of the two purine nucleobases used in forming nucleotides of the nucleic acids DNA and RNA. It occurs free in tea and in combined form in nucleic acids, ATP, vitamin B12, and several coenzymes. Adenine nucleobases provides interesting building blocks for forming extended structures, not only by the multiple possibilities in which bases may interact by hydrogen bonds, but also for the possible π-stacking between them (Houlton, 2001). Adenine and guanine form hydrogen bonds with other nucleobases that can lead to the formation of supramolecular structures, which can be of chemical and biological interest. Protonated nucleobases are present in many biochemical processes such as enzymatic reaction, stabilization of triplex structures, and they play a key role in a newly emerging feature of nucleic acid chemistry, namely acid-base catalysis. The asymmetric unit of (I) contains two adeninium cations (1 and 2), two half phthalate dianions having crystallographic C_2 symmetry, one neutral phthalic acid molecule, and one fully occupied and one partially occupied site (0.45) for water molecules, while, (II) contains one adeninium cation, one phenylacetate anion, one neutral phenylacetic acid and one water molecule, and (III) comprises one adeninium cation, one succinate anion and one water molecule with one of the carboxyl groups in the succinic acid deprotonated. In all the structures, the adeninium cations form N---H...O hydrogen bonds with their anion counterparts and adeninium-adeninium self-association base pairs with the $R_2^2(10)$-type motif. Conventional hydrogen-bonds lead to layer structures in (I) and (II) and two-dimensional infinite polymeric ribbons in (III). The details about the crystal structure, conformation and hydrogen bonding aspects will be presented and discussed.

P05-120

CRYSTAL OF 6-[BIS(2-CHLOROETHYL)AMINO]-12-OXO-DIBENZO [d,g] [1,3,2]DIOXAPHOSPHOCIN 6-OXIDE

Jadaprolu Radha Krishna[a], Musali Krishnaiah[a], Vedavati G. Puranik[b]

[a]*Department of Physics, Sri Venkateswara University, Tirupati-517502-India;* [b]*Centre for Material Characterization, National Chemical Laboratory, Pune-411 008, India*

The crystal structure and conformation of organophosphorus compounds have become the subject of intense study due to their involvement in many biological processes. The proven toxic effects of phosphoric acid esters on pests and their possible application as lubricant additives prompted the synthesis of a new class of organophosphorus heterocyclic esters. To our knowledge, there have been few reports of structural studies on eight-membered heterocyclic organophosphorus compounds, and hence undertaken the crystal structure of the title compound.

Crystal data: $C_{17}H_{16}Cl_2NO_4P$, Mr = 400.18, Rectangular yellow crystals, monoclinic, $P2_1/c$, a= 21.273(4), b = 8.538(11), c = 19.353(7) Å, β =90.864(6)°, V= 3514.7(12) $Å^3$, ρ_m= 1.50, ρ_c= 1.513 Mg/m^3, Z = 8, (MoKα) = 0.71073Å, & **F**(000)= 1648. Final **R**= 0.039 and **Rw**= 0.081 for 6585 with [$I \geq 2\ \sigma\ (I)$].

The eight-membered dioxaphosphocine ring adopts a distorted boat conformation with the phosphoryl O atom equatorial and ‘oxo’ group in a pseudo equatorial arrangement. The planar benzene groups fused to heterocyclic ring makes an angle of 53.7º in molecule-I and 50.3º in molecule-II with one another. The bond lengths around **P**-atom and ‘oxo’ group (C=O) are increased due to N-mustered group attached as exocyclic substitution. The structure is stabilized by intra- and intermolecular C-H---O hydrogen bonds, linking the molecules into chains.

P05-121

CRYSTAL STRUCTURE OF 4-(4-CHLORO-PHENYL)-5-PHENYL ISOXAZOLE

A.K.Balaji[a], J.Radha Krishna[a], M.Krishnaiah[a], Than Zaw Oo[b], Thetmar Win[b] and Pho Kaung[b]

[a] *Department of Physics, Sri Venkateswara University, Tirupati-517502, INDIA*

[b] *Department of Physics, Yangon University, Myanmar.*

The isoxazoles are a group of heterocycles, generated by the insection of nitrogen atom at 2nd –position of the furan. Isoxazoles are unique in their chemical behaviour like aromatic system particularly at the N-O bond.

The structural studies of isoxazoles and their derivatives have attracted considerable attention with their multifaceted applications as monoamine oxidase inhibitors used in psychotherapy, anti-inflammatory and anti-tumer agents. Some of them are industrial important as semiconductors and corrosion inhibitors in fuels and lubricants. In agriculture applications, herbicidal activity has been identified for some isoxazoles. The X-ray structure determination of some isoxazoles have been undertaken to investigate the effect of the substituents on the conformation of the heterocyclic ring with respective to their orientations.

Crystal data: C30 H20 Cl2 N2 O2, Mr = 511.38, Colourless transparent crystals, triclinic, P- $\bar{1}$, a = 6.554(7), b =25.966(17), c=7.472(10) Å, α = 90.07(9), β = 106.17(9) γ = 89.78(7)°, V= 1221(2) $Å^3$, ρ_c = 1.391 Mg/m^3, Z = 2, (MoKα) = 0.71073Å, & **F**(000) = 528, Final **R**= 0.0554and **Rw**= 0.1691for 2845 with $[I \geq 2\ \sigma\ (I)]$.

Isoxazole ring is planar. At the point of linkage of substituents to the isoxazole ring enlargement in bond lengths, bond angles and torsion of the substituted moieties with respect to isoxazole ring are observed. In the crystal, molecules are packed with van der Waals interactions.

P05-122

MOLECULAR RECOGNITION OF 2-PHENOXYBUTANOIC ACID BY CHIRAL AROMATIC AMINES

Ryoma Aoki,[a] Yukio Takahashi, [b] and Isao Fujii[a]

[a]*Department. of Biological Sci. and Tech., Tokai Univ., Japan.,* [b]*Daito Chem. Co., Ltd, Japan*

The production of non-naturally occurring-amino acids or amines has great importance in the pharmaceutical industry. An aqueous solution of racemic compound and optically pure 2-phenoxypropionic acid [PPA] has been applied in the diastereomer salt separation. We have applied PPA in the resolution of such compounds, 2-methylpiperadine, pipecolic acid, alanine, valine, 2-aminobutanoic acid.[1-3)] We recently reported that the chiral interface between hydrophobic and hydrophilic layers (chiral shallow pockets on the hydrophobic layers) formed by PPA recognizes the chirality of compounds.[4)] The CH…π interaction between the methyl and phenyl groups of PPA strongly affects the stability of pockets on the hydrophobic layers. In this study, we focused to clarify the inherent structure of substituted 2-phenoxybutanoic acid [PBA], and disclose the varieties of chiral interface formed by PBA molecules. The complexes of *S*-1-naphtylethylamine [*S*-NAP] and *S*-2-phenylethylamine [*S*-PEA] with *S*-PBA, and the pure *S*-PBA were examined by X-ray analysis.

Reference:

1) T Watadani, Y Takahashi & I Fujii, *Anal Sci*, **21**, x25 (2005).
2) I Fujii, T Watadani, S Nunomura & Y Takahashi, *Anal Sci*, **21**, x41 (2005).
3) I Fujii, H Baba & Y Takahashi, *Anal Sci*, **21**, x175 (2005).
4) I Fujii, T Watadani, S Nunomura & Y Takahashi, *Anal Sci*, **22**, x75 (2006).

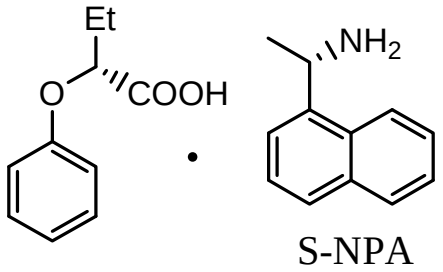

S-NPA

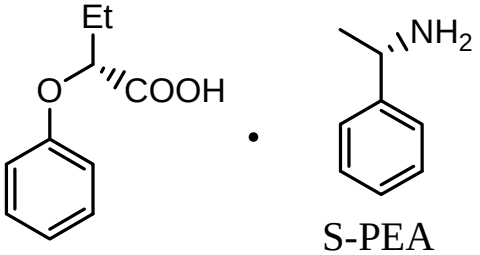

S-PEA

P05-123

STRUCTURE DETERMINATION OF PENTACENE DERIVATIVE BY SYNCHROTRON POWDER DIFFRACTION DATA

Hwo-Shuenn Sheu,[a] Wei-Ju Shih,[a] Wei-Tsung Chuang,[a] and Yu-Tai Tao[b]

[a] National Synchrotron Radiation Research Center, Taiwan. [b] Institute of Chemistry, Academia Sinica, Taiwan.

Organic thin-film transistors have attracted much attention for their potential application as alternatives to the traditional amorphous silicon-based TFTs. The pentacene derivative stands out as a promising material because of its ability to form ordered films and its reasonably high field-effect mobility and on/off ratio. Numerous efforts were attempted aiming at improving the electronic properties of pentacene-based devices. The crystal structure of the pentacene derivative thin film is the main theme to understand the physical properties and provide the base for theoretical calculation. We have solved the crystal structure of tetra chlorodiazapentacene (TCDAP) by synchrotron powder diffraction data. The compound is difficult to growth large enough crystal for single crystal diffraction study. From the powder diffraction data we found that TCDAP crystallize in monoclinic of space group P 2_1/n, a=17.0302(17), b=12.1166(11), c=4.0236(2)Å, beta=91.29(1), vol=930.06(9), Z=2. The unit cell is indexed by DICVOL. Structure determination from powder diffraction data was carried out using monte carlo simulation of DASH program. The final Rietveld refinement by GSAS program gave Rwp= 0.0675, Rp=0.0425, and X^2= 1.56. The powder structure of TCDAP fit well to its thin film diffraction pattern. Some other powder structures of pentacene derivatives will also reported in the meeting.

P05-124

PREPARATION, PROPETIES, AND STRUCTURAL STUDIES OF [MCl(diphosphine)]$_2$ (M = Rh, Ir; diphosphine = BINAP)

Tsuneaki Yamagata,[a] Aika Iseki,[a] Kazunori Hoshida,[a] Hiromitsu Nagata,[a] Kazuhide Tani,[a,b,] and Kazushi Mashima[a]

[a]*Department of Chemistry, Graduate School of Engineering Science, Osaka University, Machikaneyama 1-3, Toyonaka, Osaka, 560-8531, Japan,* [b]*Higashiosaka College, Nishitutumi Gakuen-chou 3-1-1, Higashiosaka, Osaka 577-8567, Japan*

Recently, we have reported the isolation and characterization of [IrCl(binap)]$_2$ **1** {BINAP = 2,2'-bis(di-phenylphosphino)-1,1'-binaphthyl}. Complex **1** reacted easily with MeOH, H_2O, PhSH, RCOOH (R = Me, Ph, *p*-tolyl), and HX (X = Cl, Br, I) to give the oxidative addition products ([{IrHCl(binap)}(μ-Cl)$_2$(μ-OMe)]Cl **2**, ([{IrHCl(binap)}(μ-Cl)$_2$-(μ-OH)]Cl **3**, [{IrHCl(binap)}(μ-Cl)$_2$(μ-SPh)]Cl **4**, *OC*-6-23-*A*-[IrCl(H)(O_2CR){(*S*)-binap}] (R = CH_3, Ph, *p*-tolyl, etc.) **5**, and [{Ir(H)-[(*S*)-binap]}$_2$(μ-X)$_3$]X (X = Cl, Br, I) **6**. These complexes were efficient for transfer hydrogenation of alkynes and alkenes with methanol as a hydrogen source (**2**), hydration of nitrile (**3**), and asymmetric hydrogenation of prochiral imines (**5** and **6**). However, [RhCl(binap)]$_2$ **7** does not react with protic molecules or Brönsted acid at ambient temperature.

We will discuss the structures of **1** and **7** and the different reactivity of them for protic molecules or Brönsted acid.

P05-125

HIGH RESOLUTION CRYSTAL STRUCTURE OF A BLUE COMMERININ PIGMENT

Naohiro Matsugaki,[a] Masaaki Shiono,[b] and Kosaku Takeda[c]

[a] *Photon Factory, High Energy Accelerator Research Organization, Oho 1-1, Tsukuba 305-0801, Japan;* [b] *Department of Physics, Graduate School of Science, Kyushu University, Hakozaki 6-10-1, Fukuoka 812-8581, Japan;* [c] *Department of Biology, Tokyo Gakugei University, Koganei, Tokyo 184-8501, Japan.*

The structure of commerinin, a pigment of a blue dayflower, was solved by Kondo et al. in 1992 [1]. The authors reported that the pigment was composed of six anthocyanin and six flavone molecules with two Mg ions, based on the crystal structure analysis at 1.0Å resolution. However, our recent research on the structure of protocyanin pigment [2] indicated that the commerinin complex pigment has other metal constituents.

We investigated the crystal structure of the commerinin pigment at the resolution of 0.7 Å using a large CCD area detector at BL-5A of the Photon Factory. The structure reveals two additional Mg ions bound to outer side of the complex pigment. The positions of Mg ions roughly corresponded to those of Ca ions in the protocyanin structure. The high resolution structure including the positions of hydrogen atoms will be presented.

P05-126

SOLID-STATE PHOTODIMERIZATION OF 6-METHYLCOUMARIN AND IT'S INCLUSION COMPLEXES, INVESTIGATED BY *Ab INITIO* POWDER CRYSTAL STRUCTURE ANALYSIS

Kotaro Fujii,[a] Hidehiro Uekusa,[a] Shunsuke Tanigawa,[b] Shinji Toyota,[b] Fumio Toda,[b]

[a]*Department of Chemistry and Materials Science, Tokyo Institute of Technology;* [b]*Department of Chemistry, Okayama University of Science*

The photoreaction of 6-methylcoumarin in solid-state produces four stereoisomeric dimers in different raitio (the major product is *syn*-Head-to-Head dimer). However, in the inclusion complex with trimesic acid, only *syn*-Head-to-Head dimer is obtained by photoreaction. In order to investigate this difference of photoreactivities, the crystal structures of each phase were analyzed.

Since 6-methylcoumarin crystal (**1**) has high tendency to crystallize in twin form, the crystal structure was successfully determined by *ab initio* powder crystal structure analysis. In the crystal structure, 6-methylcoumarin aligned by 4.73Å parallel translation and dimerization to the major product of *syn*-Head-to-Head dimer is well expected(Fig. 1).

The inclusion complex of 6-methylcoumarin and trimesic acid (**2**) was obtained as single crystalline form from the ethanol solution. The single crystal analysis revealed the complex consists of 1:2:2 of 6-methylcoumarin, trimesic acid, and ethanol molecules. While the alignment of 6-methylcoumarin in the inclusion complex is favorable for the *anti*-Head-to-Tail dimer by photoreaction(Fig. 2), however, it is not consistent with the actual photo-product of *syn*-Head-to-Head dimer. Desolvation of ethanol from this crystal and the following crystal structure change may explain this inconsistency of photo-reactivity.

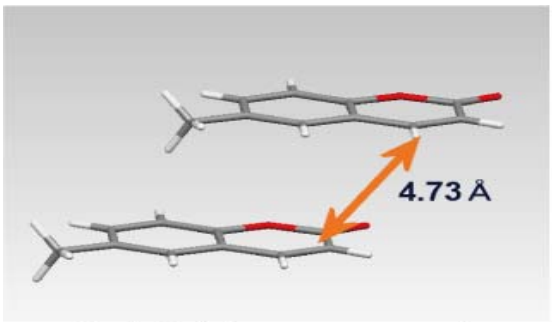

Fig.1 : Relative arrengement of 6-methylcoumarin in crystal 1

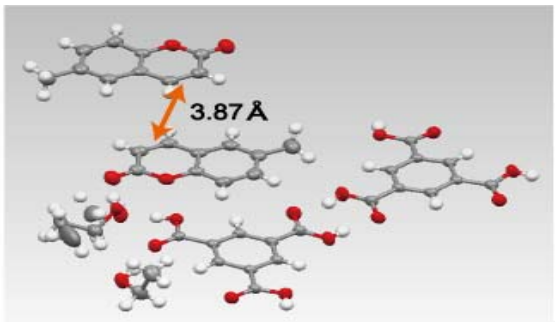

Fig.2 :crystal structure of **2**

P05-127

GUEST EXCHANGE MECHANISM OF ORGANIC INCLUSION CRYSTAL INVESTIGATED BY POWDER X-RAY DIFFRACTION ANALYSIS

Yasunari Ashida,[a] Hidehiro Uekusa,[a] Natsuki Amanokura,[b] and Masami Kaneko[b]

[a]*Department of Chemistry and Materials Science, Tokyo Institute of Technology, Japan*
[b]*Nippon Soda Co., Ltd.*

1,1,2,2-tetrakis(4-hydroxyphenyl)ethane, TEP, is an commercially used host molecule which crystallizes with small guest molecules such as organic solvents. By application of water vapor, inclusion crystal of TEP with methanol (**1**) showed guest exchange phenomenon and was transformed into TEP with water inclusion crystal (**2**). Interestingly, TEP is insoluble to water; therefore the inclusion crystal of **2** is obtained only through the guest exchange of methanol for water in powder crystalline state. Thus the crystal structure was successfully determined directly from powder diffraction data (SDPD technique) using direct space method. The crystal structure has a solvent channel structure and also it is very similar to that of **1**, which are the reason of the easy guest exchange. Heating of both inclusion crystals of **1** and **2** transformed them into apohost crystal (**3**), however, the reverse process, vapor absorption of the apohost, was observed only for methanol inclusion crystal. The crystal structure of apohost of **3** was also determined from powder diffraction data indicating that the SDPD technique is very powerful for investigation of this kind of phase transition process in which single crystal is usually disintegrated.

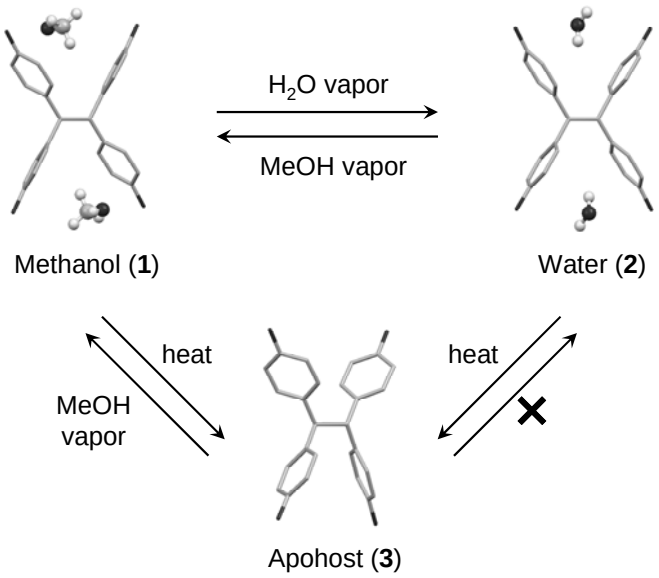

P05-128

HYDROGEN BONDING DYNAMICS OF THE STRUCTURE 4,5-DIMETHYL-N-(2-METHYL PHENYL)-2-{[(1E)-3,4,5-TRIMETHOXY PHENYLMETHYLENE] AMINO} THIOPHENE-3-CARBOXAMIDE.

Vasu,[a] K. A. Nirmala,[b] Deepak Chopra,[c] S. Mohand and J. Saravanan [d]

[a] *Vivekananda Degree College, Bangalore 560 055, Karnataka, India,*
[b] *Department of Physics, Bangalore University, Bangalore 560 056, Karnataka, India,*
[c] *Solid State and Structural Chemistry Unit, Indian Institute of Science, Bangalore 560 012, Karnataka, India,*
[d] *PES College of Pharmacy, Hanumanthanagar, Bangalore 560 050, Karnataka, India*

The title compound shows promising antibacterial activity against subtilis aureus, Escherichia coli compared with Ampicilin. The molecular structure is primarily stabilized by intra-molecular N-H...O interactions forming pseudo-six membered S(6) ring forming hydrogen bonded pattern. The crystal packing is governed by a diverse set of C-H...O head-tail interactions and π...π interactions. These dimers connected another C-H…O dimers.

The structure was determined by direct methods using SHELXS-97 and refined to a final *R*-value0.045. In the title compound, the geometry of the thiophene ring is planar and is good agreement with the data obtained for thiophene by electron diffraction. The *ortho*-toluidine is in the gauche position. The angle between thiophene and *ortho*-toluidine is 59.24(2)^{o}. The S-C bond distances are not equal due to π-delocalisation. The methyl group of the p-methoxy connected to oxygen is not in the plane and is deviated from the phenyl plane by 0.095(1)Å. The methyl groups attached at m-positions point away from each other. The inclination angles in the methoxy parts are not equal due to steric environment. The bond distances in the methoxy groups agree with values observed in other methoxy benzene derivatives. The non-planar part of the molecule i.e., *ortho*-toluidine is characterised by the torsion angle 72.84(2)^{o} indicating the conformation of the *ortho*-toluidine is bent in the compound.

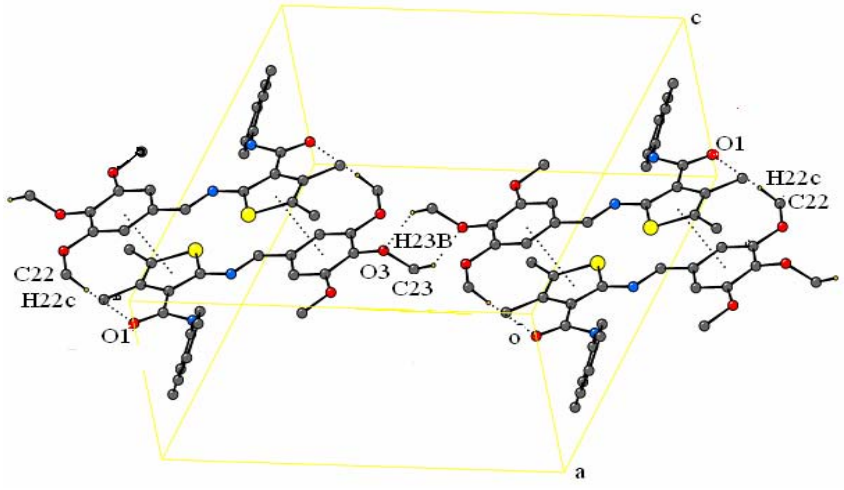

Fig. packing diagram. The dotted lines show C - H…O and π-π hydrogen bonds

P05-129

THE PHICIAL PROPERTIES OF S DOPANT IN InP UNDER HIGH-PRESSURE BY ADX AND RAMAN METHDOS

Yen-Ting Liu[1], Chih-Ming Lin [1] and Hwo-Shuenn Sheu [2]

[1]Department of Applied Science National Hsinchu University of Education, Hsinchu 30014, Taiwan; [2]Synchrotron Radiation Research Center, No. 1 R &D Road VI, Hsinchu Science-based Indust. Park, Hsinchu 30011, Taiwan

Angle-dispersive x-ray diffraction (ADXD) and Raman scattering methods have been performed for the Sulphur-dopand Indium Phosphide (InP:S) under high-pressure at ambient temperature. The ADXD results show that possible structure transitions from zinc-blende (B3) to rock-salt phase (B1) and rock-salt to Cmcm phase for InP:S occur at 8.1 and 22.3 GPa, respectively. The ambiguous regions in which the B3 and B1 phases and B1 and Cmcm phases mixed together, exists from 8.1 to 11.3 GPa and from 22.3 to 35.0 GPa for InP:S, respectively. The unloading run reveals that a reversible phase transition exists in the InP:S bulk. Raman scattering results show that the structure transitions from zinc-blende to rock-salt and rock-salt to Cmcm phase occur at 8.3 and 23.0 GPa. The ambiguous regions exists from 8.3 to 15.2 GPa and from 23.0 to 34.4 GPa for InP:S. Those two methods were matched very well.

P05-130

DIMERIZATION IS IMPORTANT FOR THE GTPASE ACTIVITY OF CHLOROPLAST TRANSLOCON COMPONENTS ATTOC33 AND PSTOC159

Yi-Hung Yeh,[a,b] Muppuru M. Kesavulu, [a] Hsou-min Li, [a] Shu-Zon Wu, [a] Yuh-Ju Sun, [b] Emadeldin H. E. Konozy [a] and Chwan-Deng Hsiao [a]

School of Molecular and Microbial Sciences and Institute for Molecular Bioscience, University of Queensland, Brisbane, Australia.

As part of our program on high-throughput crystallography of macrophage proteins, we have carried out a comprehensive structural and functional characterisation of mouse acyl-CoA thioesterase 7 (Acot7). Acots catalyse the hydrolysis of fatty acyl-CoA to free fatty acid and coenzyme A and thereby regulate lipid metabolism and cellular signalling. While prokaryotic homologues possess a single thioesterase domain, mammalian Acot7 contains a pair of domains in tandem. We determined the crystal structures of both the N- and C-terminal domains (1.8 and 2.5 Å resolution, respectively) of the mouse enzyme, and the structure of the full-length enzyme using a combination of chemical crosslinking, mass spectrometry, and molecular modelling. The novel quaternary arrangement features a trimer of hotdog fold dimers. We show that both domains of Acot7 are required for activity, that only one of two possible active sites in the dimer is functional, and identify Asn24 and Asp213 (from N- and C-domains, respectively) as the catalytic residues through site-directed mutagenesis. We also designed an enzyme with higher activity than wild-type Acot7 by mutating the residues in the non-functional active site. Because Acot7 shows the highest activity towards arachidonoyl-CoA (a precursor of eicosanoids), is highly expressed in macrophages and upregulated by pro-inflammatory factors, and its over-expression in macrophages alters the production of prostaglandins D2 and E2, we propose a role in inflammatory processes. Together, our results provide a foundation to relate the molecular and cellular functions of Acot7 in macrophages and other mammalian tissues.

Forwood JK, Thakur AS, Guncar G, Marfori M, Mouradov D, Meng W, Robinson J, Huber T, Kellie S, Martin JL, Hume DA and Kobe B (2007). Structural basis for recruitment of tandem hotdog domains in acyl-CoA thioesterase 7 and its role in inflammation. Proc Natl Acad Sci USA 104: 10382-10387

P05-131

EFFECTS OF TERMINAL SUBSTITUENTS AND SEED CRYSTALS ON THE MODE OF POLYMORPHIC TRANSITION INDUCING PREFERENTIAL ENRICHMENT

Masahiro Horiguchi, Shinichiro Okuhara, Eiji Shimano, Daisuke Fujimoto, Hiroki Takahashi, Hirohito Tsue, and Rui Tamura

Graduate School of Human and Environmental Studies, Kyoto University, Kyoto 606-8501, Japan

In 1996 we reported the first instance in which enantiomeric resolution by simple recrystallization of a racemic crystal from organic solvents was feasible; this unusual symmetry-breaking enantiomeric resolution phenomenon regarded as an event of complexity system was referred to as Preferential Enrichment [1].

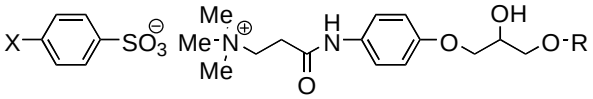

(±)-**1a**, X=NO_2, R=Ph
(±)-**1b**, X=NO_2, R=*p*-FC_6H_4
(±)-**3**, X=Cl, R=Ph
(±)-**5**, X=I, R=Ph
(±)-**2a**, X=Me, R=Ph
(±)-**2b**, X=Me, R=*p*-FC_6H_4
(±)-**4**, X=Br, R=Ph

Recently we have found a new type of polymorphic transition (γ to α_1-form) inducing Preferential Enrichment for (±)-**3**~(±)-**5** having a phenoxy group at the terminal position of the ammonium cation (Figure 1) [2]. Here we report (i) the mode of polymorphic transition with respect to the novel terminal phenoxy derivatives (±)-**1a** and (±)-**2a** and the *p*-fluorophenoxy ones (±)-**1b** and (±)-**2b**, and (ii) the effects of seed crystals of (±)-**2a** and (±)-**2b** on the Preferential Enrichment of (±)-**1** and (±)-**2** (Table 1). (±)-**1a**, (±)-**1b**, and (±)-**2b** showed Preferential Enrichment, whereas (±)-**2a** failed to do so. In this case, addition of the α_1-form seed crystals of (±)-**2b** to the supersaturated EtOH solution of (±)-**2a** induced the Preferential Enrichment of (±)-**2a**.

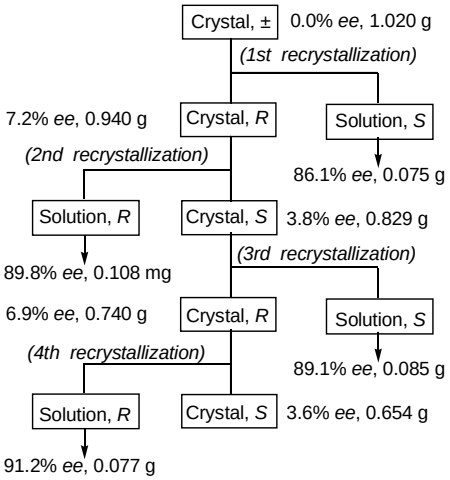

Figure 1. Preferential Enrichment of (±)-**4** in EtOH.

Table 1. Induction or inhibition of Preferential Enrichment by seeding for (±)-1 and (±)-2.

	Solubility in EtOH (mg/mL)	Without seeding [a]	Seed crystal [b]	
			(±)-**2a** (μ-form)	(±)-**2b** (α_1-form)
(±)-**1a**	6.1	yes [c] (γ to α_1 and μ) [d]	inhibition [e] (μ) [g]	restraint [f] (α_1) [g]
(±)-**1b**	1.9	yes [c] (γ to α_1) [d]	inhibition [e] (μ) [g]	restraint [f] (α_1) [g]
(±)-**2a**	2.0	no [h] (γ to μ) [d]	no effect [h] (μ) [g]	induction [i] (α_1) [g]
(±)-**2b**	4.9	yes [c] (γ to α_1) [d]	inhibition [e] (μ) [g]	inhibition [e] (α_1) [g]

[a] Recrystallization was carried out without seed crystals. [b] 5 wt% of seed crystals were added. [c] Preferential Enrichment occurred. [d] Mode of polymorphic transition. [e] Preferential Enrichment was completely inhibited by seeding. [f] Preferential Enrichment was restrained by seeding. [g] Polymorphic form of the deposited crystals. [h] Preferential Enrichment did not occur. [i] Preferential Enrichment was induced by seeding.

Reference:

[1] *Top. Curr. Chem.* **2007**, *269*, 53-82.
[2] *Cryst. Growth Des.* in press.

P05-132

STRUCTURE-ASSISTED DISCOVERY OF *HELICOBACTER PYLORI* SHIKIMATE KINASE (HpSK) INHIBITORS

Wen-Chi Cheng[a], Yen-Fu Chen[b], Jinn-Moon Yang[b] and Wen-Ching Wang[a]

[a]*Institute of Molecular and Cellular Biology and Department of Life Science, National Tsing Hua University;* [b]*Department of Biological Science and Technology, Institute of Bioinformatics, National Chiao Tung University, Hsinchu, Taiwan, 300, R.O.C.*

Helicobacter pylori, a Gram-negative bacterium, colonizes in approximately half of human population, induces chronic inflammation in gastric epithelial cells, and may further develop into various gastrointestinal diseases such as peptic ulcers and gastric cancer. Shikimate pathway plays an important role in aromatic amino acid biosynthesis in bacteria, fungi, and plants, but not mammals, in which enzymes of this pathway represent attractive targets for the development of new antimicrobial agents, herbicides and antiparasitic agents. We have determined the structure of the fifth enzyme, shikimate kinase (HpSK) that catalyzes the specific phosphorylation of the 3-hydroxyl group of shikimic acid in the presence of ATP in its apo form (1.8 Å) and the HpSK·shikimate·PO_4 (2.3 Å) binary complex structures. The binary structure reveals induced fit movement on substrate binding and the detailed enzyme-substrate interactions. Several highly conserved charged residues including Asp33 (in a conserved Asp31Thr/Ser32Asp33 motif), Arg57, and Arg132 (interacting with shikimate) are identified, guiding the development of novel inhibitors of shikimate kinase. We have currently conducted virtual drug screening utilizing the DOCK4.0 and GEMDOCK molecular docking tool among compounds of ZINC database which is a free database from University of California, San Francisco. Top hits obtained from DOCK4.0 were additionally filtered with GEMDOCK. Several molecules were identified that inhibited the HpSK activity with IC50 values in the micromolar range.

P05-133

AB INITIO STRUCTURAL DEFERMINATION OF PHARMACEUTICAL COCRYSTAL FROM POWDER X-RAY DIFFRACTION DATA

Chihiro Itoga[a], Kotaro Fujii[a], Hidehiro Uekusa[a], Noriyuki Takata[b], Koji Shiraki[b]

[a]*Department of Chemistry and Materials Science, Tokyo Institute of Technology,* [b]*Chugai Pharmaceutical Co.Ltd* .

The solubility and other properties of pharmaceutical compounds can be controlled by forming cocrystals with small molecules. Because the solubility of compounds relates to the molecular structure and interactions in the crystal, the crystal structure information is the most important to control the solubility and other properties. Also, pharmaceutical compounds usually obtained and handled in poly-crystalline form. Thus the crystal structure analysis should be performed to the powder crystals without recrystallization using *ab initio* structure determination from powder X-ray diffraction data.

The powder cocrystal of spironolactone (a), which is hypotensive and diuretic medicine, and the saccharin (b), which is artificial sweetener, was obtained from water solution. Powder X-ray diffraction data were collected in SPring-8, BL19B2, and the structure determination was performed by direct space method, using simulated annealing optimization. The crystallographic data for the cocrystal are *monoclinic*, space group *C*2 with *a*=25.2550, *b*=6.4045, *c*=23.4824Å, *β*=126.1552°, and *V*=3066.73Å^3, T=298K. Rietveld refinement was performed using the best solution of the simulated annealing calculation. The bond length and angles are restrained to it's own crystal structure reported in CSD.

There is an intermolecular H-bond, N-H…O in cocrystal between N atom in Saccharin and O atom in spironolactone carbonyl. Both N-H…O and C-H…O H-bond make each molecule stacked along *b* axis to form a column structure. Because of these intermolecular interactions, the solubility was decreased in cocrystal comparing with spironolactone crystal.

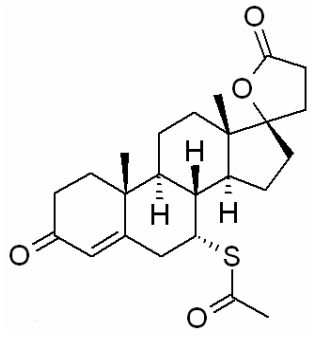

(a)

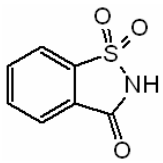

(b)

(a) spironolactone , (b) saccharin

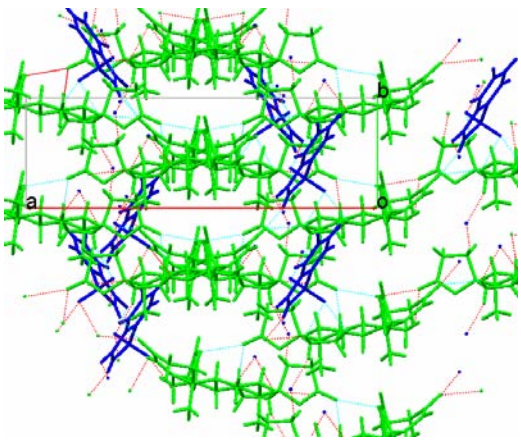

crystal structure

P05-134

PROBING INTER MOLECULAR INTERACTIONS IN FUNCTIONALISED THIOPHENES

K.A.Nirmala [a], Vasu [b]

[a] *Department of Physics, Bangalore University, Jnanabharathi, Bangalore-560056.*

[b] *Department of Physics, Vivekananda Degree College, Malleshwaram west, Bangalore-560055.*

Probing inter molecular interactions in functionalised thiophenes has been carried out to understand the influence of various substituents on the bond parameters and the conformation.

The research work reported describes the crystal structure and conformational studies of 2-amino thiophenes, and Schiff bases of thiophenes, which serves as a starting materials for number of intermediate derivatives. These compounds are antibacterial, antitubercular, antifungal, anti-inflammatory, and antitoxic. The crystallographic studies throw light on molecular structure which helps in understanding the activities of the biological molecules. The X-ray structure determination of 17 compounds has been carried out in the above family.

The experimental steps consist of growing single crystals by slow evaporation method by selecting the right solvents. After careful examination under polarising microscope (for transparent crystals) suitable crystal is selected which is free from defects such as twinning or cracks and it is mounted on the single crystal diffractometer equipped with SMART APEX CCD. The crystal structures were solved using SHELXS97 program, and refined using SHELXL97 program. Molecular and packing diagrams were generated by ORTEP32. The geometric calculations were done using PARST.

The structural comparisons of all the thiophene compounds are as follows: There are certain similar and dissimilar molecular and crystal packing features are described among 2-amino thiophene derivatives and Schiff bases of thiophene derivatives. The thiophene moiety is planar in all the compounds. It is noticed that from the comparative study that the conformation of the six-membered ring does not make any change from the half-chair conformation with different substituents. Strong intra-molecular interations which locks the molecular conformation is observed in all the compounds. In addition to this the presence of intermolecular interactions within the crystal lattice is influencing the packing of the molecules which modifies the properties.

P05-135

MOLECULAR RECOGNITION OF SYNEPHRINE BY CHIRAL ORGANIC ACIDS

Taira Kimino,[a] Yukio Takahashi, [b] and Isao Fujii[a]

[a]Department of Biological Sci. and Tech., Tokai Univ, Japan,[b] Daito Chemical Co., Ltd, Japan

Production of optically active aminoalcohols and amines, such as ephedrine and 1-phenylethylamine [PEA], has a great importance in the pharmaceutical industry. PEA is one of intermedicines and ephedrine has a variety of potent bioactivities, e.g. adrenergic activity. On the other hand, an aqueous solution of racemic compound and optically pure ephedrine has been widely applied in the diastereomer salt separation. One of such alkaloids, synephrine [SYN], systematic name: 4-(1-hydroxy-2-(methylamino)ethyl)phenol, is lower toxic and natural product without law control. The racemic compound was also found in citrus commonly. [1),2)] The enantiomers were considered to be potentially chiral resolution agents.

In this study, we focus on the molecular-recognition mechanism of SYN and optically-active organic acids. The complexes of rac-SYN and (1*R*, 2*R*)-tartrate [R-TART], and rac-SYN and *S*-ibuprofen [S-IBU] were examined by X-ray analysis. From the limited information, the SYN molecules recognize the chiral carboxy groups by its amino-ethernol group and *p*-hydroxy group in the columnar hydrophilic region with intermolecular hydrogen bonds. Two independent S-IBU molecules in the asymmetric unit are almost identical, but the difference between the enantiomers of rac-SYN mainly existed at the torsion angles of aminoethane moiety. This tendancy was also found in R-TART complex. It reveals that the molecular recognition system of chirality differs in the diastereomer.

Reference:

1) M. Datta *et. al*, *Acta Cryst.* (1994), **C50**, 1132-1135.
2) M. Sajid *et. al*, *Acta Cryst.* (2005), **E61**, o2534-o2536.

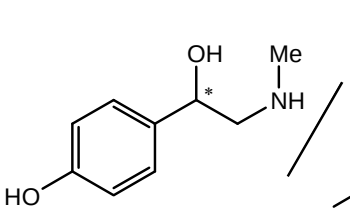

rac-SYN

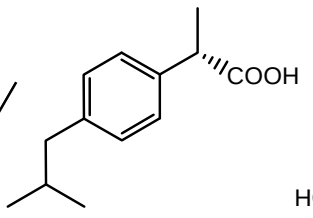

S-IBU

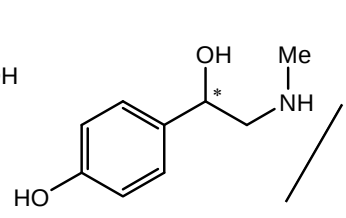

rac-SYN

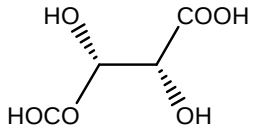

R-TART

P05-136

CRYSTAL STRUCTURE OF 2-PHENYL-2,3-DIHYDRO-4*H*-CHROMEN-4-ONE

Nongnaphat Khosavithitkul,[a] Kenneth J. Haller[b]

[a] *The Centre for Scientific and Technological Equipment;* [b] *School of Chemistry, Institute of Science, Suranaree University of Technology, Nakhon Ratchasima 30000 Thailand*

E-mail: nkhosavithitkul@yahoo.com

Flavonoids are a group of polyphenolic compounds of low molecular weight that present a common benzo-γ-pyrone structure. They occur naturally in fruits, vegetables, nuts, seeds, flowers, and bark. They are categorized into various subclasses including flavones, flavonols, flavanones, isoflavanones, anthocyanidins, and catechins. Their various properties make them attractive for applications in the pharmaceutical, cosmetic and nutrition fields. They are pharmacologically active, and some are currently used in a wide range of medical preparations, including antibacterial, antiviral, anti-inflammatory, and vasodilatory preparations.

The crystal structure of the title compound was determined by single crystal X-ray analysis. Data were collected on a Nonius KappaCCD diffractometer equipped with a fine focus molybdenum X-ray source, and a 0.3 mm *ifg* capilliary collimator. Structure solution and refinement utilized SIR97, MaXus, and the SHELXTL system.

***Crystal data*:** $C_{15}H_{12}O_2$; M_r = 224.26 Daltons; transparent colorless; monoclinic; $P2_1/n$ (No.14); a = 10.611(5), b = 5.531(5), c = 19.362(5) A, V = 1136.32 A^3; Z = 4; D_{calc} = 1.230 Mgm^{-3}; $\lambda_{MoK\alpha}$ = 0.71073 A; μ = 0.9 cm^{-1}; T = 298(2) K. 16,476 data collected, R_{int} = 0.0752 1068 unique data.

P05-137

CRYSTAL STRUCTURE OF 'N-(4-METHOXYPHENYL)-2-{[(1E)-(4-METHYLPHENYL) METHYLENE]AMINO}-4,5,6,7-TETRAHYDRO-THIENO[2,3-C]PYRIDINE-3-CARBOXAMIDE'

G. N. Anilkumar [a], M. K. Kokila [b], Puttaraja [b], S. Mohan [C] and J. Saravanan[c].

[a] *Department of Physics, M. S. Ramaiah Institute of Technology, MSRIT Po, Bangalore, Karnataka. 560054.* [b] *Department of Physics, Bangalore University, Bangalore, Karnataka. 560056.* [c] *PES College of Pharmacy, Hanumanthanagar, Bangalore, Karnataka. 560050.*

e-mail: anilkumargn@gmail.com

The title compound, is one of the series of is one of a series of 3-arylcarboxamides and was found to exhibit antibacterial and antifungal activities. Various derivatives of thiophenes and Schiff bases are known to possess different biological activities, such as antitubercular, bacteriostatic and antifungal activities. Sulfur containing Schiff bases are the most effective.

The compound $C_{24}H_{25}N_3O_2S$, crystallizes under Triclinic system, Pī space group, a = 8.3905 (11) Å, b = 9.9883 (13) Å and c = 12.9549 (17) Å, α = 91.375 (2)º, β = 94.789 (3)º, γ = 96.121 (2)º, V = 1075.2 (2) $Å^3$, Z= 2, μ = 0.18 mm−1, & D= 1.296 Mgm^{-3}.

The three dimensional intensity data were collected using Bruker Smart CCD diffractometer using graphite monochromated MoK_α radiation. The data of the compound was corrected for LP factors and used for structure solution. The structure was solved using SHELXS-97 program and and refined using full-matrix least squares on F2 to an R value of 0.085 using SHELXL-97 Program for 2645 reflections with I>2σ(I). The geometry, mode of packing and the hydrogen bonds of the compound will be presented and discussed.

P05-138

CRYSTAL STRUCTURE OF 'N-(4-METHOXYPHENYL)-2-{[(1E)-(4-METHYLPHENYL) METHYLENE]AMINO}-4,5,6,7-TETRAHYDRO-THIENO[2,3-C]PYRIDINE-3-CARBOXAMIDE'

G. N. Anilkumar [a], M. K. Kokila [b], Puttaraja [b], S. Mohan [C] and J. Saravanan[c].

[a] *Department of Physics, M. S. Ramaiah Institute of Technology, MSRIT Po, Bangalore 560056, Karnataka, India.* [b] *Department of Physics, Bangalore University, Bangalore 560056 Karnataka, India.* [c] *PES College of Pharmacy, Hanumanthanagar, Bangalore 560050, Karnataka, India.*

e-mail: anilkumargn@gmail.com

The title compound is one among the series of 3-arylcarboxamides and was found to exhibit antibacterial and antifungal activities. Various derivatives of thiophenes and Schiff bases are known to possess different biological activities, such as antitubercular, bacteriostatic and antifungal activities. Sulfur containing Schiff bases are the most effective.

The compound $C_{24}H_{25}N_3O_2S$, crystallizes under Triclinic system, P$\bar{1}$ space group, a = 8.3905 (11) Å, b = 9.9883 (13) Å and c = 12.9549 (17) Å, α = 91.375 (2)º, β = 94.789 (3)º, γ = 96.121 (2)º, V = 1075.2 (2) Å^3, Z= 2, μ = 0.18 mm−1, & D= 1.296 Mgm^{-3}.

The three dimensional intensity data were collected using Bruker Smart CCD diffractometer using graphite monochromated MoK$_\alpha$ radiation. The data of the compound was corrected for LP factors and used for structure solution. The structure was solved by Patterson technique using SHELXS-97 program and refined using full-matrix least squares on F^2 to an R-value of 0.085 using SHELXL-97 Program for 2645 reflections with I>2σ(I). The conformation, mode of packing and the hydrogen bonding geometry of the compound will be presented and discussed.

P05-139

CRYSTAL CHEMISTRY OF CYCLODEXTRINS AND THEIR INCLUSION COMPOUNDS WITH BIOLOGICALLY-ACTIVE GUESTS

Mino R Caira

Department of Chemistry, University of Cape Town, Rondebosch 7701, South Africa

Results of our recent studies of the crystal chemistry of cyclodextrins (CDs) and their inclusion compounds are described under three headings, namely structures and conformations of sterically crowded host compounds, the isolation and structural characterization of multiple crystalline forms of individual CD inclusion complexes, and novel modes of inclusion of biologically-active molecules in both native and derivatised CDs.

Chemical modification of native CDs (e.g. alkylation/acetylation of their hydroxyl groups) has a dramatic effect on their structures and conformations. 'Self-inclusion' of sterically bulky substituents may render these modified hosts unsuitable for inclusion of sizeable guest molecules. The structures of representative examples of such host molecules are compared with those of previously reported analogues and their limited extent of guest inclusion is illustrated.

Variation of crystallization conditions can give rise to different crystal forms of a CD inclusion complex. This was reported earlier for the β-CD inclusion complex of methyl paraben, where a triclinic and a monoclinic crystal form with the same 1:1 host-guest stoichiometry were isolated and structurally characterized. An important feature of these complexes is the significant difference in their thermal stabilities. This has obvious implications for crystallization control in the production of CD inclusion complexes, especially those of pharmaceutical relevance. Our recent studies indicate that, as in the conventional generation of polymorphs, the chances of isolating multiple forms of a given inclusion complex may be significantly enhanced by systematic variation of the crystallization conditions,

Accurate prediction of the mode of inclusion of a given guest in a CD host molecule is not yet possible and the empirical approach often yields novel findings in this regard. Representative structures of CD inclusion complexes containing antibacterials, anti-hypertensives and potential anti-cancer agents are described to illustrate some of the diversity of inclusion modes observed in the solid state. Guest disorder may prevent satisfactory structural elucidation even from X-ray data recorded at relatively low temperatures. However, examples are presented in which more than two disordered guest components have been successfully modelled within their CD host cavities.

While the focus in this presentation is on single crystal X-ray studies, the utility of complementary techniques such as powder X-ray diffraction and thermal analysis in the investigation of these compounds is also illustrated.

P05-140

CRYSTAL STRUCTURE OF '2-AMINO-N-(2-METHOXYPHENYL)-5,6,7,8-TETRAHYDRO-4H-CYCLOHEPTA[B]THIOPHENE-3-CARBOXAMIDE'

K. Chandra Kumar [a], M. K. Kokila[b], Puttaraja [b], S. Mohan [C] and J. Saravanan[c].

[a]*Department of Engineering Physics, HKBK College of Engineering, Nagawara, Bangalore 560 045, Karnataka, India.* [b] *Department of Physics, Bangalore University, Bangalore 560056, Karnataka, India.* [c] *PES College of Pharmacy, Hanumanthanagar, Bangalore 560050, Karnataka, India.*

Schiff bases and various derivatives of thiophenes are known to possess different biological activities, such as antitubercular, bacteriostatic and antifungal activities. Sulfur containing Schiff bases are the most effective. The title compound shows above mentioned properties.

The compound $C_{17}H_{20}N_2O_2S$, crystallizes under Monoclinic system, $P2_1/n$ space group, a = 9.228(2) Å, b = 8.413(2) Å and c = 20.839(5) Å, β = 95.798(4)º, V = 1609.5(6) $Å^3$, Z= 4, μ = 0.210 mm^{-1}, & D= 1.306 Mgm^{-3}.The three dimensional intensity data were collected using Bruker Smart CCD diffractometer using graphite monochromated MoK_α radiation. The data of the compound was corrected for LP factors and used for structure solution. The structure was solved using SIR92 program and refined using full-matrix least squares on F^2 to an R value of 0.0510 using SHELXL-97 Program for 2238 reflections with $I>2\sigma(I)$. The structural details of the compound will be presented and discussed.

P05-141

HIGH RESOLUTION, HIGH THROUGHPUT X-RAY POWDER DIFFRACTION EXPERIMENTS AND DATA ANALYSIS

A. Stefanovic, D. Beckers, T. Degen, S. Prugovečki

PANalytical B.V., Almelo, The Netherlands

Advances in X-ray optics, detector technology and software enabled new application areas that previously were not feasible on a laboratory powder diffractometer. Until recently, e.g. XRPD experiments on small sample amounts were either time consuming or needed to be performed with compromises in resolution, limiting the information content that could be extracted from the data.

New optical modules - like the focusing X-ray mirror - and new stages that can be added to modular systems now allow to optimize the optical configuration for a particular sample – and not vice versa. With these new options in particular high resolution, high throughput X-ray powder diffraction comes within reach of laboratory instrumentation.

Samples coming from high throughput crystallization experiments, typically only available in small amounts, can now be measured with drastically enhanced speed without compromising the resolution. High quality data can be obtained either in transmission or reflection geometry. Optimal instrument configurations, measurement strategies and data treatment tools will be discussed on pharmaceutical examples.

P05-169

RNA DEGRADATION BY ESCHERICHIA COLI POLYNUCLEOTIDE PHOSPHORYLASE

Zhonghao Shi,[a,b] Wei-Jen Yang,[b] Kin-Fu Chak[a] and Hanna S. Yuan[b]

[a]*Institute of Biochemistry and molecular Biology, National Ying-Ming University*
[b]*Institute of Molecular Biology, Academia Sinica, Taipei, Taiwan*

RNA degradation is an important biological process in regulating mRNA levels in cells. In eukaryotes, a protein complex, exosome, plays a major role for mRNA degradation in cytoplasm. The bacterial trimeric polynucleotide phosphorylase (PNPase) shares similar sequence and domain organization and bears similar function in mRNA degradation to that of eukaryotic exosome. We determined the crystal structure of *E. coli* PNPase at a resolution 2.7 Å. PNPase, containing two RNase PH domains and a S1/KH domain, forms a trimer. The six RNase PH domains of the trimeric PNPase fold into a ring-like structure containing a central channel for RNA binding and degradation. This ring-like architecture of bacterial PNPase is similar to those of archeal and human exosomes, supporting the hypothesis that a common mechanism for RNA degradation is used in all kingdoms of life. We also found that the wild-type PNPase produces a final end product of 4-nucleotide RNA. However, a R106A mutant and a S1/KH domain truncated PNPase produce different RNA end products, indicating that R106 located inside the channel and S1/KH domain are likely involved in RNA recognition.

P05-170

UNDERSTANDING OF D-STAGGER IN COLLAGEN FIBERS BASED ON THE 7/2-HELICAL STRUCTURE AND AMINO ACID SEQUENCE

Koichi Masakiyo, Tatsuya Kawaguchi and Kenji Okuyama

Department of Macromolecular Science, Graduate School of Science, Osaka University, Toyonaka, Osaka, 560-0043, Japan

Collagen is the most abundant protein in animals, responsible for structural integrity in their bodies. It is composed of three polypeptide chains containing more than 1000 amino acid residues, and has a triple helical structure. Since each polypeptide chain requires Gly at every third position, the amino acid sequence of collagen can be designated by $(Gly\text{-}X\text{-}Y)_n$, in which the X and Y positions are frequently occupied by Pro and Hyp, respectively. During these five decades, the molecular structure of collagen was believed to be the 10/3-helical structure (the Rich & Crick model). Recently, we reported that both the 7/2- and 10/3-helical models could explain quantitatively the fiber diffraction data from native collagen (Okuyama, et al., *Biopolymers* 2006). On the other hand, all the conformations found in single crystals of collagen-model peptides showed 7/2-helical symmetry rather than 10/3-helical one (Okuyama, et al., *Biopolymers* 2006). Based on these evidences it is now clear that the average conformation of collagen is the 7/2-helical structure.

In the fiber-forming collagen, like type I, II and III collagen, molecules spontaneously associate in a specific way to form fibers in the extracellular matrix. These fibers exhibit cross striations every 670 Å (= D) in electron microscopic observations and also a series of meridional Bragg reflections in X-ray small angle diffraction based on this period. Although this period was explained by the D-stagger of collagen molecules along the molecular axis (Figure 1), there is no clear explanation why they assemble with this stagger based on the amino acid sequence. In other words, we do not know the specific interaction between adjacent molecules which cause this D-stagger. In this study we examined electrostatic interactions between source and target molecules to understand the origin of the D-stagger.

The amino acid sequence of α1(II) chain of the human type II collagen was used in this analysis. Charged residues were supposed to have +1 or -1 charge on their C_β atom as a first approximation. Collagen molecules were constructed from three such peptide chains by applying 7/2-helical symmetry. Staggering the source molecule 5 residues at a time, electrostatic energy between source and target molecules was calculated. The local minimum of energy was found at the 1D-stagger (= 235 amino acid residues), which showed that the electrostatic interaction is one of important driving forces for the D-stagger in collagen fiber.

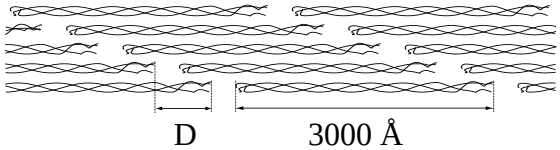

P05-171

X-RAY CRYSTAL STRUCTURE ANALYSIS OF HEMOGLOBIN FROM DOMESTIC PIGEON (*COLUMBA LIVIA*) AT 1.44Å RESOLUTION

P.Charles[1], K.Neelagandan[1], S.Sundaresan[1], Jürgen J. Müller[2], Udo Heinemann[2] and M.N.Ponnuswamy[1*]

[1]*Department of Crystallography and Biophysics, University of Madras*
Guindy Campus, Chennai-600 025, India,
*e-mail: mnpsy2004@hotmail.com[1]**
[2] *Max-Delbrück-Center for Molecular Medicine,Department of Crystallography*
Robert-Rössle-Straße 10, D-13122 Berlin, Germany

Hemoglobin is an oxygen carrier protein in the red cells of the blood in mammals and other animals. The oxygen binding properties of hemoglobin are regulated by binding of allosteric effectors. The data were collected at 1.44 Å resolution using synchrotron radiation at BESSY, Germany. Crystals of pigeon hemoglobin belong to the orthorhombic space group $P2_12_12_1$ with cell dimensions: a = 81.086 Å, b = 81.543 Å, c = 79.214 Å. The structure solution was carried out by molecular replacement method using graylag goose hemoglobin as the starting model (PDB id: *1FAW*) using the program A*MORE* implemented in *CCP4* suite. The structure refinement was done using *REFMAC 5.0*. About 5% of the reflections were used for the test set. The resultant model obtained from the structure solution was subjected to 20 cycles of rigid body refinement, which led to an R-factor of 37.7% (R_{free}=38.1%). At this stage restrained refinement was carried out and the final R-factor converged to 19.6% (R_{free}= 23.4%). The detailed results will be presented.

P05-172

SMALL-ANGLE X-RAY SCATTERING EXPERIMENTS TO DETERMINE THE STRUCTURAL TRANSITIONS IN THE INSULIN RECEPTOR ECTODOMAIN UPON INSULIN BINDING

Andrew E. Whitten,[1] Jill Trewhella[2], Colin W. Ward[3] and Michael C. Lawrence[3]

[1]Bragg Institute, ANSTO, Australia, [2]Department of Biochemistry, University of Sydney, New South Wales, Australia; [3]Walter and Eliza Hall Institute of Medical Research, Parkville, Australia.

The human insulin receptor (hIR) is a disulphide-linked homodimeric tyrosine kinase (TK) receptor. The crystal structure of the apo form of the hIR ectodomain has recently been determined to 3.8 Å resolution (McKern *et al.*, *Nature*, 2007) and revealed the ectodomain to have an inverted "V" structure with two-fold symmetry. Each leg of the inverted "V" is composed of the L1, CR and L2 domains of one monomer juxtaposed against the FnIII-1, FnIII-2 and FnIII-3 domains of the other monomer (domain nomenclature is described in Adams *et al.*, *Cell Mol. Life Sci.*, 2000). The C-termini of the FnIII-3 domains lie at base of the legs of the inverted "V", poised to extend through the cell membrane towards the intracellular TK domains. The structure revealed, importantly, that the L1 and FnIII-1 domains, both known to be involved in hormone binding, are juxtaposed in such a way that insulin can bind with its dimer-forming face interacting with L1 and elements of its hexamer-forming face interacting with the C-terminal loops of FnIII-1.

However, nothing is known about the conformational changes that occur in hIR upon insulin binding and how these effect signalling, and we are thus seeking to investigate these by small-angle X-ray scattering (SAXS) from the hIR ectodomain in solution. As part of this study, we are investigating the extent to which simulated, one-dimensional SAXS data derived from the crystal structure of the ectodomain is capable of yielding an adequately unique reconstruction of the three-dimensional shape of the particle. We have shown that the ectodomain particle is mono-dispersed in solution and have thus begun SAXS studies of the hIR ectodomain to investigate whether the solution structure agrees with the crystal structure. The final task is to determine from SAXS data the structural transitions in the hIR ectodomain upon complexation with insulin. Progress towards these goals will be presented.

P05-173

CRYSTAL STRUCTURE OF THE HUMAN FOXO3A-DBD/DNA COMPLEX SUGGESTS THE EFFECTS OF POST-TRANSLATIONAL MODIFICATION

Kuang-Lei Tsai,[a,b] Yuh-Ju Sun,[b] Cheng-Yang Huang,[a] Jer-Yen Yang,[c] Mien-Chie Hung[c] and Chwan-Deng Hsiao[a]

[a]*Institute of Molecular Biology, Academia Sinica, Taipei, 115, Taiwan*

[b]*Institute of Bioinformatics and Structural Biology, National Tsing Hua University, Hsinchu, 300, Taiwan*

[c]*Deaprtment of Molecular and Cellular Oncology, The University of Texas M. D. Anderson Cancer Center, Houston, Texas 77030, USA*

FOXO3a is a transcription factor of the FOXO family. The FOXO proteins participate in multiple signaling pathways, and their transcriptional activity is regulated by several post-translational mechanisms, including phosphorylation, acetylation, and ubiquitination. Because these post-translational modification sites are located within the C-terminal basic region of the FOXO DNA-binding domain, it is possible that these post-translational modifications could alter the DNA-binding characteristics. To understand how FOXO-mediated transcriptional activity, we report here the 2.7 Å crystal structure of the DNA-binding domain of FOXO3a (FOXO3a-DBD) bound to a 13-bp DNA duplex containing a FOXO consensus binding sequence (GTAAACA). Based on a unique structural feature in the C-terminal region and results from biochemical and mutational studies, our studies may explain how FOXO-DBD C-terminal phosphorylation by protein kinase B (PKB) or acetylation by cAMP-response element binding protein (CBP) can attenuate the DNA-binding activity and thereby reduce transcriptional activity of FOXO proteins. In addition, we demonstrate that the methyl groups of specific thymine bases within the consensus sequence are important for FOXO3a-DBD recognition of the consensus binding site.

P05-174

CRYSTAL STRUCTURE OF HUMAN TUDOR-SN AND IMPLICATION OF ITS ROLES IN RNA INTERFERENCE

Chia-Lung Li and Hanna S. Yuan

Institute of Molecular Biology, Academia Sinica, Taipei, Taiwan, R.O.C.

The human Tudor-SN (also called p100) is a multiple function protein. So far Tudor-SN has been reported to function as a transcriptional co-activator, participate in RNA interference silencing complex assembling and hyper-edited microRNA cleavage. Although extensive functional studies have been carried out, the structure and domain arrangement of Tudor-SN is unknown. The structural based analysis of Tudor-SN is thus imperious for better understanding of the role of this protein in RNA interference and transcription activation.

We crystallized a stable 70-kD truncated form of human Tudor-SN and solved the structure by MAD method at a resolution of 1.9 Å. X-ray diffraction data were recorded at the Taiwan beamline BL-12B in SPring-8. The overall Tudor-SN structure contains three intact SN domains (SN3, SN4 and SN5) and one Tudor domain which is a insertion domain between second and third β-strands of SN5. Superposition of Tudor-SN with staphylococcal nuclease shows that some of the important active site residues of SN3 and SN4 domains are missing, indicating that some of the SN domains, including SN4, may not be active in RNA cleavage. Structural superposition of the OB fold in the SN domain of Tudor-SN with the OB-fold structure of Sac7d/DNA complex reveals a substrate binding cleft located between SN3 and SN4 interface. We suggest that SN3 domain is likely responsible for RNA cleavage and SN4 domain is likely involved in substrate binding but not in cleavage. These results are consistent with the activity assays for different truncated forms of Tudor-SN in RNA cleavage. In conclusion, the structural analysis of Tudor-SN suggests a coordination between two SN domains in RNA binding and cleavage and provides some clues for further functional investigations.

P05-175

CRYSTAL STRUCTURE OF DNAC REPLICATIVE DNA HELICASE REVEALS THE MECHANISM OF HEXAMERIZATION AND POSSIBLE PROTEIN-PROTEIN INTERACTIONS NETWORK

Cheng-Yang Huang, Kuang-Lei Tsai, Wei-Ti Chen, Chwan-Deng Hsiao

Institute of Molecular Biology, Academia Sinica, Taipei, Taiwan, Republic of China

Helicases are motor proteins which play an essential role in DNA replication, recombination, and transcription. The *GK3476* gene encoding a replicative DNA helicase (*Gk*DnaC helicase) of *Geobacillus kaustophilus* HTA426 is a hexameric ring helicase belonging to the AAA+ family. DnaC helicase can interact with several proteins required for DNA replication, such as DnaA initiator protein, DnaI helicase loader protein, and DnaG primase. Here, we cloned, overexpressed, purified, crystallized, and determined the crystal structure of DnaC helicase at 3.6 Å resolution. Unlike other crystal structures of hexameric helicase, the six monomers of the DnaC helicase adopt predominantly a 3-fold symmetric morphology (trimer of dimers) to the hexameric ring, made by forming a four-helix bundle in the cooperation between the two N-terminal regions (residues 110-150) of the dimer, and thus creates three significant holes on the surfaces of DnaC helicase. The orientation and position of the RecA-like helicase domains are almost identical. However, the N-terminal domain interacting modes with the helicase domain are different. Based on this crystal structure of full length version of DnaC helicase, we renew the hexamerization mechanism of replicative helicase and propose the interaction regions of DnaC helicase for DnaA, DnaI, and DnaG binding. This study provides a molecular insight into why DnaC helicase can not unwind double-stranded DNA in the absence of the N-terminal domain and may contribute to an understanding of the protein-protein interactions map in DNA replication.

P05-176

PYROCOCCUS HORIKOSHII ARGINYL-TRNA SYNTHETASE LACKING ADDITIONAL N-TERMINAL DOMAIN WITH AMINOACYLATION ACTIVITY

Emiko Uchikawa,[a] Shun-ichi Sekine,[b] Shigeyuki Yokoyama,[b] and Michiko Konno[a]

[a]*Department of Advanced Sciences, Chemistry and Biochemistry course, Graduate School of Humanities and Sciences, Ochanomizu University, 2-1-1 Otsuka, Bunkyo-Ku, Tokyo 112-8610, Japan;* [b]*The Department of Biophysics and Biochemistry, Graduate School of Science, University of Tokyo, Hongo, Bunkyo-Ku, Tokyo 113-0033, Japan.*

Since there are six kinds of codons (CGX (X stands for U/C/A/G), AGA, AGG) for arginine, and arginyl-tRNA synthetase (ArgRS) has the additional N-terminal domain, a hypothesis that the recognition of $tRNA^{Arg}$ is determined mainly by the interaction between 20^{th} base of D-loop of tRNA and N-terminal domain on ArgRS has been believed. On the other hand, in the aminoacylation reaction for tRNA of N106A and G111A mutants yeast ArgRS substituted to Ala of Asn106 and Gln111, which D20 base of the D-loop of tRNA (ICG) was observed to have contacts with in crystal structure, it was revealed that *K*m and *k*cat values of these mutant ArgRSs are the same as that of wild type ArgRS and the interaction between the N-terminal domain and D loop of tRNA is not required in the aminoacylation reaction [1]. The main codon usages of Arg are CGX for *E. coli*, CGG/AGG for *T. thermophilus* and CGX/AGA/AGG for yeast and distribution of usage is broad for these species, whereas for *Pyrococcus horikoshii* (Ph), codons of AGA and AGG occupy 98 % of Arg codon usage. Therefore, we selected tRNA with anticodon CCU and determined the crystal structure of the ternary complex of Ph ArgRS, Ph $tRNA^{ARG}$ (CCU) and AMP-PNP with R_{factor} = 0.22 (R_{free} = 0.26) at 2.0 Å resolution. It was observed that in this complex, the base of A20 of D loop of tRNA stacks on the aromatic ring of the side chain of Tyr85 and forms hydrogen bonds with Asn87 in the last β-strand in the N-terminal domain. In order to clarify the role of the N-terminal domain, we constructed Ph ArgRS (92-629 residues) lacking the N-terminal domain and measured kinetic parameters in the aminoacylation reaction for mutant ArgRS and wild type ArgRS. For wild type ArgRS, *k*cat and *K*m values for tRNA are 0.075 s^{-1} and 3.3 μM at 100 mM HEPES-NaOH buffer pH 7.5, respectively and for mutant ArgRS, those are 0.006 s^{-1} and 13 μM at the same buffer and 0.013 s^{-1} and 5.1 μM at 100 mM trisHCl buffer pH 8.0, respectively. This indicates that the fixing of tRNA by the N-terminal domain is not essential in the aminoacylation reaction. We obtained also sensitive crystals of a complex of mutant ArgRS and tRNA from solution containing 2 % PEG and 2.0 M ammonium sulfate.

Reference:

[1] R. Geslain, G. Bey, J. Cavarelli & G. Eriani, *Biochemistry* 2003, 42, 15-92-15101.

P05-177

CRYSTAL STRUCTURE OF 5-METHYLTHIORIBOSE 1-PHOSPHATE ISOMERASE PRODUCT COMPLEX FROM *BACILLUS SUBTILIS*: IMPLICATIONS FOR CATALYTIC MECHANISM

Haruka Tamura[a], Yohtaro Saito[b], Hiroki Ashida[b], Tsuyoshi Inoue[a, c], Yasushi Kai[a], Akiho Yokota[b], and Hiroyoshi Matsumura[a, c]

[a]Department of Applied Chemistry, Osaka University, Suita, Japan; [b]Department of Molecular biology, Nara Institute of Science and Technology (NAIST), Ikoma, Japan; [c]CREST (Sosho Project), JST, Suita, Japan

Methionine salvage pathway (MSP) plays an important role in recycling the methylthio moiety of methylthioadenosine into methionine. Recently, the genes and reactions in MSP from *Bacillus subtilis* have been identified, where 5-methylthioribose 1-phosphate isomerase (MtnA) catalyzes a reversible conversion of 5-methylthioribose 1-phosphate (MTR-1-P) to 5-methylthioribulose 1-phosphate (MTRu-1-P). According to Pfam database, MtnA belongs to a superfamily of translation initiation factors.

Herein, we report the crystal structures of *B. subtilis* MtnA (Bs-MtnA) in complex with its product MTRu-1-P, and a sulfate at 2.4 and 2.7 Å resolution, respectively. The electron density clearly shows the presence of each compound (MTRu-1-P and sulfate) bound to the active site. Bs-MtnA exhibits a Rossman-fold (αβα-sandwich) and forms a homo-dimer.

The three-dimensional structure of MtnA product complex and the structural comparison with MtnA homologous proteins suggest an open/close transition as well as novel catalytic mechanism. The several highly conserved residues in the active site, namely Arg94, Cys160 and Asp240 are most likely involved in catalysis. The details of the catalytic mechanism will be proposed and discussed.

P05-178

STRUCTURAL DIFFERENCE BETWEEN RICE AND RED ALGA RUBISCO COMPLEXED WITH SULFATE

Yasuhiro Komura[a], Hiroyoshi Matsumura[a, d], Hiroyuki Ishida[c], Hiroki Ashida[b], Eiichi Mizohata[a], Tsuyoshi Inoue[a, d], Amane Makino[c], Tadahiko Mae[c], Akiho Yokota[b], Yasushi Kai[a]

[a]Department of Applied Chemistry, Osaka University, Suita, Japan; [b]Department of Molecular biology, Nara Institute of Science and Technology (NAIST), Ikoma, Japan; [c]Department of Applied Plant Science; Tohoku University, Sendai, Japan, [d]CREST (Sosho Project), JST, Suita, Japan

Ribulose 1,5-bisphosphate carboxylase/oxygenase (Rubisco; EC 4.1.1.39) catalyzes the addition of gaseous CO_2 to ribulose 1,5-bisphosphate (RuBP) and produces two molecules of 3-phosphoglycerate (3-PGA). The carboxylation of plant Rubisco is the rate-limiting step of photosynthesis due to the following reasons. First, Rubisco has an extremely slow rate of catalysis with a very low turnover rate (3-4 / seconds per active site). Second, the enzyme cannot exert its maximum ability to fix CO_2, since the concentration of CO_2 in the stroma is smaller than the Michaelis constant (*K*m) for CO_2. Third, the carboxylation and oxygenation reactions are catalyzed in the same active site on the enzyme, with CO_2 and O_2 being competitive substrates. Compared to plant Rubisco, Rubisco from a red alga *Galdieria partite* catalyzes its carboxylation with high affinity to CO_2, but with low maximum turnover number.

In order to investigate the difference in enzymatic properties, rice and *Galdieria* Rubiscos were crystallized in presence of sulfate. The two crystal structures complexed with sulfate show the apparent structural difference of their catalytic loop. The details of structural analysis and structure-function relationship of the two Rubiscos will be presented and discussed.

P05-179

CRYSTAL STRUCTURE OF IcaR, A REPRESSOR OF THE TetR FAMILY IMPLICATED IN BIOFILM FORMATION IN *STAPHYLOCOCCUS EPIDERMIDIS*

Wen-Yih Jeng,[*, 1, 2] Tzu-Ping Ko,[*, 1, 2] Rey-Ting Guo,[1, 2, 3] Chien-Liang Liu,[1, 4] Chia-I Liu,[1, 2, 3] Hui-Lin Shr[1, 2] and Andrew H.-J. Wang[1, 2, 3]

[*]These authors contributed equally to this work. [1]Institute of Biological Chemistry, [2]Core Facility for Protein Crystallography, Academia Sinica, Taipei 115, Taiwan; [3]Institute of Biochemical Sciences, National Taiwan University, Taipei 106, Taiwan; [4]Structural Biology Program, Institute of Biochemistry and Molecular Biology, National Yang-Ming University, Taipei 112, Taiwan

Expression of the gene cluster *icaADBC* is necessary for biofilm production in *S. epidermidis*. The *ica* operon is negatively controlled by the repressor IcaR. Here, the crystal structure of IcaR was determined by multiple anomalous diffraction methods, using a seleno-methionine derivative. It revealed a homodimer comprising entirely α-helices, typical of the tetracycline repressor protein family for gene regulations. The N-terminal domain contains a conserved helix-turn-helix DNA-binding motif. Conformational variation indicates flexibility in this region. The C-terminal domain shows a complementary surface charge distribution about the dyad axis, ideal for efficient and specific dimer formation. The results of electrophoretic mobility shift assay suggest that a 28-base-pairs core segment of the *ica* operator is implicated in cooperative binding of two IcaR dimers on opposite sides of the DNA. Computer modeling based on the known DNA-complex structure of QacR showed that direct protein-DNA interactions are mostly conserved, but with slight variations for recognizing the different sequence. By interfering with the binding of IcaR to DNA, gentamicin and other antibiotics may elicit biofilm production in *S. epidermidis*, as a defense mechanism.

P05-180

STRUCTURAL BASIS FOR THE DISTINCTIVE SUBCHLOROPLAST LOCATION OF THREE MAIZE LEAF FERREDOXIN:NADPH OXIDOREDUCTASES

N. Muraki,[a] G. T. Hanke,[b] T. Shiba,[a] T. Hase,[b] and G. Kurisu[a]

[a]*Department of Life Sciences, University of Tokyo, 3-8-1 Komaba, Meguro-ku, Tokyo 153-8902, Japan,*
[b]*Institute for Protein Research, Osaka University, 3-2 Yamadaoka, Suita, Osaka 565-0871, Japan.*

Ferredoxin:NADPH oxidoreductase (FNR) catalyzes reduction of $NADP^+$ in the final step of linear photosynthetic electron transport and is also implicated in cyclic electron flow that facilitates H^+ pumping for ATP production without producing new reducing species. In higher plants, it has been reported that FNR is localized on the stromal side of thylakoide membranes through association with membrane protein complexes. We have identified that there were three leaf FNR isozymes (LFNR1, LFNR2, and LFNR3) in maize chloroplasts at approximately equivalent concentration and they varied in subchloroplast location (Okutani et al., 2005). LFNR1 was only found at the thylakoide membrane, LFNR3 was exclusively soluble and LFNR2 had a dual location, although three FNRs showed high (>80%) amino acid sequence homologies. In addition, LFNR1 and LFNR2 were found to associate with the cytochrome b_6f complex as a result of its partial purification. Since no one has succeeded in crystallizing the FNR:cytochrome b_6f super complex from higher plants, we crystallized and analyzed the structures of three FNR isozymes, to elucidate the structural basis for their distinctive localization in chloroplast. Main-chain structures of functional domains were very similar (rmsd = 0.58-0.92 Å). A significant structural difference was found at the N-terminal region consisting of about 20 residues. A protruding N-terminal region from the globular domains of LFNR1 seemed to be suitable for interaction with membrane proteins, while the N-terminal of LFNR3 was folded globular across the catalytic domains. These results are discussed in terms of the functional differentiation of maize LFNR isozymes.

P05-181

PREPARATION, CRYSTALLIZATION AND PRELIMINARY CRYSTALLOGRAPHIC ANALYSIS OF OLD YELLOW ENZYME FROM *TRYPANOSOMA CRUZI*

Naoki Okamoto[a], Shigeru Sugiyama[b], Keiji Tokuoka[a], Nahoko Uchiyama[c], Yousuke Okano[a], Hiroyoshi Matsumura[a], Yasushi Kai[a], Koji Inaka[d], Yoshihiro Urade[c] and Tsuyoshi Inoue[a]

[a]Department of Applied Chemistry, Graduate School of Engineering, Osaka University, 2-1 Yamadaoka, Suita, Osaka 565-0871, Japan; [b]CREST, JST, Honcho, Kawaguchi-shi, Saitama 332-0012, Japan; [c]Department of Molecular Behavior Biology, Osaka Bioscience Institute, Osaka 565-0874, Japan; [d]Maruwa Foods Co., Ltd., Tsutsui-cho 170-1, Yamatokoriyama, Nara 639-1123, Japan

Trypanosoma cruzi (*Tc*) is the etiological agent of Chagas' disease which is a major public health and economic problem in South America. The development of new chemotherapeutic agents becomes an urgent need because the anti-chagasic drugs in use have been shown to have undesirable side effects in addition to the emergence of parasite resistance.

Old yellow enzyme (OYE) is an NADPH oxidoreductase that contains flavin mononucleotide as prosthetic group. The OYE from *Tc* (TcOYE) produces prostaglandin (PG) $F_{2\alpha}$ from PGH_2 as a potent mediator of various physiological and pathological processes. However, the detailed mechanism has remained obscure.

In order to investigate the relationship between structure and function of TcOYE, the recombinant enzyme was expressed and purified from *Escherichia coli* and crystallized by the hanging-drop vapor diffusion method. The crystal belongs to the monoclinic space group of $P2_1$ with unit-cell parameters of a = 56.3 Å, b = 78.8 Å, c = 78.8 Å, and β = 93.4° showing that there are two molecules per asymmetric unit. The crystals diffracted up to 1.7 Å resolution, and were suitable for X-ray crystallographic studies. A Patterson search method using the structure of OYE from *Pseudomonas putida*, as a starting model, is in progress.

P05-182

CRYSTALLIZATION AND PRELIMINARY X-RAY ANALYSIS OF THE CERAMIDASE FROM *PSEUDOMONAS AERUGINOSA*

Hiroyuki Okano[a],Koji Kambayashi[a], Nozomu Okino[b], Hatsumi Monjusyo[b], Yoshimitsu Kakuta[c] Makoto Ito[b] and Tsuyoshi Inoue[a]

[a]*Department of Applied Chemistry, Graduate School of Engineering, Osaka University, 2-1 Yamada-oka, Suita, Osaka 565-0871, Japan,* [b]*Department of Bioscience and Biotechnology, Graduate School of Bioresource and Bioenvironmental Sciences,Kyushu University, 6-10-1, Hakozaki, Higashi-ku, Fukuoka 812-8581, Japan,* [c]*Laboratory of Biochemistry, Department of Bioscience and Biotechnology, Faculty of Agriculture, Graduate School, Kyushu University, Fukuoka 812-8581, Japan*

Ceramidase (CDase, EC 3.5.1.23) is an enzyme that catalyzes the hydrolysis of the N-acyl linkage of ceramide to generate sphingosine and fatty acids. Based on optimal pH and primary structure, CDases are classified into three groups: acid, neutral, and alkaline enzymes. Bacterial CDases cloned from *Pseudomonas aeruginosa* are classified as neutral CDases based on the primary structure.

In this study we performed the overexpression, purification and crystallization of a neutral CDase from *Pseudomonas aeruginosa.* Crystals grew with PEG1000 and PEG8000 as the precipitant at 293 K. They diffracted up to 2.6 Å at 100 K using synchrotron radiation and were found to belong to an orthorhombic space group of $P2_12_12_1$, with unit-cell parameters of a = 127.7, b = 206.6,and c = 204.8 Å. The asymmetric unit contains twelve molecules of CDase, showing the V_M value of 2.4 $Å^3$ Da^{-1} and a solvent content of 49%. The search for heavy atom derivatives is in progress.

P05-183

WHY DO NITRILASES NEED TO FORM HELICES TO BE ACTIVE?

Trevor Sewell[a], Serah Kimani[b] and Muhammed Sayed[c]

[a]Electron Microscope Unit; [b]Department of Molecular and Cell Biology, University of Cape Town;[c]Department of Biotechnology, University of the Western Cape, South Africa.

We have recently solved the crystal structure of the amidase from *Geobacillus pallidus* RAPc8. The structure of this enzyme, which has approximately 20% identity to the fibre forming, cyanide hydratases, cyanide dihydratases and nitrilases gives a series of previously inacessible insights. Firstly the extended C-terminus is forms an interlock on at the "A surface" which we have described previously - giving the reason for the stability of this interface. Furthermore a hydrogen bond across this interface stabilises the position of the 3_{10} helix on which the catalytic cysteine is located. The most interesting obsevation arises from the very small active site of the amidase. Because of this it can be seen that the oxygen of the acyl intermediate restricts access to glu59 thought to be the general base catalyst responsible for assisting the hydrolysis of the acyl intermediate. An alternative choice for general base catalyst is glu142 which is located in a loop which we have previously identified as being part of the "C surface" which together with the "A surface" form the interactions along the one-start left handed helix. We postulate, based on a series of cryo and negative stain structures, that the formation of the "C surface" moves glu142 into position so that it can perform a catalytic role in the nitrilases.

P05-184

THE PRESENT STATUS OF ACCURATE STRUCTURE REFINEMENTS FOR MACRO MOLECULES BY THE MAXIMUM ENTROPY METHOD

Makoto Sakata,[a] Eiji Nishibori,[a] , Takahiro Nakamura,[a] Masanori Arimoto,[a] Shinobu Aoyagi,[a] Hideo Ago,[b] Masashi Miyano[b] and Toshikazu Ebiszaki[c]

[a]Department of Applied Physics, Nagoya University;Chikusa-ku, Nagoya, 464-8603 Japan, [b]Miyano Structural Biophysics Laboratory, RIKEN SPring-8 Centre, Harima Institute, 1-1-1 Kouto, Mikazuki, Sayo, Hyogo, 679-5148 Japan, , [c]Ebisuzaki Computational Astrophysics Laboratory, RIKEN 2-1 Hirosawa, Wako, Saitama, 351-0198 Japan

It seems very obvious that the Maximum Entropy Method (MEM) has a great potential to improve the accuracy of crystal structure refinements for macromolecules, e.g. proteins. In a sense, protein crystals are open system, for which unknown number of water molecules is included. Therefore, it is absolutely necessary to determine the structure of water molecules included in protein crystals.

Conveniently, such determination of water molecules is replaced by bulk solvent correction, which assumes homogeneous distribution of water among protein molecules. This assumption should become crude as the accuracy of structure refinements increases. For better refinements, every water molecules has to be assigned in a unit cell of the crystal structure.

It would be not difficult to understand that MEM has essential superiority to the conventional Fourier method. MEM never produces physically meaningless negative density region and hence positive region due to termination effects in resolution. Such positive region of electron density map could be easily misinterpreted as water molecules in protein crystals.

Although MEM has an essential advantage of accurate structure analyses for macromolecules, there are very few examples of actual structure analyses of protein crystals by the MEM. A part of reasons is MEM requires a huge computation loads. The purpose of this study is to demonstrate how accurately a protein crystal can be analysed by taking advantage of MEM in the case of relatively a small protein crystal from extreme thermopile (TT189) using near atomic resolution diffraction data set. It was possible 1) to determine probably all water molecules in a protein crystal, 2) to find out disordered structures in many cases, 3) to detect hydrogen atoms and 4) to refine anisotropic thermal parameters if necessary. However, it was not possible to find out all the atoms in a crystal. The small number of atoms, which seemed severely disordered, could not be detected.

P05-185

CRYSTALLIZATION OF THE COLD-ADAPTED ARABINANASE FROM PENICILLIUM CRYSOGENUM

Kyoko Ikoma,[a] Yuri Sogabe,[a] Asako Yamaguchi,[b] Tetsuko Nakaniwa,[a] Takayoshi Kinoshita,[a] Tatsuji Sakamoto,[b] Hideshi Ihara[a] and Toshiji Tada[a]

[a]*Department of Biological Science, Graduate School of Science, Osaka Prefecture University, Osaka, Japan;* [b]*Department of Applied Life Sciences, Graduate School of Life and Environmental Sciences, Osaka Prefecture University, Osaka, Japan*

Arabinanase hydrolyzes the α-1,5-L-arabinofuranoside linkage of arabinan distributed in hemicelluloses, which comprise a large fraction of plant cell walls. An endo-arabinanase (Abnc) from *Penicillium crysogenum* 31B showed optimal activity at 303 to 313 K and retained about 40% of its optimal activity at even 273 K. We have initiated an X-ray structure analysis of Abnc to clarify the structural features that participate in having activity at low temperature. Here we report the expression system, purification and crystallization of Abnc.

The recombinant Abnc was overexpressed in *E. coli* as fusion protein with maltose binding protein (MBP-Abnc). MBP-Abnc purified by affinity chromatography was cleaved by Factor Xa. The resulting mixture was chromatographed on UNO Q and Superdex 75 columns. The purity of Abnc was confirmed by SDS-PAGE. Prior to crystallization trials, the purified protein was concentrated to 6 mg ml^{-1} in 0.02 M Tris-HCl buffer, pH 8.0, containing 0.1 M NaCl. Crystallization were performed using the sparse matrix screening kit Crystal Screen I from Hampton Research by the sitting drop vapor diffusion method at 277 K. Small crystals were obtained from a drop containing ammonium sulfate as a precipitant at pH 8.5. The optimization of crystallization conditions is currently under way.

P05-186

RIETVELD ANALYSIS SOFTWARE FOR J-PARC

Ryoko Oishi,[a] Masao Yonemura,[b] Shuki Torii,[c] Akinori Hoshikawa,[d] Toru Ishigaki,[b] Yuichiro Nishimaki,[a] Takahiro Morishima[c] and Takashi Kamiyama[c]

[a]*Visible Information Center Inc., Tokai-mura,* [b]*Ibaraki University; Hitachi-city,* [c]*High Energy Accelerator Research Organization; Tsukuba-city,* [d]*Japan Atomic Energy Agency, Tokai-mura, Japan*

As a part of the project creating the world brightest pulsed neutron beam facilty in Japan Proton Accelerator Research Complex(J-PARC), we are developing software for data acquisition, data handling, analysis and visualization.

Here we report on the present status of structure analysis software for J-PARC, especially development of the Rietveld analysis code whose provisional name is Z-Rietveld. The features of this software and results will be presented.

P05-187

VISUALISING AND QUANTIFYING INTERMOLECULAR INTERACTIONS WITH HIRSHFELD SURFACES AND CRYSTALEXPLORER

Joshua J. McKinnon,[a] Mark A. Spackman,[a] and Dylan Jayatilaka[a]

[a]*School of Biomedical, Biomolecular & Chemical Sciences, The University of Western Australia, Crawley, WA, Australia.*

The Hirshfeld surface [1] and associated 2D-fingerprint plot [2] encourage a new kind of understanding of intermolecular interactions in molecular crystals by emphasising a *whole-of-structure* approach. The Hirshfeld surface is determined by the full local environment - the combination of intermolecular contacts - rather than concentrating on those contacts perceived to be important.

The latest release of *CrystalExplorer* [3] incorporates our recent developments[4] which enable the Hirshfeld surface and fingerprint plot to focus on specific interaction types (for instance, O•••H, C–H•••π, etc.) by highlighting regions of the molecule or fingerprint involving those specific types of interaction.

By dividing the Hirshfeld surface into regions involved in different types of interaction, *CrystalExplorer* allows the user to quantify the contribution of these interactions based on their contribution to the Hirshfeld surface area. Quantifying intermolecular interactions in this way provides a truly novel tool for comparing related structures such as polymorphs.

Reference:

1. McKinnon, J. J., Spackman, M. A. & Mitchell, A. S. (2004). *Acta Crystallographica Section B*, 60, 627-668.
2. Spackman, M. A. & McKinnon, J. J. (2002). *CrystEngComm* 4, 378-392.
3. Wolff, S. K., Grimwood, D. J., McKinnon, J. J., Jayatilaka, D. & Spackman, M. A. (2007). CrystalExplorer. Version 2.0. http://hirshfeldsurface.net/CrystalExplorer
4. McKinnon, J.J., Jayatilaka, D., Spackman, M.A., *Chem. Commun.*, 2007, DOI: 10.1039/b704980c

P05-188

THE EFFECT OF AMINO ACIDS AND AMINO ACID DERIVATIVES ON PROTEIN CRYSTALLIZATION

L. Ito[1], T. Kobayashi[1], K. Shiraki[2], T. Narukawa[1], A. Oosuka[1] and H. Yamaguchi[1]

[1]*Sch of Sci and Tech, Univ of Kwansei Gakuin, 2-1 Gakuen, Sanda, Hyogo 669-1337,*
[2]*Inst of Appl Phys, Univ of Tsukuba, 1-1-1 Tennodai, Tsukuba, Ibaraki 305-8573*

Protein crystallography is an indispensable technique for biological, biotechnological, and pharmaceutical researches. The structure determination by X-ray crystallography has been dramatically developed by progress in sample preparation, data collection and computation. To obtain high quality single crystals, however, still remains as the great problem. The difficulty depends on the many parameters that influence protein crystallization, including protein concentration, pH, ionic strength and precipitant concentration. Recently, many researchers adopt the sparse-matrix including different mother liquors that cover many chemical factors, in order to determine the primary crystallization conditions. Single crystals suitable for X-ray diffraction experiment are not always obtained by the procedure. Such screening procedures are not effective enough.

Prevention of protein aggregation plays a key role in the formation of single crystals in the aggregation-prone solution condition. Guanidine and urea are well known as aggregation suppressors that weaken the hydrophobic intermolecular interaction of proteins. Such denaturants are contained in a commercially available additive-screen kit, but decrease the stability of the native state. Recently, amino acids and amino acid derivatives, which are non-denaturating reagents, such as arginine have been used for additives to decrease the aggregation during a refolding process and a heat treatment process. In this study, we investigated the effect of amino acids and amino acids derivatives on protein crystallization.

As a result, protein crystals were obtained in expanded concentration range of the known precipitant in the presence of some kind of these reagents. Especially, crystals were obtained from many conditions including precipitants that crystal did not appear in the absence of the reagents. For example, in the presence of arginine, HEWL crystals were obtained from ammonium sulfate solution. It is considered that the basic additive and amino acid derivatives promote the crystallization of positively charged HEWL. These results show that these reagents are very effective for crystallization and promote success ratio of it and suggests a new strategy to improve the performance of the protein crystallization by addition of amino acids.

P05-189

COMPUTATIONAL METHODOLOGY TO ANALYZE VARIOUS DEFECTS IN CUBIC CRYSTALS

S. T. Nakagawa

Material Science, Graduate School of Science, Okayama Univ. of Science, Okayama, JAPAN

In the field of crystal engineering, an important issue is the innovative synthesis with a new effect. In order to make a breakthrough in the material design, it has been confirmed that the key is hidden in the sequence of time-developed intermediate processes following certain disturbances. In experiments, the sign of such an intermediate process emerges occasionally as imperfections in a perfect crystal. To the contrary, computation can thoroughly trace the time-dependent processes in principle, and we can see the detail of the response mechanism of materials. For such computation, Molecular dynamic (MD) simulation is often used. Unfortunately for the same event or quantity, we cannot always compare experimental and computational results with same accuracy, while those two means are rather complementary.

We have developed a computational methodology to analyze atomistic defects in cubic crystals based on crystallography under the name of Pixel Mapping (PM). An empirical MD monitors the atomic configuration under annealing or ion bombardment. PM method can identity various types of atomistic defects from microscopic to macroscopic scale including long-range-order (LRO) parameters. The essential difference of the PM from other analyses is in the coarse-grained recognition of atoms. Crystalline space is segmented into cubic pixels and atoms are identified by integer address of its belonging cubic pixel. This definition makes it possible to identify Miller indices of atomic planes and indicate crystallographic directions for atoms in crystals, even at higher temperatures than absolute 0 K. This coarse-grained viewpoint is a breakthrough that our computational analysis can identity planar defects with Miller index as is observed by microscopes.

The PM is available for 24 prototype cubic crystals listed in a crystallographic database called StrukturBericht. The classification of prototypes arranges crystals based on the ligand-field of composite atoms in a crystal. For MD simulations, such a classification has the merit that the same formula of interatomic potentials can be expected for crystals belonging to the same prototype. We have defined the set of LRO parameters for each prototype group. Judging from LRO information, we can identify structure changes as amorphization or transformation from one cubic crystal to another. Applications of PM are to be shown in the presentation.

P05-190

DDLM: A NEW DICTIONARY LANGUAGE SUBMITTED TO COMCIFS FOR APPROVAL

Nick Spadaccini,[a] John Westbrook,[b] and Syd Hall[c]

[a]*School of Computer Science and Software Engineering, The University of Western Australia, AUSTRALIA;* [b]*Protein Data Bank, Rutgers Univ., New Jersey, USA;* [c]*School of Biomedical, Biomolecular and Chemical Sciences, The University of Western Australia, AUSTRALIA*

DDLm is a data definition language that provides a rich but simple syntax for constructing data definitions. It includes facilities for relating derivative data via method expressions that are symbolic, easy to read as text, but are computer interpretable and executable [2]. DDLm provides a wider range of data types and allows for lists, arrays, tuples and tables. DDLm also provides for real-time merging of dictionaries, thus allowing for the greater modularisation of discipline dictionaries and the avoidance of definition duplication. A long-term aim of DDLm is to provide a common syntax and structure to all crystallographic dictionaries. It is currently available for examination and comment by all members of the crystallographic community [3]. The community is invited to review and comment on the proposed definition language as part of the approval process.

The paper will describe the major features of DDLm and their importance in the more comprehensive definition of all data used our discipline.

Reference:

[1] International Tables for Crystallography Volume G: Definition and Exchange of Crystallographic Data. (2005) Editors Sydney Hall and Brian McMahon. Springer, Dordrecht.

[2] Spadaccini, N., Hall, S.R., & Castleden, I.R. (2000) J. Chem. Inf. Comput., Sci. 40. 1289-1301.

[3] www.iucr.org/iucr-top/cif/ddlm/

P05-191

MULTIPLE STRATEGIES IN HIGH-THROUGHPUT CLONING, EXPRESSION AND PRODUCTION OF RECOMBINANT PROTEINS FOR STRUCTURAL PROTEOMICS

Hao Xu, Jin-Yi Zhu, Mervin Zhao, Quentin Florence, James Tucker Swindell II, Bret Dillard, Dayong Zhou, Angela Yang, John Rose, and Bi-Cheng Wang

Southeast Collaboratory for Structural Genomics, Department of Biochemistry and Molecular Biology, University of Georgia, Athens, GA 30602, USA

The determination of "three-dimensional protein structures with unique chemical sequences" has been an emphasis of the Southeast Collaboratory for Structural Genomics (SECSG) in target selection.

Six biologically important organisms have been chosen as initial genome resources in our studies and more than 3,000 pfam or non-pfam ORFs have been cloned. We have found that recombinant protein yield and solubility of these ORFs is highly dependent on the specific sequence, as well as on the vector, fusion construct, host cell, and culture conditions used. For high-throughput processing, initial efforts have focused on soluble (Tier-1) and insoluble (Tier-2) purification strategies using the cost-effective His-tag. In Tier-1 processing ~50% of the cloned targets are expressed and ~25% of the expressed proteins are soluble and have been purified for crystallization. In the Tier-2 process, insoluble Tier-1 targets are salvaged using a variety of cloning and production strategies in parallel. For difficult yet biologically important targets including membrane proteins, HIV-related human proteins, or protein complexes, new technologies have been developed to improve expression and explore high throughput production.

Work is supported in part with funds from the National Institutes of Health (GM62407), the Georgia Research Alliance and the University of Georgia Research Foundation.

P06-004

PERFORMANCE OF THE HIGH-THROUGHPUT PROTEIN CRYSTALLOGRAPHY BEAMLINE BL13B1 AT THE NSRRC

Chun-Hsiung Chao,[a] Yuch-Chen Jean,[a] Yu-Shan Huang,[a] Chien-Chang Tseng[a], Cheng-Hung Chiang[a], Chun-Jung Chen[a], Shih-Chun Chung,[a] Ching-Shiang Hwang,[a] King-Long Tsang[a] and Chien-Te Chen[a]

[a]*National Synchrotron Radiation Research Center, Hsinchu 30077, Taiwan, ROC*

A high-throughput Protein Crystallography facility was constructed for the National Synchrotron Radiation Research Center (NSRRC) super-conducting super-wiggler beamline BL13B1. This 28-pole wiggler, with a magnetic field of 3.2 Tesla, increases the critical energy from 2.14 keV for a 1.25 Tesla normal conducting magnet to 4.82 keV, and is capable to provide an intensive X-ray beam up to 19 keV, which made it possible for hard x-ray experiments to be conducted at the relatively low energy NSRRC ring (1.5 GeV).

BL13B1 covers an energy range from 6.5 keV to 19 keV, which is suitable for both MAD and monochromatic diffraction experiments. The major optical components of this beamline include a front end, a cylindrical vertical collimating mirror, a double-crystal Si (111) monochromator, and a toroidal focusing mirror. The end stations is equipped with an ADSC Quantum315 CCD area detector, with a high precision single-phi axis goniometer, a sample cooling system, a robotic sample changer for automatically sample mounting and centering. BLU-ICE and HKL2000 provides user-friendly interfaces to the data acquisition and data processing tasks. The design and performance characteristics of this beamline will be described.

P06-005

STANDARD OPERATION SYSTEM FOR STRUCTURAL BIOLOGY BEAMLINES AT SPRING-8

Go Ueno[a], Kazuya Hasegawa[b], Nobuo Okazaki[b], Kunio Hirata[a], Takashi Kumasaka[a, b] and Masaki Yamamoto[a, b]

[a]*RIKEN SPring-8 Center, Kouto, Sayo, Hyogo, Japan.,* [b]*Japan Synchrotron Radiation Research Institute, Kouto, Sayo, Hyogo , Japan*

The standard operation system for structural biology beamlines at SPring-8 has been first developed at RIKEN Structural Genomics Beamlines (BL26B1 & BL26B2) [1], where the high throughput data collection with sample auto-changer SPACE (SPrign-8 Precise Automatic Cryo-sample Exchanger) is carried out with automatic beamline operation. The control system is designed based on the client-and-server architecture in which each device is controlled by distributed server programs. User interface BSS (Beamline Scheduling Software) provides the centralized control of entire beamline instruments with an intuitive GUI. The hardware components in the end station such as x-ray shutter, crystal goniometer, equipment stage etc. are controlled by VME bus modules through MADOCA device control framework [2], which is commonly used for beamline and storage ring operation of SPring-8. By communicating with MADOCA system, as well as other equipment servers such as area detector, sample changer etc., BSS realizes the all-in-one and automatic operation of the beamlines. Successive data collections for multiple samples can be easily scheduled and executed by utilizing BSS, starting with setting x-ray wavelength, exchanging sample, setting up detector, and taking diffraction photos with monitoring the storage ring status.

Since this control system is scalable and configurable to other hardware, the same architecture has been similarly implemented to many of other structural biology beamlines at SPring-8, providing users a common look and feel at all beamlines.

Presently, development of some new features, such as automatic crystal screening, real-time monitoring of radiation damage, automatic crystal centering etc. are attempted by associating the beamline operation with the automatic diffraction image analysis.

Reference:

[1] Ueno, G., et al., (2006). J. Struct. Funct. Genomics. **7**, 15-22.

[2] Tanaka, R. et al., Proc of ICALEPCS ’95, Chicago, USA, 1995 p.201.

P06-006

HOMELABS VS. SYNCHROTRONS: THE FACTS WILL SURPRISE YOU

Joseph D. Ferrara, Cheng Yang

Rigaku Americas Corporation, The Woodlands, USA

This presentation will be divided into two parts. The first part will comprise a review of the current state-of-the-art in home lab x-ray sources from both performance and environmental impact perspectives. In the second part will present the results of data mining of the RCSB PDB (H.M. Berman, J. Westbrook, Z. Feng, G. Gilliland, T.N. Bhat, H. Weissig, I.N. Shindyalov, P.E. Bourne: The Protein Data Bank. (2000) *Nucleic Acids Research.* **28**, 235-242) , and will compare and contrast the productivity of home labs and synchrotrons. The results of the survey will surprise you.

P06-007

NEXT GENERATION X-RAY DETECTOR FOR IN-HOUSE XRD SYSTEM

Takeyoshi Taguchi,[a] Christian Broennimann[b] and Eric F. Eikenberry[b]

[a]*X-rayResearch Laboratory, Rigaku Corporation, 3-9-12 Matsubara-cho, Akishima-shi, Tokyo, Japan;*
[b]*DECTRIS Ltd., 5232 Villigen PSI, Switzerland*

A novel type X-ray detector, called PILATUS, has been developed at the Paul Scherrer Institut (PSI) during the last decade. PILATUS detectors are two-dimensional hybrid pixel array detectors, which operate in single-photon counting mode. The PILATUS detectors have a very wide dynamic range (1:1,000,000), very short read out time (< 3.0msec), and very high counting rate (> 2 x 106 counts/sec/pixel). Additionally, the PILATUS detector can set energy threshold individually for each pixel. Thus the PILATUS can suppress fluorescence background. These features are superior to existing area detectors and PILATUS is the next generation X-ray detector.

The PILATUS detector systems have a few different configurations. A single module of PILATUS detector, or the PILATUS 100K, has 487 x 195 pixels with a pixel size of 172 x 172μ2. The active area is 83.8 x 33.5mm2. Large area systems consist of 20 to 60 modules and can cover up to 424 x 435mm2 area. Such systems are mainly used for macromolecule analysis, i.e. protein crystallography. The single module detector is small and easy to handle and can be adapted to many systems with small modification. The PILATUS 100K detector is integrated to an in-house X-ray diffraction system and demonstrates superior performance. Some examples of XRD measurements with the PILATUS 100K detector will be given.

P06-008

STRUCTURAL BIOLOGY BEAMLINES AT SPring-8

Masaki Yamamoto[a,b], Go Ueno[a], Takaaki Hikima[a], Atsushi Nisawa[a], Kunio Hirata[a], Tetsuya Shimizu[a], Nobutaka Shimizu[a,b], Masahide Kawamoto[b], Kazuya Hasegawa[b], Hisanobu Sakai[b], Seiki Baba[b], Nobuo Okazaki[b], Aik Hong Teh[b], Takashi Kumasaka[a,b]

[a]*RIKEN SPring-8 Center, Kouto, Sayo, Hyogo, Japan.*, [b]*Japan Synchrotron Radiation Research Institute, Kouto, Sayo, Hyogo , Japan*

In the third generation synchrotron radiation, structural biology research is one of the major subjects in the past decade. At SPring-8, eight beamlines are operating for protein crystallography (PX). We have been constructing and developing the beamlines with the view of two objectives. One objective is improvements of the applicable crystal size and the data quality, and the other is the high throughput protein crystallography. After the completion of the Human Genome Project, structural genomics research projects have been progressing worldwide. At SPring-8, the Protein 3000 project, a Japanese structural genomics project, has been progressing rapidly owing to high-throughput PX beamlines.

BL41XU is an undulator beamline with the high brilliance of 4.8×10^{14} photons/sec/mm^2. The new K/B mirror system was installed for micro crystals (~ 25 μm) using a micro beam. The beam size at sample position is controllable from 25 × 25 to 70 × 100 μm^2 using two quadrant slits. SAD measurements of Se-methionine samples with the crystal size from 15 to 50 μm were performed using multiple positions on a crystal, and we solved the initial phase at the resolutions from 2.7 to 3.9 Å. A new micro focus beamline, aimed at the target beam size of 1 × 1 μm^2, is planning.

BL26B1&B2 have been constructed for Structural Genomics research. The beamline operation is automated cooperating with the sample changer robot named SPACE, the operation software BSS and beamline management database D-Cha. Combination of BSS, SPACE and D-cha also enables Mail-in data collection, and the Web interface of D-Cha allows users to deposit measurement condition or to observe recorded images from distant place.

We will present the present status and the future plan of protein crystallography beamlines at SPring-8.

P06-009

STATISTICAL PROPERTIES OF X-RAY INTENSITY MEASURED WITH A COUNTING SYSTEM WITH FINITE DEAD-TIME

Takashi Ida, Akihisa Oya, Hisashi Hibino

Ceramics Research Laboratory,Nagoya Institute of Technology, Tajimi, Gifu, 507-0071, Japan

Counting method is widely used to measure the intensity of X-ray. Independently generated signal pulses are expected to obey the Poisson distribution, which predicts the probability for the number of pulses n during the measurement period T is given by

$P_{Poisson}(n) = (n!)^{-1} (rT)^n \exp(-rT)$,

where r is the average rate of generated pulses. The mean μ and variance σ^2 of the number of the Poisson pulses are simply given by

$\mu = \sigma^2 = rT$

The statistical errors of the intensity measured by a counting method can naturally be modelled by the square root of the measured count, if the Poisson distribution of the pulses is assumed.

The probability for the number of counted Poisson pulses m based on the non-extended dead-time model can be expressed as

$P_{non}(m) = (m!)^{-1} (1+r\tau) [r(T - m\tau)]^m \exp[-r(T - m\tau)]$

where τ is the dead-time of a detector and/or the electronic circuits of the detection system. The mean μ_{non} and variance σ_{non}^2 of the counted pulses are given by

$\mu_{non} = rT / (1 + r\tau)$

$\sigma_{non}^2 = \mu_{non} / (1 + r\tau)^2$

Recently, Laundy & Collins [1] have reported analytical expressions about the statistical properties of a pulse-overlap model for the counting loss, which includes the extended dead-time model as a special case. According to their results, the mean μ_{ext} and variance σ_{ext}^2 for the extended dead-time model are given by

$\mu_{ext} = rT \exp(-r\tau)$,

$\sigma_{ext}^2 = \mu_{ext} [1 - 2r\tau \exp(-r\tau)]$.

The above expressions for the non-extended and extended dead-time models for counting loss applied to the Poisson pulses has been validated by a Monte Carlo simulation with simple computer algorithm. Variance of pulses counted with a detection system on the powder diffraction beam-line BL-4B2 at the Photon Factory in Tsukuba, evaluated by repeated measurements of the beam diffracted from mica standard powder (NIST SRM675), will be compared with the theoretical prediction.

Reference:

[1] Laundy, D. & Collins, S. (2003). *J. Synchrotron Rad.* **10**, 214-218

P06-010

MAIL-IN DATA COLLECTION AT SPRING-8 STRUCTURAL BIOLOGY BEAMLINES

Seiki Baba[a], Kazuya Hasegawa[a], Go Ueno[b], Nobuo Okazaki[a], Hisanobu Sakai[b], Hironori Murakami[b], Takashi Kumasaka[a] and Masaki Yamamoto[a,b]

[a]*Japan Synchrotron Radiation Research Institute, Kouto, Sayo, Hyogo , Japan,* [b] *RIKEN SPring-8 Center, Kouto, Sayo, Hyogo, Japan*

The mail-in data collection at SPring-8 structural biology beamlines makes use of automated beamline operation system using the sample changer SPACE, the beamline control software BSS and the web interface D-Cha. Data collection can be readily carried out without visiting SPring-8 by following procedures: 1) Target crystals are stored in the sample tray at laboratory. 2) The tray is sent to the beamline via home-delivery service. 3) The information of the tray such as sample name, experimental conditions of content samples is input into D-Cha by users. 4) Diffraction data is collected at the beamline utilizing automatic system with SPACE and BSS. 5) Collected data is downloaded via the Internet using D-Cha.

At the beamline, all crystals are once screened by using synchrotron radiation. In this process, crystal centering is carried out by beamline operator. Users can monitor the experimental results via D-Cha at their laboratory in real time. The complete data set is collected only for crystals qualified by users. Since SPACE has the special feature to assure the reproducibility of the crystal mount position, the data sets can be automatically collected once the crystal centering is performed.

By following the screening process on our system, users can definitely select the best crystal to collect the data set and also can make an efficient experimental schedule, which leads to the improvement of the throughput.

At BL26B1, BL26B2 and BL38B1, mail-in data collection system has been operated since September 2005. Currently, the commercial mail-in service has started in July 2006, as the joint project among JASRI, RIKEN and analysis service companies.

P06-011

HIGH THROUGHPUT PROTEIN CRYSTAL EXCHANGE ROBOTS OF THE PHOTON FACTORY BEAMLINES

Masahiko Hiraki, Shokei Watanabe, Nobuo Honda, Yusuke Yamada, Naohiro Matsugaki, Noriyuki Igarashi, Yurii Gaponov and Soichi Wakatsuki

Structural Biology Research Center, Photon Factory (*PF*), *Institute of Materials Structure Science, High Energy Accelerator Research Organization* (*KEK*), *Tsukuba, Ibaraki, 305-0801, Japan*

In order to execute diffraction experiments of protein crystals by remote-control, process of sample exchange must be automated. In addition, the sample exchange robots can liberate users from slavish work at the beamlines. Therefore, we have developed sample exchange robots that can exchange protein crystals according to the instructions from out of the experimental hutches. The robots were designed based on the SAM system (SSRL Automated Mounting system) with cooperation of SSRL (Stanford Synchrotron Radiation Laboratory) macromolecular crystallography group. In order to reduce the required time for the sample exchange, we modified the single-tongs of the SAM system and developed a double-tongs system that can hold two cryo pins at the same time. The robot with double-tongs can move to the goniometer head holding the next cryo pin by one of the tongs, dismounts the used cryo pin with the other tongs and mounts the next pin onto the goniometer head without leaving the diffractometer area.

Two different types of tongs have been installed; the single-tongs at the beamlines BL-5A and AR-NW12A, and the double-tongs at the BL-17A. The same GUI software for the operation of the sample exchange robots is used at all beamlines, however, so that the users do not need to consider the differences of the tongs. An intermediate computer works for communication between the GUI and the robot controller. When it receives "exchange" command from the GUI, it translates suitable commands for the type of tongs and sends them to the robot controller.

We will introduce our sample exchange robot system including the beamline computer network, and report on the state of the user operation.

P06-012

UPGRADE OF THE STRUCTURAL BIOLOGY BEAMLINES AT THE PHOTON FACTORY

Noriyuki Igarashi, Naohiro Matsugaki, Yusuke Yamada, Masahiko Hiraki and Soichi Wakatsuki

Photon Factory, Institute of Materials Structure Science, High Energy Accelerator Research Organization 1-1 Oho, Tsukuba, Ibaraki 305-0801, Japan

Structural Biology Research Center at the Photon Factory currently operates four structural biology beamlines. The AR-NW12A, BL-5A and BL-17A are the insertion device beamlines, while the BL-6A is a conventional bending magnet beamline. The micro-focus beamline BL-17A was newly constructed and opened for general users in 2006. In the next two years, two more construction plans of a pharmaceutical beamline and another micro-focus beamline are scheduled.

The BL-17A was designed for micro-crystal structure analysis. In addition, the intense lower energy beam at around 6 keV is used for structure determination by SAD phasing with light atoms. The source of the beamline is a newly developed short-gap undulator installed in one of four short straight sections of PF 2.5GeV ring. The measured focused beam size (FWHM) with the K-B mirror system was about 0.03mm (V) x 0.23 mm (H). The photon flux at 12 keV collimated by 100 and 20 μm^2 were 8 x 10^{10} and 7 x 10^9 photons/sec, respectively. Further optimization and stabilization of the optics have been executed; suppressing vibration of the optical elements, fixing beam position by feedback control, etc. In this June, a brand-new CCD detector ADSC Quantum 270 was installed and used for experiments.

Automation of the beamlines is facilitated by installing sample changers, automatic sample centering system and beamline control software. The changers, modified from the original SSRL-SAM system, have been operated at all the insertion device beamlines. The automatic sample centering system, including diffraction-based evaluation algorithm, is under development. The beamline control software based on a relational database allows secure remote access and automatic scheduled experiments together with the sample changer. All the information stored in the database during experiments can be easily tracked and managed.

A pharmaceutical beamline will be built at the PF-AR NE3A in the summer of FY2008 and opened to users from April, FY2009. The beamline is expected to show a higher performance than the high-throughput beamlins AR-NW12A and BL-5A. The beamline will be mainly dedicated to drug design.

Construction of a new micro-focus beamline at the PF ring in FY2009 is scheduled. The goal is to deliver brilliant lower energy beam at around 4-5 keV (dedicated to sulphur SAD experiment) and more photon flux at around 12keV than that of BL-17A.

P06-013

THE SIDE LINE OF TAIWAN CONTRACT BEAMLINE BL12XU AT SPRING-8 FOR HIGH ENERGY PHOTOEMISSION

Chi-Yi Huang, Ku-Ding Tsuei, Yong Q. Cai, Cheng-Chi Chen, Yen-Fang Song and Shih-Chun Chung

National Synchrotron Radiation Research Center, Hsinchu, Taiwan, 300, R.O.C.

High energy photoemission spectroscopy presents new opportunities in the study of the electronic structure of novel materials with increased bulk sensitivity. This characteristic is particularly useful to study strongly correlated systems with different bulk properties from surface, and the properties of berried interface of devices. For these experiments, we are constructing a new side beamline branching off from the main line of BL12XU at SPring-8. A single bounce diamond monochromator (DM) will be used to deliver monochromatic X-rays to the side beamline from 6 keV to 12 keV. After the DM, we have designed a high resolution monochromator to reduce the energy resolution to 60 meV (FWHM). The total flux will be $2x10^{11}$ photons/sec at 6 keV. Finally, the X-ray is focused to 30 x 30 μm^2 (HxV) (FWHM) at the sample position. The whole beamline except the DM will be supported on a platform that swings with photon energy. We intend to start commissioning this beamline by the end of 2007.

P06-041

RATIOS OF ELASTIC CONSTANTS OF CdTe DERIVED FROM X-RAY THERMAL DIFFUSE SCATTERING UNDER HIGH PRESSURE

Daisuke Ohtsu,[a] Maki Okube,[a] Takahiro Kuribayashi,[b] Yasuhiro Kudoh,[b] Taiki Nakanishi,[a] Hiroyuki Katsuragawa,[a] Akiko Nakao,[c] and Satoshi Sasaki[a]

[a]*Materials and Structures Laboratory, Tokyo Institute of Technology, Yokohama, 226-8503;*
[b]*Institute of Mineralogy, Petrology and Economic Geology, Tohoku University, Sendai, 980-8578;*
[c]*Photon Factory, Institute of Materials Structure Science, KEK, Tsukuba, 305-0801, Japan*

Cadmium telluride (CdTe) has attracted to various applications to optoelectronic devices. The II-VI semiconductor has the zinc-blende structure at ambient pressure and transforms to the intermediate cinnabar phase in a pressure range of about 2.5 to 4 GPa, before reaching the rock-salt structure. An accurate description of the elastic property for CdTe is important because it provides a link between the mechanical and dynamical behaviours of crystals in concerning the nature of phase transition. The elastic constants can be related to the X-ray intensity of thermal diffuse scattering (TDS), which arises from the scattering of the incident beam by phonons. The TDS approach is useful even for a small and opaque crystal loaded in a diamond-anvil cell (DAC). In this study, the pressure dependence of the elastic constant of CdTe is investigated on the basis of the observation of TDS.

At each experiment, a single crystal of CdTe was loaded in a modified Merrill-Bassett-type DAC with a gasket made from stainless steel. The pressure was measured using the ruby-fluorescence method. Only zinc-blende phase was investigated in the pressure range close to the phase boundary. The TDS intensity was measured with a vertical-type four-circle diffractometer at the BL-10A of Photon Factory. A wavelength of λ = 0.7 Å was selected by a Si(111) monochromator. The TDS intensities were measured in two-dimensional reciprocal area with two of [100], [010] and [001] passing through 004, 220 and 111 reciprocal lattice points at room temperature. Based on the diffuse intensity measured at each point of the grid, the shape of curves of isodiffusion surrounding the Bragg point were obtained and compared with the theoretical isodiffusion surfaces (Jahn, 1942). The shape of the isodiffusion surface was examined whether to change by the pressure. Then, the ratios of elastic constants of c_{11}/c_{44} and c_{11}/c_{12} were determined from the relative diffuse intensities as a function of pressure. The presentation will be made in the context of the merits and demerits of the TDS method.

P06-042

SITE OCCUPANCY AND MAGNETIC STRUCTURE OF $BaTiMnFe_{10}O_{19}$ HEXAFERRITE

Taiki Nakanishi,[a] Maki Okube,[a] Hiroyuki Katsuragawa,[a] Daisuke Ohtsu,[a] Takeshi Toyoda,[b] Akiko Nakao,[c] and Satoshi Sasaki[a]

[a]*Materials and Structures Laboratory, Tokyo Institute of Technology, Yokohama, 226-8503, Japan;*
[b]*Industrial Research Institute of Ishikawa, Kanazawa, 920-8203, Japan;*
[c]*Photon Factory, Institute of Materials Structure Science, KEK, Tsukuba, 305-0801, Japan*

M-type barium hexaferrite, $BaFe_{12}O_{19}$ is ferrimagnetic below T_c = 723 K. The magnetic structure can be described with the spin collinear model, where all the magnetic moments are ordered parallel or antiparallel to *c* axis. Ti^{4+} and Mn^{2+} substitution for Fe^{3+} results the reduction of the strong uniaxial magnetic anisotropy. In the solid solution including Ti^{4+} and Co^{2+} ions, the neutron and synchrotron X-ray diffraction studies have revealed the existence of a magnetic helix propagated along the hexagonal *c* axis in $BaTi_{0.8}Co_{0.8}Fe_{10.4}O_{19}$. Therefore, in this study, another hexaferrite of $BaTiMnFe_{10}O_{19}$ has been examined with the ion-size effect to study crystallographically the mechanism of the magnetic anisotropy change.

The powder crystals were prepared by the conventional solid-state reaction using appropriate molar mixtures of $BaCO_3$, TiO_2, $MnCO_3$ and Fe_2O_3 as starting materials. The products preheated at 1073 K for an hour were ground again and heated at 1473 K for 2 hours. A flux method was used for single crystal growth. The chemical analysis was made using a Horiba XGT-2000 X-ray fluorescence spectrometer. The cell dimensions are a = 5.902(3), c = 23.209(4) Å ($P6_3/mmc$). Conventional and synchrotron X-ray diffraction experiments were carried out using Rigaku AFC-7R and PF-BL10A four-circle diffractometers, respectively. The X-ray magnetic circular dichroism (XMCD) experiments were performed at the Fe *K* absorption edge with a diamond(001) phase retarder and rare-earth magnets at the BL-6C.

The structural parameters of $BaTiMnFe_{10}O_{19}$ were determined using full-matrix least-squares software RADY with the Mo *K* data. The site occupancies of Fe ions in five different sites were determined with the anomalous scattering effects of synchrotron X-rays at a wavelength λ = 1.7485 Å. Then, site occupancies of Ti ions were determined within two selective sites with the Mo *K* data. The final result on the cation distribution is: 100% Fe in Fe(1) [2*a* site]; 100% Fe in Fe(2) [2*b*]; 58.0% Fe, 35.1% Ti and 6.9% Mn in Fe(3) [4f_1]; 100% Fe in Fe(4) [4f_2]; 80.7% Fe, 5.0% Ti and 14.3% Mn in Fe(5) [12*k*]. In XMCD measurements, a negative peak was clearly observed near E = 7.120 keV, having a similar pattern to that of typical M-type ferrites. Progress on the determination of the magnetic structure will be presented.

P06-043

VALENCE AND SPIN STATE OF Co IONS IN $La_{1-X}Ca_XCoO_3$

Hiroyuki Katsuragawa,[a] Maki Okube,[a] Takayasu Hanashima,[b] Taiki Nakanishi,[a] Daisuke Ohtsu,[a] and Satoshi Sasaki[a]

[a]*Materials and Structure Laboratory, Tokyo Institute of Technology, Yokohama, 226-8503;*
[b]*Organization for Promotion of COE, Ritsumeikan University, Kusatsu, 525-8577, Japan.*

Broad magnetic-electronic transition of $LaCoO_3$ above 90 K can be interpreted with the existence of the intermediate spin (IS) of Co^{3+}. It is known in $La_{1-x}Sr_xCoO_3$ that the IS state with hole doping or a superexchange of Co^{3+}-O-Co^{4+} gives the magnetic moments such as spin glass when Sr^{2+} is substituted for La^{3+}. Ca^{2+} substitution for La is expected to have the hole doping with weak lattice distortion because of resemble ionic radii (r_{La} = 1.32 Å, r_{Ca} = 1.35 Å, r_{Sr} = 1.44 Å). A careful comparison of magnetic and electronic state is needed for $La_{1-x}Ca_xCoO_3$ and $La_{1-x}Sr_xCoO_3$.

Powder crystals of $La_{1-x}Ca_xCoO_3$ were synthesized from appropriate molar mixtures of Co_2O_3, La_2O_3 and $CaCO_3$. The mixtures were ground in an agate mortar, prepared in an aluminum crucible, and heated up to 1273 K and maintained for 36 hours. The products were ground again and heated at 1273 K for 12 hours and quenched. X-ray powder diffraction measurements were performed to confirm a single. The effect of Ca doping on the magnetic structure of $La_{1-x}Ca_xCoO_3$ (x = 0, 0.1, 0.15, 0.2, 0.25, 0.3, 0.35, 0.4, 0.5, 0.6, 0.65 and 0.8) was examined by measurements of SQUID and X-ray magnetic circular dichroism (XMCD). The XMCD experiments were carried out at the Co *K* absorption edge on the BL-6C(3A). The Si(111) double-crystal monochromator and a diamond(001) phase retarder were used with X-rays of $3^{(H)}$ x $2^{(V)}$ mm^2. The powder samples were mounted on several sheets of transparent tape, which were used in the Faraday arrangement with a pair of rare-earth magnets in a magnetic field of 0.4 T. Two ionization chambers were used for absorption experiments, where the second one is 300 mm in length and filled with 75% N_2 + 25% Ar gas. A completely standard transmission setup was used with the

The XMCD signal was observed in a difference of absorption coefficients with the right and left circularly polarized X-rays. It reflects the local spin and orbital polarization of the final states at the inner core absorption edges. A negative peak of XMCD was clearly observed at E = 7.719 keV within the threshold region, suggesting the existence of the IS state of Co^{3+}. By Ca substitution for La, a positive peak appeared at E = 7.723 keV of the main edge. The presentation will discuss the electronic state of Co ions.

P06-044

MIXED-VALENCE STATES OF TRANSITION-METAL ATOMS IN A SOLID SOLUTION BETWEEN Fe_3O_4 AND Co_3O_4

Yoshihiro Yamamoto,[a] Norio Shimizu,[a] Maki Okube,[a] Atsuko Ohno[a] and Satoshi Sasaki[a]

[a]*Materials and Structures Laboratory, Tokyo Institute of Technology, Yokohama, 226-8503, Japan;*

The spinel structure has the geometrical frustration of a pyrochlore type, which is important in the superexchange interaction between tetrahedral A and octahedral B sites. The valence states of iron and cobalt atoms are a key factor to control the conductivity and magnetism in ferrites and cobaltites. A combination study of single-crystal X-ray diffraction (SCXD), X-ray absorption near edge structure (XANES) and X-ray magnetic circular dichroism (XMCD) is useful to clarify the valence and spin states in the mixed-valence compounds.

Synchrotron experiments for $Fe_xCo_{3-x}O_4$ (x = 0, 0.8, 1.0, 1.1, 1.4, 1.8, 2.0, 2.1 and 3.0) were carried out at BL-10A and BL-3A/6C of Photon Factory. The horizontally polarized X-rays were monochromatized by Si(111) monochromators to select the wavelengths near Fe *K* and Co *K* absorption edges. Diffraction intensities for some single crystals were measured by a ω-2θ step-scan technique in a vertical-type four-circle diffractometer. The cation distribution between iron and cobalt atoms was determined with a large difference in anomalous scattering factors. The XMCD experiments were made to use a phase retarder of a synthetic diamond crystal, ionization chambers and rare-earth magnets. The difference in the absorption coefficients for right- and left-circularly polarized X rays can be used with spins parallel and antiparallel to the direction of light travel.

XANES and XMCD spectra of $Fe_xCo_{3-x}O_4$ gave the following results on the compositional dependence of the valence states: (1) iron ions are trivalent for the samples having $x \leq 2$, (2) trivalent cobalt ions exist at least for $x \leq 2$ and (3) Fe^{3+}, Co^{2+} and Co^{3+} ions equally occupy the B sites in $Fe_{4/3}Co_{5/3}O_4$. The samples for $x \leq 1.4$ have the split XMCD peaks at E = 7707 and 7715 eV of the Co *K* edge, suggesting the change of the spin state of cobalt atoms. The presentation will discuss the electronic states of iron and cobalt atoms in the solid solution of Fe_3O_4 and Co_3O_4.

P06-045

X-RAY SCATTERING STUDY OF YTTRIUM-DOPED HfO_2 THIN FILMS

C.-H. Hsu[a,] Z. K. Yang,[a,b] K. L. Yu[a,], M.-T. Tang,[a] M. L. Huang,[a,b] W. C. Lee,[b] Y. J. Lee,[b] P. Chang,[b] M. Hong,[b] and J. Kwo[c]

[a]National Synchrotron Radiation Research Center; [b]Department of Materials Science and Engineering, National Tsing Hua University; [c]Department of Physics, National Tsing Hua University, Hsinchu, Taiwan, 300, ROC

We have successfully converted the structure of monoclinic HfO_2 thin films to a cubic one by yttrium doping. These yttrium-doped HfO_2 (YDH) ultra-thin films were grown epitaxially on GaAs (001) and Si (111) substrates by molecular beam epitaxy (MBE). The electric measurements of a film of 7.7 nm thick yielded an enhanced dielectric constant κ~32, close to the theoretical value of cubic phase HfO_2. We have performed x-ray scattering and transmission electron microscopy measurements to thoroughly investigate the structure and surface morphology of the YDH thin films. The interfaces between YDH and both kinds of substrates are atomistic sharp and free of reacted interfacial layer. The surface of YDH layers grown on Si (111) are rather flat but well resolved {111} facets were observed on those grown on GaAs (001). We have also determined yttrium content of YDH films to be 19% by using anomalous x-ray diffraction (AXD) across Y *k*-edge and angle resolved X-ray photoelectron spectroscopy (AR-XPS). The agreement between the AXD and AR-XPS results manifests that the incorporated Y atoms indeed homogeneously substitute Hf atoms in the crystalline lattice and form a substitutional solid solution.

P06-046

STUDIES ON FERROMAGNETIC CARBONS

Prabal Dasgupta

Department of central scientific services
Indian Association for the cultivation of science
2A&2B, Raja S.C. Mullick Road
Kolkata-700032
India

The structure of commerinin, a pigment of a blue dayflower, was solved by Kondo et al. in 1992 [1]. The authors reported that the pigment was composed of six anthocyanin and six flavone molecules with two Mg ions, based on the crystal structure analysis at 1.0Å resolution. However, our recent research on the structure of protocyanin pigment [2] indicated that the commerinin complex pigment has other metal constituents.

We investigated the crystal structure of the commerinin pigment at the resolution of 0.7 Å using a large CCD area detector at BL-5A of the Photon Factory. The structure reveals two additional Mg ions bound to outer side of the complex pigment. The positions of Mg ions roughly corresponded to those of Ca ions in the protocyanin structure. The high resolution structure including the positions of hydrogen atoms will be presented.

P06-047

CRYSTAL STRUCTURE AND MAGNETIC PROPERTIES OF $NaFe(WO_4)_2$ AND $NaCr(WO_4)_2$

D.Sangaa[a], L.Nyam-Ochir[a,b], H.Ehrenberg[b,c], D.Mikhailova[b], H.Fuess[b]

[a]*National University of Mongolia, Ikh Surguuli1, Ulaanbaatar, Mongolia*

[b]*Darmstadt University of Technology, Petersenstrasse 23, 64287 Darmstadt, Germany*

[c]*Institute for Complex Materials, IFW Dresden, Helmholtzstrasse 20, 01069 Dresden, Germany*

Powder samples of $NaFe(WO_4)_2$ and $NaCr(WO_4)_2$ were prepared and studied by X-ray diffraction and SQUID measurements at low temperature. The structure of sodium iron and chromium tungstate, $NaFe(WO_4)_2$ and $NaCr(WO_4)_2$, is similar to the structure of wolframite-type $FeWO_4$ with the same space group P2/c, but with doubled *a* parameter [1,2].

Therefore, less magnetic coupling paths between $M^{3+}O_6$-octahedra exist in $NaM^{3+}(WO_4)_2$ because of additional diamagnetic units in the structure. Nevertheless, magnetisation data show that $NaFe(WO_4)_2$ and $NaCr(WO_4)_2$ are antiferromagnetic at low temperature. A maximum in the temperature dependence of magnetisation is observed at 11(1)K for $NaFe(WO_4)_2$ and for $NaCr(WO_4)_2$ at 32(1)K, which is an upper estimate of the Néel temperature.

This system provides a suitable test for the proposed dominance of supersuperexchange couplings M^{3+}-O-O-M^{3+}, with M^{3+}-O-O and O-O- M^{3+} angles close to 180° and both bridging oxygens belonging to the same coordination polyhedra of a diamagnetic ion [3].

Reference:

[1] P.V.Klevtsov and R.F.Klevtsova, J. Solid State Chem. 2, 278-282 (1970)

[2] R.F.Klevtsova and N.V.Belov, Soviet Physics-Crystallography Vol.15, No.1 July-Aug., 1970

[3] H.Ehrenberg, K.G.Bramnik, E.Muessig, T.Buhrmester, H.Weitzel, C.Ritter, J. Magn. Magn. Mater. 261, 353-359 (2003).

P06-048

THE METHOD OF DETERMINATION OF STRUCTURAL IN STRETCHED POLYMERS

Aida Martirosyan

Physical department,Yerevan State University , Yerevan, Armenia

The suggested method has high sensitivity towards structural changes occurring in substances ; it allows us to observe particularly supramolecular changes in stretched or textured polymers.In the given work, by the example of stretched polychloroprens (300%), it is shown the regularity of intercristalline distance changes along and across the stretched axes, depending on the medium density of the stretched sample. If in the three – block interferometer we put a stretched polymeric film on the way of one of the split X-ray beams and get moir patterns in two positions – along and across the stretching axes, according to the formula $\delta = \frac{(l - l_0)}{l_0}\frac{\lambda}{D} + \delta_0$ (l and l_0 are the distances between moiré stripes, received from the interferometer with and without the sample, accordingly; D- is the sample thinckness; λ is the wave length of the falling X-ray radiation; δ is the decree-ment of the refractive index of air), it will be possible to determine the decrement of X-ray beams, and to calculate the density alond and across the stretching axes of polymer. The density was defined according to the formula $\rho = 3{,}67 \cdot 10^{-11}\frac{A}{Z}\frac{\delta}{\lambda}$, where A and Z are the atomic weigt and the full number of electrons in the atom, accordingly .

The relation of the calculated densities is back proportional to intercrystalline distances along and across the stretching axes of the polymeric film (irradiated volumes are equal in both cases) : $V_1 = V_2 = \frac{N_1 m_{kr} + N_1 m_{am}}{\rho_1} = \frac{N_1 m_{kr} + N_2 m_{am}}{\rho_2}$, where N_1 and N_2 are the numbers of crystalline and amorphic fields in the irradiated area, along and across the stretching axes, accordingly, m_{kr} and m_{am} are the masses of crystalline and amorfic unit sections, accordingly, ρ_1 and ρ_2 are the medium densities along and across the stretching axes. Taking into account the fact that the intercrystalline distance is $d = \frac{t}{N_i}$, where *i*= 1,2,… , and it is the length of the irradiated section, from here it follows that $\frac{d_1}{d_2} = \frac{\rho_2}{\rho_1}$. In the given method the accuracy of the density definition is 10^{-4}-$10^{-5}\frac{g}{cm^3}$.

P06-049

CRYSTAL ENGENEERING OF NEW 4,4'-BIPYRIDINES AND RELATED COMPOUNDS

Olexii V. Gutov, Eduard B. Rusanov, Alexander N. Chernega, Mark I. Povolotskii

Institute of Organic Chemistry NAS Ukraine, Murmanska st. 5, 02094, Kyiv-94, Ukraine (AVGutov@mail.ru)

4,4'-bipyridine derivatives are widely used on the practice as the electrochromic materials, electron transfer mediators, biosensors, matrices of molecular electronic devices etc. The viologens, 4,4'-bipyridine tertiary salts (**I**), are the most useful of them.

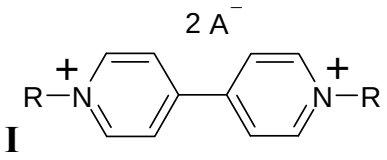

I

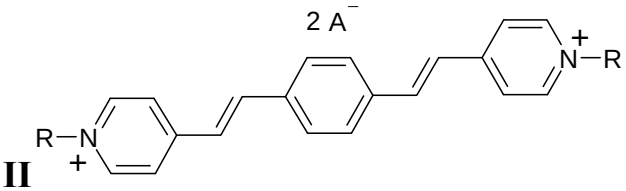

II

R = Alk, -$(CH_2)_n$-X. X – functional group.

We have recently synthesized new substituted viologens contained various functional groups (amide, amino, urea, carboxylic etc), conjugation-extended viologen analogues (**II**) bearing stilbene motif as a spacer between the pyridine moieties and some other 4,4'-bipyridine derivatives. Single-crystal X-ray diffraction was used for the determination of the molecular and crystal structure peculiarities of these compounds. It was found that in the most cases pyridine moieties of viologens and their analogues are coplanar. But there are also some exceptions that demonstrate twisted bipyridine structures. X-ray diffraction has showed that the viologens bearing hydrogen-contained functional groups usually formate intermolecular chains, helices or nets by different types of hydrogen bonds.

Spectral and optical properties of the all new compounds were studied. It was found that the extended viologen-analogues demonstrate strong luminescence properties in contrast to the corresponding original viologens.

P06-050

COCRYSTALS OF OXALIC ACID WITH DERIVATIVES OF TRICYCLIC QUINAZOLONE-4

Akmal Tojiboev,[a] Kambarali Turgunov,[a] Bahodir Tashkhodjaev[a]

[a]*Institute of Chemistry of Plant Substances, Academy Sciences of Uzbekistan, Tashkent, Uzbekistan.*

The design of organic solids by crystal engineering is presently of high interest [1]. Tricyclic quinazoline derivatives are potentially valuable synthons in crystal engineering: their electron donating nitrogen atom holds out the promise of different complexes with a range of electron acceptors.

Recent x-ray investigations of crystals obtained by cocrystalization of tri-, tetra- and pentamethylene-3,4-dihydroquinazolin-4-one homologues with oxalic acid shows that in the case of first two homologues cocrystal structures is formed without protonation of quinazolin-4-one molecule in the ratio 2:1, in contrast to first crystallization of pentamethylene-3,4-dihydroquinazolin-4-one with oxalic acid gives salt type crystals in the 1:1 ratio. In this case protonation occurs through nitrogen atom of quinazolone molecule and it reflects in changing of some bond lengths in the molecules of quinazoline and oxalic acid.

For comparison to first structures also the crystals of 2,3-pentamethylene-3,4-dihydroquinazolone-4 hydrochloride oxalic acid is obtained and structure is investigated.

Such research of a structure of this cocrystals of biologically active tricyclic derivatives of quinazoline [2] are important in crystal engineering terms since they offer the possibility of designing new materials through control of hydrogen bonding

Reference:

[1] Desiraji, G.R. Crys.Engineer. The Design of Organic Solids, Elsevier: Amsterdam, 1989.
[2] Shakhidoyatov, Kh.M. Quinazolin-4-one and their application. Tashkent: Fan, 1989.

P06-051

CRYSTAL STRUCTURES OF TWO ALIPHATIC AMIDASES AmiE AND AmiF FROM *HELICOBACTER PYLORI* REVEAL A CONSERVED CATALYTIC TRIAD

Wen-Ching Wang, Chiu-Lien Hung, Cheng-Yu Chen, and Yu-Wen Hua

Institute of Molecular and Cellular Biology and Department of Life Science, National Tsing Hua University, Hsinchu, Taiwan

Helicobacter pylori AmiE and AmiF are two aliphatic amidases and belong to members of the nitrilase superfamily. The crystal structure of AmiF was solved to 1.75 Å resolution using single-wavelength anomalous dispersion methods. The structure consists of a homohexamer related by 3-fold symmetry in which each subunit has an α-β-β-α four-layer architecture characteristic of the nitrilase superfamily. One exterior α layer faces the solvent, whereas the other one associates with that of the neighbor subunit, forming a tight α-β-β-α-α-β-β-α dimer. The apo and liganded crystal structures of an inactive mutant C166S were also determined to 2.50 and 2.30 Å, respectively. These structures reveal a small formamide-binding pocket that includes C166, E60, and K133 catalytic residues, in which C166 acts as a nucleophile. The crystal structure of AmiE was also solved to 2.38 Å resolution with molecular replacement methods. The AmiE structure also reveals the homologous architecture and conserved catalytic residues (C165, E59, and K133). Molecular dynamic simulations show that the conserved triad has minimal fluctuations, catalyzing the hydrolysis of a specific nitrile or amide in the nitrilase superfamily efficiently.

P06-052

POLYTYPE TRANSFORMATION DURING NITROGEN DOPING OF SiC CRYSTALS

Jinli Chen[a] and Zhe Chuan Feng[b,*]

[a] *Physics Department, National University of Singapore, Singapore 117542;* [b] *Institute of Photonics & Optoelectronics and Department of Electrical Engineering, National Taiwan University, Taipei, Taiwan 106-17, ROC.*

** E-mail: zcfeng@cc.ee.ntu.edu.tw*

SiC, because of its excellent properties, is very attractive in high power, high frequency, and high temperature electronic and optoelectronic device applications, including as substrates for III-Nitrides materials and devices. It has been noticed recently that polytype transformation in SiC crystals has large impact on the quality of SiC-based materials and microelelctronic devices. The occurrence of stacking faults (SF) and the polytype transformation in SiC thin films or bulk wafers will cause severe problems in the devices. In deed, the polytype transformation is also a type of stacking fault - periodical stacking fault. The uncontrolled polytype transformation in SiC wafers could degrade micro-electronic device properties. On the other hand, if polytype transformation can be controlled, it may lead to new devices based on the heterojunction between different polytypes.

In this paper, we study the structural variations of a set of SiC bulk crystal wafers prepared by Physical Vapore Deposition (PVD), with different Nitrogen (N) doping levels. The initial growth conditions were used to produce 6H-poly type SiC, which has been approved by high resolution X-ray diffraction (HR-XRD), Raman scattering (RS) and high resolution transmission electron microscopy (HR-TEM). However, when extreme high N-dopants were applied, the obtained wafer was found with 4H-polutype features. Experimental results from HRTEM, RS and HR-XRD measurements are presented in details for above observations. We propose a mechanism for the experimental findings. A possible reason of the polytype transformation is that the introduction of N enhanced the formation of clusters on the growing surface which act as nucleation centers of other polytypes or affects the reaction surface C/Si ratio.

P06-053

FORMATION OF LARGE LANTHANIDE CLUSTER HAVING CHIRAL LIGANDS AND THEIR MOLECULAR ASSEMBLY IN THE CRYSTALLINE STATE

Chizuko Kabuto [a)], Kenji Omata [b)], Kuninobu Kabuto [b)], and Yoichi Sasaki [c)]

[a)]Research and Analytical Center for Giant Molecules and [b)]Graduate School of Science, Tohoku University, Aramaki, Aoba-ku, Sendai, 980-8578, [c)]Graduate School of Science, Hokkaido University, Kita-ku, Sapporo, 060-0810

It is well known that the structures of lanthanide-based supramolecular systems are hardly predictable and often quite peculiar. Recently we reported an unprecedented tetrahedral cage-like of lanthanide cluster $[La^{III}_{18}(D\text{-bpba})_{18}(H_2O)_{36}]Cl_{18}$ {D-bpba = *N*,*N*'-bis(2- pyridylmethyl)-*N*,*N*'-1,2-ethanediyl-bis(D-alaninate)} **1**, revealed by X-ray crystallographic study. To the best of our knowledge, **1** is the largest lanthanide cluster so far reported not only in the number of metal ions but in the size of cluster (Figure 1). This octadecamer cluster is built up with twelve *cis*- and six *trans*-complexes, where the bpba ligands coordinate in the *cis* and *trans* position with respect to the two pyridines, respectively.

Another interesting feature is the formation of the trinuclear core in **1**, being the smallest assembled unit utilizing the carboxylate-bridging mode. Very recently we found out that the similar trinuclear core is formed in various kinds of $M^+[Ln(pdta)\ (H_2O)_2]^-$ complexes **2** {pdta = propylenediamine-*N*,*N*, *N*',*N*'-tetraacetate}. Furthermore the trinuclear core of **2** forms a hexamer unit via M^+ ion, eventually forming a two-dimentional network architecture in the crystalline state (Figure 2). Since no such assembly has been observed in Ln(etda) {edta = ethylenediamine-*N*,*N*, *N*',*N*'-tetraacetate}, we consider that the chirality of the ligand might be essential for the formation of the trinuclear core and for the large cluster formation.

We wish present and discuss here the details about the crystal structures of lanthanide complexes **1** (X = Cl, Br) and **2** (M = Na, K; Ln = Pr^{III}, Sm^{III}, Eu^{III}, Gd^{III})

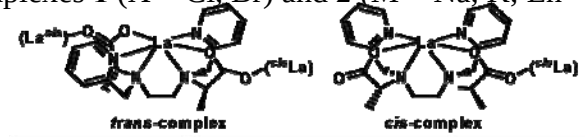

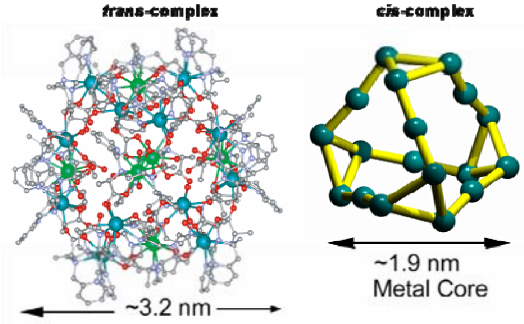

Figure 1: La(bpba)

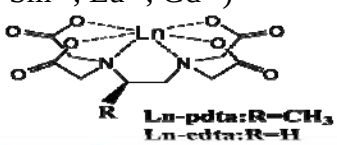

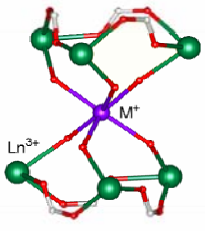

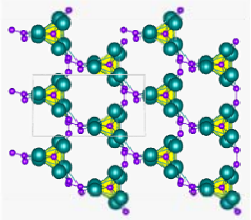

Figure 2 : Ln(pdta)

P06-054

HOST FRAMEWORK OF INCLUSION CRYSTAL OF 1,1,2,2-TETRAKIS(4-CARBOXYPHENYL) ETHANE

Michiko Iriyama[a], Natsumi Sakuma[a], Hidehiro Uekusa[a], Natsuki Amanokura[b], Masami Kaneko[b]

[a]*Department of Chemistry and Materials Science, Tokyo Institute of Technology, Japan*
[b] *Nippon Soda Co.,Ltd.*

Tetrapodal organic host molecule, 1,1,2,2-tetrakis (4-carboxyphenyl) ethane, TEP-COOH (Fig.1), is expected to form inclusion host framework via strong hydrogen bonding (carboxylic dimer motif) and also weak π-π interaction (phenyl group). In order to investigate the dimensionality of the host framework, the crystal structures of inclusion compounds of TEP-COOH with small solvent molecules and amines were determined by single crystal X-ray structure analysis.

As expected, methanol inclusion crystal shows two-dimensional framework with large cavity (Fig.2). The methanol molecules are connecting the TEP-COOH hosts by O-H…O hydrogen bonds. Interestingly, the TEP-COOH molecules also form a one-dimensional linear chain using carboxylic dimer hydrogen bond (Fig.3) and fill the host cavity. As seen in this structure, the connections between TEP-COOH hosts are not always directly (dimr motif), but have “joints” by guests. These structural elements of “chain”, “net”, and “joint” form variety of host-frameworks in TEP-COOH inclusion crystals.

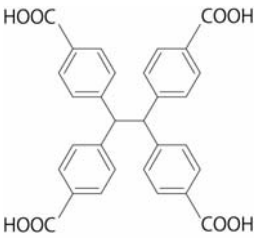

Fig. 1 TEP-COOH

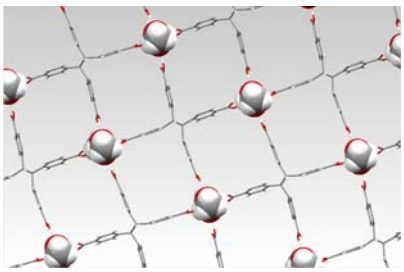
Fig. 2 net framework

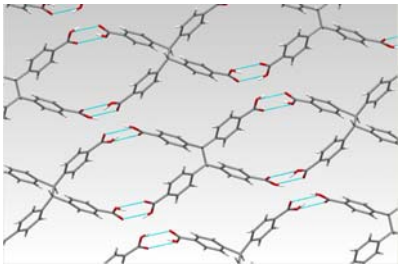
Fig. 3 one-dimensional liner chain

P06-055

CRYSTAL STRUCTURE ANALYSIS OF 1,1,2,2-TETRAKIS(3-METHYL-4-HYDROXYPHENYL)ETHANE INCLUSION CRYSTALS

Kazuyuki Toyota[a], Hidehiro Uekusa[a], Natuki Amanokura[b], and Masami Kaneko[b]

[a]*Depertment of chemistry and materials science, Tokyo institute of technology, Tokyo*
[b]*Nippon Soda Co.,Ltd*

Enclosed in the host frameworks, physical properties of guest molecule such as solubility or guest release speed can be controlled by inclusion mode. 1,1,2,2-tetrakis (4-hydroxyphenyl)ethane, TEP, is known as a tetrapodal flexible host molecule which crystallizes with small guest molecules such as organic solvents.

In our previous study, three characteristic host frameworks were recognized in TEP inclusion crystal, which governed guest release properties. We focused on a TEP derivative, 1,1,2,2-tetrakis(3-methyl-4-hydroxyphenyl)ethane, TEOC (Fig.1), in which the methyl group next to hydroxy group deteriorates the hydrogen bonding capability. It is of interests to investigate the effect of methyl group to the framework structure and guest inclusion ability of TEOC comparing with TEP inclusion crystal.

Unexpectedly, crystal structure analysis revealed that TEOC-acetone and TEP-acetone inclusion crystals have similar structure. Also, in the case of TEOC-methanol (Fig.2) and corresponding TEP crystal, same 1D chain framework with guest joints was observed. Although the TEP-methanol has flat chain structure, the TEOC chain was zigzag shape due to steric effect of methyl group, and additional host molecules were attached to the chain. From these results, the influence of methyl substitution would be limited if the host framework has enough cavity around itself.

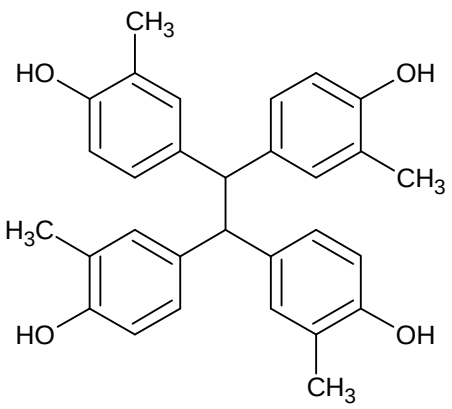

Fig. 1

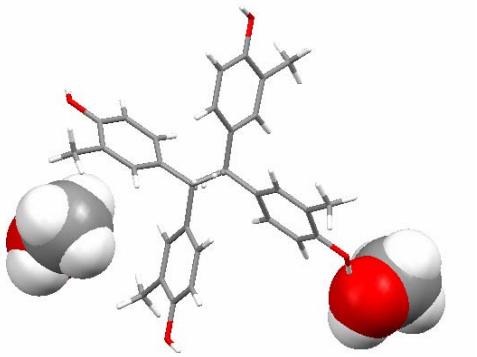

Fig. 2

P06-056

STRUCTURAL DIVERSITY OF [M(SCN)$_2$] FRAGMENTS WITH N,N'-BISPYRIDINE-TYPE LIGANDS, 4-BPD (4-BPD = 1,4-BIS(4-PYRIDYL)-2,3-DIAZA-1,3-BUTADIENE)

Chih-Chieh Wang,[a]* Wei-Zeng Lin,[a] Yu-Ruei Guo,[a] Wei-Ting Huang,[a] Shuen-Jie Dai,[a] Mei-Ju Ke,[a] Gene-Hsiang Lee[b]

[a]*Department of Chemistry, Soochow University,;* [b]*Instrumentation Center, National Taiwan University, Taipei, Taiwan, R.O.C.*

The Schiff base ligand, 1,4-bis(4-pyridyl)-2,3-diaza-1,3-butadiene (4-bpd), was used in the synthesis of six new coordination polymers, $[Fe_6(NCS)_{12}(4\text{-bpd})_{11}(H_2O)]\cdot(4\text{-bpd})\cdot3(H_2O)$ (**1**), $[Fe(NCS)_2(4\text{-bpd})_2]$ (**2**), $[Ni(NCS)_2(4\text{-bpd})_2]\cdot3(EtOH)\cdot(H_2O)$ (**3**), $[Ni(NCS)_2(4\text{-bpd})_2]\cdot2(EtOH)\cdot2(H_2O)$ (**4**), $[Zn(NCS)_2(4\text{-bpd})_2]$ (**5**) and $[Cd(NCS)_2(4\text{-bpd})]$ (**6**), each of them adopting a different structural topologies. Synthesis, X-ray structural determinations and thermogravimetric analyses are presented. The reaction of $FeCl_2\cdot4H_2O$, KSCN and 4-bpd afforded compounds **1** and **2**, in which the former one shows a two-dimensional (2D) [Fe_6] interpenetrating structure constructed by two T-shape terminal Fe(II) and four central square-grid Fe(II) building units and the latter one shows a 2D 4^4 square grid framework. Three symmetrically identical layers in **2** are mutually interpenetrated with a repeating ABCABC--- sequence. The reaction of $NiCl_2\cdot6H_2O$, KSCN and 4-bpd was found to be solvent-sensitive and resulted in the formation of two supramolecular isomers, compound **3**, which adopts a 2D square-grid MOF and $[Ni(NCS)_2(4\text{-bpd})_2]\cdot2(EtOH)\cdot2(H_2O)$ and compound **4**, which adopts a 3D $6^5\cdot8$ $CdSO_4$ MOF, respectively. The 2D layered MOF in **3** adopts an ABAB-- arrangement forming a 3D network with two 1D channels intercalated with solvent molecules. In **4**, the much larger intra-framework spaces of the3D NbO MOF are occupied by two other identical but independent networks, which interpenetrate the first and each other forming 1D channels intercalated with solvent molecules. The reaction of $ZnCl_2\cdot6H_2O$ or $Cd(NO_3)_2\cdot6H_2O$ with KSCN and 4-bpd afforded compound **5** with a one-dimensional zigzag chain and compound **6** with a 2D rectangle-grid layer, respectively. The rotational freedom of the diaza group of 4-bpd ligand plays an important role on the structural diversity of theses MOFs.

P06-057

STRUCTURAL DIVERSITY OF [M(SCN)$_2$] FRAGMENTS WITH BPHD (BPHD = 2,5-BIS(4-PYRIDYL)-3,4-DIAZA-2,4-HEXADIENE)

Chih-Chieh Wang,[a*] Yi-Tzu Lin,[a] Yu-Hsuan Lee,[a] Gene-Hsiang Lee[b]

[a]*Department of Chemistry, Soochow University,;* [b]*Instrumentation Center, National Taiwan University, Taipei, Taiwan, R.O.C.*

Five metal coordination polymers with interesting supramolecular architectures, $\{[Zn(bphd)_2(NCS)_2][Zn_{0.5}(bphd)(NCS)(H_2O)]\}_n$ (**1**), $[Mn(bphd)_2(NCS)_2]_n$ (**2**) $\{[Mn_{0.5}(bphd)_{0.5}(NCS)(H_2O)](H_2O)(bphd)\}_n$ (**3**) , $[Fe(bphd)_2(NCS)_2]_n$ (**4**), and $[Co(bphd)_2(NCS)_2]_n$ (**5**), (bphd=2,5-Bis(4-pyridyl)-3,4-diaza-2,4-hexadiene), have been synthesized and structurally determined by X-ray diffraction method, each of them adopting a different structural metal-organic frameworks (MOFs). Compound **1** are divided into two parts, the first part is a hexa-coordinated Zn(II) center bonded with two NCS^- and four bridging bphd ligands. A 2D layered MOF is constructed by a square-grid as the basic building unit. The second part is a five-coordinated Zn(II) center bonded with two bridging bphd, two NCS^- and one water molecule forming a 1D chain-like MOF Adjacent 2D layers are parallel arranged and penetrated by 1D chains. In compound **2**, the Mn(II) ion is hexacoordinated by two NCS^- and four bphd ligands. The bphd acts a bridging ligand to connect the metal ions forming a 2D square-grid wave-liked layer. Three identical but independent layers are mutually interpenetrated. In compound **3**, the Mn(II) ion is hexa-coordinated bonded with two NCS^-, two water molecules and two bridging bphd ligands to form 1D chains. A 3D supramolecular architecture is constructed by hydrogen-bonds among the free bphd ligand and water molecules and π–π interactions between the pyridyl rings of the bphd ligands. In compound **4** and **5**, the metal centers are bonded with two NCS^- and four bridging bphd ligands to afford a 2D noninterpenetrating square-grid layered MOF. These 2D layered MOFs adopt an ABAB arrangement forming a 3D network with two 1D channels intercalated with solvent molecules. The rotational freedom of the diaza group of bphd ligand plays an important role on the structural diversity of theses MOFs.

P06-058

CRYSTAL STRUCTURE AND VIBRATIONAL SPECTRA OF *μ*-OXO-*BIS*[TETRA(*p*-METHOXYPHENYL)PORPHYRINATOIRON(III)]

Ratchadaporn Puntharod,[a,b] Bayden Wood,[b] Don McNaughton,[b] and Kenneth J. Haller[a]

[a]*School of Chemistry, Institute of Science, Suranaree University of Technology, Nakhon Ratchasima, Thailand, 30000;* [b]*School of Chemistry, Faculty of Science, Monash University, Melbourne, Australia, 3800.*

The compound, *μ*-oxo-bis[tetra(*p*-methoxyphenyl)porphyrinatoiron(III)] was prepared following the method of Cheng (include the reference), and recrystallized by vapor diffusion of acetonitrile into a dichloromethane solution. The structure was determined from single-crystal X-ray data collected at 123 K. The space group is monoclinic C2/c: a = 17.1330(6), b = 27.1339(10), c = 18.0900(11) Å, β = 98.2980(10)°, V= 8321.7(7) Å^3, and contains four molecules of the title compound with iron atoms located on 2-fold axes. The Fe–N distances are 2.072(8), 2.078(8), 2.080(9), and 2.087(8) Å; the Fe–O distance is 1.7624(13) Å; and the Fe–O–Fe angle is 179.7(6)°. The domed five-coordinate geometry around each iron atom is entirely typical for a high-spin ferric porphyrin, and corresponds with the resonance Raman spectra which shows the oxidation state marker band (ν_4) at ~1359 cm^{-1} for high-spin iron(III) porphyrin. The ATR/infrared spectrum displays the μ-oxo Fe–O–Fe absorption at 871 cm^{-1}.

P06-059

$[H_2en]^{2+}$ CATION DISORDER IN A NETWORK OF VANADIUM POLYBORATE CLUSTERS

Aungkana Chatkon,[a] Kenneth J. Haller,[a] and Ian D. Williams[b]

[a] *School of Chemistry, Suranaree University of Technology, Nakhon Ratchasima 30000 Thailand*
[b] *Department of Chemistry, Hong Kong University of Science & Technology, Hong Kong*

Hydrothermal reaction of vanadium pentoxide, boric acid, ethylenediamine, and hydrofluoric acid (1:10:3:3) at 180 °C for 3 days gave the anionic vanadium polyborate cluster, $[V_6B_{20}O_{50}H_8]^{10-}$ which has been characterized by single crystal X-ray crystallography. Charge balance is maintained by conversion of amine groups to ammonium groups on the associated ethylenediamine molecules. The approximately S_6 cluster, which consists of a central V_6O_{18} band of six square-pyramidal vanadyl groups capped top and bottom through the basal oxygen atoms by triangular raft-like $B_{10}O_{16}H_4$ polyborate ligands, was easily located by conventional direct methods using SIR97. Electron density difference maps based on this preliminary model showed a plethora of peaks in the intercluster region. Some peaks were rational for the organic amine component, but several regions were not recognizable due to disorder of cations and solvent water molecules. Successful solution of this structure was possible through an iterative process of examination/interpretation of electron density maps followed by model building and constrained/restrained refinement. The resulting three dimensional supramolecular array of cations, anions, and solvent water molecules, interconnected by extensive hydrogen bonding will be described.

Crystal data: $\{[H_2en]^{2+}\}_5[V_6B_{20}O_{50}H_8]^{10-} \cdot 7H_2O$; *Mr* = 1766.6; light green; 0.20 x 0.25 x 0.32 mm; monoclinic; *C2/c* (No. 15); a = 20.0513(2), b = 13.4444(1), c = 21.6003(2) Å, β = 97.332(1)°, V = 5775.34(9) Å^3; Z = 4; $\lambda_{MoK\alpha}$ = 0.71073 Å; T = 200 K. Data collection: Nonius KappaCCD; 16,769 data collected; R_{merge} = 0.019; 8425 unique data; 7105 observed data ($I_o > 4\sigma(I_o)$); R = 0.048.

P06-060

A THREE-DIMENSIONAL SUPRAMOLECULAR STRUCTURE OF ZINC VANADATE: $Zn(2\text{-}EtIm)_2(VO_3)_2$

Orrasa In-noi,[a] Samroeng Krachodnok,[a] Kenneth J. Haller,[a] Herman H.-Y. Sung,[b] Fanny L.-Y. Shek[b] and Ian D. Williams[b]

[a]*School of Chemistry, Suranaree University of Technology, Nakhon Ratchasima 30000 Thailand;*
[b]*Department of Chemistry, Hong Kong University of Science and Technology, Hong Kong.*

Pale yellow crystals of the title compound were obtained from the hydrothermal synthesis of vanadium pentoxide, zinc acetate, and 2-ethylimidazole in the mole ratio 1:1:4 at 110°C for 2 days, and structurally analyzed by single crystal X-ray diffraction. The compound crystallizes in monoclinic space group $P2_1/c$ with a = 10.8319(10), b = 14.7575(14), c = 10.8554(10) Å, β = 92.821(2)°, and V = 1733.15 Å^3, T = 298(2) K. Intensity data were collected on a Bruker-Nonius Smart Apex CCD diffractometer using graphite monochromated Mo Kα X-radiation.

The structure contains polyoxovanadate chains parallel to the *b* axis, interconnected with corner-sharing ZnN_2O_2 tetrahedra to form 2D networks in the *bc* plane, with 6-membered $[Zn_2V_4O_6]$ rings and 10-membered $[Zn_2V_8O_{10}]$ rings. The strength of the layers is reinforced by strong N–H···O and weak C–H···O hydrogen bond interactions. Adjacent layers are held together via strong N–H···O hydrogen bond interactions (d[N···O] = 2.776(7) Å, d[H···O] = 1.95(5) Å) to generate a 3D supramolecular framework (**Fig. 1**).

Crystal data: $C_{10}H_{16}N_4O_6V_2Zn$; M_r = 455.52 Daltons; pale yellow crystals 0.10 x 0.15 x 0.20 mm; monoclinic; space group $P2_1/c$ (No. 14); a = 10.8319(10), b = 14.7575(14), c = 10.8554(10) Å^3, β = 92.821(2)°, and V = 1733.25; Z = 4;T = 298(2) K; μ = 2.460 mm^{-1}; d_{calc} = 1.746 Mgm^{-3}; 10642 data collected; θ_{max} = 28.31°; 4145 unique (2/m), *Rint* = 0.0696; R_1= 0.0574 and wR_2= 0.1028 for 2519 observed $Fo > 4\sigma(Fo)$; $\Delta\rho_{max,\ min}$ = 0.50, -0.44 e A^{-3}.

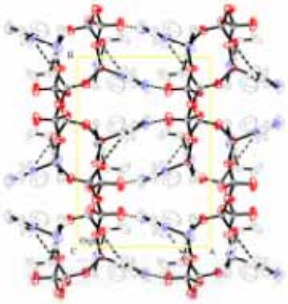

Fig. 1 Strong N–H···O hydrogen bond interactions forming a 3D network.

P06-061

LAYERED AND NETWORK STRUCTURES OF HYBRID ZINC VANADATES CONTAINING BRIDGING AZOLE LIGANDS

Samroeng Krachodnok,[a] Kenneth J. Haller,[a] Herman H-Y. Sung,[b] Fanny L-Y. Shek[b] and Ian D. Williams[b]

[a]*School of Chemistry, Suranaree University of Technology, Nakhon Ratchasima 30000 Thailand;*
[b]*Department of Chemistry, Hong Kong University of Science and Technology, Hong Kong*

Vanadium oxide and hybrid organic-inorganic vanadate compounds have been the subject of extensive study in the past decade with a wide range of applications in catalysis, Liion batteries, magnetism, and medicine. Hybrid zinc vanadates remain relatively unexplored when compared with hybrid cobalt, manganese, nickel, and copper vanadates with their demonstrated rich structural chemistry.

Herein, we report three hybrid zinc vanadates synthesized with three different types of bridging azole ligands, namely 2D $Zn_4(\mu\text{-}3,5\text{-}Me_2pz)_4(3,5\text{-}Me_2pzH)_4(V_4O_{12})$ **(1)** from 3,5-dimethylpyrazole, 3D $Zn(Im)(\mu\text{-}Im)VO_3$ **(2)** from imidazole, and 3D $Zn(\mu_3\text{-}1,2,4\text{-}tz)V_2O_5(OH)$ **(3)** from 1,2,4-triazole. All compounds were synthesized under hydrothermal conditions from mixtures of vanadium pentoxide and zinc acetate dihydrate with the different azole bases in the mole ratio 1:1:1 at 140°C for 2 days. **1** consists of the $[V_4O_{12}]_{4-}$ tetracyclovanadate sharing the corners with four dimeric zinc tetrahedra, formed by two doubly bridged μ-3,5-Me_2pz, through μ-O oxygen atoms lying across inversion centers to generate 2D layers parallel to the *ac* plane. The layer and neighbors are held together via weak C–H···X (X = O and π) hydrogen bond interactions into a 3D network. **2**, presenting imidazolate-doubly bridged binuclear zinc units and the complexes are alternately linked to disordered polyoxovanadate chains by sharing the corners. Finally, **3** shows the triply bridged μ_3-1,2,4-triazolate to zinc centers to build up cationic polymeric layers. The cationic layers are connected to the anionic polyoxovanadate layers by μ-O oxygen atoms into a 3D network. Strong D–H···O (D = N and O) and weak C–H···X (X = O and π) hydrogen bond interactions in **2** and **3** will be presented and discussed.

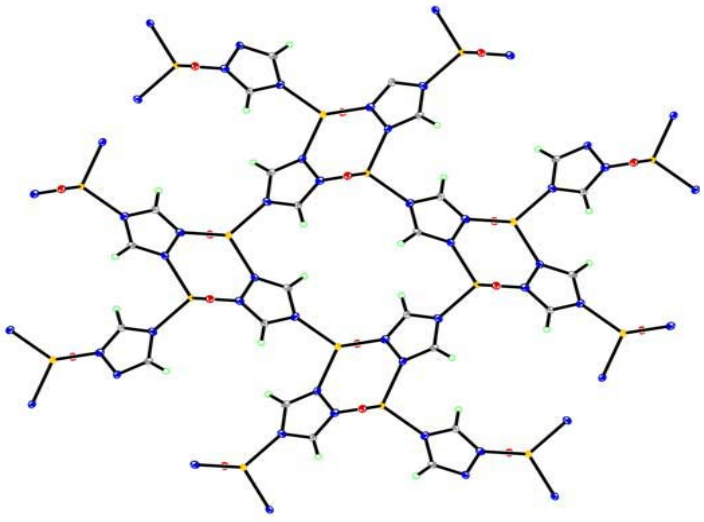

Fig. Perspective view of the cationic polymeric layers of triply bridged μ_3-1,2,4-tz in **3**

P06-062

OPEN COPPER TARTRATE BIPYRIDINE 3D FRAMEWORKS WITH VARYING WALL CHIRALITIES

Pokka K-C. Pang, Herman H-Y. Sung and Ian D. Williams

Department of Chemistry, Hong Kong University of Science and Technology, Clear Water Bay, Kowloon, Hong Kong, China. Email: pokka@ust.hk

Hydrothermal synthesis has been carried out for the chiral porous lanthanide tartrates $[Ln_2(L\text{-}TAR)_3(H_2O)_2]3H_2O$ [1] as well as open framework indium tartrates [2]. In order to further extend this we have examined the possibility for transition metals of combining tartrate with other neutral ligands which may act as spacers to create larger channels. Reaction of copper acetate, 4,4-bipyridine and L-, D/L- or meso-tartaric acids leads to a related set of 3D network polymers [Cu($_3$, ^{3}-TAR^{2-}) (bipy)], in which sheets of copper tartrate are connected by the bipyridine spacer groups. The inherent chirality of L-tartrate leads to rectangular chiral 1D channels, of dimension 4 x 6Å which can contain further uncoordinated bipyridine (left). In D/L and meso-tartrate cases similar network polymers are also formed in which the chirality of the uncoordinated C(2) and C(3) -CH(OH)- alcohol centers are varied. Furthermore differentiation of the faces of the copper tartrate sheets can create two alternating channel types, through head-to-head and tail-to-tail ordering, shown best in the case of [Cu(meso-TAR)(bipy)] (right) which has been crystallized with the alternating channels containing oxalic acid and water. The sorption selectivity of these channels in these novel porous solids is now under investigation. The Research Grants Council (HKSAR) is thanked for financial support of this work, grant 603307.

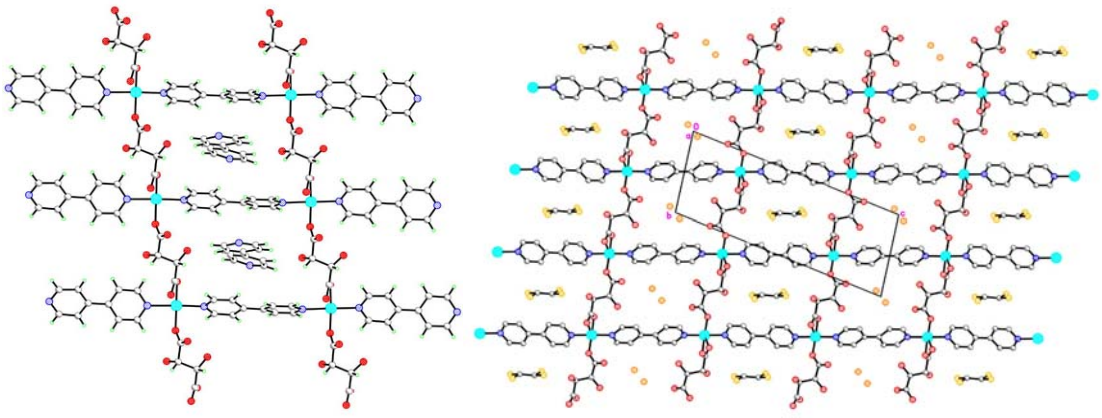

Reference:

1. S. Thushari, J.A-K. Cha, H. H-Y. Sung, S. S-Y. Chui, I. D. Williams, *Chem.Commun*., **2005**, 5515.

2. A. S-F. Au-Yeung, J.A-K. Cha, H. H-Y. Sung, S. S-Y. Chui, I. D. Williams, *Inorg. Chem. Commun*., **2006**, 9, 507.

P06-063

FLUX SYNTHESIS OF NEW TARTRATOBORATE POLYMERS AND CYCLIC OLIGOMERS

Alex S-F. Au-Yeung, Herman H-Y. Sung and Ian D. Williams

Department of Chemistry, Hong Kong University of Science and Technology, Clear Water Bay, Kowloon, Hong Kong, China. Email: alexwill@ust.hk

Molten boric acid 'flux' synthesis was initially developed by us for the preparation of borate-rich clusters [1], recently we found these conditions can lead to new bis(salicylato)borates through direct reaction of boric and salicylic acids with either inorganic or organic bases.[2] We were interested to see whether this could be extended to other chelating ligands involving carboxylate and alcohol groups. The use of chiral ligands is of further interest since their bis-chelation leads to new stereogenic center at boron. Reaction of L-tartaric acid with boric acid and KOH yields either the known monomeric salt K[B(L-TAR^{2-})$_2$]nH_2O or the new chiral chain polymer K[B(L-TAR^{4-})] H_2O depending on reaction stoichiometry. The chain polymer has a novel 3-fold helical structure. If *meso*-tartaric acid is used an analogous chain polymer K[B(*meso*-TAR^{4-})] H_2O is formed, which has 2-fold screw translational symmetry. Different reaction conditions in this case can lead to phase-pure isolation of the novel cyclic oligomer $K_4[B_4(meso\text{-}TAR^{4-})_4]$, shown below. This has a central cavity which binds a potassium ion in the solid state, which presumably assists its supramolecular formation. The *meso*-polymers and oligomers are chiral since the stereochemistry of the boron centers is the same within each molecule. The integrity of these tartratoborate chains and rings in solution and their use in further preparation of chiral solids is under investigation. The Research Grants Council (HKSAR) is thanked for financial support of this work (grant 6043-05)

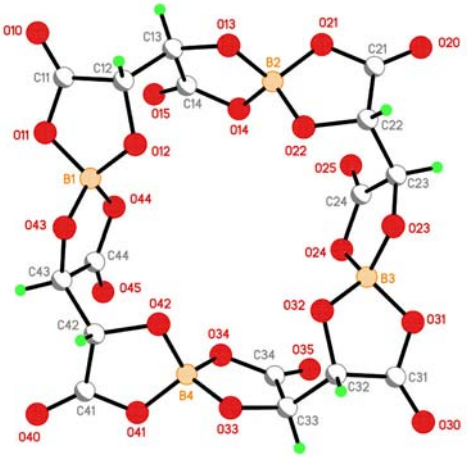

Reference:

1. I. D. Williams, M. Wu, H. H-Y. Sung, X. X. Zhang and J. Yu, Chem. Commun., **1998**, 2463.

2. A. S-F. Au-Yeung, H. H-Y Sung, M. G. Lesley, I. D. Williams Mol. Cryst., Liq Cryst submitted

P06-064

CRYSTAL STRUCTURE OF COMPLEX BIMETALLIC SALTS OF NICKEL(II): $[Ni(ter)_2(H_2O)_4][Ni(4\text{-}CNpy)_2(H_2O)_4].H_2O$ AND $[Ni(H_2O)_6][Ni(ter)(4\text{-}CNpy)(H_2O)_4].(ter)$

Sanchay J. Bora and Birinchi K. Das*

Department of Chemistry, Gauhati University, Guwahati – 781 014, India

Two supramolecularly aggregated Ni(II) compounds containing terephthalato (ter) and 4-cyanopyridine (4-CNpy) as the common ligands, *viz.* $[Ni(ter)_2(H_2O)_4][Ni(4\text{-}CNpy)_2(H_2O)_4].H_2O$ (**1**) and $[Ni(H_2O)_6]$ $[Ni(ter)(4\text{-}CNpy)(H_2O)_4].(ter)$ (**2**) have been synthesized and structurally characterized. Compound **1** is triclinic (Pī) with unit cell parameters a = 6.3355(2)Å, b = 7.1529(3)Å, c = 20.3808(7)Å, = 90.342(2)˚, = 96.227(1)°, = 114.980(2)˚, V = 830.89(5)Å^3, Z = 2, $D_{calc.}$= 1.315g cm^{-3}. The structure was solved by direct method and refined by full-matrix least squares to final *R1* = 0.0323, *wR2* = 0.0694 for 3991 reflections with I>2 (I) and 310 parameters. The asymmetric unit of **1** contains two Ni(II) centres having different coordination spheres. One of the Ni atoms contains two monodentate terephthalate dianions and four water molecules whereas the other Ni centre contains two 4-cyanopyridine ligands and four water molecules.

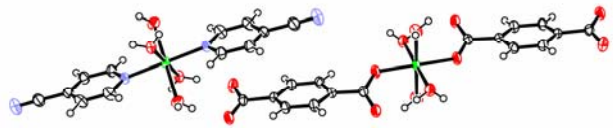

ORTEP diagram of **1**

Compound **2** is also triclinic (Pī) with unit cell parameters a = 6.2609(4)Å, b = 12.1153(9)Å, c = 15.3239(11)Å, α = 78.479(1)˚, β = 86.865(1)°, γ = 79.698(1)˚, V = 1120.36(14)Å^3, Z = 2, $D_{calc.}$ = 0.942g cm^{-3}. The structure refined to final *R1* = 0.0291, *wR2* = 0.0774 for 5063 reflections with I>2 (I) and 409 parameters. Like **1**, the asymmetric unit of **2** also contains two different Ni(II) centres. The neutral part which consists of a Ni^{2+} ion surrounded by a monodentate terephthalate dianion, an N-bound 4-cyanopyridine and four water molecules as ligands, while the positive charge on the $[Ni(OH_2)_6]^{2+}$ cation is compensated by the presence of an uncoordinated terephthalate dianion in the crystal lattice.

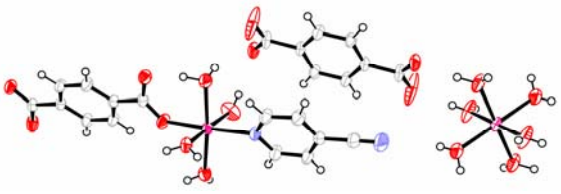

ORTEP diagram of **2**

Extensive hydrogen bonding interactions in both crystal structures lead to interesting supramolecular architectures for **1** and **2** in the solid state.

P06-065

A NOVEL 3D INTERPENETRATING FRAMEWORK CONTAINING 1D LADDERS COORDINATION POLYMERS WITH MIXED ORGANIC LIGANDS: $[Ni_2(H_2O)_2(BDC)_2(bpp)_2]$

Chia-Her Lin* and Tai-Hsing Tsao

Department of Chemistry, Chung-Yuan Christian University, Chungli 320, Taiwan
**Corresponding author. Tel: +886-3-2653315; Fax: +886-3-2653399*
E-mail address: chiaher@cycu.edu.tw (C. H. Lin).

A novel nickel (II) coordination polymer, $[Ni_2(H_2O)_2(BDC)_2(bpp)_2]$ (**1**) (BDC = BDC = 1,4-benzene dicarboxylate anion; bpp = 4,4'-trimethylene dipyridine), was synthesized by hydrothermal reaction and structurally characterized. Single crystal X-ray diffraction showed that **1** consists of a 3D framework contracture by interpenetrated 1D ladders. The luminescent and magnetic properties of **1** in the solid state were investigated.

Keywords:
Nickle, Crystal structure; Magnesium; Photoluminescence, hydrothermal Synthesis

P06-066

HYDROTHERMAL SYNTHESIS OF METAL HYDROXIDE IMIDAZOLIDE 3D FRAMEWORK POLYMERS

Fion T-Y. Yeong, Fanny L-Y. Shek, Herman H-Y. Sung and Ian D. Williams

Department of Chemistry, Hong Kong University of Science and Technology, Clear Water Bay, Kowloon, Hong Kong, China.

Metal imidazolides $[M(Im)_2]$ are metal organic analogues of SiO_2 and possess tetrahedral metal centers with bent ligand bridges. They can be found in a variety of topological networks similar to zeolites. (K.S. Park et al, *Proc. Natl. Acad. Sci*, **2006**, 103, 10186) Little work has appeared on their hydrothermal preparation, however for zinc, cobalt and cadmium facile preparation is possible under basic conditions. Other phase types have also emerged from this work and we have now prepared three mixed imidazolide-hydroxides with open 3D frameworks $[Zn_3(2\text{-MeIm})_5(\mu\text{-OH})]$ forms I and II (framework shown below) and $[Zn_2(2\text{-EtIm})_3(\mu\text{-OH})]$. Studies of the thermal stability and sorption character of these new hybrid polymers and comparison with the $[Zn(Im)_2]$ parent materials are underway. The Research Grants Council (HKSAR) is thanked for financial support of this work.

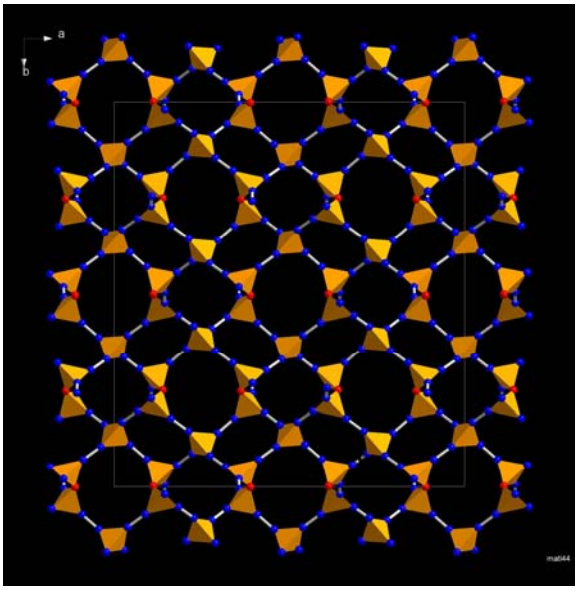

P06-067

SOLVING ZEOLITE STRUCTURES FROM POWDER DATA USING DENSITY BUILDING FUNCTIONS AND HISTOGRAM MATCHING

Chris Gilmore, Gordon Barr, Wei Dong, Andrew Parkin, Duncan Sneddon, Chick Wilson

Department of Chemistry, University of Glasgow, Glasgow G12 8QQ,UK.

Cambridge Structural Database (CSD) searches can produce thousands of 'hits' especially if a simple fragment is used, and as a result processing and interpreting the results becomes a considerable task, and one in which it is easy to make mistakes. Cluster analysis using dendrograms, metric multidimensional scaling and suitable visualization tools can reduce the workload to a few hours with minimal user intervention, and minimal user bias. The real beauty of the method is in its interactivity and scalability: it allows you to go from an overview of the entire dataset and easily spot any outliers or errors, to the ability to ‘drill down’ within a cluster, looking at more and more detailed differences between different fragments. The computer program we have developed to do this is dSNAP [1]. The formalism and the associated program are also invaluable in a crystal engineering environment since it can readily identify the basic motifs in a structure and how they pack in the unit cell. It is available free of charge to all interested researchers from the web site http://www.chem.gla.ac.uk/snap

Reference:

[1] G. Barr, W. Dong, C. J. Gilmore, A. Parkin and C. C. Wilson *J. Appl. Cryst,*. 2005, **38**, 833-841.

P06-068

AN OBSERVATION ON THE WETTING PHENOMENON OF GALLIUM NANO DROPLETS BY X-RAY DIFFRACTION

Masanori Tanaka,[a] Takehiro Noda, [a]Osami Sakata,[b]Hikaru Terauchi,[a] and Isao Takahashi [a]

[a]*Faculty of Science and Technology, Kwansei Gakuin University Sanda, Japan;* [b]*Japan Synchrotron Radiation Research Institute, Sayo, Japan.*

Precise measurements of the contact angle of droplet provide us fundamental information on wetting phenomenon. Instruments for macroscopic observation like an optical microscope with digital view-recording devices have usually been adopted for determining the "macroscopic" contact angle. However, wetting is a cooperative phenomenon associated with microscopic interaction between substrate and numerous atoms. In order to comprehend this phenomenon, it is thus critical to study the average contact angle and its deviation from it for many droplets which consist of a relatively small number of atoms. Size dependence of contact angle of metallic substance gives us the essential knowledge which would encompass all the mechanical properties of electrons dispersed into anion-core gels. In the present study, we evaluate the average contact angle of nano-sized Ga droplets formed on an inert diamond substrate by surface-sensitive X-ray diffraction techniques. So as to avoid the oxidation of Ga surface, whole the process was performed in an ultra high vacuum chamber installed on a multi-axis diffractometer BL13XU, SPring-8. After annealing the diamond(100) substrate at 500^{o}C, gallium was evaporated onto the substrate to form a 3.5nm thick Ga layer. As surface-sensitive X-ray diffractions, we exploited X-ray Reflectivity (XR) and Grazing Incidence Small Angle X-ray Scattering (GISAXS). The combination of XR and GISAXS is quite useful to construct the average shape of nano-sized droplets, since electron density profile normal to the substrate surface is precisely obtained by XR and that in lateral direction is easily evaluated from GISAXS.

We carried out the measurements of XR and GISAXS at various temperatures up to 500^{o}C, where X-ray wavelength was 0.08nm and degree of vacuum was maintained better than 1.67X10^{-5}Pa. From the fitting procedures on XR and GISAXS data, the average contact angle of nano-sized Ga droplets shows about 110 degrees, which is substantially smaller than that of macroscopic Ga droplets. Considerable variation in electron density and size of the droplets is also confirmed.

P06-069

BEAM COMPRESSION AND LATTICE-CONSTANT VARIATIONS IN CURVED X-RAY CAVITY

S.-Y. Chen,[a] Y.-Y. Chang,[a] Y.-J. Liu,[a] M.-T. Tang,[b] Yu. P. Stetsko,[b] H.-H. Wu,[a] Y.-R. Lee,[a] M. Yabashi,[c] B.-Y. Shew,[b] and S.-L. Chang[a]

[a]Department of Physics, National Tsing Hua University; [b]National Synchrotron Radiation Research Center, Hsinchu, Taiwan, 300, R.O.C.; [c]Spring-8/RIKEN Mikazuki, Hyogo 679-5148, Japan

We report the unusual optical effects for curved multi-plate x-ray crystal cavities consisting of compound refractive lenses (CRL). X-ray (12 4 0) back diffraction from these monolithic silicon crystal devices clearly showed interference fringes due to cavity resonance. However, the expected focusing effect from the CRL was not observed, but rather beam compression was detected. That is, the incident x-ray beam size of about 90 μ m across the CRL was reduced to 20 μ m. The beam size remained the same at different positions after the cavity. Namely, a small sized parallel x-ray beam was produced. The origin of this beam compression mechanism is believed to due to the competition between the multiple back reflection of the crystal cavity and the focusing of the CRL, in addition to crystal absorption.

On the other hand, when the photon energy was close to the exact energy for cavity resonance, the exact energy required for resonance became very sensitive to the irradiated position on the cavity crystal. By tuning the crystal position along the wafer surface-normal for the back diffraction, the nominal exact energy could vary. This meant the variation of the lattice constant at different crystal positions came into play. In turn, the analysis of the change in the crystal positions and nominal exact energy allowed us to determine the local lattice deformation. The lattice-constant variation resolved is of the order of 10^{-7} Å.

P06-070

DETERMINATION OF LATTICE PARAMETERS OF $FeSi_2$/Si QUANTUM DOT NANO-STRUCTURES BY X-RAY BRAGG-SURFACE DIFFRACTION

Yi-Wei Tsai,[a] Chia-Hung Chu ,[a] Wen-Ching Sun,[a] and Shih-Lin Chang[a]

[a]*Department of Physics, National Tsing Hua University, Hsinchu, Taiwan, R.O.C.*

The method of using Bragg surface diffraction (BSD) for structural investigation of thin film/substrate systems has recently been introduced and demonstrated successfully for interfacial strain analysis. With the BSD method, the strain field can be determined by measuring the variations of lattice constants of iso-strained substrate layers at different penetration depths. This method is now applied to investigate the strain field of quantum dots nano-structures of $FeSi_2$/Si. Choosing one secondary diffracted beam along the interface (parallel to the surface of the substrate) between the quantum dots and the Si substrate, the diffraction images of the secondary diffraction, recorded on a charge coupled device (CCD), provide the information of the interfacial structures. A theoretical model of X-ray scattering in quantum dots at the Bragg-surface diffraction geometry will be also reported.

P06-071

CRYSTALLINE LAMELLAE IN THIN FILM OF BIODEGRADABLE POLYMER POLY(HYDROXYBUTYRATE) STUDIED BY SURFACE X-RAY DIFFRACTION

Shota Mukoyama,[a] Kazuhiro Yamasaki,[a] Hikaru Terauchi,[a] Harumi Sato,[a] Yukihiro Ozaki,[a] Isao Noda,[b] and Isao Takahashi[a]

[a] *Faculty of Science and Technology, Kwansei Gakuin University, Sanda, Hyogo 669-1337, Japan ;*
[b]*The Procter & Gamble Company, 8611 Beckett Road, West Chester, Ohio 45069, USA*

Much attention has been paid to biodegradable polymers due to its biodegradability and presumably due to the anxiety for our society deeply relying upon the limited petroleum. Poly(hydroxybutyrate) (PHB) is one of the most studied polymers which shows decent thermo-plasticity, high crystallinity and prompt biodegradability. A PHB-based random copolymer Poly(hydroxybutyrate-*co*-hydroxyhexanote) (P(HB-*co*-HHx)) indicates remarkable flexibility because of its lower crystallinity. Our recent study revealed that inter- and intra-molecular interaction of C-H…O type along the *a*-axis plays an essential role for crystallization, melting and morphology of lamellae crystallites embedded in bulk matrix [1]. In the present study, we focus on crystalline lamellae in ultrathin films of PHB and that of the random copolymer, formed on Si substrates. The thin films were prepared by spin-coating method with hot chloroform solutions. We exploit two surface-sensitive X-ray diffractions to characterize the polymer layers: one is X-ray reflectivity which affords nano-meter level information on surface morphology such as average thickness, surface roughness and electron density; the other is the grazing incidence X-ray diffraction (GIXD) for investigating crystalline objects in surface region e.g., crystallinity, average crystallites size and preferred orientations. PHB thin films with a smooth surface are abtained only for samples with thickness less than 60nm. For P(HB-*co*-HHx), we form a fairly flat surface even for the films with 120nm thick. From the GIXD data collected at various temperatures up to 130^{o}C, we find that unstable-type lamellae which would be referred to as loosely packed lamellae display a novel thermal behavior in the surface region. In addition to the measurements stated above, we study surface morphology of atactic PHB in which no crystallite is grown. It would afford a clue to understand the effects of crystallinity on surface morphology.

Reference:

[1]H.Sato et al., Macromolecules, 39(2006) 1525-1531

P06-072

CORE-SHELL COMPOSITION AND ITS INFLUENCES ON THE PROPERTIES OF MATERIALS

Vo Vong [a], Luu Tien Hung[a] and Michael Hietschold[b]

[a] *Laboratory of Electron Microscopy,Institute of Materials Science,Vietnamese Academy of Science and Technology;*[b] *Institute of Physics , Technical University of Chemnitz,Germany*
18 Hoangquocviet str. Caugiay Hanoi Vietnam

In recent years, nano materials have been widely applied in many fields of high technology . Besides scientists have been using the nano materials,which have core-shell composition, in order to treat the dangerours diseases such the cancer. In these materials there are two parts : The core and the shell. The first is the main one, which is a medicament or a chemical substance . The second plays the role of showing the way. In other words , it directs the core (medicament) to target (cancer cells).

The nano materials are fabricated by special method and we received many sorts of materials,which have core-shell composition. They are : 1) the volume of the core and the shell is the same 2) the volume of the core is biger than of the volume of the shell 3) vice versa ,the volum of the core is smaller than of the volum of the shell.

In the paper we will present the details about preparation of these nano materials and discuss application in high technology and the life .

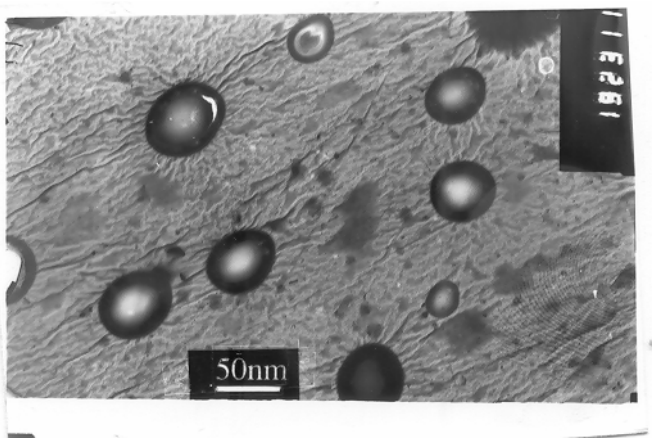

TEM image of the $Sn(y)O_x$ sensor –material,which have core-shell composition

P06-073

GLASS TRANSITION TEMPERATURE OF ULTRATHIN POLYMER UNDER ULTRASLOW HEATING: AN X-RAY REFLECTIVITY STUDY ON POLYSTYRENE FILMS SUPPORTED ON Si

Chun-Ming Yang, Hikaru Terauchi, and Isao Takahashi

Faculty of Science and Technology, Kwansei Gakuin University, Gakuen 2-1, Sanda 669-1337, Japan

For glass-forming polymers, glass transition temperature (T_g) is known to vary with heating/cooling rate. According to the cooperative molecular motion theory, the possible lowest glass transition temperature T_g^L for bulk sample can be as low as ((T_g determined by experiments with conventional cooling rates) – 50K). Whole the picture of glass transition phenomenon would finally be understood in a hyper-phase diagram spanned by a combination of non-thermodynamic variables like “time” and conventional thermodynamic variables including pressure and temperature. For thin polymer films, “thickness” and “substrate” should emerge as additional non-thermodynamic parameters. In the present study, we perform precise measurements on X-ray reflectivity (XR) of thin polystyrene (PS) films under various heating rates. Atactic PS thin layers were prepared by spin-coating method with Si substrates and toluene solutions. Before the XR measurements, samples were annealed above bulk T_g for 12 h. The range of film thickness investigated is between 4 nm and 60 nm, which are comparable to radius of gyration. Typical heating rate is 0.05 K/min. and 0.5 K/min., both of which fully elucidate the temporal character of glass transition of ultrathin PS layers supported by Si(100) wafers. From the thickness vs. temperature curve obtained under various heating rates, substantial reduction in T_g is clearly observed for the sample with 5.8 nm thick; the glass transition temperature is evaluated as 333K (= T_g(Bulk) – 40 K) with heating rate of 0.05K/min. Systematic variations in T_g with heating rate and thickness are also confirmed.

P06-074

CRYSTAL STRUCTURE OF β-LACTOGLOBULIN AND VITAMIN D COMPLEX. IDENTIFICATION OF A SECOND BINDING SITE FOR VITAMIN D: A THERMAL INDEPENDENT SITE.

Hong -Hsiang Guan[2,3], Ming -Chi Yang[1], Ming -Yih Liu[2], Jinn -Moon Yang[1],Wen -Liang Chen[1], Simon JT Mao[1] and Chun- Jung Chen[2]

[1]*College of Biological Science and Technology, National Chiao Tung University, Hsinchu, Taiwan*

[2]*Life Science Group, Research Division, National Synchrotron Radiation Research Center, Hsinchu, Taiwan*

[3]*Institute of Bioinformatics and Structural Biology, National TsingHua University, Hsinchu, Taiwan.*

β-lactoglobulin (β-LG) is a bovine milk protein sensitive to thermal denaturation belonging to the lipocalin family. It is predominantly a β-sheet configuration containing nine antiparallel β-strands from A to I, strands A-D form one surface of the barrel (calyx) while strands E-H form the other. The only α-helical structure with three turns is at the C-terminus, which follows strand H lying on the outer surface of the calyx. A remarkable property of the calyx is its ability to bind hydrophobic molecules such as retinol, fatty acids, and vitamin D. Whether there is another binding site for vitamin D is physiologically important, but remains controversial. The opening of calyx (located at the EF loop) is responsible for the entrance of vitamin D and such binding ability of β-LG is conformationally and pH dependent known as Tanford transition. In the present study, we observed that the molar binding ratio between vitamin D to β-LG was 2:1 at pH above the Tanford transition, but for retinol and palmitate was 1:1. However below the transition (pH 2-6), only vitamin D was able to retain the binding with a ratio almost 1:1. We also observed that heating β-LG above 80°C abolished its binding to retinol and palmitic acid, while heated β-LG (heated at 100°C for 16 min) still binding to vitamin D_3. Titration curve shows the maximal binding ratios of heated β-LG to vitamin D_3 to be 1:1. Taken together, the data suggest that there is a second binding site beyond the calyx that is specific only for vitamin D_3, but not for retinol and palmitate. Using synchrotron X-ray diffraction on the crystal of β-LG-vitamin D_3 complex (at a resolution 2.4 Å, R = 0.2369, R_{free} = 0.2989; space group $P3_221$ with unit-cell parameters $a = b$ =53.78 Å and c = 111.58 Å), we demonstrate that one vitamin D_3 molecule bound to the calyx (central binding site) of β-LG and the other bound to a specific remote exosite. It is located near the surface of C-terminal -helix (residues 130-141) and -strand I (residues 146-151), where the OH group of vitamin D3 interacts with 1 N of Arg-148. This binding domain provides strong van der waals forces to stabilize vitamin D_3 binding, whereas the charged group of Asp-137, Lys-138, and Lys-141 congregate and stick outside of the binding pocket and therefore enhance the hydrophobic interaction between the exosite and vitamin D_3. The significance and physiologic role of this additional binding site is discussed in the light of vitamin D supplemented milk.

P06-075

NANOSTRUCTURED FILMS CONSTITUTED OF TiO_2 AND SnO_2 PREPARED BY MEANS OF SPRAY PYROLYSIS

Pham-Van Nho[a], Pham-Hoang Ngan[b], Tran-Kim Cuong[c]

[a] *Applied Physics Lab, Hanoi University of Science, and* [b] *Faculty of Engineering Physics and Nano Technology, College of Technology, Vietnam National University, Hanoi;* [c] *Faculty of Physics, Dalat University, Dalat City,Vietnam*

Nano TiO_2 is one of the perspective materials in nanoscience and nano technology. This material has been effectively applied to photo catalysis for environmental purification, photo electrochemical solar cell…However, in order to heighten efficiency, nano TiO_2 is usually used in the form of as either dye sensitized or nitrogen doped materials...

In this work we present another way to enhance activities of TiO_2 materials. That is the preparation of TiO_2 in conjugation with SnO_2 using spray pyrolysis technique. The starting materials are solutions from commercial $TiCl_4$ and $SnCl_4$, which were sprayed by help of the atomizer operated by pressed air. Solutions were sprayed onto glass slide substrates preheated up to 400^oC under open air condition. At high temperature pyrolysis of chloride salts were took place resulting in the formation of the films of nano TiO_2 crystalline and SnO_2. Obtained films were characterized by XRD and SEM and photoconductivity measurement. It was found that in this method TiO_2 was deposited in anatase phase with average crystalline size of 15-20nm and photoelectrical properties of it strongly depends on both SnO_2 concentration and method of spraying constituent solutions.

This is inexpensive method but obtained results have been successfully used for manufacture of high performance UV detectors. They also can be applied to photo electrochemical solar cell based on nano crystalline TiO_2.

Corresponding Author: Pham Van Nho, nhopv@vnu.edu.vn

P06-076

STRUCTURAL STUDY OF ARSENATE INCORPORATION INTO CALCIUM PHOSPHATE HYDROXYAPATITE

Winya Dungkaew*, Weenawan Somphon**, Kenneth J. Haller*

**School of Chemistry, Institute of Science, Suranaree University of Technology, Nakhon Ratchasima,Thailand ** National Synchrotron Research Center (NSRC), Nakhon Ratchasima, Thailand*

Calcium Phosphate Hydroxyapatite ($Ca_{10}(PO_4)_6(OH)_2$, CaHAP) is a naturally occurring material as a major component of animal bones and teeth. Apatite structure $[(A^{I}_4)(A^{II}_6)((BO_4)_6)X_2]$ contains several exchangeable positions resulting in the apatite structure being tolerant to ionic substitutions. Due to this property CaHAP has been widely used as a host for heavy metal substitution for contaminant immobilization. CaHAP has also been considered as an ideal adsorbent for long term storage due to its high sorption property, high stability under reducing and oxidizing conditions, low water solubility, and low cost.

The structural study of arsenate incorporated CaHAP structure was performed. The effect of the amount of arsenate incorporation on the CaHAP structure was investigated using XRD and Ca K-edge XAS (XANES and EXAFS) techniques at the Siam Photon Laboratory of the National Synchrotron Research Center (NSRC). This study is useful in understanding arsenate immobilization using CaHAP. Arsenate immobilization occurs by incorporating arsenate into CaHAP structure at phosphate positions due to the similarity of arsenate and phosphate.

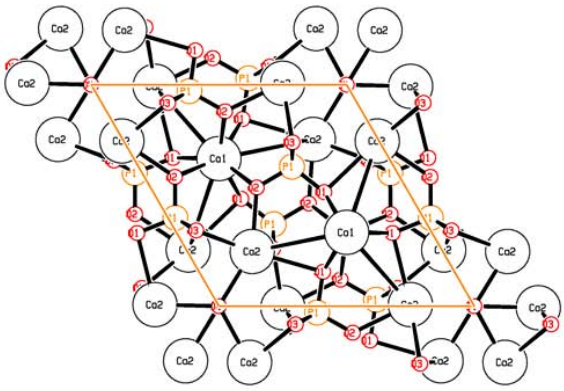

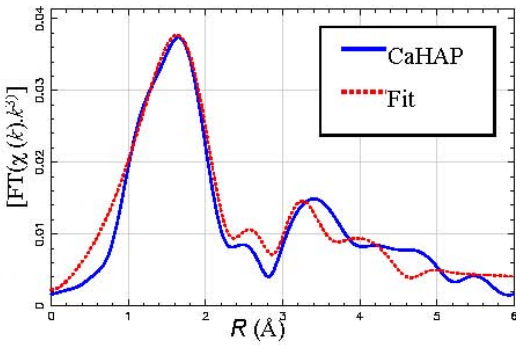

P06-077

STRUCTURAL STUDY OF COPPER INCORPORATION INTO CALCIUM PHOSPHATE HYDROXYAPATITE

Oratai Saisa-ard, [a] Winya Dungkaew, [a] Weenawan Somphon[b] and Kenneth J. Haller [a]

[a] *School of Chemistry, Institute of Science, Suranaree University of Technology, Nakhon Ratchasima 30000 Thailand.* [b] *Siam Photon Laboratory of the National Synchrotron Research Center (NSRC), Nakhon Ratchasima 30000 Thailand.*

Calcium phosphate with apatite structure [$Ca_{10}(PO_4)_6(OH)_2$, CaHAP] crystallizes in the hexagonal space group $P6_3/m$. The CaHAP structure consists of a calcium/phosphate framework surrounding a pseudo hexagonal channel as shown in the figure. The material can accept a series of cationic and anionic substitutions in its structure, both in the framework itself and inside the hexagonal channel. From this property CaHAP has been proposed for the removal of heavy metal from wastewater.

Cu^{2+} ions can ions exchange with Ca^{2+} ions in the CaHAP structure resulting in copper immobilization. Substitution of Cu^{2+} at Ca^{2+} positions affects the CaHAP structure due to their different sizes. This work studies the structure of copper incorporation into CaHAP based on XRD and Ca K-edge XAS (XANES and EXAFS) techniques.

Acknowledgement: OS and WD thank the Thai government for supporting this work through

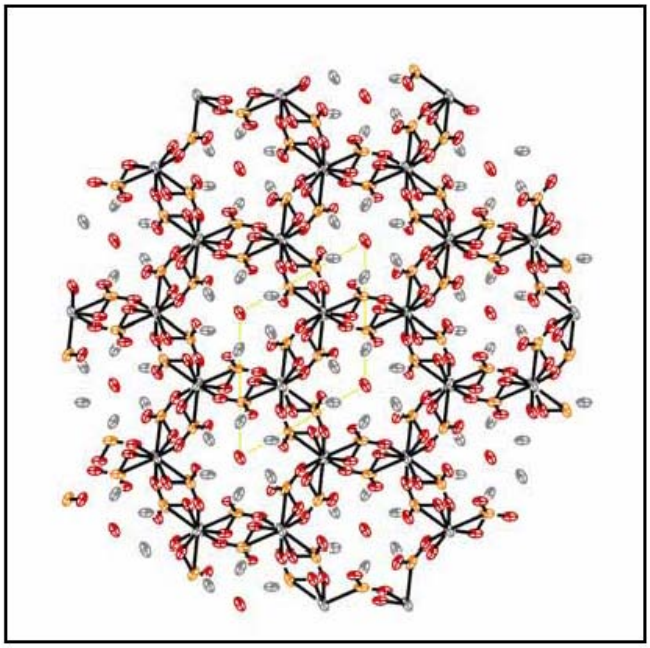

Ph.D. scholarships.

P06-078

CHROMIUM AND CADMIUM IMMOBILIZATION BY PORTLAND CEMENT SOLIDIFICATION

Weenawan Somphon, [a] Samroeng Krachodnok,[b] Angkana Kiatpichitpong [c]

[a]National Synchrotron Research Center (NSRC), Nakhon Ratchasima 30000 Thailand; [b]School of Chemistry, Institute of Science, Suranaree University of Technology, Nakhon Ratchasima 30000 Thailand; [c]Thai Pride Cement Co., Ltd., Saraburi 18110 Thailand

.

Cement-based solidification/stabilization (S/S) is an important technology used for heavy metal immobilization due to low water solubility, non-flammability, durability, and low cost of the final materials. Ordinary Portland Cement (OPC) is the most common cement binder in S/S technology. This research aims to improve understanding of the chromium and cadmium immobilization process. The mechanisms of S/S technology for toxic metal immobilization are significantly controlled by surface, near-surface, and interfacial phenomena. OPC was mixed with $K_2Cr_2O_7$ (Cr^{6+}), Cr_2O_3 (Cr^{3+}), and $Cd(NO_3)_2{\cdot}4H2O$ (Cd^{2+}). The pH value of the cation solutions was varied between 6 and 8. The mixture was cured at room temperature for 7 and 28 days, and the analyzed using XRD and SEM. X-Ray Photoemission Spectroscopy (XPS) was used for chemical analysis on the cement surface. X-Ray Absorption Spectroscopy (XAS) was then applied to powder samples to examine of the hydration state of chromium and cadmium.

P06-079

NANOCRYSTALLINE COPPER SULPHIDE: SYNTHESIS AND ITS CHARACTERIZATION

N.Vasumathi, B.B.Nayak and B.S.Acharya

Materials Characterization Dept., Institute of Minerals and Materials Technology, Bhubaneswar, Orissa, India – 751013.

Copper chalcogenides have been studied for their use as optical filter, solar cell materials and superionic materials. Although several methods like templated assisted sonochemical synthesis, hydrothermal synthesis and facile solution reaction in ethylene glycol etc have been proposed, large scale preparation of copper monosulphide in nano regime has not been successful so far. In the present investigation, the authors have modified technique proposed by Wu et al (J.Am.Chemical Soc.June-2006) to produce CuS nanospheres having size in the range of the 10nm to 250nm.

The powders were characterized by x-ray diffraction, transmission electron microscopy and laser raman spectroscopy. X-ray diffraction studies reveal the average crystallite size to be 14nm and the phase identified to be $Cu_{1.8}S$ (PDF card no 646) with hexagonal structure. Morphological study of the powder was carried with a high resolution TEM (TechnaiG20 – 200KV). Two types of particles were observed; one in the size range of 10nm to 60nm and another in the range of 150nm to 250nm, also particles were spherical in nature. Selected area diffraction pattern of these particles confirm the monophasic nature of CuS. The powder was tested for its stability at room temperature (≈ 27°C). The nano CuS powders kept at RT for 6 months show interesting result as regards the laser raman spectra are concerned. The raman spectra observed for freshly synthesized CuS and 6 months stored CuS powders were 162, 275, 479, 1453 and 172, 494, 1262, 1444 cm^{-1} respectively. The sharp band observed at 479cm^{-1} for as prepared $Cu_{1.8}S$$cm^{-1}$ shifts to 494cm^{-1} when the sample was stored at RT for 180days. Although structurally, the sample remains the same, the size of the crystallites reduces to 8.0nm. These observations have been confirmed from TEM photographs and size distribution analysis. This indicates that surface oxidation plays an important role in amorphization of the sample thereby reducing the particle size and shifting the raman peak to high wavenumber side. These results will be presented and discussed in this paper.

P06-080

X-RAY DIFFRACTION STUDY ON THERMAL BEHAVIORS OF SHAPE MEMORY ALLOY $AU_{50.5}CD_{49.5}$

Michinori Yoshikawa,[a] Genki Kikuma,[a] Takuya Ohba,[b] Hikaru Terauchi,[a] and Isao Takahashi [a]

[a]*Faculty of Science and Technology, Kwansei Gakuin University, Sanda, Japan*
[b]*Interdiscipilinary Faculty of Science and Engineering Shimane University, Matsue Japan.*

Martensitic transformation is a diffusionless transformation which is considered to serve a substantial role for both of the shape memory effect and superelasticity in Shape Memory Alloys (SMA). Although the Martensitic transformation is a cooperative phenomenon in solid states, conventional thermodynamic variables e.g., temperature, pressure, are insufficient to determine the physical properties of SMA; additional parameters like heating rate, cooling rate, ageing time, and thermal history etc., sometimes greatly affect them. $Au_{50.5}Cd_{49.5}$ is one of the most intensively studied SMA which also exhibits superelasticity. The parent phase of the CsCl-type is stable above 309K. Under cooling, it undergoes a transformation to the trigonal phase (ζ'_2 phase) at 303K. Theζ'_2 phase consists of a multi-domain structure called variant [1]. Despite the large number of published papers, information on spatial-temporal development of domain structure in bulk as well as in the surface region seems to be highly limited. In the present study, we investigate the time & temperature dependent domain formation of $Au_{50.5}Cd_{49.5}$ by exploiting X-ray diffraction techniques.

An electro-polished 112 surface of $Au_{50.5}Cd_{49.5}$ with 5mmX5mm in area was prepared to measure the (112) Bragg reflection and X-ray reflectivity. High resolution diffractometers equipped with rotating-anode X-ray generators were used (Rigaku TTR-450, SLX2000+UltraX). For measurements of temporal fluctuations, synchrotron radiation at BL13XU, SPring-8 was also used. The temperature varied from the room temperature to 350K within a precision of 0.1K. The (112) reflection is measured by longitudinal and transverse scans, usually referred to as ω scan and θ-2θscan respectively. X-ray reflectivity is collected with a very shallow angle of incidence close to the critical angle of total reflection. A peak splitting of (112) Bragg reflection and that of X-ray reflectivity is clearly observed throughout the transformation, indicating the domain formation. Inζ'_2 phase, long-tailed fluctuations in (112) reflection are observed, although the X-ray reflectivity does not show the fluctuation of this type.

Reference:

[1]T. Ohba and K. Otsuka, Jpn.J.Appl.Phys.Vol37 (1998) L64-L66

P06-081

OBSERVATION ON TRANSITIONS IN SURFACE REGION OF COCOA BUTTER BY X-RAY DIFFRACTION

Yusuke-Hayashi,[a] Yoshihito-Uozaki,[a] Hikaru-Terauchi,[a] and Isao-Takahashi[a]

[a]*Department of Science and Technology, Kwansei Gakuin Universiy, Hyogo,Japan*

Cocoa butter, which constitutes chocolate, is known to have at least six phases [1]. There are a lot of studies on phase transition of bulk cocoa butter, but little has been reported on surface. In this paper, we perform comparison between phase transitions in bulk and those in the surface region by combination of conventional wide angle X-ray diffraction (WAXD) and surface sensitive X-ray diffraction techniques. As for the X-ray diffraction for investigating the surface region, we exploited X-ray reflectivity (XR) and grazing incident X-ray diffraction (GIXD). XR gives us information on sample surface, e.g., thickness, electron density, and roughness of surface. GIXD detects the crystal structure, crystallinity, preferred orientations of crystalline in surface region.

Natural cocoa butter is composed of some similar oils: POP (sn-1,3-dipalmitoyl-2-oleoylglycerol), SOS (sn-1,3-dipalmitoyl-2-stearoyl-glycerol), POS (1,3-rac-palmitoyl-stearoyl-2-oleoylglycerol). Thin films of cocoa butter are formed on Si(100) wafers by spin coating method. Since the melting points of polymorphisms of cocoa butter are I: 17.3^{o}C, II: 23.3^{o}C, III: 25.5^{o}C, IV: 27.5^{o}C, V: 33.8 ^{o}C, and VI: 36.3 ^{o}C in bulk, we measured XR and GIXD of thin film in this temperature range.

Figure1 shows XR at various temperatures. At 24^{o}C, thickness of the cocoa butter layer is estimated as 4.8 nm. With elevating the temperature, coverage of the layer increased from 80% to 100% indicating the formation of completely wetting layer. Increase in the thickness was also recognized presumably due to the melting of residual cocoa butter particles which incoherently scatter X-ray. Results on GIXD will also be discussed.

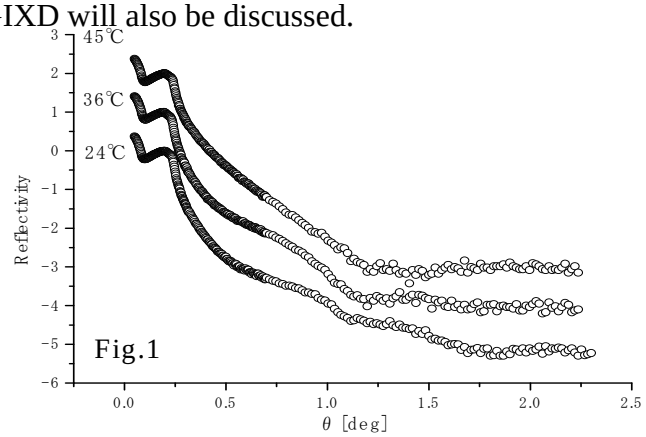

Fig.1

Reference:

[1] R.L. Wille and E.S. Lutton : J. Am. Oil Chem. Soc. Vol.43, 491 (1966)

P06-082

COMPARATIVE STUDY ON THE I-V CHARACTERISICS OF METAL STRING COMPLEXES EXPERIMENT VS THEORY

Liang-Yan Hsu, Bih-Yaw Jin, Chun-Hsien Chen, Shie-Ming Peng

Department of Chemistry, National Taiwan University, Taipei, 106, Taiwan.
Institute of Chemistry, Academia Sinica, Taipei, 115, Taiwan.
smpeng@ntu.edu.tw; Tel:(886)-2-2363-8305; Fax:(886)-2-8369-3765

I. Linear Metal String Complexes [1, 2, 3]
- ∗ Synthesis, Structure, Bonding

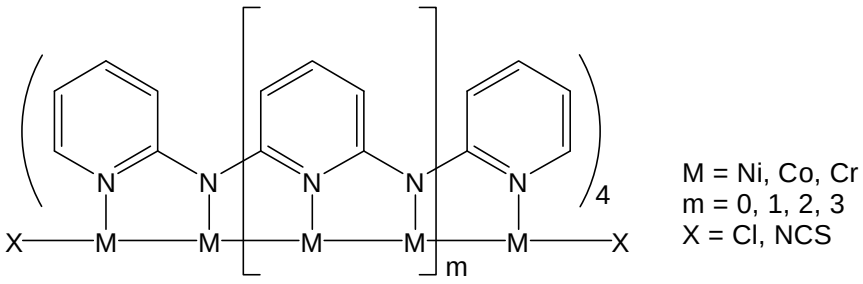

II. Potential Application as Molecular Metal Wires & Molecular Switches [4,5]
- ∗ STM Study on the Conductivity of Metal Strings
- ∗ C-AFM Measurements of Single Metal String Molecules
- ∗ Comparative Study on the I-V Characterisics (Theory V.S. Experiment)

III. Tuning of the Metal Strings [6]
- ∗ Naphthyridyl Amino Ligands: Low Oxidation Mixed Metal Strings
- ∗ Asymmetrical Ligands: Toward Molecular Rectifier

IV. Conclusion

Reference:

1. C.-Y. Yeh, C.-C. Wang, Y.-H. Chen and S.-M. Peng, in *Redox Systems Under Nano-Space Control*, Ed: T, Hirao, Springer, Germany, 2006, Ch. 5.
2. S.-Y. Lai, T.-W. Lin, Y.-H. Chen, C.-C. Wang, G.-H. Lee, M.-H. Yang, M.-K. Leung and S.-M. Peng, *J. Am. Chem. Soc.*, **1999**, *121*, 250.
3. S.-J. Shieh, C.-C. Chou, G.-H. Lee, C.-C. Wang and S.-M. Peng, *Angew. Chem. Int. Ed. Engl.*, **1997**, *36*, 56.
4. S.-Y. Lin, I.-W. P. Chen, C.-H. Chen, M.-H. Hsieh, C.-Y. Yeh, T.-W. Lin, Y.-H. Chen and S.-M. Peng, *J. Phys. Chem. B*, **2004**, *108*, 959.
5. I.-W. P. Chen, M.-D. Fu, W.-H. Tseng, J.-Y. Yu, S.-H. Wu, C.-J. Ku, C.-H. Chen, and S.-M. Peng, *Angew. Chem. Int. Ed. Engl.*, **2006**, 5414.
6. (a) C.-H. Chien, J.-C. Chang, C.-Y. Yeh, G.-H. Lee, J.-M. Fang and S.-M. Peng, *Dalton Trans.*, **2006**, 2106. (b) C.-H. Chien, G.-H. Lee, Y. Song and S.-M. Peng, *Dalton Trans.*, **2006**, 3249.

P06-142

CRYSTAL STRUCTURES OF THE CYTOSOLIC DOMAIN OF THE Mg^{2+} TRANSPORTER MgtE

Yoshiki Tanaka [a], Motoyuki Hattori [a], Shuya Fukai [b], Ryuichiro Ishitani[a] and Osamu Nureki[a]

[a]Department of Biological Information, Graduate School of Bioscience and Biotechnology, Tokyo Institute of Technology, Yokohama, Japan; [b]Center for Biological Resources and Informatics, Tokyo Institute of Technology, Yokohama, Japan

The magnesium ion, Mg^{2+}, is one of the most abundant divalent cations in biological systems and is vital for all living organisms. Three distinct classes of Mg^{2+} transporters have been identified from eubacteria and archaea. The MgtE Mg^{2+} transporter, which is ubiquitously conserved in all of the kingdoms of life, has not been thoroughly characterized, and it is not even clear whether MgtE acts as a channel or an active transporter. MgtE consists of an N-terminal cytosolic domain and a C-terminal transmembrane domain. The cytosolic domains include a cystathionine-β-synthase (CBS) domain, which reportedly plays a regulatory function in other transporter proteins, e.g. human chloride channels and the osmoregulated ABC transporter, OpuA. Therefore the cytosolic domain of MgtE is expected to have a regulatory function.

We solved the structures of the cytosolic domain of the MgtE in the presence and absence of Mg^{2+} at 2.3 Å and 3.9 Å resolutions, respectively. The cytosolic domain consists of two subdomains. The N-terminal subdomain (N domain) forms a right-handed superhelix. The C-terminal subdomain is composed of typical duplicated CBS domains. In the cytosolic domain structure in the presence of Mg^{2+}, the electron densities presumably corresponding to Mg^{2+} were clearly observed between the N and CBS domains, and might be related to a regulatory function.

A structural comparison of the cytosolic domains in the presence and absence of Mg^{2+} revealed that the domain organization is drastically changed. Such domain reorganization might be essential for gating of the MgtE pore.

P06-143

CRYSTAL STRUCTURE OF THE MgtE Mg^{2+} TRANSPORTER

Motoyuki Hattori [a], Yoshiki Tanaka [a], Shuya Fukai [b], Ryuichiro Ishitani[a] and Osamu Nureki[a]

[a]*Department of Biological Information, Graduate School of Bioscience and Biotechnology, Tokyo Institute of Technology, Yokohama, Japan;* [b]*Center for Biological Resources and Informatics, Tokyo Institute of Technology, Yokohama, Japan*

The magnesium ion, Mg^{2+}, is one of the most abundant divalent cations in biological systems and is vital for all living organisms. Mg^{2+} has the largest hydrated radius among all cations, while its ionic radius is the smallest. It remains obscure how Mg^{2+} transporters selectively recognize and dehydrate the large, fully-hydrated Mg^{2+} cation for its transport.

The MgtE family of Mg^{2+} transporters is ubiquitously distributed in all three kingdoms, and human homologues were functionally characterized and suggested to be involved in magnesium homeostasis However, the MgtE transporters have not been thoroughly characterized, and it is even not clear whether MgtE works as a channel or an active transporter.

We determined the crystal structure of the full-length *Thermus thermophilus* MgtE at 3.5 Å resolution. The transporter adopts a homodimeric architecture, consisting of the C-terminal five transmembrane (TM) domain, and the N-terminal cytosolic domains, composed of the superhelical N domain and the following typical duplicated cystathionine-β-synthase domains, which reportedly plays a regulatory function in other transporter proteins, e.g. human chloride channels and the osmoregulated ABC transporter. A solvent-accessible pore nearly traverses the TM domains, with one potential Mg^{2+} bound to the conserved Asp residues within the pore, which might be related to the ion selectivity by MgtE. The TM5 helices from both subunits close the pore through interactions with the "connecting helices", which connect the cytosolic and TM domains. Four putative Mg^{2+} ions are bound at the interface between the connecting helix and the other domains, which may lock the closed conformation of the pore. A structural comparison of the Mg^{2+}-bound and Mg^{2+}-free cytosolic domains showed the Mg^{2+}-dependent movement of the connecting helices, which might reorganize the TM helices to open the pore. These findings suggest a Mg^{2+} homeostasis mechanism, in which the cytosolic domains regulate the gating of the pore by sensing the intracellular Mg^{2+} concentration.

P06-144

STRUCTURAL BASIS OF PROSTACYCLIN BIOSYNTHESIS

Yi-Ching Li[1], Chia-Wang Chiang[1], Hui-Chun Yeh[2], Frank G. Whitby[3], Lee-Ho Wang[2], and Nei-Li Chan[1]

[1]*Institute of Biochemistry, College of Life Sciences, National Chung Hsing University, Taichung City 402, Taiwan.*

[2]*Division of Hematology, Department of Internal Medicine, University of Texas Health Science Center at Houston, 6431 Fannin, Houston, TX 77030, USA.*

[3]*Department of Biochemistry, 15 North Medical Drive East, Room 4100, University of Utah, Salt Lake City, UT 84103, USA*

Prostacyclin synthase (PGIS) converts prostaglandin H_2 to prostacyclin, which is a highly potent vasodilator and inhibits platelet aggregation. This enzyme is located to the endoplasmic reticulum membrane and was assigned to the P450 superfamily as CYP8A1 when its cDNA sequence was determined. Unlike other microsomal P450s that catalyze mono-oxygenation or hydroxylation reaction, PGIS catalyzes an isomerizaton and does not need molecular oxygen, reductase or any other external electron donor. Various genome projects have identified PGIS-like sequence in the animals as low as amphibians and fish (http://drnelson.utmem.edu/CytochromeP450.html), suggesting that PGIS emerged early in vertebrate evolution. Using the recombinant human PGIS obtained from a prokaryotic expression system, we had previously determined the crystal structure of this atypical and yet physiologically important P450 in its ligand-free state. However, critical questions regarding the regioselectivity of PGIS-catalyzed isomerization and the catalytic roles of active residues remain to be answered. To this end, we have now determined the crystal structures of the ligand-free and substrate analog-bound zebrafish PGIS. The structural basis for the regioselectivity and how the enzyme may facilitate the isomerization reaction were recognized. In addition, the substrate entrance and product exit channels of PGIS were identified. Detail structural analysis and functional significance of the ligand-bound zPGIS will be presented and discussed.

P06-145

STRUCTURAL STUDIES OF THE HUMAN PROSTACYCLIN SYNTHASE

Chia-Wang Chiang[1], Hui-Chun Yeh[2], Lee-Ho Wang[2*], and Nei-Li Chan[1*]

[1]*Institute of Biochemistry, College of Life Sciences, National Chung Hsing University, Taichung City 402, Taiwan.*

[2]*Division of Hematology, Department of Internal Medicine, University of Texas Health Science Center at Houston, 6431 Fannin, Houston, TX 77030, USA.*

Prostacyclin synthase (PGIS) catalyzes an isomerization of prostaglandin H_2 to prostacyclin, a potent mediator of vasodilation and anti-platelet aggregation. Here we report the crystal structure of human PGIS (hPGIS) at 2.15 Å resolution, which represents the first three-dimensional structure of a Class III cytochorme P450. While notable sequence divergence has been recognized between PGIS and other P450s, hPGIS exhibits the typical triangular prism-shaped P450 fold with only moderate structural differences. The conserved acid-alcohol pair in the I helix of P450s is replaced by residues G286 and N287 in hPGIS, but the distinctive disruption of I helix and the presence of a nearby water channel remain conserved. The side chain of N287 appears to be positioned to facilitate the peroxide bond cleavage, suggesting a functional conservation of this residue in activating oxygen. A combination of bent I helix and tilted B' helix creates a channel extending from the heme distal pocket, which seemingly allows binding of various ligands; however, residue W282, placed in this channel at a distance of 8.4 Å from the iron with its indole side chain lying parallel to the porphyrin plane, may serve as a threshold to exclude most ligands from binding. In addition, we have also determined the crystal structure of hPGIS in complex with the known inhibitor minoxidil at 1.62 Å. A clear piece of electron density in the heme distal pocket which corresponds to the bound minoxidil was easily recognized in the weighted Fo-Fc map. Interestingly, in contrast to the previous thought that a primary amine nitrogen may serve as the distal ligand, it was found that the oxygen of minoxidil is ligated to the heme-iron at a distance of 2.2 Å. The minoxidil binding prompts the formation of water-mediated hydrogen bonds between the heme propionates and residues from the B and C helices, turning the termini of both helices toward the heme. The functional significance of these findings will be presented during the meeting.

P06-146

HIGHLY AMPHIPHILIC INTERFACE IN THE COMPLEX FORMED BETWEEN DPPIV (CD26) AND ADENOSINE DEAMINASE

Wolfram Saenger[a], Wilhelm A. Weihofen[a], Jiango Liu[b], Werner Reutter[b], Hua Fan[b]

[a]*Institute for Chemistry and Biochemistry/ Crystallogra- phy, Freie Universitaet Berlin, Takustrasse 6, D-14195 Berlin, Germany.* [b]*Institute for Molecular Biology and Biochemistry, Charité-Universitaetsmedizin Berlin, Arnimallee 22, D-14195 Berlin, Germany*
E-mail: saenger@chemie.fu-berlin.de

Dipeptidyl-peptidase IV (DPPIV or CD26) is a homodimeric type II membrane glycoprotein in which the two monomers are subdivided into a propeller domain and an α/β-hydrolase domain.

As dipeptidase, DPPIV modulates the activity of various biologically important peptides and, in addition, DPPIV acts as a receptor for adenosine deaminase (ADA), thereby mediating co-stimulatory signals in T-lymphocytes.

The 3.0 Å resolution crystal structure of the complex formed between human DPPIV and bovine ADA presented here shows that each β-propeller domain of the DPPIV dimer binds one ADA [1]. At the binding interface, two hydrophobic loops protruding from the β-propeller domain of DPPIV interact with two hydrophilic and heavily charged α-helices of ADA, giving rise to the highest percentage of charged residues involved in a protein-protein contact reported thus far. Additionally, four glycosides linked to Asn229 of DPPIV bind to ADA. In the crystal structure of porcine DPPIV, the observed tetramer formation was suggested to mediate epithelial and lymphocyte cell-cell adhesion [2]. ADA binding to DPPIV could regulate this adhesion, as it would abolish tetramerization.

Reference:

[1] Weihofen W. A., Liu J., Reutter W., Saenger W., Fan H., *J. Biol. Chem.* 2004, 279, 43330..
[2] Engel M., Hoffmann T., Wagner L., Wermann M., Heiser U., Kiefersauer R., Huber R., Bode W., Demuth H.-U., Brandstetter H., *Proc Natl Acad Sci U S A* 2003, 100, 5063.

P06-147

CRYSTAL STRUCTURE OF BOVINE LACTOPEROXIDASE AT 2.3 Å RESOLUTION

Amit Kumar Singh, Nagendra Singh, Sujata Sharma, Mau Sinha, Punit Kaur, A. Srinivasan and T. P. Singh

Department of Biophysics, All India Institute of Medical Sciences, New Delhi, India, 110029

Lactoperoxidase (LPO, E.C. 1.11.1.7) is a redox enzyme with antibacterial properties found in several biological fluids, like milk, tears, saliva etc. In vivo, LPO catalyzes the oxidation of thiocyanate, iodide and bromide. The crystal structure of bovine lactoperoxidase (CLPO) has been determined at 2.3 Å resolution. It crystallizes in space group $P2_1$ with unit cell dimensions, a = 53.9 Å, b = 80.0 Å, c =75.7 Å and β = 103.2°. The structure has been refined to an R – factor of 23.1 % (R_{free} = 24.7 %). The structure revealed the presence of a heme group which is covalently attached to the protein via two ester linkages between carboxyl groups of Glu258 and Asp108 and modified methyl groups on pyrrole rings A and C of the heme. Ser198 is phosohorylated in CLPO, which apparently facilitates the intake of calcium ion. The calcium ion forms distorted pentagonal bipyramidal coordination. Sixteen anion-binding sites have been observed in the structure. The amino acid sequence of CLPO reveals four potential N- gycosylation sites, with Asn-X-Ser/Thr sequence motifs, these are at Asn95, Asn205, Asn205, Asn332 and structure shows that all the four sites are actually glycosylated. The structure shows five buried water molecules and His266 form a chain of hydrogen bonds extending from the Nδ of the distal His109 to the surface of molecule.

P06-148

CRYSTAL STRUCTURE OF CAMEL PEPTIDOGLYCAN RECOGNITION PROTEINS AT 3.0 Å RESOLUTION

Pradeep Sharma, Nagendra Singh, Sujata Sharma and T.P.Singh

Department of Biophysics, All India Institute of Medical Sciences, New Delhi, India, 110029

Peptidoglycan recognition protein (PGRP) is a soluble, conserved pattern recognition protein of vertebrates and invertebrates that binds to peptidoglycans (PGNs). PGNs forms a group of conserved microbial motifs (Pathogen- associated molecular patterns- PAMPs) that are unique products of microbial metabolism not produced by the host. PGNs are located on the surface of virtually all bacteria and fungi as such, constitute excellent targets to recognition by PGRP. We have isolated a 20 kDa PGRP from camel mammary secretions. It has been crystallized in the space group I 222 with cell dimensions, a =89.9Å, b = 102.5Å, c = 164.2Å with 32 molecules within unit cell. The structure reveals the presence of a tertrameric association unlike human PGRP, which is monomer. PGN binding groove is located in the domain close to C-terminus. The molecular structure contains a central β-sheet composed of five β-strands, four parallel and one (β5) antiparallel and three α- helices. PGN binding site resides in a long cleft whose walls are formed by helix α1 and five loops β3 – α1, α1- β4, β5 – β6, β6 – α2 and β7 – α3. The second site is located on the opposite side of the protein to the PGN- binding site, apparently accommodates host effector or signaling molecules. It is formed by the variable PGRP-specific segment and helix α2.

P06-149

CRYSTAL STRUCTURE OF THE COMPLEX OF SHEEP SIGNALING GLYCOPROTEIN WITH 2-METHYL-2,4-PENTANEDIOL AT 1.65Å RESOLUTION

Mau Sinha, Pradeep Sharma, Nagendra Singh, Sujata Sharma, Punit Kaur and Tej P. Singh

Department of Biophysics, All India Institute of Medical Sciences, New Delhi, India

The onset of the involution represents a period of large scale tissue remodeling in mammary glands. During this process the production of a new class of signaling glycoproteins is induced that binds to viable tissues and protect s them from programmed apoptosis. The binding proteins are designated as SPX-40 where X represents a species with a molecular weight of 40 kDa. The present protein is isolated from sheep dry secretions which crystallized in orthorhombic space group $P2_12_12_1$ with cell dimensions, a=62.9Å, b=66.4Å, c=105.7Å having four molecules in the unit cell. The structure was determined by molecular replacement method and refined to a R factor of 16.7% (R_{free}=21.7%) using data to 1.65Å resolution. A Ramachandran plot for the whole molecule shows 92.1% of residues in the most favoured regions and 7.9% in the additionally allowed regions. The structure reveals that the ligand binds in the sugar-binding groove with protein residues Trp10, Arg14, Tyr185 and Trp331 involved in direct interactions whereas residues Thr8, Tyr120, Arg242 and Asp334 interact through solvent water molecules. Residues Trp78, Leu183, Tyr185, Asp186, Ile 272 and Thr267 form Van der Waals interactions. The overall strength of interactions is of the order of 10^{-8}M.

P06-150

CRYSTAL STRUCTURES OF COMPLEXES OF C-LOBE OF BOVINE LACTOFERRIN WITH VARIOUS SACCHARIDES AT HIGH RESOLUTIONS REVEAL A COMMON BINDING SURFACE IN THE C-LOBE

Rafia Mir, Mau Sinha, Nagendra Singh, Vikram Gopalakrishnapillai, Sujata Sharma, Punit Kaur and Tej.P.Singh

Department Of Biophysics AIIMS, New Delhi India

Lactoferrin is a monomeric, iron binding 80kDa glycoprotein with antibacterial activity against Helicobacter pylori. In order to understand the role of lactoferrin against gastric damage caused by NSAIDS and bacterial colonization, a number of crystal structures of complexes of C-lobe of bovine lactoferrin with various saccharides were determined. Lactoferrin was proteotically cleaved into N- and C-lobes. The structure of C-lobe was determined at high resolution. It revealed the presence of the shallow saccharide binding site. C-lobe was crystallized with at least more than two dozens of different mono- and di-saccharides. The structures of these complexes showed that all the sugars bind at the same site but the numbers of interactions were different between the C-lobe and sugars indicating varying degree of affinities between them. The sugars used in the complexes were: Lactose, maltose, galactose, glucose, xylose, mannose, sucrose, fucose, N-acetylglucoseamine, cellobiose, raffinose, sorbitol, trehalose, melibiose, rhamnose, arabinose, melezitose, fructose, ribose, N-acetylgalactoseamine, methyalpha-D-mannopyranoside, adenosine, trisaccharide, tetrasaccharide, pentasaccharide. The resolution of structures varied from 1.5Å to 2.8Å. The protein residues that were involved in the interactions with ligands were Glu 659, Tyr 660, Leu 661 and Glu 664.

P06-151

CRYSTAL STRUCTURE OF GOAT LACTOPEROXIDASE AT 2.4Å RESOLUTION

Nagendra Singh, Amit Kumar Singh, Sujata Sharma, Asha Bhushan, Punit Kaur and Tej P. Singh

Department of Biophysics, All India Institute of Medical Sciences, New Delhi-110029, India

Lactoperoxidase (LPO) is a Fe (III) – heme enzyme belonging to the mammalian peroxidase family. LPO catalyzes the oxidation of SCN^- to hypothiocyanate. This enzyme was isolated from goat secretion. It was sequenced and crystallized. The crystals diffracted to 2.4Å resolution and belong to monoclinic space group $P2_1$ with cell dimensions, a=54.2Å, b=80.8Å, c=77.0Å, β=102.9°. The first crystal structure has been determined by molecular replacement method and refined to an R factor of 0.196 (R_{free}=0.203). The structure shows that the heme group is covalently bonded to the protein via two ester linkages between the carbonyl groups of Glu^{258} and Asp^{108} and modified methyl groups on pyrrole rings A and C of the heme. The iron is positioned slightly to the proximal side. On the distal side a funnel shaped channel filled with water molecules leads from the narrow opening to the surface of the protein. The distal heme cavity is occupied by the side chains of Glu^{105}, His^{109} and Arg^{255} together with five water molecules. The structure also has a calcium binding site with typical pentagonal bipyramidal coordination geometry.

P06-152

CRYSTAL STRUCTURE OF A COMPLEX OF PHOSPHOLIPASE A_2 (PLA_2) WITH A NEW GRAMINE DERIVATIVE AT 2.2 Å RESOLUTION

Sanjit Kumar, Nagendra Singh, Sujata Sharma, Tej.Pal.Singh

Department of Biophysics, All India Institute of Medical Sciences, New Delhi-110029, India

PhospholipaseA$_2$ (PLA_2) constitute a family of signal transduction enzymes. PLA_2 catalyzes the hydrolysis of fatty acids from the sn-2 position of phospholipd in the first step of the inflammatory pathway resulting in the production of key inflammatory lipid mediators e.g. prostanoids, leukotrenes and platelet activating factor. Several PLA_2 isoforms are consider as potential target for this role. Therefore inhibition of PLA_2 may reduce the concentration of proinflammatory compounds. We have obtained a new gramine (DAIP) derivative that binds to PLA_2 with a very high affinity.PLA_2 was complexed with DAIP and crystallized .The crystal belong tetragonal space group P4 with cell dimensions, a = b = 53.0Å ,c = 48.5 ÅThe x-ray intensity data were collected using in house facility to 2.2 Å resolution.The structure has been refined to an R-factor of 0.182(R_{Free} = 0.226) The structure revealed an excellent electron density for the Ligand.The Ligand is located in the substrate binding site.The OH group forms hydrogen bonds with a catalytically important water molecules and carboxyl oxygen of Tyr 22.The aromatic moiety is nicely stacked with Trp31 and fills the hydrophobic channel significantly.

P06-153

CRYSTAL STRUCTURES OF THREE ACTIVE SITE MUTANTS OF BOVINE PANCREATIC PHOSPHOLIPASE A_2

Shankar Prasad Kanaujia and Kanagaraj Sekar

Bioinformatics Centre and Supercomputer Education & Research Centre, Indian Institute of Science, Bangalore 560 012, India.

Phospholipase A_2 hydrolyzes the phospholipids at the *sn*-2 position to form fatty acid and lysophospholipid products. The enzyme Phospholipase A_2 is of high pharmaceutical concern since it is responsible for the release of arachidonic acid from membranes and its subsequent conversion produces leukotrienes and prostaglandins, which are part of the inflammatory response. The catalytic diad (Asp-His) along with a nucleophilic water molecule forms the active site of the enzyme. It has been known that the two nitrogens of His 48 play an important role in the active site. Biochemical and biophysical studies have shown that the single mutant H48N results in unstable conformation of the enzyme with almost negligible activity. The residue, Asp 49, in the calcium binding loop is essential for controlling the binding of the calcium ion and the catalytic action of phospholipase A_2. Solution studies reveal that the single mutants D49N and D49K show no binding to the calcium ion and hence no catalytic activity. To further elucidate the structural role of His 48 and Asp 49 at the active site, the crystal structures of the active site mutants, H48N, D49N and D49K, have been determined at high resolutions (1.9 Å). Although the catalytically important calcium ion binds to H48N, the crystal structure reveals the loss of the critical hydrogen bonding network and provides explanation as observed in proton NMR experiments. However, the tertiary structures of the three active site mutants are similar to that of wild type. The details will be presented.

P06-154

CRYSTAL STRUCTURE OF BOVINE C-LOBE WITH RIBOSE AT 2.5 Å RESOLUTION

G. Vikram, R. Mir, M. Sinha, N.Singh, S. Sharma, P. Kaur and T.P. Singh

Department of Biophysics, All India Institute of Medical Sciences, New Delhi, India

The lactoferrin molecule consists of a single polypeptide chain with a molecular mass of about 80 kDa and is folded into two similarly sized homologous N- and C-lobes. Two lobes are connected by a single bridge peptide segment. The proteolytic studies have shown that N- and C-lobes can be produced by enzymatic digestion. It has also been shown that the C-lobe is resistant to further enzymatic digestion indicating its role as a functional protein. Studies have also been reported showing that C-lobe provides relief in certain forms of gastropathy. In order to understand the medicinal effects of C-lobe, we have been carrying out systemic structural studies of the complexes of C-lobe with various carbohydrates and anti-inflammatory agents. For this purpose bovine C-lobe has been cocrystallized with ribose sugar. The crystals belong to monoclinic space group $P2_1$ with a = 59.0 Å, b = 49.6 Å, c = 64.7 Å and β = 105.8˚. The crystal structure has been determined at 2.5 Å resolution and refined to an R-factor of 20.9% (R_{free}=23.4%). The structure revealed two ribose binding sites, one at Glu659 - Tyr660 and the second at the cleft involving residues Asp378 and Asp462. Although both sites are shallow in shape but at both sites ribose molecules interact extensively with protein residues. The interaction include atleast five hydrogen bonds at each location indicating a moderate level of specificity.

P06-155

FRAGMENT-BASED INHIBITION OF PROTEINASE K: CRYSTAL STRUCTURE OF A COMPLEX OF PROTEINASE K WITH BORONIC ACID AT 0.83 Å RESOLUTION

R. Jain[1], N. Singh[1], M. Perbandt[2], C. Betzel[2], S. Sharma[1], P. Kaur[1], A. Srinivasan[1], T.P. Singh[1]

1-Department of Biophysics, All India Institute of Medical Sciences, New Delhi, India

2- Department of Biochemistry and Molecular Biology, University of Hamburg, Germany

Fragment-based design of tight inhibitors offers good scope of developing new medicines. More than one compound can be designed to occupy subsites in the ligand binding space of the target protein. Proteinase K is a fungal protease which has been implicated as a key enzyme in certain fungal based disorders. In order to understand the mechanism of ligand binding with Proteinase K, the crystal structure of a complex of Proteinase K with boronic acid has been determined at 0.83Å resolution. The complex was co- crystallized. The X-ray intensity data were collected at 100 K using Synchrotron beamline. The unit cell dimensions were a = b = 67.3Å, c = 106.5Å. The structure has been refined to an R-factor of 12.0% (R_{free} 13.6%). The structure contains 2118 protein atoms and two boronic acid molecules bound at subsites S1 and S1'. Both molecules are held tightly with atleast five hydrogen bonds between individual ligands and protein molecule. Residues His69, Gly134, Asn161, Ser221, Thr223 and Ser224 are involved extensively in the interactions with boronic acid. The building of boronic acid also perturbs the stereochemical arrangement between His69 and Ser224.

P06-156

CRYSTAL STRUCTURE OF BUFFALO LACTOPEROXIDASE AT 2.8Å RESOLUTION

Ishfaq Ahmed Sheikh, Nagendra Singh, Sujata Sharma, Asha bhushan and T.P. Singh

Department of Biophysics, All India Institute of Medical Sciences, New Delhi-110029, India

Mammalian peroxidases include lactoperoxidases (LPO), myeloperoxidase (MPO), eosinophil peroxidase (EPO), and thyroid peroxidase (TPO) utilize H_2O_2 to catalyze a diverse set of reactions. LPO is found in milk and other biological fluids like tears, saliva etc. and is a component of an antimicrobial defense system that catalyzes the bielectronic oxidation of thiocynate to hypothiocynate. It is a glycoprotein characterized by a single polypeptide chain of 78KDa whose carbohydrate content is of the order of 10%. LPO has been isolated from buffalo milk (BLPO) and crystallized using PEG 3350.The crystals belong to monoclinic space group P_2, with cell dimensions, a =54.5Å, b =80.8Å, c =77.6Å, ß = 102.9º. The structure has been determined by molecular replacement method and refined to an R value of 0.186 (R_{free} =0.217). The structure reveals that heme is covalently attached to the protein via two ester linkages between the carboxyl groups of Glu 258 and Asp109 and modified methyl groups on pyrrol rings A and C of the heme. The structure has a calcium binding site with a typical pentagonal bipyramidal coordination geometry. The linkages to proximal and distal sites reveal several novel features.

P06-157

CRYSTAL STRUCTURE OF MAMMARY SECRETORY GLYCOPROTEIN FROM BUFFALO AND ITS COMPLEXES WITH OLIGO-SACCHARIDES

Punit Kaur, A.K. Singh, Rishi Jain, N. Singh, S. Sharma and T.P. Singh

Department of Biophysics, All India Institute of Medical Sciences, New Delhi, India

Mammary involution in buffalo is characterized by a rapid loss of tissue function and degeneration of the alveolar structure and massive loss of epithelial cells. This cell loss is due to programmed cell death or apoptosis. During this period of large scale tissue destruction, a 40 kDa glycoprotein is secreted in significantly high concentrations which is implicated to be binding to viable cells and protects them from the process of programmed cell death. The protein has been isolated from buffalo dry secretions and crystallized. It has also been cocrystallized with tetrasaccharide. The crystals belong to orthorhombic space group $P2_12_12_1$ with cell dimensions a = 62.8 Å, b = 66.5 Å, c = 107.1 Å. The structure determination reveals that the tetrasaccharide residues occupy subsites S2 - S5. The conformation of Trp 78 is unperturbed because S1 subsite is not occupied. The shape of sugar-binding groove is considerably distorted particularly beyond S2 subsite. The flexible domain which is assumed to be involved in the intermolecular recognition through protein-protein interactions is unaffected by carbohydrate binding. Protein has an N-linked glycan chain which is integrated well with protein structure near the covalent linkage but extends into space indicating its participation as a glycan chain - protein interactions. All the binding components are independently involved in the recognition making this protein as a binding protein with high affinity.

P06-158

X-RAY CRYSTAL STRUCTURE ANALYSIS OF ERK1/IODOTUBERCIDIN COMPLEX

Ikuyo Yoshida,[a] Takayoshi Kinoshita,[a] Masaki Gouda,[b] Mamoru Matsubara,[b] Hiroshi Ishiguro,[b] Toshiji Tada[a]

[a]*Department of Biological Science, Graduate School of Science, Osaka Prefecture University, Osaka, Japan;* [b]*CARNA BIOSCIENCES, INC., Hyogo, Japan*

ERK is a member of MAP kinase family that contributes to the coordination and regulation of cell growth and differentiation in response to extracellular stimulation. ERK consists of two isoforms, ERK1 and ERK2, which have a high degree of amino acid sequence homology. ERK1 and ERK2 are different from each other in the intravital behavior. Mice lacking ERK1 are viable and fertile, but have a deficient thymocyte maturation, while mice lacking ERK2 die during embryogenesis due to a defect in trophoblast development.

In order to clarify the difference in the in vivo function between ERK1 and ERK2, we determined the crystal structure of human ERK1/Iodotubercidin complex. Crystals of the complex were obtained at 277 K using a reservoir solution of 1.6 M - 1.8 M ammonium sulfate, 100 mM MES buffer, pH 6.5, and 3% - 5% PEG 400. Diffraction data were collected to 3.2 Å resolution at beamline BL6A, Photon Factory, Tsukuba. The crystal belongs to the space group $P2_1$, with unit-cell parameters, a = 62.11 Å, b = 90.91 Å, c = 63.41 Å, β = 91.58° and Z = 4. ERK1 structure was solved by molecular replacement method. The structural refinement and model modification are currently in progress. A detailed comparison of the structure of ERK1 with that of ERK2 will be reported.

P06-159

CRYSTAL STRUCTURE OF HUMAN LYN KINASE DOMAIN

Nao Miyano,[a] Takayoshi Kinoshita,[a] Koichi Yokota,[b] Hiroshi Ishiguro[b] and Toshiji Tada[a]

[a]*Department of Biological Science, Graduate School of Science, Osaka Prefecture University, Osaka, Japan;* [b]*Carna Biosciences, Hyogo, Japan*

Lyn tyrosine kinase is a member of Src family kinases and plays a critical role in the signal transduction of immune system. Its excess activity is involved in cancer and inflammatory diseases. The crystal structure of Lyn kinase domain would help to design novel inhibitors of Lyn.

Human Lyn kinase domain (233 - 513) fused to His-tag at C-terminal was expressed in *Sf9* insect cells and purified using a Ni-column, His trap HP, and an anion exchange column, MonoQ (GE Healthcare). A crystal of Lyn was obtained with the sitting drop vapor diffusion technique at 4ºC with a reservoir buffer containing 0.2 M proline, 10% (w/v) PEG 3350 and 0.1 M HEPES (pH 7.5). Diffraction data were collected at 3.2 Å resolution using synchrotron radiation at Photon Factory beamline BL-17A. The data were processed and scaled using the program HKL2000. The crystal belongs to rhombohedral space group *R*3, with unit-cell parameters $a = b = 129.6$ Å, $c = 58.6$ Å, $\alpha = \beta = 90°$, $\gamma = 120°$. The crystal structure was solved by the molecular replacement method using a Lyn homology model derived from human Fyn kinase domain. Further, structural refinement and model modification are currently in progress.

P06-160

PROTEOMIC ANALYSIS OF MANGANESE REGULATION OF *NEISSERIA GONORRHOEAE*

Hsing-Ju Wu[1], Kuan-Tin Pan[1], He-Hsuan Hsiao[1], Chen-Wen Yao[3], Alastair G. McEwan[2], Michael P. Jennings[2] and Andrew H-J. Wang[1]

[1] Core Facilities for Proteomics Research, Institute of Biological Chemistry, Academia Sinica, Taipei, Taiwan; [2] School of Molecular and Microbial Sciences & Centre for Metals in Biology, The University of Queensland, Brisbane, Australia; [3] Chinese Herbal Medicine Research Center, Tri-Service General Hospital, Taipei, Taiwan

Neisseria gonorrhoeae is an important human pathogen which causes gonorrhoea and pelvic inflammatory disease. It is a facultative aerobe with a high iron requirement and a highly active aerobic respiratory chain. These factors would suggest that this bacterium would require defense systems to respond to toxic oxygen species. In the previous studies, we have shown that the accumulation of manganese (Mn) and Mn(II) uptake system, MntABC, in *N. gonorrhoeae* protected against killing by superoxide anion, and was independent of superoxide dismutase activity. Also, investigation of a regulatory role for Mn(II) in *N. gonorrhoeae* has revealed that a key virulence factor, pili, is repressed by Mn via a PerR-independent post-transcriptional mechanism. To provide a more comprehensive view of the regulatory network and its molecular mechanism, the shotgun proteomic approach, i.e. one dimensional (1D) sodium dodecyl sulfate-polyacrylamide gel electrophoresis (1D-SDS-PAGE) coupled with 1D liquid chromatography (LC) - tandem mass spectrometry (MS/MS) and the quantitative method, i.e., isotope coded affinity tag (ICAT) were performed.

N. gonorrhoeae cells were grown in the presence and absence of Mn and cell lysates were fractionated into cytoplasmic, inner membrane and outer membrane components. These results revealed that 98 proteins were differentially regulated at the post transcriptional level under conditions of increased or decreased Mn. The Mn-regulated proteins have a broad range of functions including oxidative stress defence (i.e. superoxide dismutase (SodB), azurin, bacterioferritin), cellular metabolism, protein synthesis, RNA processing, cell division, pilin and the proteins involved in the pilus assembly, such as PilC1 and PilQ. This confirms our previous study and may explain how the expression of pili was downregulated when cells were grown in the Mn supplement. Taken together, these data give us a proteomic view of Mn regulation and provided us with leads to correlate protection against oxidative stress with pilus formation and surface protein expression.

P06-161

MOLECULAR BASIS FOR RECOGNITION OF A SELECTIVE NUCLEOSIDE INHIBITOR BY *PLASMODIUM FALCIPARUM* *S*-ADENOSYL-L-HOMOCYSTEINE HYDROLASE

Yoshio Kusakabe,[a] Nobutada Tanaka,[a] Ken-ichi Aoki,[a] Masayuki Nakanishi,[b,e] Yukio Kitade,[b,c,d] and Kazuo T. Nakamura[a]

[a]School of Pharmaceutical Sciences, Showa University, Tokyo 142-8555, Japan; [b]Department of Biomolecular Science, Faculty of Engineering, Gifu University, Gifu 501-1193, Japan; Centers for [c]Infectious Diseases and [d]Advanced Drug Research, Gifu University, Gifu 501-1193, Japan; College of Pharmaceutical Sciences, Matsuyama University, Ehime 790-8578, Japan

The human malaria parasite *Plasmodium falciparum* is responsible for the death of more than a million people each year. The emergence of strains of malarial parasite resistant to conventional drug therapy has stimulated searches for antimalarials with novel modes of action.

S-Adenosyl-L-homocysteine hydrolase (SAHH) is a regulator of biological methylations. In 2004, we reported the crystal structure of *Plasmodium falciparum* SAHH (PfSAHH) complexed with a reaction product adenosine [Tanaka et al., *J. Mol. Biol.*, 2004]. A structural comparison of PfSAHH with human SAHH (HsSAHH) revealed that a single substitution between the PfSAHH (Cys59) and HsSAHH (Thr60) accounts for the differential interactions with nucleoside inhibitors. Chemical studies suggested that introduction of a fluorine atom at the 2-position of an adenine nucleoside derivative improve the selectivity index between HsSAHH and PfSAHH inhibition. To obtain an insight into molecular basis for selective inhibition of SAHHs by the inhibitors, structural analyses of PfSAHH complexed with the selective inhibitors are essential.

Here we report the crystal structure of PfSAHH complexed with a selective inhibitor, 2-fluoronoraristeromycin (2-F-NAM).

P06-162

CRYSTAL STRUCTURE OF *MYCOBACTERIUM TUBERCULOSIS* *S*-ADENOSYL-L-HOMOCYSTEINE HYDROLASE

Nobutada Tanaka,[a] Yoshio Kusakabe,[a] Masayuki Nakanishi,[b,f] Koichi Maruyama,[b] Takayuki Ezaki,[e] Yukio Kitade,[b,c,d] and Kazuo T. Nakamura[a]

[a]*School of Pharmaceutical Sciences, Showa University, Tokyo 142-8555, Japan;* [b]*Department of Biomolecular Science, Faculty of Engineering, Gifu University, Gifu 501-1193, Japan; Centers for* [c]*Infectious Diseases and* [d]*Advanced Drug Research, Gifu University, Gifu 501-1193, Japan;* [e]*Department of Microbiology, Gifu University School of Medicine, Gifu-501-1193, Japan;* [f]*College of Pharmaceutical Sciences, Matsuyama University, Ehime 790-8578, Japan*

Mycobacterium tuberculosis is a main pathogen causing tuberculosis (TB). It currently infects one-third of the world's population, resulting in 2 million deaths annually. The increased prevalence of drug-resistant and multi-drug-resistant strains, together with the lethal combination that tuberculosis and AIDS represents, makes the need for new and better drugs urgent. Given the multiple problems in fighting TB, effective control of the disease requires the identification of new drug targets and discovery of novel drugs.

S-Adenosyl-L-methionine (SAM) is the most widely used methyl donor. Numerous methyl transferases transfer the methyl group from SAM to their respective biologic acceptors, forming *S*-adenosyl-L-homocysteine (SAH). SAH is hydrolysed by *S*-adenosyl-L-homocysteine hydrolase (SAHH, EC 3.3.1.1) to adenosine (Ado) and L-homocysteine (Hcy). Inhibition of SAHH results in a cellular accumulation of SAH, which is a potent feedback inhibitor of SAM-dependent biological methylation. Thus, SAHH inhibitors can be potent inhibitors against various pathogenic organisms.

To design selective inhibitors for *Mycobacterium tuberculosis* SAHH (MtSAHH), we initiated structural analysis of recombinant MtSAHH. Medium-resolution crystal structure analyses of human, rat, and *Plasmodium falciparum* SAHHs have been reported, however, high-resolution crystal structure analysis of SAHH has not been reported yet. Here we report the crystal structure of MtSAHH complexed with the reaction product Ado at 1.75 Å resolution. This is the first high-resolution crystal structure analysis of SAHH.

P06-163

ELUCIDATION OF A CATALYTIC-CRITICAL HYDROGEN BOND NETWORK IN THE ACTIVE SITE OF ANIMAL GLUTAMINYL CYCLASES SUGGESTS AN ESSENTIAL PROTON TRANSFER PROCESS DURING CATALYSIS

Kai-Fa Huang[‡§], Yu-Ruei Wang[¶], En-Cheng Chang[‡], Tsung-Lin Chou[†], and Andrew H.-J. Wang[‡§†]

[‡]*Institute of Biological Chemistry, Academia Sinica, Taipei 115, Taiwan*

[§]*National Core Facility of High-Throughput Protein Crystallography, Academia Sinica, Taipei 115, Taiwan*

[¶]*Department of Biochemical Science and Technology, College of Life Science, National Taiwan University, Taipei 106, Taiwan*

[†]*Institute of Biochemical Sciences, National Taiwan University, Taipei 106, Taiwan*

Glutaminyl cyclases (QCs) catalyze the N-terminal pyroglutamate (pGlu) formation of numerous bioactive peptides. The enzymes were reported to relate to several pathological processes, such as amyloidotic diseases, osteoporosis, rheumatoid arthritis, and melanoma. The crystal structure of human QC revealed an unusual hydrogen bond network in the active site, formed by several highly conserved residues (Ser^{160}, Glu^{201}, Asp^{248}, Asp^{305}, and His^{319}), within which Glu^{201} and Asp^{248} were found to bind to substrate. In this study, we combine steady-state enzyme kinetic and X-ray structural analyses of eleven single-mutation human QCs to investigate the roles of the hydrogen bond network on catalysis. Our results demonstrated that disrupting one or both of the central hydrogen bonds, *i.e.*, Glu^{201}•••Asp^{305} and Asp^{248}•••Asp^{305}, reduced the steady-state catalysis dramatically. The roles of these two COOH•••COOH bonds on catalysis could not be replaced by COOH•••$CONH_2$ bonds, but could be slightly replaced by COOH•••HOH bonds. Mutations on Asp^{305}, a residue locating at center of the hydrogen bond network, raised the K_m value of the enzyme 3.6-17.5-fold and, surprisingly, decreased the k_{cat} value 89-3267-fold, indicating that Asp^{305} primarily plays a catalytic role. In addition, results from mutational studies on Ser^{160} and His^{319} suggest that they might help to stabilize the conformations of Asp^{248} and Asp^{305}, respectively. These data allow us to propose an essential proton transfer process during catalysis of animal QCs.

P06-164

STRUCTURAL COMPARISON STUDIES FOR 2H PHOSPHOESTERASE SUPERFAMILY PROTEINS

Yasumitsu Sakamoto,[a,b] Nobutada Tanaka,[a] Tomomi Ichimiya,[c] Tadashi Kurihara,[c] and Kazuo T. Nakamura[a]

[a]*School of Pharmaceutical Sciences, Showa University, 1-5-8 Hatanodai, Shinagawa-ku, Tokyo 142-8555, Japan,* [b]*School of Nursing and Rehabilitation Sciences, Showa University, 1865 Tokaichiba-cho, Midori-ku, Yokohama, 226-8555 Japan,* [c]*Department of Bioinformatics, Faculty of Engineering, Soka University, 1-236 Tangi-cho, Hachioji-shi, Tokyo 192-8577, Japan*

Recently, the structures of several 2H phosphodiesterase super family proteins have been determined by X-ray crystallography and NMR spectroscopy. Here we report the structure-function relationship studies of two hydrophobic residues in cyclic-nucleotide phosphodiesterase (CNP) family proteins.

The structures of CNP family proteins are highly similar to each other in the active site region. Our previous crystallographic study of human CNP (hCNP-CF) implies that Phe236 and Val322 are involved in non base-specific substrate recognition. Among the seven vertebrate CNPs, Val322 is completely conserved in seven cases (human, bovine, rat, mouse, chicken, frog, and goldfish). Structural superpositions using recently published NMR structures (rat CNP-CF (rCNP-CF): PDB code 1ILX; goldfish RICH protein (gRICH): PDB code 2I3E) and the crystal structure of hCNP-CF (PDB code 1WOJ) indicate that Phe236 and Val322 in hCNP-CF are structurally equivalent to Phe235 and Val321, and Phe239 and Val332, respectively, in rCNP-CF and in gRICH. These results support our previous study and imply functional significance of these residues.

P06-165

CRYSTAL STRUCTURE OF PARASPORIN-2, AN ANTI-TUMOR TOXIN FROM BACILLUS THURINGIENSIS

Toshihiko Akiba,[a] Yuichi Abe,[b] Sakae Kitada,[b] Yoshitomo Kusaka,[b] Akio Ito,[b] Tokio Ichimatsu,[c] Hideki Katayama,[c] Tetsuyuki Akao,[c] Kazuhiko Higuchi,[c] Eiichi Mizuki,[c] Michio Ohba,[d] Ryuta Kanai [a] and Kazuaki Harata [a]

[a]Biol. Info. Res. Center, AIST, Tsukuba; [b]Dept. Chem., Kyushu Univ., Fukuoka; [c]Biotech. Food Res. Inst., Fukuoka Ind. Tech. Center, ; [d]Dept. Appl. Gen. Pest Manage., Kyushu Univ., Fukuoka, Japan

Parasporin-2 is a protein toxin isolated from parasporal inclusions of a Gram-positive bacterium, *Bacillus thuringiensis*, strain A1547. While the bacterium is generally known as a valuable source of protein toxins that are harmless to mammals but specifically effective against insect pests, parasporin-2 does not have insecticidal activity but has a strong cytocidal activity against various human cells with markedly divergent target specificity, preferentially effective to liver and colon cancer cells. The 37-kDa inactive nascent protein is proteolytically converted to the 30-kDa active form, which causes susceptible cells rapid ballooning and subsequent burst to death. To elucidate the basis for toxicity and specificity, the crystal structure of the recombinant active-form has been determined at 2.65 Å by the MAD method.

The protein has an unusually elongated structure dominated by b-strands, many of which are remarkably long, running all or two-thirds of the longer axis of the molecule. The molecule can be divided to three domains: the N-terminal domain 1 is composed of a small four-stranded b-sheet surrounded by three short a-helices; domains 2 and 3 are both b-sandwiches. The overall structure of the protein resembles those of epsilon-toxin from *Clostridium perfringens* and domains 2-4 of aerolysin from *Aeromonas hydrophila*. Since these toxins belong to the b-pore-forming toxin, parasporin-2 would also develop toxicity by perforation of target cell membrane through formation of a large multimeric b-sheet-walled channel. This assumption agrees with reported changes in susceptible cells treated with the protein. Comparison of each domain with counterparts of those structural homologues highlights remarkable structural conservation in domains 2 and 3, suggesting they may be responsible for pore formation. Particularly interesting is an elongated patch of hydroxylated amino acid residues on the surface of these domains; a non-toxic structural homologue, the 26-kDa crystal protein from *B. thuringiensis*, strain A1470, lacks this feature. On the other hand, there is noticeable structural divergence between the domain 1 parts of the homologues, suggesting its involvement in target specificity. There is an extensive cluster of aromatic residues in domain 1 of parasporin-2, which could be suitable for binding to sugar moieties of glycoproteins or glycolipids on the cell surface.

P06-166

CRYSTAL STRUCTURE OF THE HRDC DOMAIN OF HUMAN WERNER SYNDROME PROTEIN, WRN.

Ken Kitano, Nozomi Yoshihara and Toshio Hakoshima

Structural Biology Laboratory, Nara Institute of Science and Technology (NAIST), Ikoma, Japan.

Werner syndrome is a human premature aging disorder characterized by chromosomal instability. The disease is caused by the functional loss of WRN, a member of the RecQ-helicase family that plays an important role in DNA metabolic pathways. WRN contains four structurally folded domains comprising an exonuclease, a helicase, a winged-helix, and a helicase-and-ribonuclease D/C-terminal (HRDC) domain. In contrast to the accumulated knowledge pertaining to the biochemical functions of the three N-terminal domains, the function of C-terminal HRDC remains unknown.

Recently we determined the crystal structure of the human WRN HRDC domain (Kitano *et al.*, 2007, *J. Biol. Chem.*). The domain forms a bundle of α-helices similar to those of *Saccharomyces cerevisiae* Sgs1 and *Escherichia coli* RecQ. Surprisingly, the extra ten residues at each of the N and C termini of the domain were found to participate in the domain architecture by forming an extended portion of the first helix α1, and a novel looping motif that traverses straight along the domain surface, respectively. The motifs combine to increase the domain surface of WRN HRDC, which is larger than that of Sgs1 and *E. coli*. In WRN HRDC, neither of the proposed DNA-binding surfaces in Sgs1 or *E. coli* is conserved, and the domain was shown to lack DNA-binding ability *in vitro*. Moreover, the domain was shown to be thermostable and resistant to protease digestion, implying independent domain evolution in WRN. Coupled with the unique long linker region in WRN, the WRN HRDC may be adapted to play a distinct function in WRN that involves protein-protein interactions.

P06-167

CRYSTAL STRUCTURE OF *FUSOBACTERIUM ADHESIN A* (FADA): IMPLICATIONS FOR ORAL DISEASES AND PRETERM BIRTH

Stanley Nithianantham,[a] Minghua Xu,[b] Mitsunori Yamada,[b] Hongqi Liu,[b] Jonathan Ross,[b] Mark Durham,[b] Hameem Kawsar,[b] Menachem Shoham[a*] and Yiping W. Han[b,c]

[a]*Departments of Biochemistry,* [b]*Periodontics and* [c]*Pathology, Case Western Reserve University, Cleveland, Ohio 44106, U.S.A.*

Epidemiological and microbiological-immunological studies have lent credence to the concept that periodontal disease is a risk factor for cardiovascular, cerebrovascular and respiratory diseases in addition to preterm delivery of low-birth-weight infants. *Fusobacterium nucleatum* is one of the predominant anaerobes associated with periodontal disease and preterm birth. It originates in the oral cavity and it is transmitted to the uterus via the blood stream. A 13.7 kDa FadA (*Fusobacterium adhesin* A) protein is required for the bacterium to attach to host mammalian cells. FadA has been expressed in Escherichia coli, purified and crystallized. The crystals belong to the hexagonal space group $P6_1$, with unit-cell parameters a = b = 59.3, c = 125.7 Å. Synchrotron X-ray data have been collected to 1.9 Å. We have solved the structure by MAD (Multiple Anomalous Dispersion) method. The analysis of FadA reveals two antiparallel coiled coil α-helices connected by an eight-residue hairpin loop. The two helices interact with each other via leucine residues. The N-terminal helix has four additional exposed leucines that interact with leucines of a neighboring molecule. This novel oligomerization motif is the leucine chain. The structure and function of FadA will be discussed in detail.

References:

[1]Nithianantham, S., Xu, M., Wu, N., Han, Y. W., and Shoham, M. (2006). Crystallization and preliminary X-ray data of the FadA adhesion from Fusobacterium nucleatum. *Acta Crystallograph Sec F* **62**, 1215-1217.

[2]Xu, M., Yamada, M., Li, M., Liu, H., Chen, S. G., and Han, Y. W. (2007). FadA from *Fusobacterium nucleatum* utilizes both secreted and non-secreted forms for functional oligomerization for attachment and invasion of host cells. *J Biol Chem (in press).*

P06-168

STRUCTURE-BASED DESIGN OF INHIBITORS OF HUMAN MTH1 PROTEIN I

Teruya Nakamura,[a] Miyuki Inazato,[a] Sinji Ikemizu,[a] Yusaku Nakabeppu,[b] and Yuriko Yamagata[a]

[a]*Graduate School of Pharmaceuical Sciences, Kumamoto University, Kumamoto 862-0973, Japan;* [b]*Medical Institute of Bioregulation, Kyushu University, Fukuoka 812-8582, Japan.*

Human MutT homolog-1 (hMTH1) hydrolyzes a variety of oxidized purine nucleoside triphosphates including 8-oxo-dGTP, 2-oxo-dATP, 2-oxo-ATP, and 8-oxo-dATP to their corresponding nucleoside monophosphates, while *E. coli* MutT possesses prominent substrate specificity for 8-oxoguanine nucleotides. Up to date, we have determined the crystal structures of hMTH1 complexed with three oxidized nucleotides, 8-oxo-dGMP, 8-oxo-dGTP, and 2-oxo-dATP. Their structures indicate that hMTH1 exhibits the broad substrate specificity for oxidized purine nucleoside triphosphates with a very novel manner.

hMTH1 suppresses the cell death occurred by oxidative stress. The expression of the hMTH1 protein increases in human cancerous tissues including brain tumors, kidney and lung cancers with an increased accumulation of 8-oxoguanine. This indicates that compounds which suppress the hMTH1 function or expression must be new candidates for chemotherapy of cancer to sensitize cancer cells against certain type of anticancer drugs. Thus we are trying to seek inhibitors of hMTH1 based on the characteristic active site structure of hMTH1. In this presentation, we will discuss the examination using the program MOE.

P06-192

CRYSTAL STRUCTURES OF D-AMINO ACID AMIDASE FROM *OCHROBACTRUM ANTHROPI* SV3 AND α-AMINO-ε-CAPROLACTAM RACEMASE FROM *ACHROMOBACTER OBAE*

Seiji Okazaki[a], Atsuo Suzuki[a], Tsunehiro Mizushima[a], Hidenobu Komeda[b], Yasuhisa Asano[b], Takashi Yamane[a]

[a]*Department of Biotechnology, School of Engineering, Nagoya University, Chikusa, Nagoya, 464-8603, Japan,* [b]*Biotechnology Research Center, Toyama Prefectural University, Imizu, Toyama, 939-0398, Japan.*

D-amino acid amidase (DAA) from *Ochrobactrum anthropi* SV3 catalyzes the stereospecific hydrolysis of D-amino acid amides to yield the D-amino acid and ammonia. And, α-amino-ε-caprolactam racemase (ACL racemase) from *Achromobacter obae* catalyzes racemization of D,L-ACL. Recently, racemase activity on amino acid amide was discovered in ACL racemase. By combinating of ACL racemase and D-stereospecific hydrolase like DAA, the production of D-amino acid in 100% theoretical yield can be possible. In ordered to clarify the structute-function relationships of DAA, the crystal structures of native DAA, D-phenylalanine complex, L-phenylalanine complex and L-phenylalanine amide complex were determined at 2.1, 2.4, 2.3 and 2.2 Å, respectively. Also to clarify the structute-function relationships of ACL racemase, the crystal structure of native ACL racemase was determined at 2.5 Å resolution. The structure of ACL racemase is composed of three segment; (1) an N-terminal segment (residues 1 to 43); (2) a large, pyridoxal phosphate (PLP) binding domain (residues 44 to 319); and (3) a C-terminal domain (residues 320 to 436). The overall structure of ACL racemase is similar to those of the other aminotransferase subgroup Ⅱ enzymes, especially γ-aminobutyrate aminotransferase (GABA-AT) from *E. coli*, and dialkylglycine decarboxylase (DGD) from *Pseudomonas cepacia*. Like GABA-AT and DGD, two monomers of ACL racemase make extensive contacts to form a dimer. Interestingly, differed from GABA-AT and DGD, ACL racemase having unique elongated C-terminus polypeptide chain (Ser423 - Trp436), and the C-terminus residue Trp436 elongated to active site. The C4' in PLP covalently bonded to the ε-amino group of Lys267 forming the internal aldimine.

P06-193

XC5848, AN ORFan PROTEIN FROM *XANTHOMONAS CAMPESTRIS*, ADOPTS A NOVEL VARIANT OF Sm-LIKE MOTIF

Ko-Hsin Chin[a], Andrew H.-J. Wang[b], & Shan-Ho Chou[a,c,*]

[a]*National Chung Hsing University Biotechnology Center, National Chung-Hsing University, Taichung, 40227, Taiwan,* [b]*Institute of Biological Chemistry, Academia Sinica, Nankang, Taipei, Taiwan, ROC,* [c]*Institute of Biochemistry, National Chung-Hsing University, Taichung, 40227, Taiwan, ROC*

The XC5848 gene from a plant pathogen *Xanthomonas campestris* pv. *campestris* str. 17 (Xcc) encodes a hypothetical protein comprising 102 amino acid residues, with a molecular weight of 11945 Da. A BLAST search using XC5848 sequence against the UniProtKB/TrEMBL database (http://us.expasy.org/sprot/) finds orthologs only in the *Xanthomonas* genus. No close sequence homologue could be detected for other organisms. We have determined the XC5858 crystal structure to 1.68 Å resolution, and found that XC5848 adopts a well-conserved Sm or Lsm (Sm-like) fold widely found in eukarya, arachea, and bacteria, despite the very low sequence identities. However, considerable differences with the Sm-like motif were observed at the N-terminal and internal regions. Since critical residues responsible for RNA recognition and oligomer formation of Sm-like proteins are generally absent, XC5848 could play biological roles other than RNA metabolism. To the best of our knowledge, this is the first structural report of the novel variant of the highly conserved Sm-like motif.

P06-194

THE CRYSTAL STRUCTURE OF XC1258 FROM XANTHOMONAS CAMPESTRIS: A PUTATIVE PROCARYOTIC NIT PROTEIN WITH AN ARSENIC ADDUCT IN THE ACTIVE SITE

Ko-Hsin Chin[a], Andrew H.-J. Wang[b], & Shan-Ho Chou[a,,b]*

[a]*National Chung Hsing University Biotechnology Center, National Chung-Hsing University, Taichung, 40227, Taiwan,* [b]*Institute of Biological Chemistry, Academia Sinica, Nankang, Taipei, Taiwan, ROC,* [c]*Institute of Biochemistry, National Chung-Hsing University, Taichung, 40227, Taiwan, ROC*

The nitrilase superfamily proteins are involved in a wide variety of non-peptide carbon-nitrogen hydrolysis reactions, characterized by a thiol acylenzyme intermediate formed through the attack of a cyano or carbonyl carbon by a novel conserved catalytic triad of Glu-Lys-Cys, to produce important natural products such as auxin, biotin, precursors of antibiotics etc. Based on extensive sequence analysis, members of the nitrilase superfamily were classified into 6 or 13 functionally district groups. However, although sequence searching can identify polypeptides as members of the nitrilase superfamily, their annotations have been perplexing. It is necessary to re-classify these protein members preferably by structure-based methods. Currently only a few protein structures are available in this superfamily, including a NitFhit protein from Caenorhabditis *elegans*, two N-carbamyl-D-amino acid amidohydrolases (DCases) from *Agrobacterium* sp. Strain KNK712 and *Agrobacterium radiobacter*, and a putative CN hydrolase from *Sacchromyces cerevisiae* strain S288C. They are either dimeric or tetrameric α–β–β–α sandwich proteins.

We now report the crystal structure of XC1258, a putative nitrilase superfamily protein from the plant pathogen *Xanthomonas campestris* pv. *campestris* str. 17 (Xcc). Based on a multiple sequence alignment, XC1258 was found to exhibit only low sequence identities with other nitrilase superfamily proteins for which the tertiary structures have been determined. We have determined the crystal structure of XC1258 to a resolution of 1.73 Å using the two-wavelength MAD approach. Interestingly, a cacodylate or dimethylarsinic acid compound was found to situate perfectly in the active region, forming a strong arsenic adduct with the active cysteine residue. This observation allows us to propose a reaction mechanism for the nitrilase superfamily proteins and suggests that their activity could be inhibited by the dimethylarsinic compound through a sulfur-arsinic covalent bond.

P06-195

KINETIC AND STRUCTURAL PROPERTIES OF TRIOSEPHOSPHATE ISOMERASE FROM *HELICOBACTER PYLORI*

Chen-Hsi Chu, Yi-Ju Lai, and Yuh-Ju Sun*

Institute of Bioinformatics and Structural Biology, National Tsing Hua University, Hsinchu 30013, Taiwan, ROC

Triosephosphate isomerase (TIM) catalyzes the interconversion between dihydroxyacetone phosphate (DHAP) and D-glyceraldehyde-3-phosphate (GAP) in the glycolysis-gluconeogenesis metabolism pathway. The *Helicobacter pylori* TIM gene (*HpTIM*) was cloned, and HpTIM was expressed and purified. The enzymatic activity of HpTIM for the substrate GAP was determined (K_m = 3.46 ± 0.23 mM and k_{cat} = 8.8 × 10^4 min^{-1}). The crystal structure of HpTIM was determined by molecular replacement at 2.3 Å resolution. The overall structure of HpTIM was (β/α)β(β/α)$_6$, which resembles the common TIM barrel fold, (β/α)$_8$; however, a helix is missing after the second β-strand. The conformation of loop 6 and binding of phosphate ion suggest that the determined structure of HpTIM was in the "closed" state. A highly conserved Arg-Asp salt bridge in the "DX(D/N)G" motif of most TIMs is absent in HpTIM because the sequence of this motif is "^{211}SVDG^{214}". To determine the significance of this salt bridge to HpTIM, four mutants, including K183S, K183A, D213Q, and D213A, were constructed and characterized. The results suggest that this conserved salt bridge is not essential for the enzymatic activity of HpTIM; however it might contribute to the conformational stability of HpTIM.

P06-196

CARBOHYDRATE-BINDING OF THE STARCH BINDING DOMAIN OF *RHIZOPUS ORYZAE* GLUCOAMYLASE IN COMPLEX WITH β-CYCLODEXTRIN AND MALTOHEPTAOSE

Jung-Yu Tung , Yen-Yi Liu, Wei-I Chou, Fang-Yu Chang, Dah-Tsyr Chang and Yuh-Ju Sun

Department of Life Science, National Tsing Hua University, Hsinchu

Glucoamylase hydrolyses starch and polysaccharides to β-D-glucose. *Rhizopus oryzae* glucoamylase (*Ro*GA) consists of two functional domains, an N-terminal starch binding domain (SBD) and a C-terminal catalytic domain. The two domains are connected by an O-glycosylated linker. The crystal structures of the SBD in complex with a cyclic carbohydrate, β-cyclodextrin (β-CD), and a linear carbohydrate, maltoheptaose (G7), were determined. The overall structures of the SBD complexes belong to a β-sandwich fold with an immunoglobulin-like structure and two carbohydrate-binding sites were observed. Site I is created by several conserved aromatic residues, Trp47, Tyr83, and Tyr94, to form a broad, flat, and firm hydrophobic surface. In addition to the hydrophobic interaction, numerous asparagine residues are involved in the hydrophilic interactions to carbohydrate. Site II is built up by Tyr32 and Phe58 to produce a protruded and narrow binding environment. Site I undergoes a bigger conformational change than site II upon the carbohydrate binding.

P06-197

ATP-DRIVEN MOTIONS OF 70-KDA HEAT SHOCK PROTEINS (HSP70S): INSIGHTS INTO STRUCTURAL DYNAMICS OF THE HSP70 POWER STROKE

Yi-Wei Chang,[a,b] Chung Wang,[a] and Chwan-Deng Hsiao[a]

[a]*Institute of Molecular Biology, Academia Sinica, Taipei, 11529, Taiwan;* [b]*Institute of Bioinformatics and Structural Biology, National Tsing Hua University, Hsinchu, 300, Taiwan*

The 70-kDa heat shock proteins (Hsp70s) are interspecific highly conserved molecular chaperones which participate in many crucial cellular functions, such as promoting the correct folding of nascent or stress-denatured polypeptides, assisting the protein translocation across membranes, and helping the assembly/disassembly of protein complexes.. Under particular control by the J-domain ATPase activating proteins and nucleotide exchange factors (NEFs), Hsp70s process their substrates in ATP-driven cycles. Previous studies clearly defined that Hsp70 protein can be distributed into two major functional domains, the NH2-terminal nucleotide-binding domain (NBD) and the COOH-terminal substrate-binding domain (SBD). To date, the ATP dependent allosterically regulating mechanism between these two domains has been long explored. However, precise structural understanding of the interdomain communication during ATPase cycle is still limited. In this report, we have determined the X-ray structures of ATP form intact Hsp70 chaperone proteins in various species, including the DnaK in eubacterium *Geobacillus kaustophilus HTA426* and the 70-kDa heat shock cognate protein (Hsc70) in mammalian *Rattus norvegicus*. Together with the result of detecting the solvent accessibility of a Trp reporter on the domain-domain interface, the structures reveal typical domain releasing behaviors of Hsp70s upon ATP binding and hydrolysis. This is in good agreement with previous studies that the hydrolysis of ATP may drives large domain movement of SBD related to NBD and provides power to allow Hsp70s serving as motors in processes such as protein translocation trough transport channels. Furthermore, the insertion of the hydrophobic linker region of gkDnaK into another crystallographic symmetry molecule's substrate binding pocket suggests a characteristic cooperative mechanism of Hsp70s. These important findings demonstrate exciting insights into structural dynamics of Hsp70 family proteins during chaperone cycles.

P06-198

CRYSTAL STRUCTURE OF PHOSPHORIBOSYLPYROPHOSPHATE BOUND NICOTINATE PHOSPHORIBOSYLTRANSFERASE FROM *PYROCOCCUS FURIOSUS*

KyuBeen Sohn[1], Yilan Fang[1], Andrea Schulte[2], Christiane Dahl[2], Sung-Hou Kim[3] and Dong Hae Shin[1*]

[1]College of Pharmacy, Ewha Womans University, Seoul 120-750, Korea, [2]Institut für Mikrobiologie & Biotechnologie, Universität Bonn, Meckenheimer Allee 168, D-53115 Bonn, Germany, [3]Department of Chemistry, University of California, Berkeley, California 94720-5230, USA,
[*]Corresponding author

The *dsrEFH* genes are part of the *dsr* (dissimilatory sulfite reductase) operon of the anoxygenic phototrophic sulfur bacterium *Allochromatium vinosum*. The *dsr* gene products are essential for the oxidation of sulfur stored in intracellular sulfur globules in this organism. The polypeptides DsrE, DsrF and DsrH are homologous to each other. From *A. vinosum* they are isolated as a soluble a2b2g2-structured holoprotein with an apparent molecular mass of 75 kDa [1]. DsrE and DsrF are the prototypes of a family of conserved proteins domains (COG 1553, 2044, 2923). DsrH is the prototype of yet another family of conserved proteins found in bacteria and archaea (COG 2168) but also fits into the DsrE/F family. In our effort to dissect functions of the proteins encoded at the *A. vinosum dsr* locus we have determined the three dimensional structure of DsrEFH by X-ray crystallography at 2.5 Å resolution to a crystallographic R-factor of 20.5 % and free R-factor of 26.2%.

P06-199

STABILIZATION OF COLLAGEN TRIPLE-HELIX BY ARG IN THE Y POSITION

Tatsuya Morimoto,[a] Mitsuru Haga,[b] Chizuru Hongo,[a] Keiichi Noguchi,[c] Kenji Okuyama[a] and Toshiki Tanaka[d]

[a]Department of Macromolecular Science, Graduate School of Science, Osaka University, Toyonaka,Osaka, Japan; [b]Department of Biotechnology and Life Science, Tokyo University of Agriculture andTechnology; [c]Instrumentation Analysis Center, Tokyo University of Agriculture and Technology; [d]Department of Materials Science and Engineering, Nagoya Institute of Technology

Because of the small number of diffraction spots, structural information available from X-ray fiber diffraction data of native collagen is very limited, which resulted in the two plausible molecular models for collagen, the Rich and Crick (10/3-helix) and Okuyama model (7/2-helix) (Okuyama, et al., *Biopolymers*, 84, 181-191, 2006). The amino acid sequence of collagen has very characteristic features with Gly in every third poison and high contents of imino acid. Collagen-model peptides with these sequence characteristics have provided valuable physicochemical information from 1960's. Especially, single crystal structures of these peptides at high resolution have provided very important structural information during the last decade. One of them is the predominant supports for the Okuyama model instead of the Rich and Crick model (Okuyama, et al., *Biopolymers*, 84, 421-432, 2006) which is believed to be correct since 1955. High resolution structures of model peptides also provide structural bases for understanding of stabilization of triple-helix by some amino acid residues. It is well known that Hyp in the Y position stabilizes the collagen triple-helix. This is very clear by comparing the helix-coil transition temperatures (T_m) of $(Pro\text{-}Pro\text{-}Gly)_{10}$ (Tm = 30 ºC) and $(Pro\text{-}Hyp\text{-}Gly)_{10}$ (T_m = 60 ºC). It was reported that the Gly-Pro-Arg sequence in the host-guest peptide showed a similar T_m compared with that of the Gly-Pro-Hyp sequence (Persikov, et al., *Biochemistry*, 39, 14960-14967, 2000) . In this study, we report the side chain conformation of Arg in the collagen triple-helix based on the single crystal structure of the host-guest peptide, $(Pro\text{-}Hyp\text{-}Gly)_3\text{-}Pro\text{-}Arg\text{-}Gly\text{-}(Pro\text{-}Hyp\text{-}Gly)_4$ (hereafter, PRG).

Single crystal structure of PRG-peptide (*a*= 23.28, *b*= 19.57, c= 49.02 Å, b= 94.51º, $P2_1$, R_{work}= 0.13, R_{free}= 0.198) was analyzed at 1.45 Å resolution by using 6808 reflections with $|Fo|>2\sigma|Fo|$ collected in the BL40B2 of SPring-8. No substantial difference of the triple-helix was observed in the peptide backbone conformation between the PRG-peptide and the homopeptide with Pro-Hyp-Gly sequence. In the structures of T3-785 (Kramer, et al., *Nature*

Structural Biology, 6, 454 – 457, 1999) and GFOGER (Emsley, et al., *Cell*, 101, 47-56, 2000) peptides, direct hydrogen bonds were reported between Arg side chain and oxygen atom in the adjacent chain. However, no such direct hydrogen bond was observed in the present case. Instead, the side chains of Arg residues seem to stabilize its triple-helix in two ways. One is van der Waals interactions between the long side chain of Arg and several parts of the adjacent chain. The other is water-mediated hydrogen bonds between one of three nitrogen atoms in the Arg side chain and one of oxygen atoms in the same molecule.

P06-200

THE STRUCTURAL ANALYSIS OF THE COLLAGEN-MODEL PEPTIDE, (Pro-Pro-Gly)$_4$-Hyp-Asp-Gly-(Pro-Pro-Gly)$_4$ CRYSTAL

Tatsuya Kawaguchi[1], Masaki Shimura[2], Chizuru Hongo[1], Keiichi Noguchi[2], Kenji Okuyama[1], Kazunori Mizuno[3] and Hans Peter Bachinger[3]

1Department of Macromolecular Science, Graduate School of Science, Osaka University, Toyonaka, Osaka 560-0043, Japan; 2Department of Biotechnology and Life Science, Graduate School of Engineering, Tokyo University of Agriculture and Technology; 3Department of Biochemistry and Molecular Biology, Oregon Health & Science University

Collagen is the most abundant protein in vertebrate. The triple-helix formation is one of the characteristics of collagen, with which collagen accomplish its functions in organism. The triple-helix formation of collagen and its stabilization mechanism had been much interesting themes. Recently, the Hyp-Y-Gly with high content of Thr in Y position was found in the *Riftia pachyptila* cuticle collagen. To investigate the stabilization mechanism of Hyp-Thr-Gly sequence in collagen, we are analyzing a series of host-guest peptides in which the guest Hyp-Y-Gly triplet is sandwiched by host Pro-Pro-Gly triplets. In this study, we determined the molecular and crystal structures of (Pro-Pro-Gly)$_4$-Hyp-Asp-Gly-(Pro-Pro-Gly)$_4$ (hereafter, ODG peptide).

The ODG peptide was crystallized by hanging-drop vapor-diffusion method. X-ray diffraction experiments were performed using the synchrotron radiation source at the BL6A beam line of PF in KEK, Ibaragi, Japan. The crystal belongs to $P2_1$ space group with cell parameters of a = 31.59, b = 21.71, c = 39.15 A, and β = 100.17°. A total of 25,367 unique reflections with [$F_o > \sigma(F_o)$] in the resolution range of 10 to 1.02 A were used for structure refinement (R_{work} = 0.128, R_{free} = 0.159).

The helical twist of each triplet had the average values of 49.0° for the host and 52.6° for the guest regions, which agreed very well with that for the ideal 7/2-helical model (51.4°; Okuyama model), and not with the 10/3-helical model (36°; Rich and Crick).

The typical interchain hydrogen-bond of (Gly)NH···O=C(X) was observed in the ODG peptide. Similar to the other Hyp-Y-G peptide, water mediated inter- and/or intra-chain hydrogen-bonds concerning Oδ of Hyp residue were observed. Water mediated inter- and/or intra-chain hydrogen-bonds concerning Asp carboxyl group were also observed. These hydrogen-bonds were thought to enhance the stability of the triple helix.

The lateral packing structure of this peptide showed the quasi-hexagonal packing, which

was usually observed for the peptides with the Pro-Hyp-Gly rich sequence. Two Asp residues in a triple helix were found to form hydrogen-bonds with Asp residues in the adjacent molecules and the third Asp was found to interact electrostatically with N-terminal of the adjacent staggered molecule. The poler side chain groups in ODG peptides enhance not only the intramolecular interaction, but also the intermolecular interaction, which stabilizes packing structure of this peptide.

P06-201

CRYSTAL STRUCTURE OF 3D8 scFv ANTI-DNA ANTIBODY, ITS SINGLE DOMAINS, AND THE COMPLEX WITH A SMALL MOLECULE

Suk-Yeol Park[1], Young-Rim Kim[2], Yong-Sung Kim[3], Myung-Hee Kwon[2], Jeong-Sun Kim[1,*]

[1]*Dept. of Chemistry, College of Natural Science, Chonnam National University, 300, Yongbong-dong, Buk-gu, Gwangju, 500-757, Korea.*

[2] *Dept. of Microbiology, Ajou Medical School, San 5, Woncheon-dong, Yeongtong-gu, Suwon 443-749, Korea.*

[3]*Dept. of Molecular Science and Technology, Ajou University, San 5, Woncheon-dong, Yeongtong-gu, Suwon 443-749, Korea.*

**Corresponding author: jsunkim@chonnam.ac.kr*

Anti-DNA antibodies (Abs) are of biomedical interests due to their association with autoimmune diseases in human and mice. The characterized anti-DNA monoclonal Ab 3D8 scFv from an autoimmune-prone MRL-pr/lpr mouse has shown the binding and hydrolyzing activities against single stranded (ss-) and double stranded (ds-) DNAs. The lack of the conserved amino acid residues of 3D8 scFv, VH, and VL for DNA-hydrolyzing activities upon comparison with other nucleases suggests that 3D8 belongs to another family of DNA-hydrolyzing enzymes. To understand the molecular mechanism of nucleotide recognition and hydrolysis, we elucidated crystal structure. The detailed structural features will be discussed.

(This work was supported by grant No. R01-2006-000-10743-0 from the Basic Research Program of the Korea Science & Engineering Foundation.)

P06-202

CRYSTAL STRUCTURE OF ydjA FROM *ESCHERICHIA COLI*

Ji-Woo Choi, Ji-Eun Lee, Che-Hun Jung, and Jeong-Sun Kim

Department of Chemistry, Chonnam National University, Gwangju, 500-757, Korea
**Corresponding author: jsunkim@chonnam.ac.kr*

Nitrogenreductases mediate the reduction of nitrogen-containing compounds. Often they require FMN as a cofactor. We elucidated the crystal structure of the putative nitrogenreductase from *E.coli*, ydjaA of 193 amino acids, without and with a FMN cofactor. The structure is composed of a beta-sheet of 5 beta-strands that are sandwiched by three alpha-helices. The detailed structural features will be discussed.

P06-203

CRYSTAL STRUCTURE OF ybfF FROM *ESCHERICHIA COLI*

Nishi Kosuke, Suk-Youl Park, Sang-Hak Lee, Ji-Woo Choi, Nguyen To Uyen, Ji-Eun Lee, Che-Hun Jung, and Jeong-Sun Kim

Department of Chemistry, Chonnam National University, Gwangju, 500-757, Korea
**Corresponding author: jsunkim@chonnam.ac.kr*

The ybfF gene from *E.coli* belongs to the putative hydrolase family upon the amino acid sequence analysis. To get the clue on the molecular function, we elucidated the crystal structure of ybfF at 1.1 Å resolution using SAD experiment. The ybfF protein is composed of two globular domains and the active site is constructed on the domain interface. The detailed structural features will be discussed.

P06-204

STRUCTURE AND FUNCTIONAL STUDY OF RICE BIFUCTIONAL ALPHA-AMYLASE/SUBTILISIN INHIBITOR FROM *Oryza sativa*

Wen-Yan Peng[a,c], Yi-Hung Lin[a], Yen-Chieh Huang[a], Hong-Hsiang Guan[a,c], Ying-Cheng Hsieh[a,c], Ming-Yih Liu[a],Tschining Chang[d], and Chun-Jung Chen[a,b]*

[a]*Life Science Group, Research Division, National Synchrotron Radiation Research Center, Hsinchu 30076, Taiwan;* [b]*Department of Physics,* [c]*Institute of Bioinformatics and Structural Biology, National Tsing-Hua University, Hsinchu 30013, Taiwan;* [d]*Department of Hospitality Management, Nan Jeon Institute of Technology, Yen-Shui, Tainan 73746, Taiwan*

Rice seeds are rich sources of different proteinaceous inhibitors with characteristic bifunctional enzyme-inhibiting activities such as α–amylase/subtilisin and trypsin /chymotrypsin inhibitors. These inhibitors were generally expressed in developing seeds and other organs, and were thought to play an important role in plant's defense system. It was generally believed that these inhibitors not only playing a role in plant development but also conferring a broad spectrum of resistance against pests and pathogens. Nevertheless, high-resolution structures of these inhibitors and in complex with target enzymes are available in other species but not in rice. Therefore, in this study, we purified RASI (rice alpha-amylase/subtilisin inhibitor, 18.9 kDa) from rice bran into homogenous and crystallized using the handing drop vapor diffusion method. According to X-ray diffraction of RASI crystals at resolution 1.80 Å, the unit cell belongs to space group $P2_12_12$ with parameters a=79.99 Å, b=62.95 Å and c=66.70 Å. Preliminary analysis of the protein indicate that there are two RASI molecules in an asymmetric unit with a solvent content of 44.05 %.Detail of the function of RASI in plant seeds seems to remain unclear. Because of its inhibition to Subtilisin and alpha-amylase of certain bacteria, RASI was considered playing a defense role. Despite it close structural relationship to other cereals showed distinct differences in sequences, in enzymatic and physico-chemical properties as well as the physiological expression to other species. Here we describe the successful purification and crystallographic characterization of RASI, and the goal of this project is to provide an alternative structural bases and ultimately functional illustration of enzyme-inhibitor interactions in rice plant which is one of the three most valuable cereal crops grown worldwide. In comparing between RASI and the homologous proteins, we can get more information about the protein functions.

P06-205

X-RAY 3D STRUCTURE AND FUNCTION STUDY OF RICE LECTIN-LIKE COMPLEX

Chin-Wen Wu,[a]Yen-Chieh Huang[b], Hong-Hsiang Guan[a], Yin-Cheng Hsieh[a], Chia-Hao Shin[a], Tschining Chang[c], Yi-Hung Lin[b] and Chun-Jung Chen[b]

[a]*Institute of Bioinformatics and Structural Biology, National TsingHua University, Hsinchu, Taiwan*
[b]*Synchrotron Radiation Research Center, Hsinchu, Taiwan*
[c]*Department of Hospitality Management, Nan-Jeon Institute of Technology, Tainan, Taiwan*

Lectins with sugar-binding specificity are widely distributed in higher plants and various other species. The expression of rice lectin from Oryza sativa is up-regulated in the growing coleoptile when anaerobic stress persists. A rice lectin of molecular weight 15.2 kDa has been crystallized using the hanging-drop vapour-diffusion method. Except the native lectin crystal, the complex of lectin and mannose has also been crystallized. In this study, three crystals (native lectin and two lectin-2αmannobiose crystal with different crystallization condition) are used to get X-ray diffraction pattern. From the diffraction of the native lectin crystals at 1.8 Å resolution, the unit cell belongs to space group P3 (1). Preliminary analysis indicates that there are two lectin molecules in an asymmetric unit. The unit cell of the lectin-2αmannobiose crystals at 1.8 Å resolution belongs to space group C222 (1). Preliminary analysis indicates that there is one lectin molecule and one 2αmannobiose in an asymmetric unit. The unit cell of the second lectin-trehalose crystals at 1.78 Å resolution belongs to space group P2 (1) 2 (1) 2 (1). Preliminary analysis indicates that there are two lectin molecules and one trehalose in an asymmetric unit.The result of study shows the rice lectin composed of 12 β sheets is a prism structure. The packing forms of the crystal under the different crystallization condition are monomer, dimmer and tetramer. Analyzing the exterior charge, there is an anion pocket at the active site composed of six amino acids: Gly14, Leu88, Gly133, Thr134, Leu135 and Asp137. In the three-dimensional structure, the interaction area of rice and mannose is in this anion pocket. Gly14, Gly133, Thr134, Leu135 and Asp137 will form the hydrogen network with O3, O4, O5 and O6 of mannose, and these hydrogen bonds can stabilize the structure of complex.

P06-206

COMPLEX STRUCTURE OF XYLANASE WITH XYLO-OLIGOSACCHARIDES FROM TRICHODERMA HARZIANUM ETS323 : STRUCTURAL EVIDENCE FOR GLYCOSYL TRANSFERASE REACTION

En-Hung Liu[e], Kun-Che Chang[c], Yuan-Lung Chiang[e], Ying-Cheng Hsieh[a,e], Chaur-Tsuen Lo[b], Yi-Hung Lin[a],Yen-Chieh Huang[a], Hong-Hsiang Guan[a,e], Kuo-Cheng Peng[c], Chun-Jung Chen[a,d]

[a] Life Science Group, Research Division, National Synchrotron Radiation Research Center, Hsinchu 30076, Taiwan;[b]Department of Biotechnology, National Formosa University of Science and Technology, Yunlin 63208, Taiwan;[c] Institute of Biotechnology, National Dong-Hwa University, Hualien, 97401, Taiwan;[d] Department of Physics, National Tsing-Hua University, Hsinchu 30013, Taiwan;[e] Institute of Bioinformatics and Structural Biology, National Tsing-Hua University, Hsinchu 30013, Taiwan

Xylanases catalyze the random hydrolysis of xylan, the most abundant hemicellulose in higher plants, to xylooligosaccharides and xylose. Trichoderma harzianum have diverse beneficial effects on plants as biocontrol agents against many soil-borne plant pathogens. Xylanase from Trichoderma harzianum ETS323, having a molecular weight of 20.5 kDa, has been crystallized using the hanging-drop vapor-diffusion method. According to X-ray diffraction data of native xylanase crystals at a resolution 1.00 Å, the unit cell belongs to space group P212121 and has parameters a = 43.21 Å, b = 51.35 Å and c = 95.07 Å. The crystals of xylanase and xylotriose complex have also been obtained by the soaking method and diffracted to 1.31 Å.

Complete model building, refinement and analysis of the structure to 1.0 Å-resolution for native xylanase; structural details of other complex, such as xylobiose, xylotriose, exlotetraose, xylopentaose and xylohexaose, will also be discussed.

P06-207

CRYSTAL STRUCTURE AND FUNCTIONAL STUDY OF THE BOWMAN-BIRK INHIBITOR FROM RICE BRAN IN TERNARY COMPLEX WITH BOVINE TRYPSIN

Hsin-Tai Li[a], Yi-Hung Lin[b], Yen-Chieh Huang[b], Ying-Cheng Hsieh[a,b], Hong-Hsiang Guan[a,b], Tschining Chang[c], Andrew H.-J. Wang[d] and Chun-Jung Chen[b]

[a]*Institute of Bioinformatics and Structural Biology, National TsingHua University, Hsinchu, Taiwan*
[b]*Synchrotron Radiation Research Center, Hsinchu, Taiwan*
[c]*Department of Hospitality Management, Nan-Jeon Institute of Technology, Tainan, Taiwan*
[d]*Institute of Biological Chemistry, Academia Sinica, Taipei, Taiwan*

The 15-kDa trypsin inhibitors from rice bran (RBTI) are members of the Bowman-Birk protease inhibitor (BBI) family. The crystal structure of a 1:1 complex between RBTI and bovine pancreatic trypsin (BPT) was determined by combination of molecular replacement and electron density modification methods. This complex model has been refined to a crystallographic R-factor of 26.2% and free R-factor of 31.6% at 3.0 Å resolution. The RBTI structure consists of seven β-strands and loops without α-helices structure and folds into two compact domains (N- and C-domain) which are similar to each domain from barley BBI. However, orientation between two domains is quite different to barley BBI, this makes the distance between two P1 residues (17Lys and 83Lys) in RBTI is only 23 Å apart rather than distance of 40 Å in barley BBI. The closer distance provides evidence to support result from activity assay that two domains show different abilities to inhibit trypsin. RBTI C-domain with protruding 84Met at P1' position, moreover, mainly leads into breakdown of the classically canonical conformation of reactive site loop. Major interaction with BPT is achieved by RBTI N-domain but C-domain plays an auxiliary role to block trypsin molecule.

P06-208

CRYSTAL STRUCTURE STUDY OF WILD TYPE AND MUTATED BACILLUS CEREUS NCTU2 CHITINASE

Yin-Cheng Hsieh[1,2], Chueh-Yuan Kuo[1,2] , Huei-Ju Tasi[3] , Yi-Hsin Pan[3] , Yaw-Kuen Li[3] , and Chun-Jung Chen[1,2]

[1]Life science Group, National Synchrotron Radiation Research Center, Hsinchu 30076, Taiwan
[2]Department of Bioinformatics and Structure Biology, National Tsing-Hua University, Hsinchu 30076, Taiwan [3]Department of Applied Chemistry , National Chiao-Tung University , Taiwan

Chitin, a β-(1,4)-linked polymer of N-acetyl D-glucosamine (GlcNAc), is widely distributed in nature, particularly as a structural polysaccharide in fungal cell walls in the exoskeleton of arthropods, the outer shell of crustaceans, nematodes, etc. Chitinases which hydrolyze chitin as carbon and nitrogen nutrient, occur in a wide range of organisms include in viruses, bacteria, fungi, insects, higher plants, and animals. A gene of family 18 chitinase from *Bacillus cereus* NCTU2 encodes a signal peptide (27 amino acids) and a mature protein (333 amino acids), The gene of family 18 chitinase from *Bacillus cereus* NCTU2 was constructed in pET-22b(+) and over-expressed by *E. coli* BL21 (DE3) strain. Amino acid multi-alignment reveals that E145 and Y227 are the potential residues mediating the catalytic function of ChiNCTU2. ChiNCTU2 and mutant E145Q of MW 36 kDa have been crystallized using the hanging-drop vapor diffusion method with solution consisted of polyethene glycerol 8000、sodium cacodylate and zinc acetate dihydrate. According to diffraction of ChiNCTU2 crystals at resolution 1.20 Å, the unit cell belongs to space group *P21* and has parameters a = 50.789 Å, b = 48.788 Å and c = 66.867 Å. And E145Q crystal at resolution 1.49, the unit cell belongs to space group *P1* and has parameters a = 61.306 50.820 Å, b =72.888 Å and c = 76.343 Å. The protein structure of ChiNCTU2 is monomer by using multiwavelength anomalous dispersion method and the crystal packing of E145Q is tetramer by using molecular replacement method. The structure of ChiNCTU2 comprises 12 α-helices and 10 β-sheets. Five residues Asp143、Glu145、Glu190、Gln225 and Tyr227 bind with zinc atoms in the catalytic domain of ChiNCTU2 protein structure. We proved that zinc atoms will cause declined activity of ChiNCTU2 by detecting the amount of chitobioside using DNS (3,5-Dinitrosalicylic acid) .We find an angular difference between residue E145 and Q145 when doing superimposition with dimer form ChiNCTU2 and E145Q protein structures reveals the declined activity of mutant E145Q. We also find that *S.marcescens* ChiA has greater catalytic velocity than *Bacillus cereus* chitinase when interact with colloidal chitin after doing DNS (3,5-Dinitrosalicylic acid) experiment .After comparing sequences and structures with other 18 family chitinase, we discover that ChiNCTU2 is the smallest protein among microbe chitinases.

P06-209

CRYSTALLOGRAPHIC STUDIES OF THE C-TERMINAL DOMAIN OF DNA GYRASE.

Tung-Ju Hsieh[a], Hsun-Tang Chang[a], Te-Sheng Lin[a], Shu-Yun Haung[a], Lynn Farh[b], and Nei-Li Chan[a].

[a]*Institute of Biochemistry, National Chung Hsing University, Taichung City 402, Taiwan, and* [b]*Department of Applied Chemistry and Life Science, National Ping Tung University of Education, Ping Tung 900, Taiwan.*

Most bacteria harbor two essential Type IIA DNA topoisomerases, DNA gyrase and topoisomerase IV (TopoIV). While these two enzymes are homologous, they exhibit distinct activities. DNA gyrase supports transcription and replication with its unique capability of introducing (−) supercoils, whereas Topo IV preferentially relaxes (+) supercoils and serves as the main decatenating enzyme during chromosome segregation. Based on crystal structures of the C-terminal domains (CTDs) from *Borrelia burgdorferi* gyrase (BbGyrA-CTD) and *Bacillus stearothermophilus* TopoIV (BsTopoIV-CTD), it was proposed previously that the divergence of enzyme function can be attributed to differences in the overall shaping of these two domains. However, recently determined CTD of *Escherichia coli* gyrase (EcGyrA-CTD) closely resembles BsTopoIV-CTD, rather than its functionally equivalent partner BbGyrA-CTD.

To understand the molecular basis of this functional divergence in greater detail, we have now determined the crystal structure of *Xanthomonas campestris* gyrase CTD (XcGyrA-CTD), and the structure of EcGyrA-CTD was re-determined in a new crystal form. These two new structures provide strong support for the idea that GyrA-CTD with canonical GyrA-box sequence most likely folds into a spiral β-pinwheel. A piece of electron density corresponds to the highly-conserved GyrA-box sequence was identified in one of the XcGyrA-CTD molecules in the asymmetric unit, representing the first structural information for this critical functional motif. In contrast to the molecular “Velcro” role of GyrA-box seen in BbGyrA-CTD, we noticed that a region downstream of GyrA-box was found to participate in the ring-closure in XcGyrA-CTD. Interestingly, the overall spiral-shape of GyrA-CTD ισ περσιστεντ ρεγαρδλεσσ ωηετηερ τηε β-pinwheel ring is closed or not. Detailed structural analysis and functional implication of our findings will be presented during the meeting.

P06-210

STRUCTURAL AND FUNCTIONAL STUDIES OF THE 6-PHOSPHOGLUCONATE DEHYDROGENASE ASSOCIATED WITH PATHOGENESIS OF *KLEBSIELLA PNEUMONIAE*

Ying-Yin Chen (陳盈穎)[1,2], Tzu-Ping Ko (柯子平)[2], Li-ping Lo(羅麗萍)[2], Chun-Hung Lin (林俊宏)[2,3], Andrew H-J Wang (王惠鈞)[2,3]

1. Institute of Biochemical Sciences, National Taiwan University, Taipei, Taiwan
2. Institute of Biological Chemistry, Academia Sinica, Nankang, Taipei, Taiwan
3. Genomics Research Center, Academia Sinica, Taipei, Taiwan

The Gram-negative bacterium, *Klebsiella pneumoniae*, is an opportunistic pathogen that is commonly isolated from urinary tract infections, nasocomial pneumonia, surgical wounds and blood stream infections. The enzymes directly related to its virulence are validated as novel targets for the understanding of the pathogenicity of *K. pneumoniae*, development of new antibiotics, as well as decoding of the structure and functional relationship of innate immunity. The 6-phosphogluconate dehydrogenase (6PGDH) has been determined and annotated as a metabolic enzyme of the pentose phosphate (PPP) pathway. Recent finding demonstrates that 6PGDH is one of cell wall lectin proteins and elicits a protective immune response in mice. Our study identifies the structures of 6PGDH from *E. coli* and *K. pneumoniae* and predicts the carbohydrates binding region for its adhesion function. The resulting high resolution three-dimensional structures will provide valuable information to design potent enzyme inhibitors as potential new drug candidates.

P06-211

CRYSTALLIZATION AND STRUCTURAL ELUCIDATION OF PLASMODIUM VIVAX DIHYDROFOLATE REDUCTASE-THYMIDYLATE SYNTHASE

Puttapol Khongsuk,[a] Ubolsree Leartsakulpanich,[b] Yongyuth Yuthavong[b] and Palangpon Kongsaeree[a]

[a]*Department of Chemistry and Center for Protein Structure and Function, Faculty of Science, Mahidol University, Rama VI Road, Bangkok 10400;* [b]*BIOTEC, National Science and Technology Development Agency, Paholyothin Road, Klong 1, Klong Luang, Pathumthani 12120, Thailand.*

The bifunctional enzyme *Plasmodium vivax* dihydrofolate reductase-thymidylate synthase (PvDHFR-TS) were purified using a single-step affinity chromatography on methotrexate-sepharose column. The PvDHFR-TS protein solution was complexed with NADPH, dUMP and pyrimethamine (Pyr) as an inhibitor. Crystallization was performed by the microbatch method and DHFR-TS crystal was collected data by using the synchrotron source equipped with a CCD detector by using beamline 13B1, NSRRC, Taiwan.

The rod-shaped crystal of PvDHFR-TS from mother liquor containing PEG, buffer and salt grew slowly within 3 weeks. The first crystal belonged to the orthorhombic space group $P2_12_12_1$ with unit-cell parameters of a = 62.36, b = 114.81, c = 198.90 Å. The calculated Metthews coefficient suggests the presence of two molecules in the asymmetric unit, with a solvent content of 50.6% and the crystal packing revealed a different dimerization mode from other bifunctional DHFR-TS. The details about the crystallization and the structural elucidation will be presented and discussed.

P06-212

THE CRYSTAL STRUCTURE OF N-TERMINAL DOMAIN OF PLANTS NADPH OXIDASE

Takashi Oda,[a] Kokoro Hayashi,[b] Chojiro Kojima,[b] Hiroshi Hashimoto,[a] Tsutomu Kawasaki,[b] Ko Shimamoto[b], Mamoru Sato[a], and Toshiyuki Shimizu[a]

[a] *International Graduate School of Arts and Sciences, Yokohama City University, Japan;* [b] *Graduate School of Biological Sciences, Nara Institute of Science and Technology, Japan*

Reactive Oxygen species (ROS) produced by NADPH oxidase play critical roles in various cellular activities including defense against pathogens by plant. To generate ROS in defense response against pathogen, plant cells need oxygen in large amounts called respiratory burst. Plant NADPH oxidase named Rboh (respiratory burst oxidase homolog), is a homolog of mammalian phagocyte NADPH oxidase catalytic subunit $gp91^{phox}$. The phagocyte NADPH oxidase forms multi-protein complex containing several membrane and cytosolic regulatory factors and small GTPase Rac. However, in plants, no homologs of these regulatory factors expect Rac have been found. Rboh possesses an extended N-terminal domain including two EF-hand motif (EF1 and EF2) which does not exist in $gp91^{phox}$, suggesting that Ca^{2+} ions are also involved in the regulation. The regulation mechanism of NADPH oxidase is different between plants and mammals. It is suggested that Rac functions as a positive regulator of Rboh. Moreover, plant Rac directly interacts with the N-terminal domain of Rboh.

To elucidate the regulation and recognition mechanism of Rhoh by Rac and Ca^{2+} ions, we determined the crystal structure of N-terminal domain of *Oryza sativa* RbohB (OsrbohB(138-313)). OsrbohB(138-313) formed homo dimer by two EF-hand motif and coiled-coil structure. Electron density of Ca^{2+} ion in EF1 was clearly detected but not in EF2. The CD spectrum of OsrbohB(138-313) is different between a Ca^{2+} loaded and free form. This result suggests that Rboh changes its conformation in a Ca^{2+}-dependent manner. While, the result of GST pull down assay suggests that Rboh interact with Rac in a Ca^{2+}-independent manner.

P06-213

HIGHER SIGNAL, LOWER NOISE: HOW TO GET THE BEST DATA FROM YOUR CRYSTALS

Martin Adam[1], Anita Coetzee[1], Bram Schierbeek[1], Cary Bauer[2] and Rob Hooft[2]

[1] Bruker AXS B.V., Delft, The Netherlands, [2] Bruker AXS Inc., Madison, WI, USA

In a macromolecular crystallography, where crystals are small and often weakly diffracting, it is imperative to obtain data with as high a signal-to-noise ratio as possible. Improving the signal usually involves using a more powerful source, since obtaining samples with larger diffraction volume is often not possible.

The contribution of the noise should not be underestimated. Especially when looking at weak reflections or small differences in anomalous signal (e.g. doing S SAD phasing on native proteins) one has to take great care to minimize the experimental noise as much as possible. This can be done by careful sample handling, minimizing the effect of background scatter from the cryo protectant and loop as well as in setting up the data collection experiment. Examples of more efficient data collection methods will be presented which can lead to a dramatic increase in signal to noise ratio, with the same amount of X-ray photons falling on the crystal. If all precautions have been taken to lower the noise of the experiment, then there is only one way to get a higher a signal-to-noise ratio: increasing the amount of X-rays on your sample. The MICROSTAR ULTRA, the next generation of the MICROSTAR series of generators, is substantially brighter than any other X-ray home source available today. With its revolutionary HyperCool™ anode cooling technology the MICROSTAR ULTRA is more intense and yet easier to maintain than other rotating anode generators.

Measurements show that this source compares with many second generation beam lines. Results of crystal data will be presented.

P06-214

CRYSTALLOGRAPHIC CHARACTERIZATION OF THE RADIXIN FERM DOMAIN BOUND TO CYTOPLASMIC TAIL OF ADHESION MOLECULE CD44

Tomoyuki Mori, Ken Kitano, Shin-ichi Terawaki, Ryoko Maesaki and Toshio Hakoshima

Structural Biology Laboratory, Nara Institute of Science and Technology (NAIST), Ikoma, Japan.

CD44 is an important adhesion molecule that specifically binds hyaluronic acid, a typical major component of the extracellular matrix, and regulates cell-cell and cell-matrix interactions. Increasing evidence has indicated that CD44 is assembled in a regulated manner into protein complexes at the membrane-cytoskeletal junction, a process mediated by ERM (Ezrin/Radixin/Moesin) proteins. Formation of this protein complex, involving both direct and indirect interactions, serves to focus downstream signal transduction events that regulate cell growth and development.

Ezrin, radixin and moesin form the ERM family of proteins, which link membrane proteins to the cytoskeleton and perform structural and regulatory roles at the polarized cell cortex. ERM proteins consist of three functional domains; an N-terminal FERM (Four point one, Ezrin, Radixin, Moesin) domain, an extended coiled-coil region and a short C-terminal domain that binds F-actin. The FERM domain associated with the plasmamembrane directly binds the juxtamembrane region of the cytoplasmic tails of the various transmembrane proteins such as intercellular adhesion molecules ICAM-1, 2, 3 of the immunoglobulin superfamily, cell-surface glycoprotein CD43, cell-surface hyaluronate receptor CD44. Thus, notwithstanding the critical role played by these protein-protein interactions from a biological and medical perspective, precise details concerning the interaction between the FERM domain and CD44 remain unknown. Crystallographic studies of the protein complex were therefore performed in an effort to delineate the interactions between ERM proteins and CD44.

Recently, we obtained the crystal of complex between the radixin FERM domain and the C-terminal cytoplasmic region of CD44. The crystal of the radixin FERM domain bound to the CD44 cytoplasmic tail peptide belong to space group $P2_12_12_1$ with unit-cell parameters a = 62.70, b = 66.18 and c = 86.22 Å, containing one complex in the crystallographic asymmetric unit. Intensity data set was collected to a resolution of 2.1 Å.

P06-215

CRYSTALLOGRAPHIC STUDIES OF A LECTIN FROM THE OCTOCORAL

Akiko Kita,[a] Mitsuru Jimbo,[b] Yukio Morimoto,[a] Ryuichi Sakai,[b] Hisao Kamiya,[b] and Kunio Miki[c]

[a]*Research Reactor Institute, Kyoto University, Kumatori-cho, Sennan-gun, Osaka 590-0494, Japan;* [b]*Department of Marine Biosciences, School of Fisheries Sciences, Kitasato University, Ofunato, Iwate 022-0101, Japan;* [c]*Department of Chemistry, Graduate School of Science, Kyoto University, Kyoto 606-8502, Japan.*

A number of lectins, sugar-binding proteins, are known to be present in a variety of animals or plants. In marine animals, lectins are believed to contribute as non-self recognition factors to the defence mechanism. Interestingly, it has been theorized that some lectins from marine animals mediate the interaction between symbiont and host.

SLL-2 is a D-galactose binding lectin isolated from the octocoral *Sinularia lochmodes*. SLL-2 is composed of 94 amino acid residues and contain one glycosylation site. It was found that SLL-2 was distributed densely on the surface of symbiotic dinoflagellate *Symbiodinium* sp. cells. Recently, SLL-2 was confirmed to transform free-swimming stage *Symbiodinium* cells into non-motile stage *Symbiodinium* cells and keep them in their non-motile stage (K. Koike, *et al*., *Biol. Bull*. 207, 80 (2004)). These results indicate that SLL-2 is a chemical cue in the symbiosis between dinoflagellates and coral. The three-dimensional structure of SLL-2 may provide information about the symbiosis mechanism. We started crystallographic works of SLL-2 to elucidate its structure.

SLL-2 was extracted and purified as previously reported (M. Jimbo *et al*., *Biochem. Biophys. Res. Commun*. 330, 157 (2005)). The protein solutions were prepared in Bis-Tris buffer at pH 6.5. The best crystals of SLL-2 were obtained from the solutions containing 2-methyl-2,4-pentanediol as a precipitant and calcium formate as an additive reagent by the sitting-drop vapour diffusion method at 20˚C. The parallelogram thin crystals were grown up to the maximum dimension of 0.5mm on one side. The crystals belonged to space group $P2_1$ with cell dimensions of a=52.7 Å, b=189.2 Å, c=57.2 Å, and β=110.8°. The crystal structure analysis is in progress.

P06-216

CRYSTALLIZATION AND STRUCTURAL ELUCIDATION OF PLASMODIUM VIVAX DIHYDROFOLATE REDUCTASE-THYMIDYLATE SYNTHASE

Puttapol Khongsuk,[a] Ubolsree Leartsakulpanich,[b] Yongyuth Yuthavong[b] and Palangpon Kongsaeree[a]

[a]*Department of Chemistry and Center for Protein Structure and Function, Faculty of Science, Mahidol University, Rama VI Road, Bangkok 10400;* [b]*BIOTEC, National Science and Technology Development Agency, Paholyothin Road, Klong 1, Klong Luang, Pathumthani 12120, Thailand.*

Antifolate drugs, such as pyrimethamine and trimethoprim, are used to treat malaria. The target enzyme of these drugs is dihydrofolate reductase (DHFR) that involves in the DNA synthesis of the malaria parasite. In nature, *Plasmodium vivax* dihydrofolate reductase-thymidylate synthase (PvDHFR-TS) is found to be the bifunctional enzyme. Drugs resistance to PvDHFR has found in many parts of the world. In order to understand the drug-resistance mechanism of the enzymes, x-ray crystallography technique has been used to determine their three dimensional structure.

Recently, PvDHFR structure has been solved by our research group and published. We found that the inhibition constant (K_i) of the double point mutation (S58R+S117N) shown 300-fold and 14-fold (*data unpublished*) higher resistant to pyrimethamine in PvDHFR and PvDHFR-TS, respectively. In this study, the first structure of PvDHFR-TS has found that its crystal packing has a different homology dimerization structure from other bifunctional DHFR-TS structures such as, *Plasmodium falciparum* and *Cryptosporidium hominis*. It speculates that its different structure might come from the interaction of protein surface in the molecule of the enzyme. This x-ray diffraction data were collected by using the synchrotron source equipped with a CCD detector by using beamline 13B1, NSRRC, Taiwan. The details of the crystallization and the structure elucidation of the enzyme will be presented and discussed.

P06-217

NOVEL DNA-BINDING FOLD AND DNA-RECOGNITION MODE DISCOVERED IN PABI FAMILY OF RESTRICTION ENZYMES

Ken-ichi Miyazono[1,7], Miki Watanabe[2,7], Jan Kosinski[3], Ken Ishikawa[2,5], Masayuki Kamo[1], Tatsuya Sawasaki[4], Koji Nagata[1], Janusz M. Bujnicki[3], Yaeta Endo[4], Ichizo Kobayashi[2,5,6], & Masaru Tanokura[1]

1 Department of Applied Biological Chemistry, Graduate School of Agricultural and Life Sciences, University of Tokyo, Tokyo, 113-8657, Japan, 2 Department of Medical Genome Sciences, Graduate School of Frontier Science, University of Tokyo, Tokyo 108-8639, Japan., 3Laboratory of Bioinformatics and Protein Engineering, International Institute of Molecular and Cell Biology, Trojdena 4, 02-109 Warsaw, Poland, 4 Department of Applied Chemistry, Faculty of Engineering, Ehime University, Matsuyama 790-8577, Japan, 5 Graduate Program in Biophysics and Biochemistry, Graduate School of Science, University of Tokyo, Tokyo 108-8639, Japan, 6 Institute of Medical Science, University of Tokyo, Tokyo 108-8639, Japan, 7 These authors contributed equally to this work

PabI is a Type II restriction endonuclease that recognizes 5'GTAC sequence and leave a 3'TA overhang (5'GTA/C). PabI and its cognate modification enzyme were identified in *Pyrococcus abyssi* through comparison of closely related genomes based on the behavior of Type II restriction-modification gene complexes as mobile elements. While the modification methyltransferase was easily recognized, PabI was predicted to have a novel three-dimensional structure by the analysis of amino acid sequence. Additionally, unlike most restriction enzymes analyzed, PabI is able to cleave a target DNA in the absence of added Mg^{2+}. It is very important to analyze PabI structure to understand its overall structure and enzymatic function. To reveal structural basis of PabI, we determined its three-dimensional structure by X-ray crystallography.

We expressed PabI in a wheat-germ cell-free translation system because protein expression systems using eukaryotic or prokaryotic cells are not suitable for the expression of cytotoxic protein. The structure of PabI was determined by the single-wavelength anomalous dispersion (SAD) method using selenomethionine derivative at 3.0 Å resolution. Structural analysis of PabI showed that this enzyme adopt a novel protein fold as predicted.

PabI form homodimer by a formation of extended anti-parallel β-sheet that is curved to form an extended groove, which is the unique architecture of PabI. We named this unique substructure "half pipe". Mutational and *in silico* DNA binding analyses have assigned the groove as the double-strand DNA binding site.

Mutational analysis has revealed that there are three residues, Arg32, Glu63, and Tyr134, which are indispensable for the catalytic activity of PabI. All of three residues are located in the "half pipe" structure of PabI dimer. These residues would act as catalytic or DNA binding residues.

Miyazono, Watanabe et al. Nucleic Acids Research 2007 35(6):1908-18.

P06-218

SINGLE MUTATIONS LEAD TO SIGNIFICANT INCREASE IN SUBSTRATE SPECIFICITY AND ACTIVITY: STRUCTURAL, ENZYME KINETICS AND MOLECULAR MODELING STUDIES FOR CYSTEINE PROTEASE FROM A TROPICAL PLANT

Raka Ghosh, Chandana Chakrabarti, Sampa Biswas and J.K. Dattagupta

Crystallography and Molecular Biology Division, Saha Institute of Nuclear Physics, 1/AF Bidhannagar, Kolkata-700064, India.

Latex of a tropical flowering plant, *Ervatamia coronaria*, contains three papain-like cysteine proteases - Ervatamin-A, -B and -C. These proteases have been isolated, purified and characterized. Among these three proteases, Ervatamin-A and Ervatamin-C, have high homology in their primary and tertiary structures and they also bear 90 % sequence identity. In spite of having high similarities, these two proteases show deviations in stability, activity and specificity. S2 subsite is the major specificity determinant for papain family cysteine proteases. Enzyme kinetics studies using chromogenic peptides revealed that both the ervatamins show preference for branched hydrophobic residues at P2 position of the peptide substrates but with different degree of efficiency. Biochemical studies show high activity of Ervatamin-A amongst ervatamins towards synthetic peptides and protein substrates. Compared to Ervatamin-A, there is only one substitution at the S2 pocket of Ervatamin-C (Tyr67 → Ala67) within 10Å sphere around catalytic cysteine. From structural point of view, this single replacement made the S2 cavity of Ervatamin-C wider preventing proper environment to bind and fix P2 residue of the above substrates. This is reflected in the higher K_M value of Ervatamin-C compared to Ervatamin-A, i.e., Ervatamin-C exhibits lower substrate affinity due to this change. There is another single substitution in the helix containing catalytic cysteine residue which have reducing effect on the catalysis rate (k_{cat}) of Ervatamin-C by reducing polarizibility of the specified helix and inter-domain plasticity. These two single substitutions reduced specificity constant (k_{cat}/ K_M) of Ervatamin-C significantly (57-times lower). This can be used as a template for SDM studies to appropriately design enzymes. Some results will be discussed.

P06-219

SYNTHESIS AND CHARACTERIZATION OF $CuMPt_6$ (M= 3D ELEMENTS) TERNARY ALLOYS

Ejaz Ahmed [a,b], Miwako Takahashi [a], Hiroshi Iwasaki [a] and Ken-ichi Ohshima [a]

[a]*Institute of Materials Science, University of Tsukuba, Tsukuba, 305-8573, Japan;* [b]*Physics Division, Pakistan Institute of Nuclear Science and Technology (PINSTECH), Nilore, Islamabad,Pakistan*

We have already identified the crystal structure of newly designed $CuMPt_6$ (M=3d elements) alloys by X-ray, electron and neutron diffraction methods [1, 2]. In the analysis, a double step ordering without any change of cubic symmetry was discovered for $CuMnPt_6$ alloy for the first time. In order to obtain more quantitative information on structure, transition temperature, electrical behavior and magnetism of this alloy group, we have performed X-ray diffraction (room temperature and in-situ), electrical resistivity and magnetic susceptibility measurements. The transition temperatures from disordered to Cu_3Au type ordered phases were determined in a temperature range from 880 ^oC for M=Co to 1320 ^oC for M=Ti [3]. The values of the resistivity were determined as $(5\sim7)x10^{-3}$ Ωm. A general trend in magnetic properties is as follows: paramagnetic – spin-glass like – ferromagnetic – paramagnetic with increasing atomic number. The variation of the structural ordering in this alloy group is found to be more systematic with increasing atomic number as compared to magnetic ordering. The nature of the magnetism is not much affected by the structural phase changes in the present alloys, though a little change is observed in T_c or T_g. The original nature of the magnetism in the ternary $CuMPt_6$ alloys remains the same as in the binary MPt_3 one. We believe that the unpaired electrons in 3d-elements are responsible for the magnetic properties of $CuMPt_6$ alloys.

P06-220

X-RAY STRUCTURE OF THE SKP1-FBS1 GLYCOPROTEIN COMPLEX

Tsunehiro Mizushima,[a] Yukiko Yoshida,[b] Taichi Kumanomidou,[a] Yuko Hasegawa,[a] Atsuo Suzuki,[a] Takashi Yamane[a] and Keiji Tanaka[b]

[a] *Department of Biotechnology, Graduate School of Engineering, Nagoya University; Nagoya, Japan*
[b] *Department of Molecular Oncology, Tokyo Metropolitan Institute of Medical Science, Tokyo, Japan*

Ubiquitin-mediated proteolysis plays a regulatory role in a number of diverse cellular processes and involves the selective destruction of short-lived functional proteins. The ubiquitin–proteasome system also is responsible for the disposal of misfolded and unfolded cellular proteins, the aberrant accumulation of which usually causes cell death, which can lead to neurodegenerative diseases. Protein ubiquitination is catalyzed by a sophisticated cascade system consisting of the ubiquitin-activating (E1), ubiquitin-conjugating (E2), and ubiquitinligating (E3) enzymes. Among these enzymes, the E3 enzymes are responsible for the selection of target proteins. The ubiquitin ligase complex SCF^{Fbs1}, which contributes to the ubiquitination of glycoproteins, is involved in the endoplasmic reticulum-associated degradation (ERAD) pathway. Misfolded proteins and unassembled protein complexes that fail to assume their functional states in the endoplasmic reticulum are subjected to ERAD, which involves retrotranslocation into the cytosol and degradation by the ubiquitin–proteasome system. In SCF ubiquitin ligases, a diverse array of F-box proteins confers substrate specificity. Fbs1/Fbx2, a member of the F-box protein family, recognizes high-mannose oligosaccharides. To elucidate the structural basis of SCF^{Fbs1} function, we determined the crystal structures of the Skp1–Fbs1 complex and the sugar binding domain (SBD) of the Fbs1–RNaseB complex at 2.4 and 2.7 Å resolutions, respectively. The structure of the Skp1–Fbs1 complex illustrates a different class of F-box proteins within the SCF ubiquitin ligase model. The mechanistic model indicated by the structures appears to be well conserved among the SCF ubiquitin ligases. The structure of the SBD–glycoprotein complex indicates that the SBD primarily recognizes Man3GlcNAc2. In addition, there are limited contacts between the SBD and RNaseB; the interface involves only 514 $Å^2$ of surface-accessible area. The surface areas occupied by Man3GlcNAc2 and the protein portion of the substrate are 349 and 165 $Å^2$, respectively, suggesting that Man3GlcNAc2, but not the protein in RNaseB, defines the interaction with Fbs1. SCF^{Fbs1} is a functionally unique molecule that recognizes the innermost Man3GlcNAc2 in N-glycans as a marker of denatured proteins. Our results provide a mechanistic basis for the recognition and ubiquitination of various glycoproteins by SCF^{Fbs1}.

P06-221

X-RAY MULTIPLE-WAVE DIFFRACTION ANOMALOUS FINE STRUCTURE

S.-C. Weng[a], Y.-R. Lee[a], Yu. P. Stetsko[b], W.-H. Sun[a], Y.-L. Soo[a] and S.-L. Chang[a]

[a]*Department of Physics, National Tsing Hua University,* [b]*National Synchrotron Radiation Research Center, Hsinchu 300, Taiwan, R.O.C.*

The combination of x-ray multiple-wave diffraction with diffraction anomalous fine structure (DAFS) technique, Multiple-wave Diffraction Anomalous Fine Structure (MDAFS), provides long-range order structure information by measuring the multiple-wave diffraction profiles in the vicinity of an absorption edge of the constituent atom of the sample crystal. The real part of dispersion correction and fine structure function can be obtained directly by multiple diffraction analysis without using Kramers-Krong relations (KKR) and kinematical fitting of diffracted intensity. The useful x-ray phase information of the structure-factor multiplets, linking the imaginary part with the real part of the structure factor, can easily replace the Kramers-Kronig relations. Moreover, the constraint imposed by the additional reflection on the diffraction geometry makes the MDAFS a much more wavevector and site-sensitive technique than the two-wave DAFS for the measurements. The three-wave diffraction measurement of GaAs single crystal near the Ga K-edge will be demonstrated as an example.

P06-222

DYNAMICAL CALCULATION FOR TWENTY-FOUR BEAM X-RAY DIFFRACTION IN A TWO-PLATE CRYSTAL CAVITY OF SILICON

M.-S. Chiu[1)], Yu. P. Stetsko[2)], and S.-L. Chang[1)]

[1)]*Department of Physics, National Tsing Hua University;* [2)]*National Synchrotron Radiation Research Center, Hsinchu 300, Taiwan, R.O.C.*

The X-ray back diffraction of (12 4 0) in a two-plate silicon resonator takes place at 14.4388 keV, at which simultaneous twenty-four beam diffraction consisting of nine coplanar reflections occurs. Based on the dynamical theory of X-ray diffraction, the numerical calculation method using a Cartesian coordinate system is employed to deal with the back diffraction, the interference due to Fabry-Perot type resonance that produces intensity undulation in both transmitted and back-reflected beams. The coordinates of tie points of the dispersion surface, linear absorption coefficients, wavefield intensities, and excitations of mode are calculated. The disentangling of 96 dispersion sheets and related linear absorption coefficients will be discussed. The involved phases in this 24-beam diffraction with X-ray cavity resonance will be discussed.

P06-223

STRUCTURAL FEATURES OF PSYCHROPHILIC MALATE DEHYDROGENASE ADAPTING TO THE EXTREME ENVIRONMENT

Yasuo Hata,[a] Tomomi Fujii, [a] Tadao Oikawa[b] and Kenji Soda [a,b]

[a]*Institute for Chemical Research, Kyoto University, Uji, Japan;* [b]*Graduate School of Engineering, Kansai University, Suita, Japan*

The psychrophilic and thermolabile malate dehydrogenase from *Flavobacterium frigidimaris* KUC-1(FfMDH) was isolated from Antarctic seawater. The enzyme is a homotetramer with a molecular weight of 123kDa and the number of amino acid residues is 311 for the subunit. To understand structural features of psychrophilic enzymes adapting to etreme environments, the structure of holo-FfMDH has been solved by X-ray crystallography and compared to those of mesophilic and thermophilic enzymes.

Holo-FfMDH was crystallized by a hanging-drop vapor diffusion method at 288 K. The crystal grew up to 1.00 x 0.15 x 0.05 mm in a few days. It has space group $P3_221$ with unit cell dimensions of a=b=147.8 Å and c=165.1 Å, and contains four subunits in the asymmetric unit. Diffraction data were collected at 100 K to 1.8 Å resolution at BL-5A, PF, Tsukuba, Japan. The crystal structure was solved by molecular replacement using the program MOLREP and search-model coordinates of a hybrid MDH (PDB code 1GUZ), and refined for 1.8 Å diffraction data to Rwork=0.146 and Rfree=0.164 with the programs CNS and Refmac5.

The tetrameric structure of FfMDH is a dimer of dimmers and similar to those of MDHs from other bacteria. A structural comparison of four MDHs from the present psychrophilic, mesophilic, moderate thermophilic and thermophilic bacteria, however, reveals several differences in molecular architecture, especially intersubunit interaction. The number of ion pairs in the FfMDH tetramer is smallest among the MDH molecules compared. Although no features are found in the number of intrasubunit ion-pairs, a remarkable difference lies in that of intersubunit ion-pairs. The present FfMDH has no intersubunit ion-pairs, although three other MDHs have two to six ion-pairs between every two subunits in each molecule. This difference becomes marked in two close dimers formed in the tetramer. The lack of intersubunit ion-pair in the oligomeric molecule results in the loose contact among the subunits in the molecule. This possibly contributes to the activity expression of the present psychrophilic enzyme at low temperatures, which may be common to other psychrophilic enzymes. Further investigations are needed to elucidate the structure-activity relationship of proteins in such extreme environments.

P06-224

GROWTH RING OF TEETH- A MICRO X-RAY DIFFRACTION STUDY

Hejing Wang[a], Jian Zhou[b], Nan Zheng[a] and Tingjing Xu[a]

[a]*X-ray Laboratory, School of Earth and Space Sciences, Peking University, Beijing 100871, P. R. CHINA;* [b]*Chinese Academy of Geosciences, 26 Baiwanzhuang Road, Beijing 100037, P. R. CHINA*

Crystallinity of hydroxylapatite in human teeth was investigated using a micro X-ray diffractometer with a beam spot of 200μm in diameter. A 10-point section crossing 10-year-old deciduous teeth was hopefully selected to clarify the growth ring in teeth. It is revealed from this 10-point section analysis that most reflections of hydroxylapatite are getting more and more outstanding and isolating from the most inner parts to the most outer parts in teeth while some reflections of hydroxylapatite are becoming weaker and weaker. This phenomenon is induced by age of teeth or crystallinity of hydroxylapatite in the sense of crystallography.

This change of hydroxylapatite in teeth is quantitatively described by the intensity ratio of reflections 112 to 211 that is decreasing from 0.84 in the most inner parts to 0.29 in the most outer parts of teeth and by the intensity ratio of reflections 300 to 211 that is generally increasing from 0.82 via 0.76 to 2.33 respectively. Meanwhile these three reflections 211, 112 and 300 gradually merge from "two rabbit-ear peaks" into "one peak" with a shoulder. Accompanying with this cluster change in hydroxylapatite the relative intensity of reflections 130 and 210 decrease from the outer parts to the inner parts and those reflections in the range of 45-54º2θ,CuKα merge into three peaks with a bump. The three peaks are reflections 222, 213 and 004 and the bump is consisting of very broad and heavily overlapped reflections 132, 230, 321, 410, 402 and 303. Therefore the intensity ratios of reflections 112 to 211 and 300 to 211 are proposed as the diagnostic indices of crystallinity of hydroxylapatite in teeth.

The TREOR method was used to refine the cell parameters of hydroxylapatite in teeth and it results a 9.456 angstroms of a and 6.889 angstroms of c lattice parameters with a 7.3 Snyder's Figure of Merit for the most outer parts hydroxylapatite in teeth. For the middle parts of hydroxylapatite, it derives the same cell parameter a as the most outer parts of hydroxylapatite and a 6.895 angstroms c which is a little bit larger than that of the outer parts of hydroxylapatite in teeth. It is failed to refine the cell parameters of hydroxylapatite in the inner parts of teeth since heavier overlapping in peak or poor crystallinity.

P06-225

STRUCTURES OF SOME CRYSTAL SOLVATES OF N-(3-ETHYLTHIO-1,2,4-THIADIAZOL-5-YL-AMINOCARBONYLMETHYL) CYTIZINE

U.S. Mahmudov, T.F. Ibragimov, K.K. Turgunov, B. Tashkhodjaev.

S.Yunusov Institute of Chemistry of Plant Substances, Kh.Abdullaev Str. 77, Tashkent 700170, Uzbekistan

Investigating structure of N-(3-ethylthio-1,2,4-thiadiazol-5-yl-aminocarbonylmethyl) cytizine have found inclusion in its crystal a solvent molecules. The crystals obtained by us for X-Ray analyses from different solvents: aqueous methanol **(1)** and a absolute acetone **(2)** had different unit cells and a space groups. Such phenomena aviable at solvatomorphism (inclusion in a crystal of different molecules of the solvent) of crystals. So N-(3-ethylthio-1,2,4-thiadiazol-5-yl-aminocarbonylmethyl) cytizine behaves as a host molecule in relation to solvent molecules and probably is potential clathratogen. For explain the causes of these phenomena are carried out a X-Ray structural analysis of crystals of titled compound , grown in above-stated solvents. Results of X-Ray analyses have shown, that crystals **(1)** and **(2)** contain molecules of water and acetone, accordingly, i.e. takes place a phenomena of inclusion. If, in a crystal **(1)** solvate (guest) and "host" molecules are in the ratio 1:1 whereas in **(2)** ratio of host and solvent molecules are as 1:2 (in the asymmetric unit there are two molecules of N-(3-ethylthio-1,2,4-thiadiazol-5-yl-aminocarbonylmethyl) cytizine and one molecule of acetone).

- H_2O **(1)**
- 0,5 $(CH_3)_2CO$ **(2)**

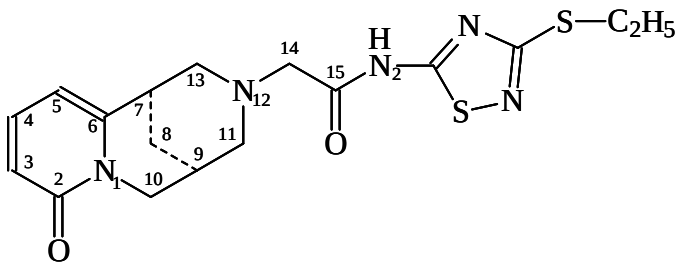

P06-226

STRUCTURAL EVIDENCE THAT AN α-PROTEOBACTERIA IS THE OLDEST SURVIVING SPECIES

William L. Duax, Robert Huether, Qilong Mao, Vladimir Pletnev, Timothy Umland and Charles M. Weeks

Structural Biology, Hauptman-Woodward Medical Research Institute, Buffalo, NY 14203, USA

The Rossmann fold is one of the most ancient and commonly encountered protein folds. From 5 to 50 members of the short-chain oxidoreductase (SCOR) enzyme family, which contains a Rossmann fold, are present in the genomes of all species sequenced to date. The SCOR family is part of a much larger superfamily of Rossmann folds that use NAD(H) or NADP(H) as cofactors. Crystallographic and biochemical studies have revealed that, in the vast majority of Rossmann folds, NAD or NADP cofactor preference is controlled by the presence of an Asp residue in a specific sequence position in the $\beta_2\alpha_3$ turn or an Arg in the adjacent sequence position, respectively.

The β-ketoacyl [acyl carrier protein] reductase (β-k-ACPR) enzymes, a 912-member subset of the SCOR family, are essential to fatty acid synthesis in bacteria and plants. By focusing analysis on the sequence and structure of the 912 β-k-ACPRs in the gene bank, we have discovered that (1) the most primitive member of the family was an NADP reductase, (2) that NADP binding was originally contingent upon a Ser or Thr residue in the $\beta_2\alpha_3$ turn (not an Arg), (3) that a specific dimer assembly is stabilized by the stacking of aromatic groups at specific sites on the α_5 and α_6 helices and (4) that a previously undetected GGMxM sequence at the C-terminus, conserved in all species of proteobacteria, stabilizes the functionally required tetramer by multiple hydrogen bonding and aromatic ring stacking crosslinking the four monomers together. We previously discovered that 20% of all the genes in the genebank have multiple open reading frames (MORFs) and a severe bias in codon use such that 85% of the coding in these genes is from the GC-rich half of the genetic code. We have been able to identify this pattern in the most ancient members of families of essential protein that are present in all species. We have found that 33% of the β-k-ACPR enzymes in α-proteobacteria have multiple open reading frames and a codon bias. Our analysis indicates that the primordial members of the β-k-ACPR family probably arose in GC-rich α-proteobacteria and that they are distinguished by the presence of multiple open reading frames (MORFs), an extreme codon bias in their DNA and an amino acid bias in their protein composition. In a separate study of the evolution of the $(\alpha/\beta)_8$ barrel *via* gene duplication we have traced the earliest members of that family to α-proteobacteria having high MORF content, and a codon bias restricted to codon ending in G or C. This research was supported by NIH grant No. DK26546.

P06-227

STRUCTURAL STUDY FOR THE ENZYME MECHANISM OF EUKARYOTIC GLUTAMINE SYNTHETASE FROM ZEA MAYS

Takeshi Ozaki[a], Hideaki Unno[b], Toshiharu Hase[a], Masami Kusunoki[a]

[a]*Institute for Protein Research, Osaka University,3-2 Yamada-oka Suita, Osaka 565-0871Japan;*
[b]*Factulty of Engineering, Nagasaki University, Japan*

Plants provide nourishment for animals and other heterotrophs as the sole primary producer in the food chain. Glutamine synthetase (GS), one of the essential enzymes for plant autotrophy catalyzes the incorporation of ammonia into glutamate to produce glutamine with concomitant hydrolysis of ATP, and plays a crucial role in the assimilation and re-assimilation of ammonia derived from a wide variety of metabolic processes during plant growth and development. The detailed reaction mechanism of higher plant GS is important to obtain insight into plant productivity and agronomical utility. Recently we determined the crystal structures of maize glutamine synthetase in complexes with three kinds of substrate analogues. From these structures we found a unique decameric structure of the enzyme which is significantly different from the bacterial glutamine synthetase and proposed a phosphate transfer reaction mechanism of ATP.

In this study, we aims at gaining insights how the enzyme recognize the substrate glutamic acid by the methods of mutagenesis and X-ray crystal structure analysis and we prepared several mutant enzymes where residues interacting substrate glutamic acid are mutated. So far we assayed the enzyme activities of the mutant enzymes and have crystallized some of them. We obtained diffraction data of one mutant. We report here the experimental procedures and results so far obtained.

P06-228

CRYSTAL SOLVATES OF N-(3-METHYLTHIO-1,2,4-THIADIAZOL-5-YL-AMINOCARBONYLMETHYL)CYTISINE

Kambarali Turgunov, Utkur Makhmudov, Temur Ibragimov, Bakhodir Tashkodjaev

S.Yunusov Institute of Chemistry of Plant Substances, Academy of Sciences of Republic of Uzbekistan, 77, Kh.Abdullaev str., Tashknent, 100170, Uzbekistan

Cytisine alkaloid (**I**) and its derivatives attract considerable attention of researchers due to a broad spectrum of physiological activities [1]. In an effort to get a new physiologic active substances by institute researchers have been synthesized a series of cytisine derivatives [2].

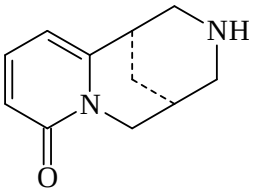

I

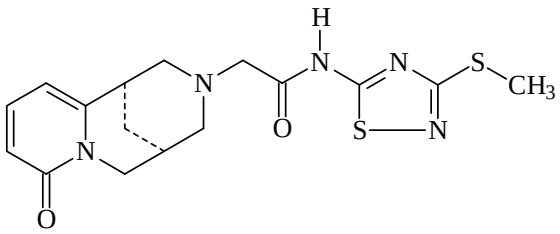

II

By crystallization of the titled cytisine derivative with structural formulas of **II** have been obtained host-guest complexes containing as guests water, methanol, chloroform, benzol and pyridine molecules. X-ray structural investigations of obtained crystals shows that molecule of **II** have taken different conformations due to its intramolecular rotate-ability. This conformation changeability allows to the molecule to forming isostructural host-guest complexes with functional and geometrical close solvent molecules (Fig.1).

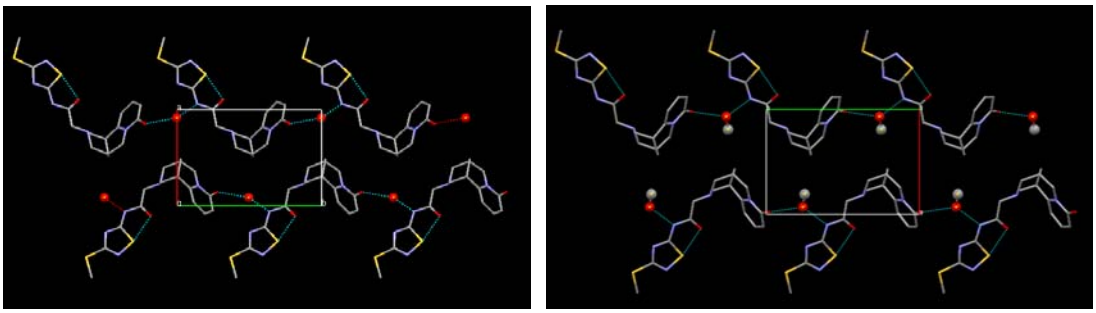

Figure 1. Water and methanol included crystal structures. (H atoms have been omitted)

Reference:

1. Boido CC, Tasso B, Boido V, Sparatore F. Farmaco, 2003, 58(3), p.265. ;
2. V.A.Saprykina, V.I.Vinogradova, R.F.Ambartsumova, T.F.Ibragimov, A.Sultankulov and Kh.M.Shakhidoyatov, *Chemistry of Natural Compounds*, 2004, **40**, p.582.

P06-229

SYNTHESIS OF NANOCRYSTALLINE $(Co,Ni)Al_2O_4$ SPINEL POWDER BY QUASICRYSTALLINE PRECURSOR

T.P. Yadav[1], N.K. Mukhopadhyay[2], R.S. Tiwari [1] and O.N. Srivastava[1]

[1]Department of Physics, Banaras Hindu University, Varanasi-221 005 (INDIA)

[2]Department of Metallurgical Engineering, Institute of Technology, Banaras Hindu University, Varanasi-221 005, (INDIA)

In the present study, attempts have been made to synthesize the nano-crystalline $(Co,Ni)Al_2O_4$ spinel powders by ball milling and subsequent annealing. An alloy of $Al_{70}Co_{15}Ni_{15}$, exhibiting the formation of a complex intermetallic compound known as decagonal quasicrystal is selected as the starting material for mechanical milling. The milling was carried out in an attritor mill at 400 rpm for 40 hours with ball to powder ratio of 20:1 in hexane medium. Subsequent to this annealing was performed in an air ambience for 10, 20 and 40 h at 600 °C in side the furnace in order to oxidize the decagonal phase and finally to form the spinel structure Significant enhancement in the magnetic properties has been found in nano-spinels compared to that of nano-decagonal phase, which can be attributed to the spinel structures. The weak ferromagnetic close to superparamagnetic behaviour is established for the first time in the nano-quasicrystalline phase. In case of nanospinels, the ferromagnetic properties are distinct although it is lower than the ferrite spinels.

P06-230

PROBING LOCAL STRUCTURES AROUND CO IN FERROMAGNETIC HfO_2:CO THIN FILMS USING EXAFS

Y. L. Soo,[a] S. C. Weng,[a] W. H. Sun,[a] S. L. Chang,[a] W. C. Lee,[a] Y. S. Chang,[a] J. Kwo,[a] M. Hong [b] J. M. Ablett,[d] C-. C. Kao,[d] D.G. Liu,[c] and J. F. Lee [c]

[a]Department of Physics;[b]Department of Materials Science and Engineering, National Tsing Hua University; [c]National Synchrotron Radiation Research Center, Hsinchu, Taiwa; [d]National Synchrotron Light Source, Upton, New York, U.S.A.

Local structure surrounding Co in MBE-grown HfO_2:Co thin films has been investigated using the extended x-ray absorption fine structure (EXAFS) technique. These films are ferromagnetic with Curie temperatures above room temperature. Our EXAFS results indicate progressive formation of Co clusters accompanied by interstitial doping of Co in samples grown at a substrate temperature of ~700ºC. On the other hand, films grown at a lower substrate temperature ~100ºC were found to be nearly Co-cluster-free. The low-temperature-grown films are also thermally stable up to an annealing temperature of ~700ºC. Our EXAFS results therefore verify the feasibility for preparing room-temperature-ferromagnetic HfO_2:Co diluted magnetic oxide without formation of magnetic Co clusters. These materials have great potential for applications in spintronic devices.

P06-231

CRYO-CRYSTALLIZATION OF DIETHYL OXALATE AND STUDIES ON INTERMOLECULAR INTERACTION

T. Vijay, S. J. Prathap and T. N. Guru Row

Solid State and Structural Chemistry Unit, Indian Institute of Science, Bangalore-12 India

In situ crystallization of a liquid, the subsequent determination of the molecular and crystal structure and consequently the study of intermolecular interactions is an area of contemporary interest. Recently, in situ cryo-crystallization has been used to crystallize liquids. In this novel methodology in our laboratory, liquid samples are solidified by selectively cooling them near crystallization temperatures with suitable ramp rates. The appearance of single crystal is followed by recording rotation photographs on the CCD detector of the Bruker Apex AXS diffractometer. The cryo-cooling is achieved using either the N_2 stream or the He stream to reach temperatures of crystallization depending on the melting point of the compound. Diethyl oxalate, a liquid at room temperature, solidifies at about 150 K, has been crystallized in a capillary of diameter 0.3 mm under the nitrogen cold stream generated by Oxford Cryostream system. The crystal belongs to a monoclinic system, space group $P2_1/c$, with Z =4.

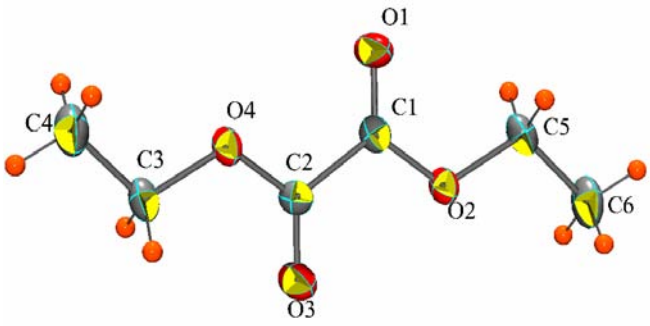

The structure is refined to a final R value of 0.08 for 1286 observed reflections. The molecules are held together via C-H…O interactions generating a sheet like structure when viewed down the b-axis.

P06-232

CRYO-CRYSTALLIZATION OF DIETHYL OXALATE AND STUDIES ON INTERMOLECULAR INTERACTION

T. Vijay, S. J. Prathap and T. N. Guru Row

Solid State and Structural Chemistry Unit, Indian Institute of Science, Bangalore-12 India

In situ crystallization of a liquid, the subsequent determination of the molecular and crystal structure and consequently the study of intermolecular interactions is an area of contemporary interest. Recently, in situ cryo-crystallization has been used to crystallize liquids. In this novel methodology in our laboratory, liquid samples are solidified by selectively cooling them near crystallization temperatures with suitable ramp rates. The appearance of single crystal is followed by recording rotation photographs on the CCD detector of the Bruker Apex AXS diffractometer. The cryo-cooling is achieved using either the N_2 stream or the He stream to reach temperatures of crystallization depending on the melting point of the compound. Diethyl oxalate, a liquid at room temperature, solidifies at about 150 K, has been crystallized in a capillary of diameter 0.3 mm under the nitrogen cold stream generated by Oxford Cryostream system. The crystal belongs to a monoclinic system, space group $P2_1/c$, with Z =4.

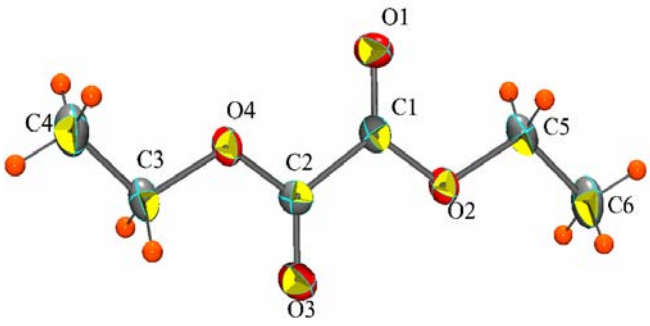

The structure is refined to a final R value of 0.08 for 1286 observed reflections. The molecules are held together via C-H…O interactions generating a sheet like structure when viewed down the b-axis.

P06-233

CRYSALIS^{Pro}'S ADVANCED STRATEGY MODULE FOR CHARGE DENSITY EXPERIMENTS

Dr. Jiwen Cai

Oxford Diffraction, 68 Milton Park, Abingdon, OX14 4RX, UK

Oxford Diffraction manufactures and supplies single crystal X-ray diffraction equipment, including a range of kappa-goniometer based Xcalibur and dual wavelength Gemini diffractometers, as well as the sub 15K base-temperature Helijet open flow helium cooler.

Our award winning hardware and CrysAlis^{Pro} software are being used in over 150 laboratories world-wide to carry out a broad range of crystallographic research, including the areas of modulated / incommensurate, quasi-crystalline materials as well as high pressure, diffuse scatter and highly demanding charge density studies.

The strategy module in CrysAlis^{Pro} takes full advantage of the agility of the four circle kappa platform and allows an unprecedented ease of use for creating data collection strategies for everyday use and for advanced charge density studies. Calculation of the most optimal, multiply-redundant, high resolution strategies are created at a click of a button, whilst maximising coverage and fully utilising the particular crystal symmetry and orientation.

P06-234

NON-CONVENTIONAL SCATTERING STUDIES OF MATERIALS USING A LABORATORY IMAGE PLATE DIFFRACTOMETER

Lynne H. Thomas[1], Sylvia E. McLain[2], Andrew Parkin[1], and Chick C. Wilson[1]

1. Department of Chemistry and WestCHEM Research School, University of Glasgow, Glasgow, G12 8QQ, U.K. 2. [2]Oak Ridge National Laboratory, PO Box 2008 MS6475, Oak Ridge TN 37831-6475, U.S.A.

Recent trends in the development of X-ray diffractometers have been towards fast readout detectors such as CCDs. Image plate detectors, however, have the advantage that long exposure times are possible due to their high dynamic range, allowing weaker scattering to be observed without suffering from detector overloads or from dark current accumulation. Experiments involving measurements such as liquid scattering and diffuse scattering which have previously required the use of high flux synchrotron radiation have been demonstrated to be possible on a laboratory diffractometer using a curved image plate detector. Diffuse scattering has been observed to arise from a wide range of different materials and its presence is often unexpected. The mechanism behind such scattering is often complex, however insights can be gained from consideration of the average structure of the material and the comparison to similar features in systems where the disorder has been characterised using modeling techniques such as Monte Carlo and Reverse Monte Carlo. The feasibility of collecting liquid diffraction patterns with the aim of studying the early stages of molecular arrangement within solution prior to crystallisation has also been investigated and preliminary results arising from this will be presented.

P06-235

CLASSIFYING MOLECULAR GEOMETRIES: APPLICATION OF FACTOR ANALYSIS TO CLUSTER FORMATION IN *d*SNAP.

Duncan Sneddon, Christopher J. Gilmore, Gordon Barr, Wei Dong, Andrew Parkin, and Chick C. Wilson,

WestChem. Department of Chemistry, University of Glasgow, Glasgow G12 8QQ, Scotland.

Cluster analysis is a well-established tool in statistics, but one that is used surprisingly little in crystallography. We have established its use in analysing the results of database searches using the Cambridge Structural Database (CSD).

CSD searches can produce thousands of 'hits' especially if a simple fragment is used as the search fragment. As a result processing and interpreting the results can be a laborious task and one where mistakes are easy to make. Cluster analysis, involving dendrograms, metric multidimensional scaling and other visualisation tools, can reduce the workload to a few hours in the hand of an experienced user. *d*SNAP is a cluster analysis program that provides these tools.

Factor analysis and other statistical methods are being used, in combination with visualisation techniques, including biplots, to uncover the latent underlying structural properties of the molecular fragments under investigation. This process is being undertaken in concert with investigations into many of the possible descriptions of the geometries of the fragments under study.

Details of this two-pronged approach will be presented, along with its utility as a method to uncover the underlying reason behind the formations of clusters in *d*SNAP. The development of this additional feature within our suite of automated methods for interpreting CSD data should substantially ease the interpretation of the results of cluster analysis.

The application of the biplots being developed will be discussed, and illustrated with a simple example to illuminate the properties of biplots and what makes them such a useful tool to a user of dSNAP.

The *d*SNAP software is available free of charge to all interested researchers, distributed through Glasgow University and Bruker-AXS (http://www.chem.gla.ac.uk/snap/).

Conference Sponsors

Academia Sinica

Asian Crystallographic Association

Bruker AXS BV

International Union of Crystallography

Marresearch GmbH

National Science Council

National Tsing Hua University

National Synchrotron Radiation Research Center

Rigaku Corporation

Rayonix

The Crystallographic Committee, Taipei